AWARD NUMBER: W81XWH-16-1-0172

TITLE: Novel mTORC1 and 2 Signaling Pathways in Polycystic Kidney Disease (PKD)

PRINCIPAL INVESTIGATOR: Charles L. Edelstein MD, PhD

CONTRACTING ORGANIZATION: University of Colorado, Denver, Aurora, CO

REPORT DATE: December 2021

TYPE OF REPORT: Final

PREPARED FOR: U.S. Army Medical Research and Materiel Command
                 Fort Detrick, Maryland 21702-5012

The views, opinions and/or findings contained in this report are those of the author(s) and should not be construed as an official Department of the Army position, policy or decision unless so designated by other documentation.

REPORT DOCUMENTATION PAGE		*Form Approved* *OMB No. 0704-0188*

Public reporting burden for this collection of information is estimated to average 1 hour per response, including the time for reviewing instructions, searching existing data sources, gathering and maintaining the data needed, and completing and reviewing this collection of information. Send comments regarding this burden estimate or any other aspect of this collection of information, including suggestions for reducing this burden to Department of Defense, Washington Headquarters Services, Directorate for Information Operations and Reports (0704-0188), 1215 Jefferson Davis Highway, Suite 1204, Arlington, VA 22202-4302. Respondents should be aware that notwithstanding any other provision of law, no person shall be subject to any penalty for failing to comply with a collection of information if it does not display a currently valid OMB control number. **PLEASE DO NOT RETURN YOUR FORM TO THE ABOVE ADDRESS.**

1. REPORT DATE December 2021	2. REPORT TYPE Final	3. DATES COVERED 01Sep2016-31Aug2021
4. TITLE AND SUBTITLE Novel mTORC1 and 2 Signaling Pathways in Polycystic Kidney Disease (PKD)		**5a. CONTRACT NUMBER** W81XWH-16-1-0172
		5b. GRANT NUMBER
		5c. PROGRAM ELEMENT NUMBER
6. AUTHOR(S) Charles L. Edelstein MD. E-Mail: Charles.edelstein@cuanschutz.edu		**5d. PROJECT NUMBER**
		5e. TASK NUMBER
		5f. WORK UNIT NUMBER
7. PERFORMING ORGANIZATION NAME(S) AND ADDRESS(ES) University of Colorado Denver Office of Grants and Contracts, Mail Stop F428, Anschutz Medical Campus, Building 500, 13001 E. 17th Place, Room W1126, Aurora, CO 80045-2571		**8. PERFORMING ORGANIZATION REPORT NUMBER**
9. SPONSORING / MONITORING AGENCY NAME(S) AND ADDRESS(ES) U.S. Army Medical Research and Material Command Fort Detrick, Maryland 21702-5012		**10. SPONSOR/MONITOR'S ACRONYM(S)**
		11. SPONSOR/MONITOR'S REPORT NUMBER(S)

12. DISTRIBUTION / AVAILABILITY STATEMENT
Approved for Public Release; Distribution Unlimited

13. SUPPLEMENTARY NOTES

Abstract: This proposal will study novel mTORC1 and 2 signaling pathways that mediate ADPKD and investigate the effects of mTORC1 (Raptor) knockout, mTORC2 (Rictor) knockout or combined mTORC1 and 2 knockout on cyst growth and kidney function. The overall hypothesis is that there is increased mTORC1 (4E-BP1) and mTORC2 (AktSer473, PKCα and SGK1) signaling in PKD kidneys and that combined mTORC1 (Raptor) knockout and mTORC2 (Rictor) knockout in Pkd1 -/- mice will slow cyst growth and improve kidney function more than mTORC1 (Raptor) knockout or mTORC2 (Rictor) knockout alone. We have published the role 4E-BP1 signaling pathways in PKD kidneys and cells. We have preliminary data in Pkd1, Rictor double knockout mice. We have published: 1) The effect of trehalose on mTOR signaling and autophagy in PKD kidneys, 2) mTOR signaling and autophagy in the heart and kidney in PKD. We have determined that both mTOR kinase inhibitors (TORKs) and sirolimus on decrease PKD and improve kidney function in the Pkd1$^{RC/RC}$ mouse model. We have continued to use FISP-MRI scanning to obtain precise measurements of kidney and cyst volume and the number of cysts in live PKD mice.

15. SUBJECT TERMS
Polycystic kidney disease, PKD, mTORC1, mTORC2, Raptor, Rictor.

16. SECURITY CLASSIFICATION OF:			17. LIMITATION OF ABSTRACT	18. NUMBER OF PAGES	19a. NAME OF RESPONSIBLE PERSON USAMRMC
a. REPORT Unclassified	**b. ABSTRACT** Unclassified	**c. THIS PAGE** Unclassified	Unclassified	98	**19b. TELEPHONE NUMBER** *(include area code)*

Standard Form 298 (Rev. 8-98)

Prescribed by ANSI Std. Z39.18

Table of Contents

1. **INTRODUCTION:**

ADPKD is the most common life threatening hereditary disease in the USA. ADPKD accounts for about 5-10% of end-stage renal failure in the USA requiring dialysis and renal transplantation. There is no effective treatment for ADPKD. This proposal will study novel mTORC1 (pS6 and 4E-BP1) and 2 (Akt, PKC alpha, SGK1) signaling pathways that mediate ADPKD and investigate the effects of mTORC1 (Raptor) knockout, or the mTORC1 inhibitor (sirolimus), mTORC2 (Rictor) knockout or combined mTORC1 and 2 knockout or the mTOR kinase inhibitor drugs (TORKs) on cyst growth and kidney function. The overall hypothesis is that there is increased mTORC1 (4E-BP1) and mTORC2 (AktSer473, PKCα and SGK1) signaling in PKD kidneys and that combined mTORC1 (Raptor) knockout and mTORC2 (Rictor) knockout in Pkd1 -/- mice will slow cyst growth and improve kidney function more than mTORC1 (Raptor) knockout or mTORC2 (Rictor) knockout alone or that the mTOR kinase inhibitors will be more effective than sirolimus in decreasing kidney cyst growth. These studies will unequivocally address whether the mTORC1 (4E-BP1) or mTORC2 pathway or both pathways is important in PKD and whether it is worthwhile performing therapeutic interventions using the novel mTORC1 and 2 inhibitors that are in clinical trials in humans

2. **KEYWORDS:**

Autosomal dominant polycystic kidney disease

mTORC1

Raptor

mTORC2

Rictor

4E-BP1

mTOR kinase inhibitor

3. **ACCOMPLISHMENTS: What were the major goals of the project?**

Major Task 1: To determine the effect of mTORC1 (Raptor) knockout in Pkd1 -/- mice (60% complete)

Subtask 1: To determine whether Raptor knockout decreases the cystic phenotype
Subtask 2: To determine the effect of Raptor -/- on 4E-BP1 signaling
Subtask 3: To determine the effect of 4E-BP inhibition on PKD

Major Task 2: To determine the effect of mTORC2 (Rictor) knockout in Pkd1 -/- mice (100% complete)

<u>Subtask 1:</u> To determine whether Rictor knockout reduces the cystic phenotype in vivo

<u>Subtask 2:</u> AktSer473, SGK1 and PKCα phosphorylation in PKD in vivo

<u>Subtask 3:</u> AktSer473, SGK1 and PKCα phosphorylation in PKD in vitro

<u>Major Task 3: To determine the effect of combined mTORC1 (Raptor) knockout and mTORC2 (Rictor) knockout in Pkd1 -/- mice (75% complete)</u>

<u>Subtask 1:</u> To determine the effect of combined mTORC1 (Raptor) knockout and mTORC2 (Rictor) knockout in Pkd1 -/- mice on apoptosis and proliferation, cyst growth and kidney function.

<u>SubTask 2:</u> To determine the effect of TORKs versus sirolimus on PKD and kidney function

What was accomplished under these goals?

(1) Major activities:

Major task 1: 4E-BP1 signaling has been studied in ADPKD kidneys and PKD cells in vitro. This study has now been published in Hum Molec. Genet.-see Major Results below.

Major Task 2: Preliminary data on the development of Pkd1 -/- Rictor -/- double knockout mice using the tamoxifen-inducible ER2 Cre is presented below. These double knockout, Pkd1 -/- Rictor -/-, mice have less cyst growth and improved kidney function compared to single knockout Pkd1 -/- mice (Fig 1).

We are continuing to breed Ksp1.3 mice with Pkd1$^{fl/fl}$ and Rictor$^{fl/fl}$ mice to develop Pkd1 -/-, Rictor -/- double knockout mice (Table 1).

Major task 3: Study of treatment of Pkd1 -/- mice with mTOR kinase inhibitors that inhibit mTORC1 and mTORC2 (TORKs) versus Sirolimus (mTORC1 inhibitor), has been published –see Major Results below.

Major Tasks 1, 2 and 3: We are using FISP-MRI scans to determine polycystic kidney volume and cyst volume and number of cysts per kidney at different time points of the disease (Fig 2).

We have published data that mTOR signaling is activated in cardiac hypertrophy in PKD mice (See Major Results below)

We have published the effect of the autophagy inducer, trehalose, on mTOR signaling in the kidney and on PKD (See Major Results below).

We have published that unilateral nephrectomy in mice results in activation of mTOR and suppressed autophagy (See Major Results below)

2) Specific objectives:

Major Task 1: To determine whether Raptor knockout decreases the cystic phenotype. To determine the effect of 4E-BP inhibition on PKD.

Major Task 2: To determine whether Rictor knockout reduces the cystic phenotype in vivo.

Major Task 3: To determine the effect of TORKs versus sirolimus on PKD and kidney function.

3) Major results:

Major Task 1: To determine whether Raptor knockout decreases the cystic phenotype. To determine the effect of 4E-BP inhibition on PKD. Study has been published.
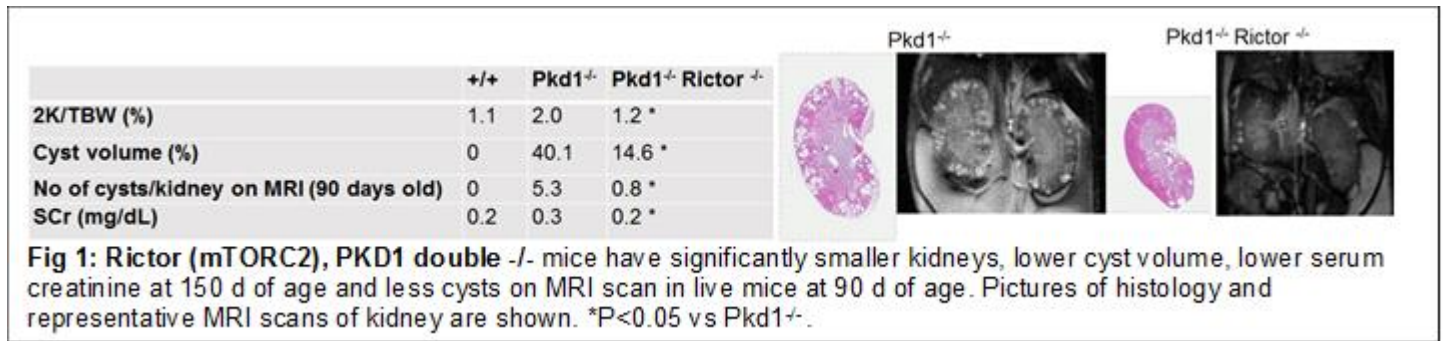
The consequences of increased 4E-BP1 in Polycystic kidney disease. Holditch SJ, Brown CN, Atwood D, Brown SE, Lombardi AM, Nguyen KN, Hill RC, Lanaspa M, Hopp K, Weiser-Evans M, Edelstein CL Hum. Molec Genet. 2019 Dec 15;28(24):4132-4147

Autosomal Dominant Polycystic kidney disease (ADPKD) is the most common hereditary renal disease, characterized by cyst formation and growth. Hyperproliferation is a major contributor to cyst growth. At the nexus of regulating proliferation, is 4E-BP1. We demonstrate that ADPKD mouse and rat models, ADPKD patient renal biopsies, and $PKD1^{-/-}$ cells exhibited hyperphosphorylated 4E-BP1, a biomarker of increased translation and proliferation. We hypothesized that expression of constitutively active 4E-BP1 constructs (4E-BP1^{F113A} and 4E-BP1^{R13AF113A}) would decrease proliferation, and reduce cyst expansion. Utilizing the $Pkd1^{RC/RC}$ mouse we determined the effect of 4E-BP1^{F113A} on PKD. Unexpectedly, 4E-BP1^{F113A} resulted in increased cyst burden and suppressed apoptosis markers, increased anti-apoptotic Bcl-2 protein and increased mitochondrial proteins. Exogenous 4E-BP1 enhanced proliferation, decreased apoptosis, increased anti-apoptotic Bcl-2 protein, impaired NADPH oxidoreductase activity, increased mitochondrial proteins and increased superoxide production in PKD patient derived renal epithelial cells. Reduced 4E-BP1 expression suppressed proliferation, restored apoptosis, and improved cellular metabolism. These findings provide insight into how cyst-lining cells respond to 4E-BP1.

Major Task 2: To determine whether Rictor knockout reduces the cystic phenotype in vivo

In new preliminary data, Rictor$^{fl/fl}$ mice were bred with the Pkd1$^{fl/fl}$; KspCad-CreERT2 mice to develop Rictor$^{fl/fl}$, Pkd1$^{fl/fl}$; KspCad-CreERT2 mice that were treated with tamoxifen to develop kidney-specific Rictor, Pkd1 double -/- mice that were evaluated at 90 and150 days post tamoxifen (Fig1). These mice develop slow PKD over a period of 150 days. gDNA was quantified by qPCR primers specific to PKD1 flox site and

RICTOR flox site in Rnase treated DNA isolated from total kidney homogenates and showed that kidney specific PKD1 and Rictor genomic flox sites significantly reduced post Tamoxifen treatment.

	+/+	Pkd1$^{-/-}$	Pkd1$^{-/-}$ Rictor $^{-/-}$
2K/TBW (%)	1.1	2.0	1.2 *
Cyst volume (%)	0	40.1	14.6 *
No of cysts/kidney on MRI (90 days old)	0	5.3	0.8 *
SCr (mg/dL)	0.2	0.3	0.2 *

Fig 1: Rictor (mTORC2), PKD1 double -/- mice have significantly smaller kidneys, lower cyst volume, lower serum creatinine at 150 d of age and less cysts on MRI scan in live mice at 90 d of age. Pictures of histology and representative MRI scans of kidney are shown. *P<0.05 vs Pkd1$^{-/-}$.

We are breeding KSP 1.3 Cre mice with Pkd floxed and Rictor floxed mice to obtain KSP 1.3 Cre Pkd floxed mice and double knockout KSP 1.3 Cre Pkd floxed Rictor floxed mice. The mice develop rapid PKD and were sacrificed at days 16-18 of age. We have obtained mice of all these genotypes and results are shown in Table 1 below. In this model, heterozygous Rictor knockout in the polycystic kidney seems to make PKD slightly worse.

Table 1	Wild type N=12	KSP1.3 Pkd1 -/- N=3	KSP1.3Pkd1-/- Rictor -/- N=4	KSP1.3Pkd1-/- Rictor +/- N=1
2K/TBW (%)	1.52 ± 0.03	38.9 ± 0.05 *	41.6 ± 1.1**	41.8
2K/TBW (%) = 2 kidney weight/total body weight as a % - a marker of cystic disease in the kidney				
*P<0.001 vs. wild type, ** P<0.001 vs. wild type, P<0.01 vs KSP1.3 Pkd1 -/-.				

Major Task 3: To determine the effect of TORKs versus sirolimus on PKD and kidney function.

We have found that in a mouse model of autosomal dominant polycystic kidney disease (ADPKD), both sirolimus and an mTOR kinase inhibitor decrease cyst volume and improve kidney function despite differential effects signaling and apoptosis. Study has been published:

Holditch S, Brown CN, Atwood DJ, Lombardi AM, Nguyen KN, Toll HW, Hopp K, Edelstein CL. A study of sirolimus and an mTOR kinase inhibitor (TORKi) in a hypomorphic Pkd1 mouse model of autosomal dominant polycystic kidney disease (ADPKD). Am J.Physiol Renal Physiol 2019 Jul 1;317(1):F187-F196

Autosomal dominant polycystic kidney disease (ADPKD) is characterized by cyst formation and growth, which is partially driven by abnormal proliferation of tubular cells. There is activation of the pro-proliferative mechanistic target of rapamycin complex 1 and 2 (mTORC1 and 2) in PKD mouse kidneys. Sirolimus indirectly inhibits mTORC1. The novel mTOR kinase inhibitors (TORKi) directly inhibit mTOR kinase resulting in inhibition of both mTORC1 and 2. The aim of the present study was to determine the effects of sirolimus versus the TORKi, torin2, on cyst growth and kidney function in the *Pkd1* p.R3277C (*Pkd1*$^{RC/RC}$) mouse model, a hypomorphic *Pkd1* model orthologous to the human condition and to determine the effects of sirolimus versus torin2 on mTORC1 and 2 signaling in *PKD1*$^{-/-}$ cells and in the kidneys of *Pkd1*$^{RC/RC}$ mice. *In vitro*, both inhibitors reduced mTORC1 and mTORC2 phosphorylated substrates, and negatively impacted cellular metabolic activity as measured by the MTT assay. *Pkd1*$^{RC/RC}$ mice were treated with sirolimus or torin2 from 50 to 120 days of age. Torin2 was as effective as sirolimus in decreasing cyst growth and improving loss of kidney function. Both sirolimus and torin2 decreased pS6, p4E-BP1, pAkt and proliferation in *Pkd1*$^{RC/RC}$ kidneys. In conclusion, both torin2 and sirolimus were equally effective in decreasing cyst burden, improving kidney function, and mediated comparable effects on mTORC1 and 2 signaling and proliferation in the *Pkd1*$^{RC/RC}$ kidney.

4) **Other achievements:** Major tasks 1, 2 and 3.

Use of FISP-MRI

We continue to use FISP-MRI to obtain measurements of kidney and cyst volume in live PKD (See Figs 2, 3 and 4).
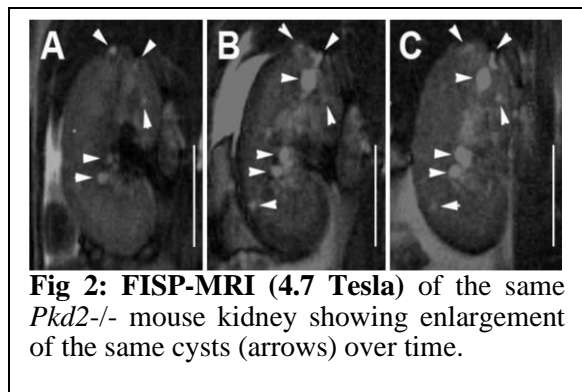

Fig 2: FISP-MRI (4.7 Tesla) of the same *Pkd2*-/- mouse kidney showing enlargement of the same cysts (arrows) over time.
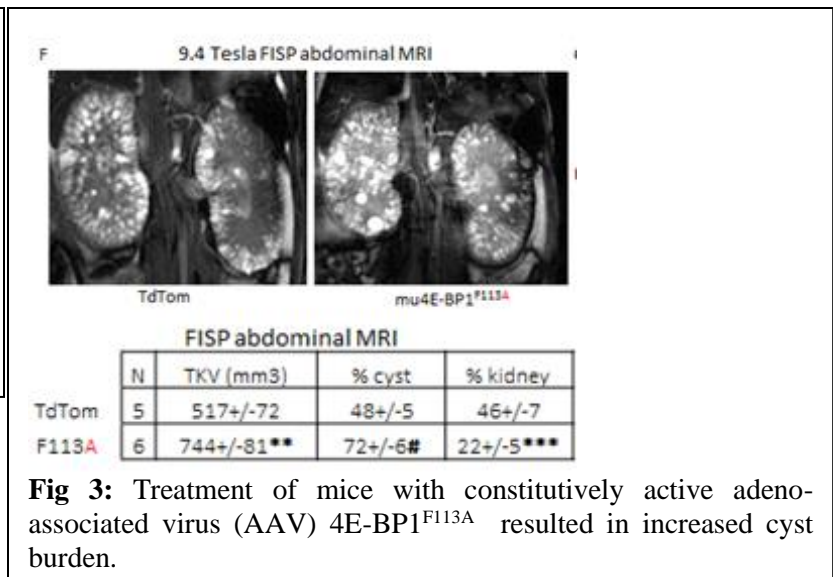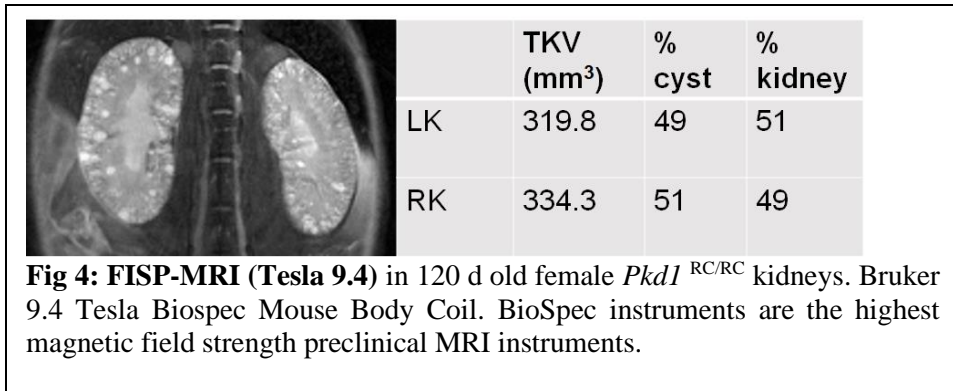

FISP abdominal MRI

	N	TKV (mm3)	% cyst	% kidney
TdTom	5	517+/-72	48+/-5	46+/-7
F113A	6	744+/-81**	72+/-6#	22+/-5***

Fig 3: Treatment of mice with constitutively active adeno-associated virus (AAV) 4E-BP1^{F113A} resulted in increased cyst burden.

	TKV (mm³)	% cyst	% kidney
LK	319.8	49	51
RK	334.3	51	49

Fig 4: FISP-MRI (Tesla 9.4) in 120 d old female *Pkd1* [RC/RC] kidneys. Bruker 9.4 Tesla Biospec Mouse Body Coil. BioSpec instruments are the highest magnetic field strength preclinical MRI instruments.

We have published two papers in the last 24 months that include mTORC1/2 signaling in the heart and kidney in PKD.

mTORC1/2 signaling in the heart in PKD:

Atwood DJ, Pokhrel D, Brown CN, Holditch SJ, Bachu DM, Thorburn A, Hopp K, Edelstein CL. Increased mTOR and suppressed autophagic flux in the heart of a hypomorphic Pkd1 mouse model of autosomal dominant polycystic kidney disease. Cell Signal. 2020 (in press)

Abstract:

Cardiac hypertrophy is common in autosomal dominant polycystic kidney disease (ADPKD) patients. We found increased heart weight in $Pkd1^{RC/RC}$ and $Pkd2^{WS25/+}$ mouse models of ADPKD. As there is a link between increased heart weight and mammalian target of rapamycin (mTOR), the aim of the study was to determine mTOR complex 1 and 2 signaling proteins in the heart in the $Pkd1^{RC/RC}$ mouse model of PKD. In 70 day old $Pkd1^{RC/RC}$ hearts, on immunoblot analysis, there was a large increase in p-AMPK^{Thr172}, a known autophagy inducer, and an increase in p-Akt^{Ser473} and p-Akt^{Thr308}, but no increase in other mTORC1/2 proteins (p-S6$^{Ser240/244}$, p-mTOR^{Ser2448}). In 150 day old $Pkd1^{RC/RC}$ hearts, there was an increase in mTORC1 (p-S6$^{Ser240/244}$) and mTOR-related proteins (p-Akt^{Thr308}, p-GSK3β^{Ser9}, p-AMPK^{Thr172}). As the mTOR pathway is the master regulator of autophagy, autophagy proteins were measured. There was an increase in p-Beclin-1 (BECN1), an autophagy regulator and activating molecule in Beclin-1-regulated autophagy (AMBRA1), a regulator of Beclin that play a role in autophagosome formation, an early stage of autophagy. There was a defect in the later stage of autophagy, the fusion of the autophagosome with the lysosome, known as autophagic flux, as evidenced by the lack of an increase in LC3-II, a marker of autophagosomes, with the lysosomal inhibitor bafilomycin, in both 70 day old and 150 day old hearts. To determine the role of autophagy in causing increased heart weight, $Pkd1^{RC/RC}$ were treated with 2-deoxyglucose (2-DG) or Tat-Beclin1 peptide, agents known to induce autophagy. 2-DG treatment from 150 to 350 days of age, a time period when increased heart weight developed, did not reduce the increased heart weight. Unexpectedly, Tat-Beclin 1 peptide treatment from 70 to 120 days of age

resulted in increased heart weight. In summary, there is suppressed autophagic flux in the heart at an early age in *Pkd1*^{RC/RC} mice. Increased mTOR signaling in older mice is associated suppressed autophagic flux. There was a large increase in p-AMPK^{Thr172}, a known autophagy inducer, in both young and old mice. 2-DG treatment did not impact increased heart weight and Tat-Beclin1 peptide increased heart weight.

mTOR signaling in the kidney in PKD:

Atwood DJ, Brown DN, Holditch SJ, Pokhrel D, Thorburn A, Hopp K and Edelstein CL. The effect of trehalose on autophagy-related proteins and cyst growth in a hypomorphic Pkd1 mouse model of autosomal dominant polycystic kidney disease. Cell Signal. 2020 (in press).

Abstract:

Autosomal dominant polycystic kidney disease (ADPKD) is a common inherited disorder characterized by kidney cyst growth often resulting in end-stage renal disease. There is growing attention on understanding the role of impaired autophagy in ADPKD. Trehalose (TRE) has been shown to increase both protein stability and aggregate clearance and induce autophagy in neurodegenerative diseases. TRE treatment in wild type mice compared to vehicle resulted in increased expression in the kidney of Atg12-5 complex and increased Rab9a, autophagy-related proteins that play a role in the formation of autophagosomes. Thus, the aim of the study was to determine the effect of TRE on cyst growth and autophagy-related proteins, in the hypomorphic *Pkd1*^{RC/RC} mouse model of ADPKD. *Pkd1*^{RC/RC} mice were treated 2% TRE in water from days 50 to 120 of age. TRE did not slow cyst growth or improve kidney function or affect proliferation and apoptosis in *Pkd1*^{RC/RC} kidneys. In *Pkd1*^{RC/RC} vs. wild type kidneys, expression of the Atg12-5 complex was inhibited by TRE resulting in increased free Atg12 and TRE was unable to rescue the deficiency of the Atg12-5 complex. Rab9a was decreased in *Pkd1*^{RC/RC} vs. wild type kidneys and unaffected by TRE. The TRE-induced increase in p62, a marker of autophagic cargo, that was seen in normal kidneys was blocked in *Pkd1*^{RC/RC} kidneys. In summary, the autophagy phenotype in *Pkd1*^{RC/RC} kidneys was characterized by decreases in crucial autophagy-related proteins (Atg12-5 complex, Atg5, Atg16L1), decreased Rab9a and increased mTORC1 (pS6, p-mTOR^{S2448}) proteins. TRE increased Atg12-5 complex, Rab9a and p62 in normal kidneys, but was unable to rescue the deficiency in autophagy proteins or suppress mTORC1 in *Pkd1*^{RC/RC} kidneys and did not protect against cyst growth.

We have published that there is increased mTORC1 and 2 signaling and suppressed autophagy caused by sham surgery in a unilateral nephrectomy (UNX) model in mice.

Surgical procedures suppress autophagic flux in the kidney

Carolyn N. Brown, Daniel Atwood, Deepak Pokhrel, Sara J. Holditch, Christopher Altmann, Nataliya I. Skrypnyk, Jennifer Bourne, Jelena Klawitter, Judith Blaine, Sarah Faubel, Andrew Thorburn, Charles L. Edelstein.

Abstract

Many surgical models are used to study kidney and other diseases in mice, yet the effects of the surgical procedure itself on the kidney and other tissues have not been elucidated. In the present study, we found that both sham surgery and unilateral nephrectomy (UNX), which is used as a model of renal compensatory hypertrophy, in mice resulted in increased mammalian target of rapamycin complex 1/2 (mTORC1/2) in the remaining kidney. mTORC1 is known to regulate lysosomal biogenesis and autophagy. Genes associated with lysosomal biogenesis and function were decreased in sham surgery and UNX kidneys. In both sham surgery and UNX, there was suppressed autophagic flux in the kidney as indicated by the lack of an increase in LC3-II or autophagosomes seen on immunoblot, IF and EM after bafilomycin A1 administration and a concomitant increase in p62, a marker of autophagic cargo. There was a massive increase in pro-inflammatory cytokines, which are known to activate ERK1/2, in the serum after sham surgery and UNX. There was a large increase in ERK1/2 in sham surgery and UNX kidneys, which was blocked by the MEK1/2 inhibitor, trametinib. Trametinib also resulted in a significant decrease in p62. In summary, there was an intense systemic inflammatory response, an ERK-mediated increase in p62 and suppressed autophagic flux in the kidney after sham surgery and UNX. It is important that researchers are aware that changes in systemic pro-inflammatory cytokines, ERK1/2 and autophagy can be caused by sham surgery as well as the kidney injury/disease itself.

What opportunities for training and professional development has the project provided?

The grant was not meant to provide training or professional development. However, starting in the summer there was a Visiting Scholar, Dr Ozgur Oto MD, working with our group as a volunteer to advance his professional skills in basic medical research.

How were the results disseminated to communities of interest?

Our results to date have been accepted as Poster Presentations at the annual American Society of Nephrology Meetings from 2016 to 2021.

We have published a review paper that includes much of our recent research and will be of interest to the PKD community:

Nowak K, Edelstein CL Apoptosis and autophagy in PKD. Cell Signal 2020 Apr;68:109518. doi: 10.1016

Apoptosis in the cystic epithelium is observed in most rodent models of polycystic kidney disease (PKD) and in human autosomal dominant PKD (ADPKD). Apoptosis inhibition decreases cyst growth, whereas induction of apoptosis in the kidney of Bcl-2 deficient mice increases proliferation of the tubular epithelium and subsequent cyst formation. However, alternative evidence indicates that both induction of apoptosis as well as increased overall rates of apoptosis are associated with decreased cyst growth. Autophagic flux is suppressed in cell, zebra fish and mouse models of PKD and suppressed autophagy is known to be associated with increased apoptosis. There may be a link between apoptosis and autophagy in PKD. The mammalian target of rapamycin (mTOR), B-cell lymphoma 2 (Bcl-2) and caspase pathways that are known to be dysregulated in PKD, are also known to regulate both autophagy and apoptosis. Induction of autophagy in cell and zebrafish models of PKD results in suppression of apoptosis and reduced cyst growth supporting the hypothesis autophagy induction may have a therapeutic role in decreasing cyst growth, perhaps by decreasing apoptosis and proliferation in PKD. Future research is needed to evaluate the effects of direct autophagy inducers on apoptosis in rodent PKD models, as well as the cause and effect relationship between autophagy, apoptosis and cyst growth in PKD.

What do you plan to do during the next reporting period to accomplish the goals?

1) This is a final report We have submitted a DOD Expansion Award to study mTOR signaling in the heart in PKD.

2) We have hearts from Pkd1 -/- mice. We are studying mTORC1 and 2 signaling pathways in hearts from Pkd1 -/- mice. It will be novel to discover that mTORC1 or 2 signaling is activated in the hearts of Pkd1 -/- mice.

4. **IMPACT:**

What was the impact on the development of the principal discipline(s) of the project?

Major findings:

1) Reduced 4E-BP1 expression suppressed proliferation, restored apoptosis, and improved cellular metabolism in Pkd1$^{RC/RC}$ mice and human Pkd1 cells. These findings provide insight into how cyst-lining cells respond to 4E-BP1. Interventions involving the 4E-BP1 system may provide a future rationale for treatment to decrease PKD (Published-see above).

2) The mTOR kinase inhibitor Torin2 is as effective as sirolimus to treat PKD in Pkd1 -/- mice despite different effects on mTOR signaling, proliferation and apoptosis. These findings provide a rationale for the testing of new generation mTOR kinase inhibitors e.g AZD 2014 in preclinical studies in animal models of PKD, These

studies provide insights into the use of combined mTORC1 and 2 inhibitors (the mTOR kinase inhibitors or TORKs) as future treatments in PKD (Published-see above).

3) Activation of the mTORC1 and 2 pathway in Pkd1 -/- mice is associated with suppressed autophagy in the kidney. These studies will provide novel insights on the potential use of autophagy inducers that are mTOR inhibitors as therapy for PKD.

4) There is suppressed autophagic flux in the heart at an early age in Pkd1$^{RC/RC}$ mice. Increased mTOR signaling in older mice is associated suppressed autophagic flux. There was a large increase in p-AMPK^{Thr172}, a known autophagy inducer and mTORC1 inhibitor, in both young and old mice. 2-DG treatment did not impact increased heart weight and Tat-Beclin1 peptide increased heart weight (Published-see above).

5) The autophagy phenotype in Pkd1$^{RC/RC}$ kidneys was characterized by decreases in crucial autophagy-related proteins (Atg12-5 complex, Atg5, Atg16L1), decreased Rab9a and increased mTORC1 (pS6, p-mTOR^{S2448}) proteins. TRE increased Atg12-5 complex, Rab9a and p62 in normal kidneys, but was unable to rescue the deficiency in autophagy proteins or suppress mTORC1 in Pkd1RC/RC kidneys and did not protect against cyst growth (Published-see above)

6) There was activation of mTORC1 and mTORC2, an intense systemic inflammatory response, an ERK-mediated increase in p62 and suppressed autophagic flux in the kidney after sham surgery and UNX. It is important that researchers are aware that changes in systemic pro-inflammatory cytokines, ERK1/2 and autophagy can be caused by sham surgery as well as the kidney injury/disease itself.

What was the impact on other disciplines?

1) Cancer: Many cancers are driven by increased 4E-BP1 signaling. We determined that inhibition of the 4E-BP1 system in PKD has different effects compared to studies in cancer. Transformed hyperproliferative breast cancer cells, lymphocytes, and epithelial cells forced to shift from cap-dependent to IRES-dependent translation results in increased apoptosis, decreased proliferation, and decreased cell size, thus retarding the growth of transformed tissues. However in PKD, a disease known for being driven by abnormal epithelial proliferation, *we observed the opposite.* In our *in vitro* studies, a shift from cap-dependent to IRES-dependent translation mediated by constitutively active 4E-BP1 suppressed apoptosis, increased proliferation, stimulated mitochondrial biogenesis, and augmented superoxide production uniquely in a PKD genotype, largely leaving non-PKD cell lines uninfluenced. *In vivo*, constitutively active 4E-BP1 resulted in mitochondrial dysregulation, and *worsened PKD disease*.

2) <u>Cancer:</u> Many cancers are driven by increased mTORC2 signaling. Demonstration that mTOR kinase inhibitors e.g. Torin2, AZD2014 decrease proliferation and have an effect on apoptosis may provide a future rationale for the use of mTOR kinase inhibitors to certain cancers.

3) <u>Aging:</u> Suppressed autophagy and increased mTOR signaling plays a role in disease processes like cancer and aging. Our studies of the effect of autophagy inducers on mTOR signaling and PKD will help in the understanding of the pathogenesis and treatment of other processes like aging and cancer.

4) <u>Cardiac hypertrophy:</u> We demonstrated increased mTORC1/2 signaling and cardiac hypertrophy in Pkd1 RC/RC mice. These studies may provide insight into the mechanisms of cardiac hypertrophy.

5) <u>In vivo models of disease:</u> Many researchers study in vivo models of disease in many different organ systems. It is important that researchers are aware that changes in systemic pro-inflammatory cytokines, ERK1/2 and autophagy can be caused by sham surgery as well as the kidney injury/disease itself.

What was the impact on technology transfer?

Nothing to report.

What was the impact on society beyond science and technology?

The study of mTOR kinase inhibitors like Torin2 or autophagy inducers to treat patients with ADPKD.

The genetic studies (Pkd1 -/- mice with additional knockout of mTORC1 or 2 or both) will offer mechanistic insights into novel mTORC1 and 2 signaling pathways in ADPKD.

The pharmacological studies (4E-BP1 inhibition, AktSer473, PKCα or SGK1 inhibition and TORKs) and gene therapy studies (AAV gene therapy against 4E-BP1) will provide insights into future therapies for PKD.

Discovery of new treatments for PKD could improve the quality of life and extend the life span of people with ADPKD.

Discovery of mechanisms and treatments for cardiac hypertrophy in ADPKD patients could impact life expectancy in PKD patients.

Our studies provided some insights on how surgery puts stresses on the body.

5. **CHANGES/PROBLEMS:**

Changes in approach and reasons for change

The tamoxifen-inducible ER2 Cre did not always work leading to mice with a very variable form of the ADPKD disease. Instead we used KSP 1.3 Cre mice that have an embronic Cre that is spontaneous (does not need tamoxifen) and the Pkd1 -/- mice develop PKD and kidney failure at a much earlier age. This model will lead to a more reproducible and faster model of ADPKD. Due to the change in our Cre mice and the Covid pandemic (see below), we were not successful in creating triple knockout Pkd, rictor, raptor mice

Both polycystin (PC-1) and polycystin-2 (PC-2) are known to modulate the mTOR pathway. PC-1 deficiency upregulates the mTOR pathway via TSC-2. PC-2 modulates the mTOR pathway in human cardiomyocytes. On further consideration, we realized that PKD mice that also have the gene defect in the heart should have upregulation of mTORC1/2 in the heart. Our published data confirmed increased mTORC1/2 signaling in the heart in PKD mice. On examining our PKD mice further, we were intrigued by the degree of cardiac hypertrophy even in heterozygous $Pkd2^{+/-}$ mice without PKD. A critical barrier to progress on understanding the causes of cardiac hypertrophy in PKD is that it is often presumed that cardiac hypertrophy is due to the hypertension and that many pre-clinical studies in PKD do not study the heart or even measure the blood pressure. Thus we are studying mTORC1/2 signaling in both the heart and kidneys in PKD. mTOR signaling in the heart is the topic of our DOD Expansion Award submission in 2021.

Actual or anticipated problems or delays and actions or plans to resolve them

Dr Holditch, the post-doctoral fellow/instructor who was performing the 4E-BP1 studies, resigned in July 2019 as her husband was transferred to another city. A new PRA, Deepak Pokhrel, was hired to continue the mTOR studies in PKD and has learnt all the necessary techniques related to mouse breeding and mTOR studies.

Laboratories were closed for 3 months, from March to end of May, 2020, at the start of the Covid-19 pandemic. This closure lead to a loss of many of our mouse breeders. We were not able to perform experiments or provide the best breeding for our PKD mice during this time. This loss of 3 months had an impact to severely slow our research and mouse breeding. Now a slowing of the supply chain due to the pandemic e.g. obtaining essential chemicals has slowed our research. As a result we were not successful in creating triple knockout Pkd, rictor, raptor mice.

Changes that had a significant impact on expenditures

Purchase of Ksp 1.3 Cre mice and increased number of breeding cages has increased expenses. Costs for FISP-MRI scans.

Less expenditures when lab was closed for 3 months due to Covid-19. Hence a second no cost extension was granted.

Significant changes in use or care of human subjects, vertebrate animals, biohazards, and/or select agents

None.

Significant changes in use or care of human subjects

Not applicable

Significant changes in use or care of vertebrate animals.

None

Significant changes in use of biohazards and/or select agents

None

6. **PRODUCTS:**

Publications, conference papers, and presentations
Nothing to report

Journal publications.

See Appendix.

Books or other non-periodical, one-time publications.

Nothing to report

Other publications, conference papers, and presentations. Recent abstract presentations.

Three abstracts accepted for presentation at the annual American Society of Nephrology virtual meeting from October 21-25, 2020.

1.   On behalf of the American Society of Nephrology (ASN) and the Kidney Week Education Committee, thank you for submitting an abstract for Kidney Week, which will be a fully digital meeting. We are pleased to inform you that your abstract 3444404 "Mechanisms of suppressed autophagic flux in the kidney caused by sham surgery and unilateral nephrectomy" has been selected by the Committee for an ePoster presentation.

2.   On behalf of the American Society of Nephrology (ASN) and the Kidney Week Education Committee, thank you for submitting an abstract for Kidney Week, which will be a fully digital meeting. We are pleased to inform you that your abstract **3442415 "The effect of trehalose on autophagy-related proteins and cyst**

growth in a hypomorphic Pkd1 mouse model of autosomal dominant polycystic kidney disease (ADPKD)" has been selected by the Committee for an ePoster presentation.

3.   On behalf of the American Society of Nephrology (ASN) and the Kidney Week Education Committee, thank you for submitting an abstract for Kidney Week, which will be a fully digital meeting. We are pleased to inform you that your abstract **3442374 "Suppressed autophagic flux in the heart in a hypomorphic Pkd1 mouse model of ADPKD**" has been selected by the Committee for an ePoster presentation.

Two abstracts accepted for presentation at the annual American Society of Nephrology virtual meeting from November 1-5, 2020.

1.   On behalf of the American Society of Nephrology (ASN) and the Kidney Week Education Committee, thank you for submitting an abstract for ASN Kidney Week 2021, which will be a hybrid format meeting. We are pleased to inform you that your abstract **3604788 "Autophagy inhibition ameliorates PKD"** has been selected by the Committee for poster presentation.

2.   On behalf of the American Society of Nephrology (ASN) and the Kidney Week Education Committee, thank you for submitting an abstract for ASN Kidney Week 2021, which will be a hybrid format meeting. We are pleased to inform you that your abstract **3604576 "Suppressed Autophagy Drives Increased Cellular Metabolic Activity in Human ADPKD Cells"** has been selected by the Committee for poster presentation.

4.   Website(s) or other Internet site(s)

Nothing to report (yet)
   Technologies or techniques

Nothing to report (yet)
   Inventions, patent applications, and/or licenses

Nothing to report (yet)
   Other Products

Nothing to report (yet)

7.   **PARTICIPANTS & OTHER COLLABORATING ORGANIZATIONS**

What individuals have worked on the project?

Provide the following information for: (1) PDs/PIs; and (2) each person who has worked at least one person month per year on the project during the reporting period, regardless of the source of compensation (a person month equals approximately 160 hours of effort). If information is unchanged from a previous submission, provide the name only and indicate "no change."

Example:

Name:	Charles Edelstein
Project Role:	PI
Researcher Identifier (e.g. ORCID ID):	
Nearest person month worked:	12
Contribution to Project:	Dr. Edelstein has overseen the design, performance and analysis of the studies
Funding Support:	DOD funding. VA Merit award funding.
Name:	Deepak Pokhrel
Project Role:	PRA
Researcher Identifier (e.g. ORCID ID):	
Nearest person month worked:	6
Contribution to Project:	Creation of double knockout mic, Mouse treatment studies mTORC1/2 signaling pathways General Lab Manager duties
Funding Support:	50% DOD funding. 50% VA Merit Award funding
Name:	Dan Atwood
Project Role:	PRA
Researcher Identifier (e.g.	

ORCID ID):	
Nearest person month worked:	6
Contribution to Project:	Breeding of single and double knockout mice Genotyping of mice Performing immunohistochemistry Mouse treatment studies mTORC1/2 signaling pathways
Funding Support:	50% DOD funding. 50% VA Merit Award funding
Name:	Nicole Brown
Project Role:	PRA
Researcher Identifier (e.g. ORCID ID):	
Nearest person month worked:	*4*
Contribution to Project:	*Autophagy studies. Genotyping animals, animal injections, Performing immunoblots,*
Funding Support:	50% DOD funding. 50% VA Merit Award funding
Name:	*Sara Holditch*
Project Role:	*Post-doctoral Fellow*
Researcher Identifier (e.g. ORCID ID):	
Nearest person month worked:	*12*
Contribution to Project:	*4E-BP1 studies, Creation of double knockout mice, Mouse treatment studies,*
Funding Support:	DOD funding. PKD Foundation Fellowship Award funding

Has there been a change in the active other support of the PD/PI(s) or senior/key personnel since the last reporting period?

1) VA Merit Award VA Merit Award to Charles Edelstein. BX003803-01A1. Autophagy in polycystic kidney disease. (Edelstein)   07/01/18-07/01/22.

2) Pharmaceutical Company support: **Title:** Effect of oxypurinol and L-arginine on PKD in the rat. XORTX Pharmaceuticals. PI Edelstein. 06/01/2021–06/01/2023.

Overlap: None

What other organizations were involved as partners?

Nothing to report

8. **SPECIAL REPORTING REQUIREMENTS**

COLLABORATIVE AWARDS:

Not applicable

QUAD CHARTS:

Not applicable

9. **APPENDICES:**

Copies of our most significant papers published during the reporting period of the DOD grant and related to the DOD grant are attached in the Appendix:

1. Holditch S, Brown CN, Atwood DJ, Lombardi AM, Nguyen KN, Toll HW, Hopp K, **Edelstein CL**. A study of sirolimus and an mTOR kinase inhibitor (TORKi) in a hypomorphic *Pkd1* mouse model of autosomal dominant polycystic kidney disease (ADPKD). Am J.Physiol Renal Physiol 2019 Jul 1;317(1):F187-F196

2. The consequences of increased 4E-BP1 in Polycystic kidney disease. Holditch SJ, Brown CN, Atwood D, Brown SE, Lombardi AM, Nguyen KN, Hill RC, Lanaspa M, Hopp K, Weiser-Evans M, **Edelstein CL**. Hum. Molec Genet, 2019 Dec 15;28(24):4132-4147

3. Nowak K, **Edelstein CL** Apoptosis and autophagy in PKD. Cell Signal 2019 (in press)

4. Atwood DJ, Pokhrel D, Brown CN, Holditch SJ, Bachu DM, Thorburn A, Hopp K, **Edelstein CL**. Increased mTOR and suppressed autophagic flux in the heart of a hypomorphic Pkd1 mouse model of autosomal dominant polycystic kidney disease. Cell Signal. 2020 (in press)

5. Atwood DJ, Brown DN, Holditch SJ, Pokhrel D, Thorburn A, Hopp K and **Edelstein CL**. The effect of trehalose on autophagy-related proteins and cyst growth in a hypomorphic Pkd1 mouse model of autosomal dominant polycystic kidney disease. Cell Signal. 2020 (in press).

6. Brown CN, Atwood D, Pokhrel D, Holditch SJ, Altmann C, Skrypnyk NI, Bourne J, Klawitter J, Blaine J, Faubel S, Thorburn A, **Edelstein CL**. Surgical procedures suppress autophagic flux in the kidney. Cell Death Dis. 2021 Mar 5;12(3):248. doi: 10.1038/s41419-021-03518-w.

7. **Edelstein CL**, Venkatachalam M, Dong Z. Autophagy inhibition by chloroquine and hydroxychloroquine could adversely affect AKI and other organ injury in critically ill patients with COVID-19. Kidney Int. 2020 (in press).

Other publications during the reporting period not directly related to DOD grant and not attached to Appendix.

1. Jain S, Edelstein CL, Jani A. Protection from apoptotic cell death during cold storage followed by rewarming in 13-lined ground squirrel tubular cells: the role of pro-survival factors XIAP and phosphoAkt. Transplantation 2016 Mar;100(3):538-45

2. Faubel S and Edelstein CL. Mechanisms and mediators of lung injury after acute kidney injury. Nature Rev Nephrol 2016 Jan;12(1):48-60

3. Kameswaran Ravichandran; Qian Wang; Abdullah Ozkok; Alkesh Jani; Howard Li; Zhibin He; Danica Ljubanovic; Mary Weiser-Evans; Raphael Nemenoff; Charles Edelstein. CD4 T cell knockout does not protect against kidney injury and worsens cancer." J. Mol. Med 2016 Apr;94(4):443-55

4. Abdullah Ozkok, Kameswaran Ravichandran, Qian Wang, Danica Ljubanovic and Charles L. Edelstein. NF-KB inhibition ameliorates cisplatin-induced acute kidney injury. Toxicol. Lett 2016 Jan 5;240(1):105-13

5. Klionsky D, Edelstein CL et al (multiple authors) . Gudelines for the use and monitoring of assays for measuring autophagy. Autophagy 2016 Jan 2;12(1):1-222.

6. Schmidt ED, Overdier LH, Dun X, Yang Y, Ammons LA, Holler T D, Sulfite M, Yu U, Chen Y, Yang S, Burley CC, Edelstein CL, Douglas I, Linhardt R. Urinary glycosaminoglycans predict outcomes in septic shock and ARDS. Am J Resp Crit Care Med 2016 Aug 5;194(4):439-49

7. Gist KM, Kaufman J, da Cruz EM, Friesen RH, Crumback SL, Linders M, Edelstein C, Altmann C, Palmer C, Jalal D, Faubel S.A Decline in Intraoperative Renal Near-Infrared Spectroscopy Is Associated With Adverse Outcomes in Children Following Cardiac Surgery. Pediatr Crit Care Med. 2016 Feb 24. [Epub ahead of print]

8. Zhao B, Lu Q, Cheng Y, Belcher JM, Siew ED, Leaf DE, Body SC, Fox AA, Waikar SW, Collard CD, Thiessen-Philbrook H, Ikizler TA, Ware LB, Edelstein CL, Garg AX, Choi M, Schaub JA, Zhao H, Lifton RP, Parikh CR; TRIBE-AKI Consortium. A Genome-Wide Association Study to Identify Single Nucleotide Polymorphisms for Acute Kidney Injury. Am J Respir Crit Care Med. 2016 Aug 30

9. de Fontnouvelle CA, Greenberg JH, Thiessen-Philbrook HR, Zappitelli M, Roth J, Kerr KF, Devarajan P, Shlipak M, Coca S, Parikh CR; TRIBE-AKI Consortium. Interleukin-8 and Tumor Necrosis Factor Predict Acute Kidney Injury After Pediatric Cardiac Surgery. Ann Thorac Surg. 2017 Dec;104(6):2072-2079.

10. Belley-Côté EP, Parikh CR, Shortt CR, Coca SG, Garg AX, Eikelboom JW, Kavsak P, McArthur E, Thiessen-Philbrook H, Whitlock RP; TRIBE-AKI Consortium. Association of cardiac biomarkers with acute kidney injury after cardiac surgery: A multicenter cohort study. J Thorac Cardiovasc Surg. 2016 Jul;152(1):245-251.

11. Torres VE, Chapman AB, Devuyst O, Gansevoort RT, Perrone RD, Koch G, Ouyang J, McQuade RD, Blais JD, Czerwiec FS, Sergeyeva O; REPRISE Trial Investigators. Tolvaptan in Later-Stage Autosomal Dominant Polycystic Kidney Disease. N Engl J Med. 2017 Nov 16;377(20):1930-1942

12. Ravichandran K, Holditch S, Brown CN, Wang Q, Ozkok A, Weiser-Evans MC, Nemenoff RA, Miyazaki M, Thiessen-Philbrook H, Parikh CR, Ljubanovic D, Edelstein CL. IL-33 deficiency slows cancer growth but does not protect against cisplatin-induced AKI in mice with cancer. Am J Physiol Renal Physiol. 2018 Mar 1;314(3):F356-F366

13. Scott Davis, Jane Gralla, Larry Chan, Alex Wiseman, Charles L. Edelstein. The Effect of Sirolimus on Native Total Kidney Volume After Transplantation in Patients with Autosomal Dominant Polycystic Kidney Disease: A Randomized Controlled Pilot Study. Transpl. Proc (in press) 2018

14. Benjamin M Fox, Hyo-Wook Gil, Benjamin Griffin, Anna Jovanovich, Lara Kirkbride-Romeo, Danielle E. Soranno, Katja Gist Julie R Haines, Matthew Wither Angelo D'Alessandro, Timothy McKinsey, Charles L Edelstein, Sara Wennersten, Nathan Clendenen, Rushita A. Bagchi, Christopher Altmann, Sarah Faubel.

Metabolomics assessment reveals oxidative stress and altered energy production in the heart after ischemic acute kidney injury in mice. Kidney International 2019 Mar;95(3):590-610

15. Lee DW, Kim JS, Kim IY, Kim HS, Kim JY, Rhee H, Seong EY, Song SH, Lee SB, Edelstein CL, Kwak IS. Catheter-based renal sympathetic denervation induces acute renal inflammation through activation of caspase-1 and NLRP3 inflammasome. Anatol J Cardiol. 2019 Mar;21(3):134-141

16. Griffin BR, Faubel S, Edelstein CL. Biomarkers of drug-induced kidney toxicity. Ther Drug Monit. 2018 Dec 10

17. Holditch SJ,. Brown CN,. Lombardi AM, Nguyen KN, Edelstein CL. Recent Advances in Models, Mechanisms, Biomarkers, and Interventions in Cisplatin-Induced Acute Kidney Injury. Int. J. Mol. Sci. 2019 Jun 20;20(12).

18. Brown CN, Atwood DJ, Pokhrel D, Ravichandran K, Holditch SJ, Saxena S, Miyazaki M, Nemenoff R, Weiser-Evans MCM, Ljubanovic DG, Joy MS, Edelstein CL. The effect of MEK1/2 inhibitors on cisplatin-induced acute kidney injury (AKI) and cancer growth in mice. Cell Signal. 2020 (in press).

19. Skrypnyk NI, Gist KM, Okamura K, Montford JR, You Z, Yang H, Moldovan R, Bodoni E, Blaine JT, Edelstein CL, Soranno DE, Kirkbride-Romeo LA, Griffin BR, Altmann C, Faubel S.IL-6-mediated hepatocyte production is the primary source of plasma and urine neutrophil gelatinase-associated lipocalin during acute kidney injury. Kidney Int. 2020 May;97(5):966-979

20. Klionsky DL, Edelstein CL et al (Multiple authors). Guidelines for the use and interpretation of assays for monitoring autophagy (4th edition)2021 Jan;17(1):1-382. Autophagy Epub 2021 Feb 8.

RESEARCH ARTICLE

A study of sirolimus and mTOR kinase inhibitor in a hypomorphic *Pkd1* mouse model of autosomal dominant polycystic kidney disease

Sara J. Holditch,* Carolyn N. Brown,* Daniel J. Atwood, Andrew M. Lombardi, Khoa N. Nguyen, Harrison W. Toll, Katharina Hopp, and Charles L. Edelstein

Division of Renal Diseases and Hypertension, University of Colorado at Denver, Aurora, Colorado

Submitted 4 February 2019; accepted in final form 29 April 2019

Holditch SJ, Brown CN, Atwood DJ, Lombardi AM, Nguyen KN, Toll HW, Hopp K, Edelstein CL. A study of sirolimus and mTOR kinase inhibitor in a hypomorphic *Pkd1* mouse model of autosomal dominant polycystic kidney disease. *Am J Physiol Renal Physiol* 317: F187–F196, 2019. First published May 1, 2019; doi: 10.1152/ajprenal.00051.2019.—Autosomal dominant polycystic kidney disease (PKD) is characterized by cyst formation and growth, which are partially driven by abnormal proliferation of tubular cells. Proproliferative mechanistic target of rapamycin (mTOR) complexes 1 and 2 (mTORC1 and mTORC2) are activated in the kidneys of mice with PKD. Sirolimus indirectly inhibits mTORC1. Novel mTOR kinase inhibitors directly inhibit mTOR kinase, resulting in the inhibition of mTORC1 and mTORC2. The aim of the present study was to determine the effects of sirolimus versus the mTOR kinase inhibitor torin2 on cyst growth and kidney function in the *Pkd1* p.R3277C (*Pkd1*$^{RC/RC}$) mouse model, a hypomorphic *Pkd1* model orthologous to the human condition, and to determine the effects of sirolimus versus torin2 on mTORC1 and mTORC2 signaling in *PKD1*$^{-/-}$ cells and in the kidneys of *Pkd1*$^{RC/RC}$ mice. In vitro, both inhibitors reduced mTORC1 and mTORC2 phosphorylated substrates and negatively impacted cellular metabolic activity, as measured by MTT assay. *Pkd1*$^{RC/RC}$ mice were treated with sirolimus or torin2 from 50 to 120 days of age. Torin2 was as effective as sirolimus in decreasing cyst growth and improving loss of kidney function. Both sirolimus and torin2 decreased phosphorylated S6 protein, phosphorylated eukaryotic translation initiation factor 4E-binding protein 1, phosphorylated Akt, and proliferation in *Pkd1*$^{RC/RC}$ kidneys. In conclusion, torin2 and sirolimus were equally effective in decreasing cyst burden and improving kidney function and mediated comparable effects on mTORC1 and mTORC2 signaling and proliferation in the *Pkd1*$^{RC/RC}$ kidney.

apoptosis; autosomal dominant polycystic kidney disease; polycystic; proliferation; sirolimus; torin2

INTRODUCTION

Autosomal dominant polycystic kidney disease (ADPKD) is one of the most common life-threatening hereditary disorders (59). In ADPKD, a mutation in the *PKD1* gene (in ~75–77% of cases) results in the slow development of kidney cysts, causing chronic kidney disease requiring dialysis or kidney transplantation, usually in the sixth decade of life (59). In a preclinical study (57) and subsequent human studies (55, 56), the drug tolvaptan was effective in slowing cyst growth and improving kidney function, resulting in United States Food and Drug Administration approval for the treatment of ADPKD (57). The development of tolvaptan as a treatment for ADPKD highlights the importance of preclinical studies for drug development for ADPKD.

Mechanistic target of rapamycin (mTOR) exists in two distinct structural and functional complexes: mTORC1 and mTORC2. mTORC1 downstream signaling is mainly via the proproliferative S6 ribosomal protein (S6) and eukaryotic translation initiation factor 4E (eIF4E)-binding protein 1 (4E-BP1) pathways. The mTORC2 protein complex associates with rapamycin-independent companion of mTOR (Rictor). mTORC2 signaling is mainly propagated via phosphorylation of Akt at Ser^{473}.

In two large randomized human studies, the effect of the rapamycin analogs (rapalogs) sirolimus and everolimus (indirect mTORC1 inhibitors) on polycystic kidney disease (PKD) was disappointing (45, 58). Apart from dose limitations due to toxicity and inconsistent timing or duration of rapalog treatment, rapalogs may not impact major downstream proproliferative substrates of mTORC1, such as the translational repressor 4E-BP1. Sirolimus does not usually directly target 4E-BP1 (16, 47); instead, sirolimus is only a partial inhibitor of mTORC1 in most cell types (16, 47, 53, 54), and phosphorylation of 4E-BP1 is usually sirolimus resistant at Thr^{46} (30). Another possible reason for the disappointing effect of rapalogs in human studies is that rapalogs do not directly target mTORC2 or its downstream substrates (16, 47).

Second-generation mTOR inhibitors, mTOR kinase inhibitors (TORKi), inhibit both mTORC1, especially 4E-BP1 (34), and mTORC2. Studies have shown 4E-BP1 phosphorylation sensitivity to TORKi (8, 52). We have previously shown that an active site TORKi, PP242, decreases PKD and improves kidney function in the Han:SPRD (Cy/+) rat model of ADPKD (38). We have also previously shown that a mTOR antisense oligonucleotide that targets both mTORC1 and mTORC2 decreases PKD and improves kidney function in the *Pkd2*$^{-/-}$ mouse (37). However, in PKD, it is unknown whether there is aberrant phosphorylation of 4E-BP1 or whether phosphorylated 4E-BP1 (pE4-BP1) species (Thr^{70}, Thr$^{37/46}$, and Ser^{65}) are sensitive to TORKi. Also, the effect of an active site TORKi has not been directly compared with the mTOR allosteric inhibitor sirolimus in PKD.

We hypothesized that a TORKi would inhibit proproliferative mTORC1 downstream substrates, such as 4E-BP1, and mTORC2, to a greater degree than the allosteric mTORC1

* S. J. Holditch and C. N. Brown contributed equally to this work.

Address for reprint requests and other correspondence: C. L. Edelstein, Div. of Renal Diseases and Hypertension, Univ. of Colorado at Denver, Box C281, 12700 E. 19th Ave., Aurora, CO 80045 (e-mail: Charles.edelstein@ucdenver. edu).

inhibitor sirolimus. Furthermore, we hypothesized that a TORKi would be as effective as, or more effective than, sirolimus in ameliorating PKD in a hypomorphic $Pkd1^{RC/RC}$ mouse model orthologous to the human disease. The aims of the study were to characterize mTORC1 and mTORC2 signaling in $PKD1^{-/-}$ cells in vitro and $Pkd1^{RC/RC}$ mice in vivo in response to sirolimus or treatment with a TORKi. This preclinical study of a TORKi in PKD may offer insights into performing future clinical studies in PKD.

METHODS

In vitro model. Human primary cells from the normal renal cortical tubular epithelium (RCTE; $PKD1^{+/+}$) and ADPKD cyst-lining epithelium [$PKD1^{-/-}$ (WT 9-12 cell line)] immortalized with ori-adenosimian virus 40, as previously described (31), were used. $PKD1^{-/-}$ cells have increased proliferation (1) and a delayed proliferative response to antiproliferative agents (49), making them a translational in vitro PKD model to study the relationship between mTOR and proliferation. Cells were cultured as previously described (31). Doses of sirolimus (1, 10, 100, and 1,000 nM) and torin2 (1, 10, 100, and 1,000 nM) were increased over a 1-h period in 10-cm^2 plates. Briefly, cells were plated 18 h in advance. Once plates had reached 80% confluence, cells were exposed to escalating doses of sirolimus or torin2. After 1 h, protein was isolated from cell lysates and immunoblotted for mTORC1 and mTORC2 substrates.

Metabolic activity was assayed using MTT according to the manufacturer's instructions. Briefly, 5,000 cells were plated per well in a 96-well plate, allowed to adhere for 5 h, exposed to sirolimus (10 nM) or torin2 (100 nM) for 2 h, and then assayed for MTT reduction. Actively respiring cells convert water-soluble MTT to insoluble purple formazan. The formazan concentration was determined by optical density measured at 590 nm.

In vivo model. $Pkd1^{RC/RC}$ mice have a hypomorphic $Pkd1$ gene mutation orthologous to that of PKD patient disease variant $PKD1$ p. R3277C ($Pkd1^{RC/RC}$) (22). $Pkd1^{RC/RC}$ mice in the C57BL/6 background have cysts at 3 mo of age (21, 24). Cyst expansion and size correlate with increased tubular cell proliferation (22). Wild-type C57BL/6J mice (stock no. 000664) were purchased from Jackson Laboratories (Bar Harbor, ME). All experiments were conducted with adherence to the National Institutes of Health *Guide for the Care and Use of Laboratory Animals.* The animal protocol was approved by the Animal Care and Use Committee of the University of Colorado at Denver. Mice were maintained on a standard diet under standard pathogen-free housing conditions, with food and water freely available.

Experimental in vivo protocol. Male and female C57BL/6 $Pkd1^{RC/RC}$ mice were treated with torin2 (10 mg/kg ip, daily on weekdays), sirolimus (0.5 mg/kg ip, daily on weekdays), or vehicle (28% DMSO in polyethylene glycol 300) from 50 to 120 days of age. There were equal numbers of male and female mice per group. PKD does not differ significantly between male and female C57BL/6 $Pkd1^{RC/RC}$ mice (24). Sirolimus was obtained from Sigma-Aldrich (St. Louis, MO). Torin2 was a gift from the developer of the compound, Dr. Nathanael Gray (Dana Farber Cancer Institute, Harvard Medical School, Boston, MA).

Dosage of sirolimus and torin2. In our previous study (61), $Pkd2^{-/-}$ mice treated with sirolimus (0.5 mg·kg^{-1}·day^{-1}) had a trough blood level of 20–22 ng/ml and a 51% decrease in the cyst index. Higher doses of sirolimus (5 mg·kg^{-1}·day^{-1}) resulted in a similar decrease in the cyst index in $Pkd1^{-/-}$ mice (46). The therapeutic blood level of sirolimus in humans is 5–15 ng/ml. In view of the sirolimus trough levels of 20–22 ng/ml with the 0.5 mg·kg^{-1}·day^{-1} treatment, it is unlikely that a higher dose of sirolimus would mediate a more therapeutic effect on PKD.

In addition, a dose experiment was performed for sirolimus and torin2 in male C57BL/6 mice at 70 days of age (see Supplemental Fig. S2; all Supplemental Data for this article can be found at https://doi.org/10.6084/m9.figshare.7949153.v1). Mice were treated with vehicle (28% DMSO in polyethylene glycol 300), sirolimus (0.1, 0.5, or 1 mg/kg), or torin2 (0.1, 1, or 10 mg/kg) on the day before they were euthanized. After 24 h, mice received a second dose of the indicated treatment and were euthanized within 1 h. Kidney tissue was analyzed for mTORC1 and mTORC2 substrates. A 0.5 mg·kg^{-1}·day^{-1} dose of sirolimus was used for long-term treatment based on the virtually complete inhibition of the mTORC1 substrate phosphorylated S6 (pS6) by sirolimus at 0.5 mg·kg^{-1}·day^{-1} (Supplemental Fig. S2A). A 10 mg·kg^{-1}·day^{-1} dose of torin2 was chosen for long-term treatment based on the virtually complete inhibition of mTORC1 and mTORC2 substrates: pS6, p4E-BP1 (Thr$^{37/46}$), and phosphorylated Akt (pAkt) (Supplemental Fig. S2B).

Measurement of kidney function. Blood urea nitrogen was measured with a urea assay kit (BioAssay Systems, Hayward, CA) according to the manufacturer's instructions (DIUR-100). Serum creatinine was measured by HPLC-tandem mass spectrometry. $^2H_3$ and creatinine were detected in multiple reaction-monitoring mode, examining transitions of m/z from 114 to 44.2 and from 117 to 47.2, respectively.

Immunoblot analysis. Protein was isolated from cells and tissues using RIPA buffer and cOmplete protease and phoSTOP phosphatase inhibitor cocktails (Sigma). Homogenates were centrifuged, and the supernatant was obtained for protein quantification by DC protein assay (Bio-Rad, Hercules, CA) according to the manufacturer's instructions. Samples were mixed with Laemmli sample buffer, boiled for 5 min, and run on 4–20% precast polyacrylamide gels. Proteins were then transferred to 0.45-µm PVDF membranes, blocked with 2.5% evaporated milk, and probed with the antibodies provided in Supplemental Table S1. The specificity of each of the antibodies has been validated by the vendor (Cell Signaling Technology, Danvers, MA) and cited in previous publications (4, 6, 12, 18, 37, 38, 61). Blots were developed by chemiluminescence and analyzed for densitometry using ImageJ.

Routine histology. Tissues were fixed overnight in 10% formalin at 4°C, transferred to fresh 70% ethanol, and left overnight at 4°C; this process was carried out a total of three times. Next, the tissues were processed and embedded in paraffin wax using Leica systems. Tissues were sectioned at 4 µm and baked at 60°C for 2 h. Kidneys were stained with hematoxylin and eosin, and the cystic index and number of cysts were quantified on 2 sections/mouse (left and right kidneys) using the NIS-Elements macro, as previously described (24). The cyst index and number of cysts were expressed as percentages of the cross-sectional area and numbers per cross-sectional area, respectively. Areas with tissue tears and bubbles that were identified with higher magnification (×40) were excluded from analysis.

Immunohistochemistry protocol. After tissue sections were deparaffinized and rehydrated, antigen unmasking was performed in sodium citrate buffer (pH 6.0) for 25 min at 100°C. Sections were rinsed for 10 min in cold tap water, immersed in 3% hydrogen peroxide for 10 min, and then rinsed in deionized water for 5 min to block endogenous peroxidase activity. Blocking was performed using Vectastain Elite ABC kit blocking serum for 30 min at room temperature. Primary antibodies were diluted in Tris-buffered saline with Tween 20, as described in Supplemental Table S1, and incubated overnight at 4°C in a humidified chamber. Immunoreactions were detected using the Vectastain standard protocol with 3,3′-diaminobenzidine tetrahydrochloride hydrate (DAB) counterstained with hematoxylin. Slides were subsequently dipped one to three times in 0.3% acid alcohol, dehydrated, and mounted. DAB-positive staining was analyzed using macros provided by Aperio ImageScope.

TUNEL protocol. TUNEL was performed on tissue sections using a DeadEnd colorimetric apoptosis detection system kit (Promega) according to the manufacturer's instructions.

Quantitation of immunohistochemistry staining. The number of positive-staining cells was counted using the Aperio ImageScope (Leica Biosystems) by an observer blinded to the treatment modality. Noncystic tubules were defined as <50-μm-diameter tubules; 15–20 fields of view (×40 magnification) devoid of cysts in the cortex per sample were randomly selected for noncystic quantitation. To avoid sensitivity and selection artifacts between noncystic and dilated, possibly precystic, tubules as well as potential changes in the tubular epithelium lining massive cysts, positive staining was counted in ~75- to 200-μm-diameter cysts. Fifty to seventy-five cortical cysts per tissue section were randomly selected for histological analysis.

Statistical analysis. Values are means ± SE. Data sets were analyzed by a nonparametric unpaired Mann-Whitney test. Multiple group comparisons were performed using ANOVA with a Newman-Keuls post test. Single group comparisons were made using a Student's *t*-test. *P* values of <0.05 were considered statistically significant.

RESULTS

Dose response of sirolimus versus torin2 on mTORC1 and mTORC2 in vitro. $PKD1^{-/-}$ (WT 9-12) cells were treated with logarithmic doses of sirolimus and torin2, resulting in a marked decrease in phosphorylation of mTORC1 and mTORC2 substrates (Supplemental Fig. S1). Sirolimus at 10, 100, and 1,000 nM decreased pS6 and p4E-BP1 (Thr$^{37/46}$) and had no effect on pAkt (Ser^{473}) in $PKD1^{-/-}$ cells (Supplemental Fig. S1*A*). Torin2 at 1, 10, 100, and 1,000 nM significantly decreased pS6. Phosphorylation of 4E-BP1 (Thr$^{37/46}$) was nearly eliminated at 10, 100, and 1,000 nM torin2; however, because of decreased total 4E-BP1 abundance, only 10 nM torin2 trended in the decreased p4E-BP1-to-total 4E-BP1 ratio (*P* = 0.05; Supplemental Fig. S1). The ratio of pAkt (Ser^{473}) to total Akt in $PKD1^{-/-}$ cells was decreased with 100 nM torin2 (Supplemental Fig. S1). Based on the dose escalation, a dose of sirolimus mediating mTORC1 inhibition (10 nM) and a dose of torin2 mediating inhibition of both mTORC1 and mTORC2 (100 nM) were chosen for further study in $PKD1^{+/+}$ and $PKD1^{-/-}$ cells.

Decreased phosphorylation of mTORC1 and mTORC2 substrates as well as decreased metabolic activity in vitro with sirolimus and torin2 treatment. Binding of 4E-BP1 to the translation initiator eIF4E is reversible (18). Hypophosphorylated 4E-BP1 binds avidly to eIF4E; 4E-BP1 hyperphosphorylation retards this interaction. mTOR signaling is the major factor in release of 4E-BP1 from eIF4E (18) and, thus, promotes translation and proliferation. Therefore, we characterized three phosphorylated isoforms of 4E-BP1 most associated with the initial phospho-priming (18) and subsequent release of eIF4E (17), namely, Thr$^{37/46}$, Thr^{70}, and Ser^{65}, in $PKD1^{+/+}$ (RCTE) and $PKD1^{-/-}$ (WT 9-12) cells exposed to sirolimus and torin2. Relative to total 4E-BP1 abundance, the Thr$^{37/46}$ and Ser^{65} phosphorylated isoforms were elevated uniquely in $PKD1^{-/-}$ compared with $PKD1^{+/+}$ cells. Sirolimus resulted in a significant decrease in p4E-BP1 (Ser^{65} and Thr$^{37/46}$) in $PKD1^{-/-}$ cells (Fig. 1*A*). Similarly, torin2 resulted in a significant decrease in p4E-BP1 (Ser^{65} and Thr$^{37/46}$) in $PKD1^{-/-}$ cells (Fig. 1*A*). Sirolimus decreased the mTORC2 substrate Akt in $PKD1^{+/+}$ cells but increased the ratio of pAkt to total Akt (Fig. 1*A*). In this regard, sirolimus-dependent inhibition of mTORC1 has been shown to increase phosphorylation of Akt (Ser^{473}) (27, 36). Sirolimus significantly decreased phosphorylation of Akt (Ser^{473}) in $PKD1^{-/-}$ cells (Fig. 1*A*). Finally, we assessed any possible suppressive metabolic effect of sirolimus

and torin2 in $PKD1^{-/-}$ (WT 9-12) and $PKD1^{+/+}$ (RCTE) cells by MTT assay (10, 48). $PKD1^{-/-}$ cells exhibited significantly higher metabolic activity than $PKD1^{+/+}$ cells (Fig. 1*B*). Both sirolimus and torin2 decreased metabolic activity, as detected by MTT assay of $PKD1^{-/-}$ cells (Fig. 1*B*). Sirolimus inhibited phosphorylation of 4E-BP1 (Thr$^{37/46}$ and Ser^{65}) and phosphorylation of Akt (Ser^{473}), a marker of mTORC2 activation, in $PKD1^{-/-}$ cells (Fig. 1*A*). From these data, we hypothesized that sirolimus and torin2 may exhibit anticystic effects in vivo, mediated through a combination of suppression of both mTORC1 and mTORC2 signaling and a decrease in metabolic activity in cystic renal epithelial cells.

Both sirolimus and torin2 decreased cyst burden and protected kidney function in Pkd1$^{RC/RC}$ mice. At 50 days of age, mice were treated with vehicle, sirolimus (0.5 mg·kg^{-1}·day^{-1}), or torin2 (10 mg·kg^{-1}·day^{-1}) for 70 weekdays. No side effects of treatment were noted on gross examination in either treatment group. Both sirolimus and torin2 resulted in a significant decrease in the kidney weight-to-body weight ratio (Fig. 2*A*), a significant improvement in kidney function, as measured by serum blood urea nitrogen and creatinine (Fig. 2, *B* and *C*), and a significant decrease in the cyst index (Fig. 2*D*), with no significant difference in efficacy between the two treatment approaches. Although the number of cysts was decreased, there was no significant reduction in the total number of cysts in PKD kidneys (Fig. 2*E*). Representative hematoxylin and eosin-stained sections showed less cystic area in both sirolimus- and torin2-treated mice (Fig. 2*F*). Thus, both sirolimus and torin2 resulted in an equivalent decrease in cyst burden and improvement of kidney function in Pkd1$^{RC/RC}$ mice, with no side effects on gross examination.

Both sirolimus and torin2 decreased proliferation and increased apoptosis in Pkd1$^{RC/RC}$ kidneys. Proliferating cell nuclear antigen (PCNA) staining, a marker of proliferation, and TUNEL staining, a marker of apoptosis, were measured in noncystic cortical renal tubules and in the cyst-lining epithelium of PKD kidneys. PCNA staining in noncystic tubules was modestly increased in PKD compared with wild-type kidneys (Fig. 3*A*). Sirolimus, but not torin2, resulted in a significant decrease in PCNA-positive nuclei in noncystic areas of PKD kidneys (Fig. 3*A*). The increase in TUNEL staining in noncystic tubules in PKD kidneys compared with wild-type control kidneys did not reach statistical significance (Fig. 3*A*). In the cystic epithelium of PKD kidneys, torin2 resulted in a significant decrease in PCNA-positive nuclei compared with vehicle and sirolimus (Fig. 3*B*). In cells lining the cysts, torin2 significantly increased apoptosis (TUNEL staining) compared with vehicle (Fig. 3*B*).

Both sirolimus and torin2 decreased mTORC1 and mTORC2 phosphorylated substrates in Pkd1$^{RC/RC}$ kidneys. Increased mTOR substrates 4E-BP1 and S6 have been associated with worsening prognosis in oncology. For example, high 4E-BP1 and S6 protein levels predict reduced benefit from treatment, poor prognosis, and endocrine resistance in breast cancer (23). For this reason, we performed immunohistochemical analysis of noncystic tubules in PKD kidneys and cells lining the cysts for p4E-BP1 isoforms and pS6. There was an increase in pS6 and p4E-BP1 (Thr$^{37/46}$ and Thr^{70}) staining in noncystic areas of PKD compared with wild-type kidneys and in cells lining kidney cysts (Fig. 4, *A* and *B*). The increase in pS6 and p4E-BP1 (Thr$^{37/46}$ and Thr^{70})
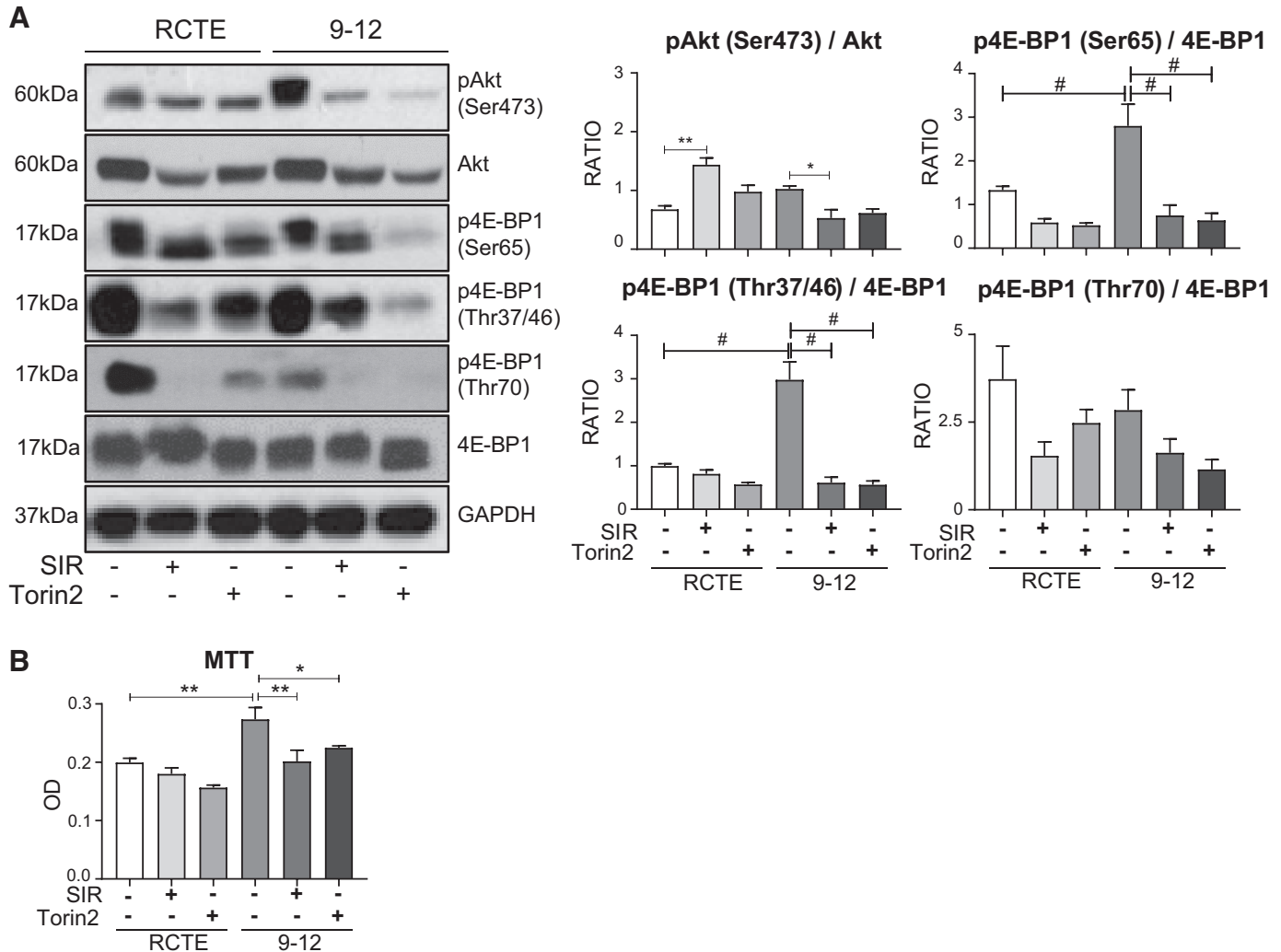
Fig. 1. Effect of sirolimus (SIR) versus torin2 on mechanistic target of rapamycin complex (mTORC)1 [phosphorylated eukaryotic translation initiation factor 4E-binding protein 1 (p4E-BP1)] and mTORC2 [phosphorylated Akt (pAkt) (Ser473)] in $PKD1^{-/-}$ cells. *A*: $PKD1^{+/+}$ [renal cortical tubular epithelium (RCTE)] and $PKD1^{-/-}$ (WT 9-12) cells were treated with sirolimus (10 nM) or torin2 (100 nM), and the effect on substrates of mTORC1 signaling [p4E-BP1 (Ser[65], Thr[37/46], and Thr[70])] and mTORC2 [pAkt (Ser[473])] was determined by immunoblot analysis. Values of the ratio of total to phosphorylated protein abundance are means ± SE; *n* = 3 per group in triplicate. *B*: MTT assay of $PKD1^{+/+}$ and $PKD1^{-/-}$ cells treated with sirolimus or torin2. OD, optical density (590 nm). Values are means ± SE; *n* = 4 per group, in triplicate. *$P < 0.05$, **$P < 0.01$, and #$P < 0.0001$ (by ANOVA with a Newman-Keuls post test).

staining in noncystic areas of PKD kidneys was decreased by both sirolimus and torin2 (Fig. 4*A*). There was an increase in p4E-BP1 (Ser[65]) staining in noncystic areas of PKD kidneys compared with wild-type control kidneys (*P* = 0.05). Staining of p4E-BP1 (Thr[37/46], Ser[65], and Thr[70]) in cells lining kidney cysts was not significantly affected by sirolimus or torin2 (Fig. 4*B*). Finally, immunoblot analysis of whole kidney homogenates revealed that pAkt (Ser[473]) was significantly increased in PKD compared with wild-type kidneys and significantly decreased in PKD kidneys treated with both sirolimus and torin2 (Fig. 4*C*). These data show, for the first time, that staining of p4E-BP1 (Thr[37/46], Ser[65], and Thr[70]) was increased in noncystic tubules in PKD kidneys and present in cells lining the cysts and was sensitive to mTORC1 and mTORC2 inhibition in vivo.

DISCUSSION

mTORC1 is associated with cell proliferation and protein synthesis via phosphoregulation of the downstream substrates

phosphorylated 70-kDa S6 kinase (and, in turn, S6) and 4E-BP1. 4E-BP1 has three main phosphorylated isoforms (18) resulting in increased translation and proliferation. Sirolimus is only a partial inhibitor of mTORC1 in most cell types (16, 47, 53, 54), and phosphorylation of 4E-BP1, especially in cancer studies, has been shown to be sirolimus resistant but sensitive to TORKi (8, 52). mTORC2 directly phosphorylates Akt at Ser[473], and a reduction in Rictor expression inhibits phosphorylation of Akt (Ser[473]). Phosphoregulation of Akt (Ser[473]) plays a crucial role in proliferation, cell survival, and growth. Both mTORC1 and mTORC2 contain a mTOR kinase that is inhibited by TORKi. Torin2 is a second-generation ATP-competitive active site inhibitor that is both potent and highly selective for mTOR kinase, exhibiting a superior pharmacokinetic profile compared with previous TORKi (63). In support of the use of combined mTORC1 and mTORC2 inhibition in PKD, our previously published data demonstrated that a mTOR antisense oligonucleotide blocks both mTORC1 and mTORC2 decreases in cyst burden and improves kidney func-
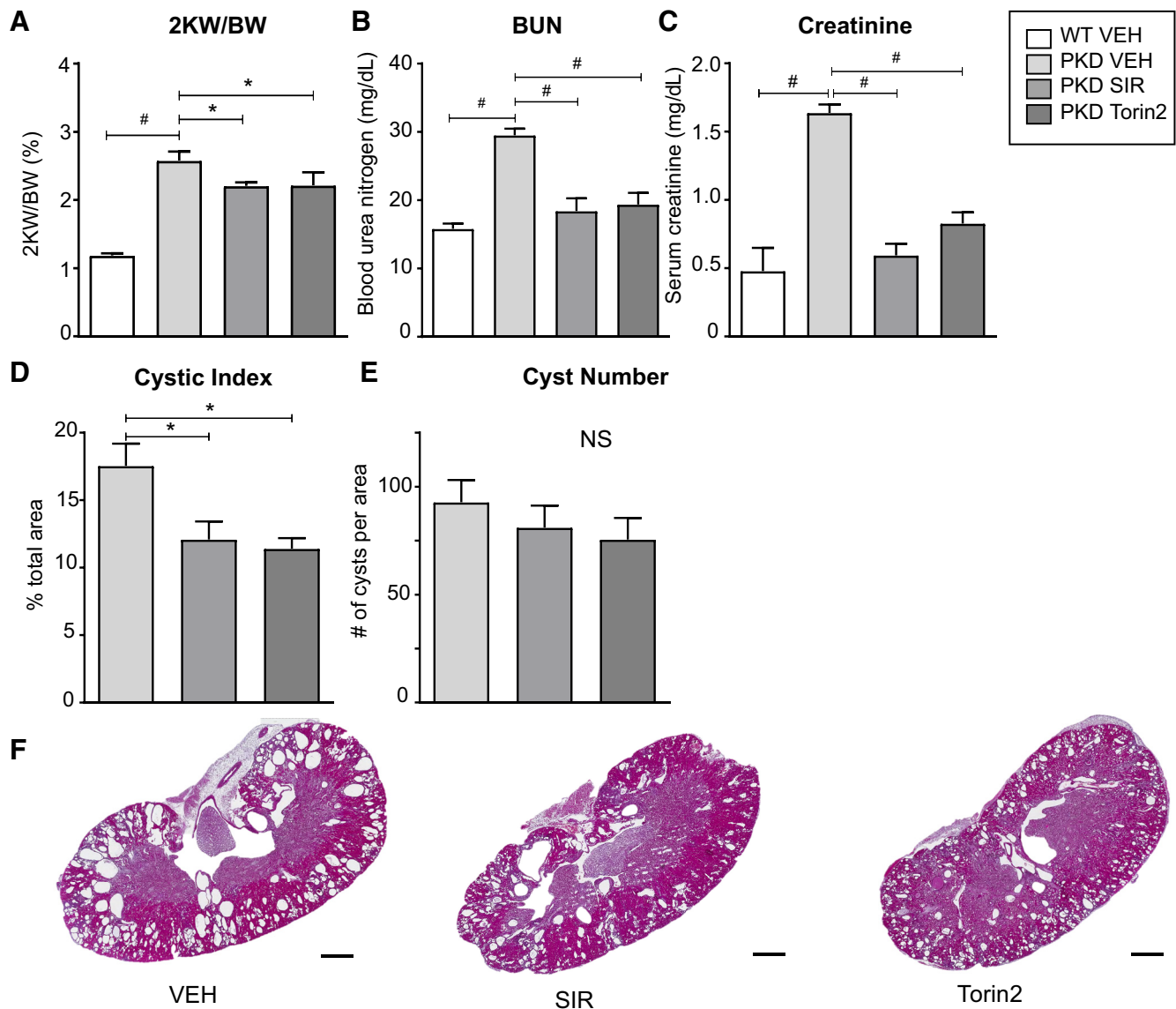
Fig. 2. Effect of sirolimus (SIR) versus torin2 on cyst burden and kidney function in $Pkd1^{RC/RC}$ mice. *A*: 2-kidney weight-to-body weight ratio (2KW/BW) in wild-type (WT) versus $Pkd1^{RC/RC}$ (PKD) mice treated with vehicle (VEH), torin2, or sirolimus. *B*: blood urea nitrogen (BUN). *C*: serum creatinine. *D*: cystic index (percentage of cross-sectional area). *E*: cyst number (per cross-sectional area). Values are means ± SE; $n = 4–5$ per group. *$P < 0.05$ and #$P < 0.0001$ (by ANOVA with a Newman-Keuls post test). NS, not significant. *F*: representative hematoxylin and eosin-stained sections. Scale bar = 1 mm.

tion in $Pkd2^{-/-}$ mice (37). Whether p4E-BP1 and pAkt (Ser[473]) are resistant to sirolimus in kidney cells and in the kidney is not known. Also, the effects of a TORKi versus sirolimus on p4E-BP1 isoforms and pAkt (Ser[473]) in kidney cells and in the kidney are not known. The major aims of the present study were to determine the effect of sirolimus versus a TORKi on cyst burden and kidney function and to characterize mTORC1 and mTORC2 signaling in in vitro and in vivo $Pkd1$ models.

First, mTORC1 and mTORC2 signaling and the effect of mTOR inhibition were determined in immortalized human cells from the normal RCTE and ADPKD cyst-lining epithelium (31). Metabolism was increased in $PKD1^{-/-}$ compared with $PKD1^{+/+}$ cells, as determined by the MTT assay. Recent studies have shown that defective glucose metabolism might be a hallmark of ADPKD, offering a new

opportunity for therapy. Metabolomic profiling using nuclear magnetic resonance of the extracellular medium of wild-type and $Pkd1^{-/-}$ cells revealed that $Pkd1^{-/-}$ cells consume high levels of glucose and preferentially use it in aerobic glycolysis for energy production (40). These data demonstrating that $Pkd1^{-/-}$ cells consume high levels of glucose and preferentially use it in aerobic glycolysis are in line with an upregulation of mTORC1 in ADPKD, as this complex regulates transcriptional programs involved in energy metabolism (33, 43). mTORC1 inhibition with sirolimus benefits glucose metabolism in five mouse models of type 2 diabetes (39), reducing weight gain, improving insulin sensitivity, and reducing hyperinsulinemia. The literature is lacking as to the glucose metabolic effects of a TORKi in diabetes or ADPKD. Thus, in wild-type and $PKD1^{-/-}$ cells, we compared the effects of sirolimus and a
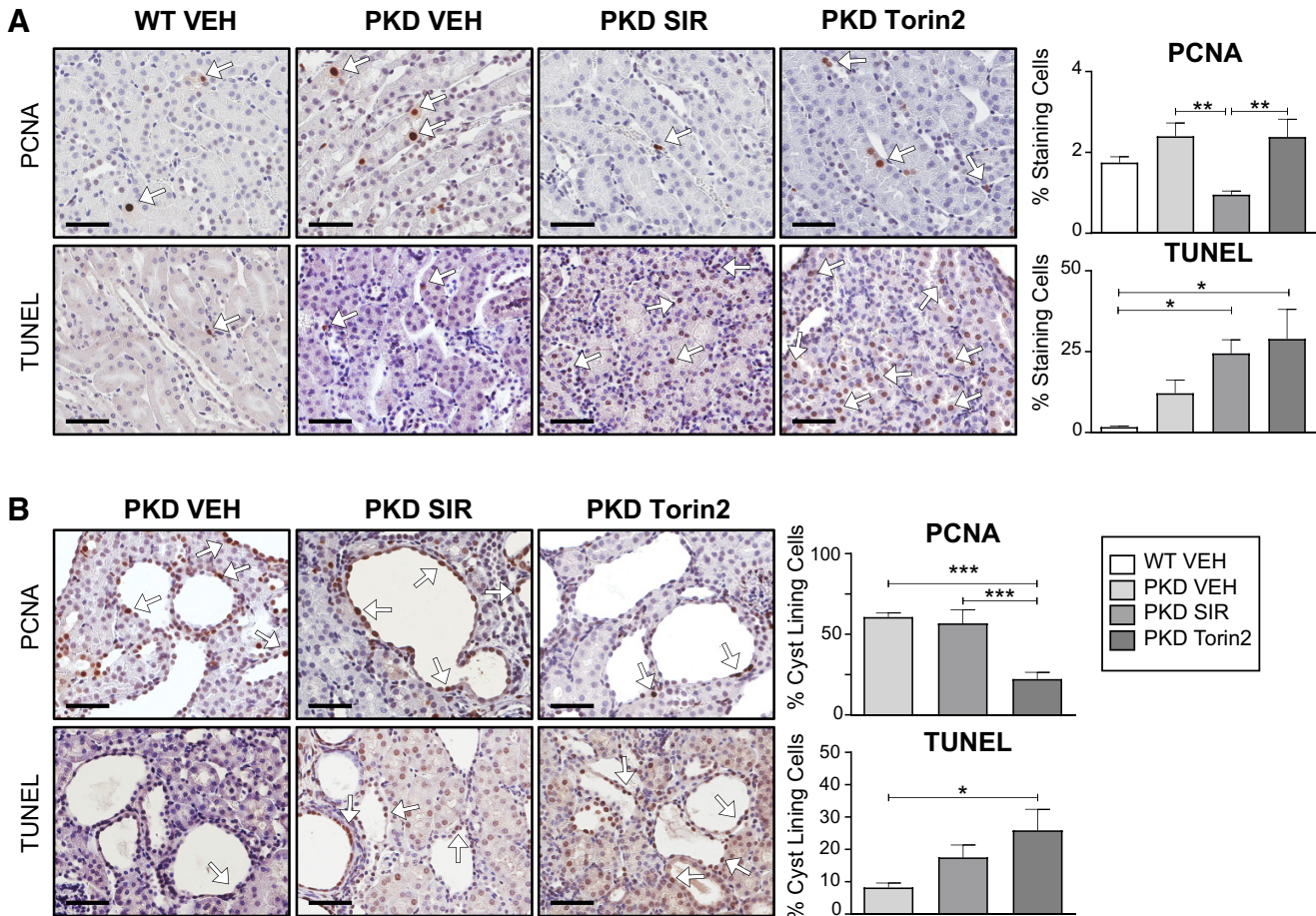
Fig. 3. Effect of sirolimus (SIR) versus torin2 on apoptosis (TUNEL) and proliferation [proliferating cell nuclear antigen (PCNA)]. *A*: PCNA and TUNEL staining in noncystic tubules from wild-type (WT) and *Pkd1*^RC/RC [polycystic kidney disease (PKD)] kidneys, expressed as the percentage of cells staining positive per 240-μm^2 area (%staining cells). *B*: PCNA and TUNEL staining in cells lining the cysts in PKD kidneys, expressed as the percentage of cells lining the cyst staining positive per cyst (%cyst-lining cells). White arrows indicate 3,3'-diaminobenzidine tetrahydrochloride hydrate-positive cells. VEH, vehicle. Scale bars = 50 μm. Values are means ± SE. *$P < 0.05$, **$P < 0.01$, and ***$P < 0.0001$ (by ANOVA with a Newman-Keuls post test).

TORKi on NAD(P)H-dependent cellular oxidoreductase activity (a direct measurement of MTT assay) and metabolic activity (an indirect measurement of MTT assay) (48). The increase in metabolism in $PKD1^{-/-}$ cells was associated with an increase in p4E-BP1 (Ser^{65} and Thr$^{37/46}$). Both sirolimus and torin2 caused a reduction in metabolic rates in $PKD1^{-/-}$ cells that was associated with decreased phosphorylation of 4E-BP1 at Ser^{65} and Thr$^{37/46}$ but not at Thr^{70}. Sirolimus decreased phosphorylation of Akt, a marker of mTORC2 in $PKD1^{-/-}$ cells. Thus, in human $PKD1^{-/-}$ cells, it is likely that metabolism is mediated by additional mTORC1-independent proproliferative pathways, as sirolimus is able to inhibit phosphorylation of 4E-BP1 and phosphorylation of Akt (Ser^{473}) (mTORC2). Also, in vitro models may have inherent artifacts of immortalization and, therefore, may not reflect an effect on the mTORC1/2 system in an in vivo model of PKD.

Human studies of sirolimus in PKD were plagued by side effects, especially mucositis (45, 58). In animal studies, the side effect profile of a TORKi was better than that of rapalogs, perhaps due to a lesser immunosuppressive effect (no bone marrow suppression and no effect on T and B cell proliferation) (2, 7, 9, 25). Human safety and tolerability studies of

TORKi have shown that the side effect profile is different from that of rapalogs and may be milder (3, 35). Thus, based on the data that a TORKi can inhibit both mTORC1 and mTORC2, including 4E-BP1, and are well tolerated in preclinical and clinical studies, a study of the TORKi torin2 versus sirolimus was performed in $Pkd1^{RC/RC}$ mice. Both torin2 and sirolimus mediated similar effects in terms of reducing kidney cyst index and maintaining kidney function, despite potentially different specificities/mechanisms of action of the two drugs. Many signaling pathways, in addition to mTOR, are involved in ADPKD (20, 41). However, both drugs effectively target pS6 in noncystic and cystic tubules, and both drugs target p4E-BP1 (Thr$^{37/46}$ and Thr^{70}) in noncystic tubules. Thus, although torin2 and sirolimus have different specificities and mechanisms of action for the effective inhibition of mTOR signaling, they do not specifically target the other pathways dysregulated in PKD (28). Regardless, the possibility that TORKi treatment may have fewer side effects than sirolimus in patients with ADPKD is encouraging.

Sirolimus decreased PCNA staining in noncystic tubules in PKD kidneys, whereas torin2 decreased PCNA staining in cystic tubules. As the mechanism for torin2 and sirolimus cellular uptake is ill defined, it is plausible that cellular

uptake for sirolimus versus torin2 may differ between cystic and noncystic tubules. Human and experimental data provide strong evidence that abnormal proliferation and apoptosis in tubular epithelial cells play a crucial role in cyst development and/or growth in PKD (59). Thus, both sirolimus and torin2 likely decreased cyst burden in $Pkd1^{RC/RC}$ mice, at least in part, by retarding cystic and noncystic cortical tubular cell proliferation.

S6 ribosomal protein is the main mTORC1 proproliferative substrate that is inhibited by sirolimus. In the present study, pS6 was increased in PKD compared with wild-type kidneys, markedly inhibited by both sirolimus and torin2 in noncystic areas of PKD kidneys, and inhibited to a lesser extent in cyst-lining epithelial cells. These data suggest that both sirolimus and torin2 may decrease proliferation in PKD kidneys via inhibition of pS6.

The role of apoptosis in cyst growth is controversial (14). Pharmacological (50) or genetic (51) inhibition of apoptosis results in less cyst growth. However, induction of apoptosis in two $Pkd1^{-/-}$ models also resulted in stunted cyst growth (15). Protection against PKD with high-dose sirolimus (1.67 or 5 $mg \cdot kg^{-1} \cdot day^{-1}$) was associated with increased apoptosis (46). Our previously published data showed that sirolimus at a much lower dose, 0.5 $mg \cdot kg^{-1} \cdot day^{-1}$, had no effect on cleaved caspase-3 or apoptosis in $Pkd2^{-/-}$ mice (61) and female Cy/+ rats (6). In the present study, torin2 resulted in increased apoptosis in cells lining the cysts. These data suggest that therapeutic effects of torin2 on PKD may be related in part to increased apoptosis in addition to decreased proliferation. While both inhibitors had effects on proliferation and apoptosis and decreased cystic index, neither significantly decreased the total number of cysts, suggesting that these inhibitors may act by preventing cyst expansion driven by proliferation and apoptosis more so than de novo cystogenesis.

4E-BP1 inhibits cap-dependent translation by binding to the translation initiation factor eIF4E. Hyperphosphorylation of 4E-BP1 disrupts this interaction and results in the activation of cap-dependent translation. Phosphorylation of 4E-BP1 at Thr[37] and Thr[46] does not prevent the binding of 4E-BP1 to eIF4E, but it does prime 4E-BP1 for subsequent phosphorylation at Ser[65] and Thr[70]. PKD rat models (Cy/+) (60) and renal tissues from both patients with autosomal recessive PKD (5, 32) or ADPKD exhibit an increase in 4E-BP1 proteins. It has been shown that p4E-BP1 is increased in the kidney of a nonorthologous PKD mouse model, transmembrane protein 67 knockout mice (13), and in $Pkd1^{-/-}$ mouse embryonic fibroblasts (11). We aimed to characterize the sensitivity of p4E-BP1 isoforms to mTORC1 and mTORC2 inhibition in a hypomorphic $Pkd1^{RC/RC}$ in vivo model. Immunohistochemical analysis revealed increased p4E-BP1 (Thr[37/46] and Thr[70]) in $Pkd1^{RC/RC}$ compared with wild-type kidneys. Both sirolimus and torin2 decreased p4E-BP1 (Thr[37/46] and Thr[70]) staining of noncystic tubular cells of PKD kidneys. These data suggest that sirolimus is as effective as torin2 at reducing 4E-BP1 phosphorylation events in $Pkd1^{RC/RC}$ kidneys.

mTORC2 directly phosphorylates Akt on Ser[473], and a reduction in Rictor expression inhibits phosphorylation of Akt (Ser[473]). Phosphoregulation of Akt (Ser[473]) plays a crucial role in proliferation, cell survival, and growth. Knockout of mTORC2 does not affect mTORC1, suggesting that mTORC2 can function independently of mTORC1, and, as such, can activate a pool of Akt that is not upstream of mTORC1. We previously demonstrated that pAkt (Ser[473]) increased in the kidney in the Han:SPRD (Cy/+) rat model and $Pkd2^{-/-}$ mouse model of ADPKD (6, 37, 38). We have previously demonstrated that silencing of Rictor in Madin-Darby canine kidney cells results in a decrease in pAkt (Ser[473]) and a decrease in cyst size that is reversed by the introduction of constitutively active Akt (37). In the present study, in vitro, the increase in the ratio of pAkt (Ser[473]) to total Akt in $PKD1^{-/-}$ compared with $PKD1^{+/+}$ cells did not reach statistical significance. However, our immunoblot analysis showed an increase in pAkt (Ser[473]) in $Pkd1^{RC/RC}$ compared with wild-type kidneys. Both sirolimus and torin2 decreased phosphorylation of Akt (Ser[473]) in $Pkd1^{RC/RC}$ kidneys. Sirolimus does not usually directly target mTORC2 or downstream substrates (16, 47); however, prolonged sirolimus treatment has been shown to inhibit mTORC2 assembly (42). Similarly, long-term administration of sirolimus can inhibit mTORC2 in some, but not all, in vitro and in vivo systems (44). In the present study, in $Pkd1^{RC/RC}$ kidneys, long-term (70 days) treatment with sirolimus was able to inhibit pAkt (Ser[473]), a marker of mTORC2 activation.

Here, we report a study of the TORKi torin2 and sirolimus in PKD. One of the limitations of the study is the much shorter half-life (~1 h) of torin2 than sirolimus (63 h) (26, 28). As the half-life is the time required for half of a compound to be removed by biological processes, it is possible that the amount of functional torin2 present to inhibit mTOR signaling and, thus, impact PKD burden chronically may have been suboptimal compared with sirolimus. In an attempt to compensate for its short half-life, torin2 was administered at the highest tolerable dose, 10 mg/kg, once daily on weekdays. It is possible that the dose of torin2 administered in a slower or more stable format, e.g., subcutaneous minipump, slow-release formulations, or compound manipulation to increase stability, will have a stronger therapeutic effect.

In summary, we report the first study of 4E-BP1 in a hypomorphic $Pkd1^{RC/RC}$ mouse model, orthologous to human PKD,

Fig. 4. Effect of sirolimus (SIR) versus torin2 on mechanistic target of rapamycin complex (mTORC)1 [phosphorylated S6 (pS6) and phosphorylated eukaryotic translation initiation factor 4E-binding protein 1 (p4E-BP1)] and mTORC2 [phosphorylated Akt (pAkt) (Ser[473])] in $Pkd1^{RC/RC}$ kidneys. The effect of sirolimus or torin2 treatment on pS6 and p4E-BP1 (Thr[37/46], Ser[65], and Thr[70]) was determined in kidneys from mice with polycystic kidney disease ($Pkd1^{RC/RC}$) and wild-type (WT) mice by immunohistochemical analysis. A: pS6 (Ser[240/244]) and p4E-BP1 (Thr[37/46], Ser[65], and Thr[70]) staining in noncystic tubules, expressed as the percentage of cells staining positive per 240-μm^2 area (%staining cells). White arrows indicate 3,3′-diaminobenzidine tetrahydrochloride hydrate-positive cells. Scale bars = 50 μm. B: pS6 (Ser[240/244]) and p4E-BP1 (Thr[37/46], Ser[65], and Thr[70]) staining in cyst-lining cells, expressed as the percentage of positive-staining cells per cyst (%cyst-lining cells). White arrows indicate 3,3′-diaminobenzidine tetrahydrochloride hydrate-positive cells. Scale bars = 50 μm. C: pAkt (Ser[473]) Akt sensitivity to torin2 and sirolimus in $Pkd1^{RC/RC}$ kidneys. The ratio of pAkt to total Akt was quantitated by densitometry. Values are means ± SE; n = 4–5 per group. *$P < 0.05$, **$P < 0.01$, and ***$P < 0.001$ (by ANOVA with a Newman-Keuls post test).

as well as a study of sirolimus versus a TORKi in PKD. Contrary to our hypothesis that torin2 would have a more potent antiproliferative effect than sirolimus by additional inhibition of both 4E-BP1 and mTORC2, we found that both drugs mediated comparable therapeutic effects, such as decreased cyst growth and improved kidney function, and both drugs increased apoptosis, decreased mTORC1 and mTORC2 signaling, and suppressed proliferation in PKD kidneys.
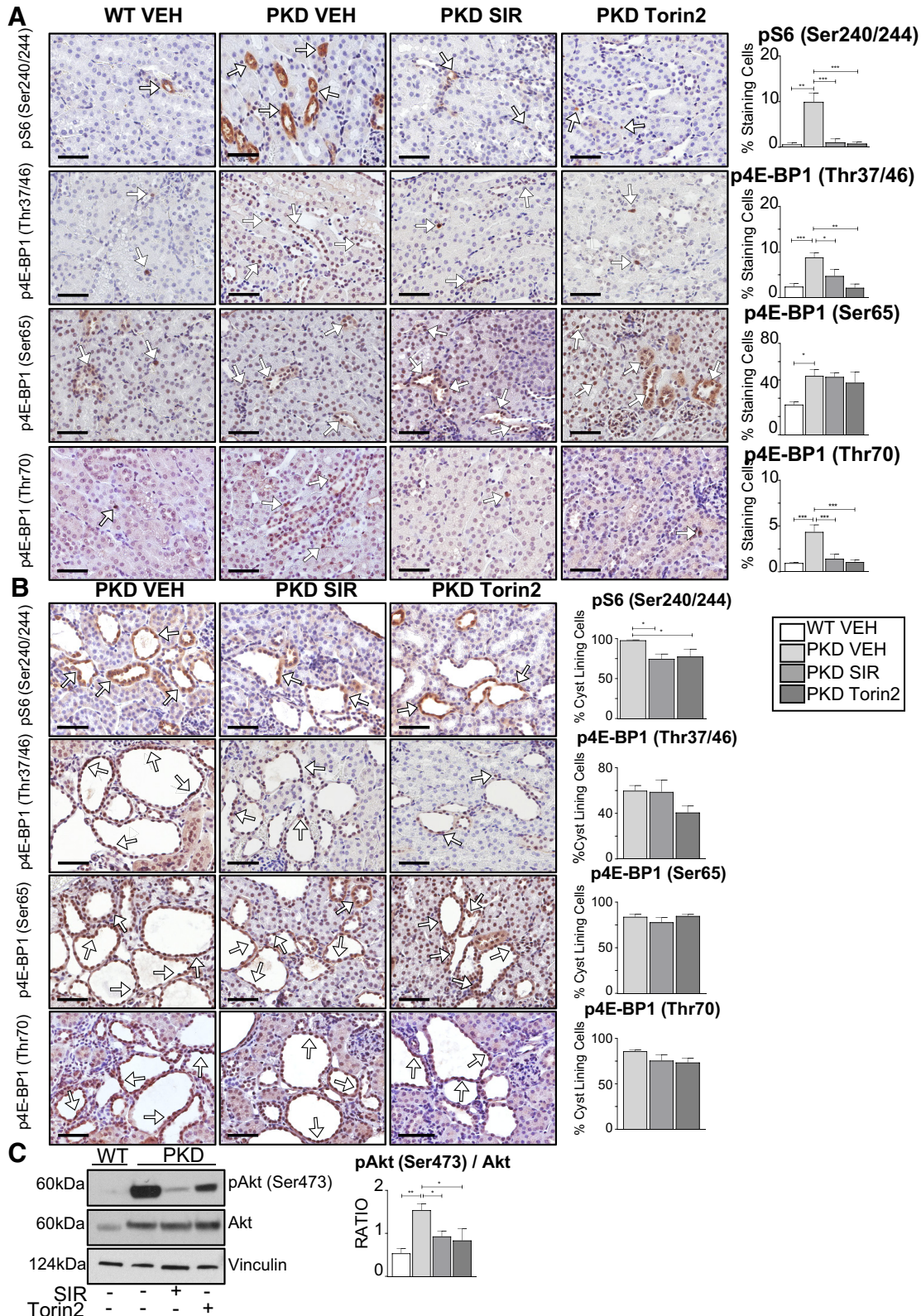
DISCLOSURES

C. L. Edelstein is on the Data Safety Monitoring Board for Conatus Pharmaceuticals.

AUTHOR CONTRIBUTIONS

S.J.H., C.N.B., and C.L.E. conceived and designed research; S.J.H., C.N.B., D.J.A., A.M.L., K.N.N., and H.W.T. performed experiments; S.J.H., C.N.B., D.J.A., A.M.L., and K.N.N. analyzed data; S.J.H., C.N.B., K.H., and C.L.E. interpreted results of experiments; S.J.H., C.N.B., D.J.A., and A.M.L. prepared figures; S.J.H., C.N.B., and C.L.E. drafted manuscript; S.J.H., C.N.B., D.J.A., K.H., and C.L.E. edited and revised manuscript; S.J.H., C.N.B., K.H., and C.L.E. approved final version of manuscript.

REFERENCES

1. **Aguiari G, Varani K, Bogo M, Mangolini A, Vincenzi F, Durante C, Gessi S, Sacchetto V, Catizone L, Harris P, Rizzuto R, Borea PA, Del Senno L.** Deficiency of polycystic kidney disease-1 gene (PKD1) expression increases A_3 adenosine receptors in human renal cells: implications for cAMP-dependent signalling and proliferation of PKD1-mutated cystic cells. *Biochim Biophys Acta* 1792: 531–540, 2009. doi:10.1016/j.bbadis.2009.03.001.

2. **Ahmed M, Hussain AR, Bavi P, Ahmed SO, Al Sobhi SS, Al-Dayel F, Uddin S, Al-Kuraya KS.** High prevalence of mTOR complex activity can be targeted using Torin2 in papillary thyroid carcinoma. *Carcinogenesis* 35: 1564–1572, 2014. doi:10.1093/carcin/bgu051.

3. **Asahina H, Nokihara H, Yamamoto N, Yamada Y, Tamura Y, Honda K, Seki Y, Tanabe Y, Shimada H, Shi X, Tamura T.** Safety and tolerability of AZD8055 in Japanese patients with advanced solid tumors; a dose-finding phase I study. *Invest New Drugs* 31: 677–684, 2013. doi:10.1007/s10637-012-9860-4.

4. **Ayuso MI, Hernández-Jiménez M, Martín ME, Salinas M, Alcázar A.** New hierarchical phosphorylation pathway of the translational repressor eIF4E-binding protein 1 (4E-BP1) in ischemia-reperfusion stress. *J Biol Chem* 285: 34355–34363, 2010. doi:10.1074/jbc.M110.135103.

5. **Becker JU, Opazo Saez A, Zerres K, Witzke O, Hoyer PF, Schmid KW, Kribben A, Bergmann C, Nürnberger J.** The mTOR pathway is activated in human autosomal-recessive polycystic kidney disease. *Kidney Blood Press Res* 33: 129–138, 2010. doi:10.1159/000314380.

6. **Belibi F, Ravichandran K, Zafar I, He Z, Edelstein CL.** mTORC1/2 and rapamycin in female Han:SPRD rats with polycystic kidney disease. *Am J Physiol Renal Physiol* 300: F236–F244, 2011. doi:10.1152/ajprenal.00129.2010.

7. **Berry T, Luther W, Bhatnagar N, Jamin Y, Poon E, Sanda T, Pei D, Sharma B, Vetharoy WR, Hallsworth A, Ahmad Z, Barker K, Moreau L, Webber H, Wang W, Liu Q, Perez-Atayde A, Rodig S, Cheung NK, Raynaud F, Hallberg B, Robinson SP, Gray NS, Pearson AD, Eccles SA, Chesler L, George RE.** The ALK(F1174L) mutation potentiates the oncogenic activity of MYCN in neuroblastoma. *Cancer Cell* 22: 117–130, 2012. doi:10.1016/j.ccr.2012.06.001.

8. **Chresta CM, Davies BR, Hickson I, Harding T, Cosulich S, Critchlow SE, Vincent JP, Ellston R, Jones D, Sini P, James D, Howard Z, Dudley P, Hughes G, Smith L, Maguire S, Hummersone M, Malagu K, Menear K, Jenkins R, Jacobsen M, Smith GC, Guichard S, Pass M.** AZD8055 is a potent, selective, and orally bioavailable ATP-competitive mammalian target of rapamycin kinase inhibitor with in vitro and in vivo antitumor activity. *Cancer Res* 70: 288–298, 2010. doi:10.1158/0008-5472.CAN-09-1751.

9. **Codeluppi S, Fernandez-Zafra T, Sandor K, Kjell J, Liu Q, Abrams M, Olson L, Gray NS, Svensson CI, Uhlén P.** Interleukin-6 secretion by astrocytes is dynamically regulated by PI3K-mTOR-calcium signaling. *PLoS One* 9: e92649, 2014. doi:10.1371/journal.pone.0092649.

10. **Dias N, Nicolau A, Carvalho GS, Mota M, Lima N.** Miniaturization and application of the MTT assay to evaluate metabolic activity of protozoa in the presence of toxicants. *J Basic Microbiol* 39: 103–108, 1999. doi:10.1002/(SICI)1521-4028(199905)39:2<103:AID-JOBM103>3.0.CO;2-D.

11. **Distefano G, Boca M, Rowe I, Wodarczyk C, Ma L, Piontek KB, Germino GG, Pandolfi PP, Boletta A.** Polycystin-1 regulates extracellular signal-regulated kinase-dependent phosphorylation of tuberin to control cell size through mTOR and its downstream effectors S6K and 4EBP1. *Mol Cell Biol* 29: 2359–2371, 2009. doi:10.1128/MCB.01259-08.

12. **Dowling RJ, Topisirovic I, Alain T, Bidinosti M, Fonseca BD, Petroulakis E, Wang X, Larsson O, Selvaraj A, Liu Y, Kozma SC, Thomas G, Sonenberg N.** mTORC1-mediated cell proliferation, but not cell growth, controlled by the 4E-BPs. *Science* 328: 1172–1176, 2010. doi:10.1126/science.1187532.

13. **Du E, Li H, Jin S, Hu X, Qiu M, Han R.** Evidence that TMEM67 causes polycystic kidney disease through activation of JNK/ERK-dependent pathways. *Cell Biol Int* 37: 694–702, 2013. doi:10.1002/cbin.10081.

14. **Edelstein CL.** What is the role of tubular epithelial cell apoptosis in polycystic kidney disease (PKD)? *Cell Cycle* 4: 1550–1554, 2005. doi:10.4161/cc.4.11.2185.

15. **Fan LX, Zhou X, Sweeney WE Jr, Wallace DP, Avner ED, Grantham JJ, Li X.** Smac-mimetic-induced epithelial cell death reduces the growth of renal cysts. *J Am Soc Nephrol* 24: 2010–2022, 2013. doi:10.1681/ASN.2013020176.

16. **Feldman ME, Apsel B, Uotila A, Loewith R, Knight ZA, Ruggero D, Shokat KM.** Active-site inhibitors of mTOR target rapamycin-resistant outputs of mTORC1 and mTORC2. *PLoS Biol* 7: e1000038, 2009. doi:10.1371/journal.pbio.1000038.

17. **Gingras AC, Gygi SP, Raught B, Polakiewicz RD, Abraham RT, Hoekstra MF, Aebersold R, Sonenberg N.** Regulation of 4E-BP1 phosphorylation: a novel two-step mechanism. *Genes Dev* 13: 1422–1437, 1999. doi:10.1101/gad.13.11.1422.

18. **Gingras AC, Raught B, Gygi SP, Niedzwiecka A, Miron M, Burley SK, Polakiewicz RD, Wyslouch-Cieszynska A, Aebersold R, Sonenberg N.** Hierarchical phosphorylation of the translation inhibitor 4E-BP1. *Genes Dev* 15: 2852–2864, 2001. doi:10.1101/gad.912401.

20. **Harris PC, Torres VE.** Genetic mechanisms and signaling pathways in autosomal dominant polycystic kidney disease. *J Clin Invest* 124: 2315–2324, 2014. doi:10.1172/JCI72272.

21. **Hopp K, Hommerding CJ, Wang X, Ye H, Harris PC, Torres VE.** Tolvaptan plus pasireotide shows enhanced efficacy in a PKD1 model. *J Am Soc Nephrol* 26: 39–47, 2015. doi:10.1681/ASN.2013121312.

22. **Hopp K, Ward CJ, Hommerding CJ, Nasr SH, Tuan HF, Gainullin VG, Rossetti S, Torres VE, Harris PC.** Functional polycystin-1 dosage governs autosomal dominant polycystic kidney disease severity. *J Clin Invest* 122: 4257–4273, 2012. doi:10.1172/JCI64313.

23. **Karlsson E, Pérez-Tenorio G, Amin R, Bostner J, Skoog L, Fornander T, Sgroi DC, Nordenskjöld B, Hallbeck AL, Stål O.** The mTOR effectors 4EBP1 and S6K2 are frequently coexpressed and associated with a poor prognosis and endocrine resistance in breast cancer: a retrospective study including patients from the randomised Stockholm tamoxifen trials. *Breast Cancer Res* 15: R96, 2013. doi:10.1186/bcr3557.

24. **Kleczko EK, Marsh KH, Tyler LC, Furgeson SB, Bullock BL, Altmann CJ, Miyazaki M, Gitomer BY, Harris PC, Weiser-Evans MCM, Chonchol MB, Clambey ET, Nemenoff RA, Hopp K.** CD8+ T cells modulate autosomal dominant polycystic kidney disease progression. *Kidney Int* 94: 1127–1140, 2018. doi:10.1016/j.kint.2018.06.025.

25. **Li C, Lee PS, Sun Y, Gu X, Zhang E, Guo Y, Wu CL, Auricchio N, Priolo C, Li J, Csibi A, Parkhitko A, Morrison T, Planaguma A, Kazani S, Israel E, Xu KF, Henske EP, Blenis J, Levy BD, Kwiatkowski D, Yu JJ.** Estradiol and mTORC2 cooperate to enhance prostaglandin biosynthesis and tumorigenesis in TSC2-deficient LAM cells. *J Exp Med* 211: 15–28, 2014. doi:10.1084/jem.20131080.

26. **Liu Q, Chang JW, Wang J, Kang SA, Thoreen CC, Markhard A, Hur W, Zhang J, Sim T, Sabatini DM, Gray NS.** Discovery of 1-(4-(4-propionylpiperazin-1-yl)-3-(trifluoromethyl)phenyl)-9-(quinolin-3-yl)benzo[h][1,6]naphthyridin-2(1H)-one as a highly potent, selective mammalian target of rapamycin (mTOR) inhibitor for the treatment of cancer. *J Med Chem* 53: 7146–7155, 2010. doi:10.1021/jm101144f.

27. **Liu Q, Thoreen C, Wang J, Sabatini D, Gray NS.** mTOR mediated anti-cancer drug discovery. *Drug Discov Today Ther Strateg* 6: 47–55, 2009. doi:10.1016/j.ddstr.2009.12.001.

28. **Liu Q, Xu C, Kirubakaran S, Zhang X, Hur W, Liu Y, Kwiatkowski NP, Wang J, Westover KD, Gao P, Ercan D, Niepel M, Thoreen CC,**

Kang SA, Patricelli MP, Wang Y, Tupper T, Altabef A, Kawamura H, Held KD, Chou DM, Elledge SJ, Janne PA, Wong KK, Sabatini DM, Gray NS. Characterization of Torin2, an ATP-competitive inhibitor of mTOR, ATM, and ATR. *Cancer Res* 73: 2574–2586, 2013. doi:10.1158/0008-5472.CAN-12-1702.

30. **Livingstone M, Bidinosti M.** Rapamycin-insensitive mTORC1 activity controls eIF4E:4E-BP1 binding. *F1000 Res* 1: 4, 2012. doi:10.12688/f1000research.1-4.v1.

31. **Loghman-Adham M, Nauli SM, Soto CE, Kariuki B, Zhou J.** Immortalized epithelial cells from human autosomal dominant polycystic kidney cysts. *Am J Physiol Renal Physiol* 285: F397–F412, 2003. doi:10.1152/ajprenal.00310.2002.

32. **Majumder PK, Febbo PG, Bikoff R, Berger R, Xue Q, McMahon LM, Manola J, Brugarolas J, McDonnell TJ, Golub TR, Loda M, Lane HA, Sellers WR.** mTOR inhibition reverses Akt-dependent prostate intraepithelial neoplasia through regulation of apoptotic and HIF-1-dependent pathways. *Nat Med* 10: 594–601, 2004. doi:10.1038/nm1052.

33. **Mao Z, Zhang W.** Role of mTOR in glucose and lipid metabolism. *Int J Mol Sci* 19: 2043, 2018. doi:10.3390/ijms19072043.

34. **Moorman NJ, Shenk T.** Rapamycin-resistant mTORC1 kinase activity is required for herpesvirus replication. *J Virol* 84: 5260–5269, 2010. doi:10.1128/JVI.02733-09.

35. **Naing A, Aghajanian C, Raymond E, Olmos D, Schwartz G, Oelmann E, Grinsted L, Burke W, Taylor R, Kaye S, Kurzrock R, Banerji U.** Safety, tolerability, pharmacokinetics and pharmacodynamics of AZD8055 in advanced solid tumours and lymphoma. *Br J Cancer* 107: 1093–1099, 2012. doi:10.1038/bjc.2012.368.

36. **O'Reilly KE, Rojo F, She QB, Solit D, Mills GB, Smith D, Lane H, Hofmann F, Hicklin DJ, Ludwig DL, Baselga J, Rosen N.** mTOR inhibition induces upstream receptor tyrosine kinase signaling and activates Akt. *Cancer Res* 66: 1500–1508, 2006. doi:10.1158/0008-5472.CAN-05-2925.

37. **Ravichandran K, Zafar I, He Z, Doctor RB, Moldovan R, Mullick AE, Edelstein CL.** An mTOR anti-sense oligonucleotide decreases polycystic kidney disease in mice with a targeted mutation in Pkd2. *Hum Mol Genet* 23: 4919–4931, 2014. doi:10.1093/hmg/ddu208.

38. **Ravichandran K, Zafar I, Ozkok A, Edelstein CL.** An mTOR kinase inhibitor slows disease progression in a rat model of polycystic kidney disease. *Nephrol Dial Transplant* 30: 45–53, 2015. doi:10.1093/ndt/gfu296.

39. **Reifsnyder PC, Flurkey K, Te A, Harrison DE.** Rapamycin treatment benefits glucose metabolism in mouse models of type 2 diabetes. *Aging (Albany NY)* 8: 3120–3130, 2016. doi:10.18632/aging.101117.

40. **Rowe I, Chiaravalli M, Mannella V, Ulisse V, Quilici G, Pema M, Song XW, Xu H, Mari S, Qian F, Pei Y, Musco G, Boletta A.** Defective glucose metabolism in polycystic kidney disease identifies a new therapeutic strategy. *Nat Med* 19: 488–493, 2013. doi:10.1038/nm.3092.

41. **Saigusa T, Bell PD.** Molecular pathways and therapies in autosomal-dominant polycystic kidney disease. *Physiology (Bethesda)* 30: 195–207, 2015. doi:10.1152/physiol.00032.2014.

42. **Sarbassov DD, Ali SM, Sengupta S, Sheen JH, Hsu PP, Bagley AF, Markhard AL, Sabatini DM.** Prolonged rapamycin treatment inhibits mTORC2 assembly and Akt/PKB. *Mol Cell* 22: 159–168, 2006. doi:10.1016/j.molcel.2006.03.029.

43. **Saxton RA, Sabatini DM.** mTOR signaling in growth, metabolism, and disease. *Cell* 168: 960–976, 2017. [Erratum in *Cell* 169: 361–371, 2017. 10.1016/j.cell.2017.03.035. 28388417]. doi:10.1016/j.cell.2017.02.004.

44. **Schreiber KH, Ortiz D, Academia EC, Anies AC, Liao CY, Kennedy BK.** Rapamycin-mediated mTORC2 inhibition is determined by the relative expression of FK506-binding proteins. *Aging Cell* 14: 265–273, 2015. doi:10.1111/acel.12313.

45. **Serra AL, Poster D, Kistler AD, Krauer F, Raina S, Young J, Rentsch KM, Spanaus KS, Senn O, Kristanto P, Scheffel H, Weishaupt D, Wüthrich RP.** Sirolimus and kidney growth in autosomal dominant polycystic kidney disease. *N Engl J Med* 363: 820–829, 2010. doi:10.1056/NEJMoa0907419.

46. **Shillingford JM, Murcia NS, Larson CH, Low SH, Hedgepeth R, Brown N, Flask CA, Novick AC, Goldfarb DA, Kramer-Zucker A, Walz G, Piontek KB, Germino GG, Weimbs T.** The mTOR pathway is regulated by polycystin-1, and its inhibition reverses renal cystogenesis in polycystic kidney disease. *Proc Natl Acad Sci USA* 103: 5466–5471, 2006. doi:10.1073/pnas.0509694103.

47. **Shor B, Gibbons JJ, Abraham RT, Yu K.** Targeting mTOR globally in cancer: thinking beyond rapamycin. *Cell Cycle* 8: 3831–3837, 2009. doi:10.4161/cc.8.23.10070.

48. **Stockert JC, Horobin RW, Colombo LL, Blázquez-Castro A.** Tetrazolium salts and formazan products in cell biology: viability assessment, fluorescence imaging, and labeling perspectives. *Acta Histochem* 120: 159–167, 2018. doi:10.1016/j.acthis.2018.02.005.

49. **Ta MH, Liuwantara D, Rangan GK.** Effects of pyrrolidine dithiocarbamate on proliferation and nuclear factor-κB activity in autosomal dominant polycystic kidney disease cells. *BMC Nephrol* 16: 212, 2015. doi:10.1186/s12882-015-0193-3.

50. **Tao Y, Kim J, Faubel S, Wu JC, Falk SA, Schrier RW, Edelstein CL.** Caspase inhibition reduces tubular apoptosis and proliferation and slows disease progression in polycystic kidney disease. *Proc Natl Acad Sci USA* 102: 6954–6959, 2005. doi:10.1073/pnas.0408518102.

51. **Tao Y, Zafar I, Kim J, Schrier RW, Edelstein CL.** Caspase-3 gene deletion prolongs survival in polycystic kidney disease. *J Am Soc Nephrol* 19: 749–755, 2007. doi:10.1681/ASN.2006121378.

52. **Thoreen CC, Chantranupong L, Keys HR, Wang T, Gray NS, Sabatini DM.** A unifying model for mTORC1-mediated regulation of mRNA translation. *Nature* 485: 109–113, 2012. doi:10.1038/nature11083.

53. **Thoreen CC, Kang SA, Chang JW, Liu Q, Zhang J, Gao Y, Reichling LJ, Sim T, Sabatini DM, Gray NS.** An ATP-competitive mammalian target of rapamycin inhibitor reveals rapamycin-resistant functions of mTORC1. *J Biol Chem* 284: 8023–8032, 2009. doi:10.1074/jbc.M900301200.

54. **Thoreen CC, Sabatini DM.** Rapamycin inhibits mTORC1, but not completely. *Autophagy* 5: 725–726, 2009. doi:10.4161/auto.5.5.8504.

55. **Torres VE, Chapman AB, Devuyst O, Gansevoort RT, Grantham JJ, Higashihara E, Perrone RD, Krasa HB, Ouyang J, Czerwiec FS; TEMPO 3:4 Trial Investigators.** Tolvaptan in patients with autosomal dominant polycystic kidney disease. *N Engl J Med* 367: 2407–2418, 2012. doi:10.1056/NEJMoa1205511.

56. **Torres VE, Chapman AB, Devuyst O, Gansevoort RT, Perrone RD, Koch G, Ouyang J, McQuade RD, Blais JD, Czerwiec FS, Sergeyeva O; REPRISE Trial Investigators.** Tolvaptan in later-stage autosomal dominant polycystic kidney disease. *N Engl J Med* 377: 1930–1942, 2017. doi:10.1056/NEJMoa1710030.

57. **Torres VE, Wang X, Qian Q, Somlo S, Harris PC, Gattone VH II.** Effective treatment of an orthologous model of autosomal dominant polycystic kidney disease. *Nat Med* 10: 363–364, 2004. doi:10.1038/nm1004.

58. **Walz G, Budde K, Mannaa M, Nürnberger J, Wanner C, Sommerer C, Kunzendorf U, Banas B, Hörl WH, Obermüller N, Arns W, Pavenstädt H, Gaedeke J, Büchert M, May C, Gschaidmeier H, Kramer S, Eckardt KU.** Everolimus in patients with autosomal dominant polycystic kidney disease. *N Engl J Med* 363: 830–840, 2010. doi:10.1056/NEJMoa1003491.

59. **Wilson PD.** Polycystic kidney disease. *N Engl J Med* 350: 151–164, 2004. doi:10.1056/NEJMra022161.

60. **Wu M, Arcaro A, Varga Z, Vogetseder A, Le Hir M, Wüthrich RP, Serra AL.** Pulse mTOR inhibitor treatment effectively controls cyst growth but leads to severe parenchymal and glomerular hypertrophy in rat polycystic kidney disease. *Am J Physiol Renal Physiol* 297: F1597–F1605, 2009. doi:10.1152/ajprenal.00430.2009.

61. **Zafar I, Ravichandran K, Belibi FA, Doctor RB, Edelstein CL.** Sirolimus attenuates disease progression in an orthologous mouse model of human autosomal dominant polycystic kidney disease. *Kidney Int* 78: 754–761, 2010. doi:10.1038/ki.2010.250.

GENERAL ARTICLE - US OFFICE

The consequences of increased 4E-BP1 in polycystic kidney disease

Sara J Holditch[1], Carolyn N Brown[1], Daniel J Atwood[1], Deepak Pokhrel[1], Sara E Brown[1], Andrew M Lombardi[1], Khoa N Nguyen[1], Ryan C Hill[2], Miguel Lanaspa[1], Katharina Hopp[1], Mary C.M. Weiser-Evans[1] and Charles L Edelstein[1],*

[1]Division of Renal Diseases and Hypertension, University of Colorado at Denver, Denver, CO, USA,
[2]Department of Biochemistry and Molecular Genetics, University of Colorado Anschutz Medical Campus, Aurora, CO 80045, USA

*To whom correspondence should be addressed at: Charles L. Edelstein Division of Renal Diseases and Hypertension, University of Colorado at Denver, Box C281, 12700 East, 19th Ave, Denver, CO 80045, USA. Tel: (303) 724-4810; Fax (303) 724-4868; Email: Charles.edelstein@cuanschutz.edu

Abstract

Autosomal dominant polycystic kidney disease (ADPKD) is the most common hereditary renal disease, characterized by cyst formation and growth. Hyperproliferation is a major contributor to cyst growth. At the nexus of regulating proliferation, is 4E-BP1. We demonstrate that ADPKD mouse and rat models, ADPKD patient renal biopsies and $PKD1^{-/-}$ cells exhibited hyperphosphorylated 4E-BP1, a biomarker of increased translation and proliferation. We hypothesized that expression of constitutively active 4E-BP1 constructs (4E-BP1^{F113A} and 4E-BP1^{R13AF113A}) would decrease proliferation and reduce cyst expansion. Utilizing the $Pkd1^{RC/RC}$ mouse, we determined the effect of 4E-BP1^{F113A} on PKD. Unexpectedly, 4E-BP1^{F113A} resulted in increased cyst burden and suppressed apoptosis markers, increased anti-apoptotic Bcl-2 protein and increased mitochondrial proteins. Exogenous 4E-BP1 enhanced proliferation, decreased apoptosis, increased anti-apoptotic Bcl-2 protein, impaired NADPH oxidoreductase activity, increased mitochondrial proteins and increased superoxide production in PKD patient-derived renal epithelial cells. Reduced 4E-BP1 expression suppressed proliferation, restored apoptosis and improved cellular metabolism. These findings provide insight into how cyst-lining cells respond to 4E-BP1.

Keywords: 4E-BP1; polycystic kidney disease; proliferation; apoptosis; mitochondrial proteins

Introduction

Autosomal dominant polycystic kidney disease (ADPKD) is characterized by cyst formation and growth which can be driven by abnormal proliferation of tubular epithelial cells (1). Aberrant cellular proliferation is a striking commonality between ADPKD and cancer. Relevant to their shared pathobiology, sustained proliferative signaling (2–4), replicative immortality (2,5,6) and deregulated cellular energetics (2,7,8) are some of the major signaling pathways dysregulated in both PKD and cancer. Further, in PKD and cancer augmented protein synthesis is a hallmark of sustained proliferation independent of genetic insult or precipitating offence (9).

Eukaryotic translation initiation factor 4E-binding protein 1 (4E-BP1) is a crucial checkpoint in protein synthesis. Hypophosphorylated 4E-BP1 strongly associates with eIF4E (10), inhibiting translation and thus inhibiting proliferation (11). For example, overexpression of 4E-BP1 can partially reverse the phenotype of cells transformed with oncogenes Src and Ras (10). Further, constitutively active 4E-BP1 which binds eIF4E avidly can lead to

cell cycle arrest, inhibit proliferation of breast cancer cells (12), block lymphocyte growth and proliferation (13) and reduce cell size (14). 4E-BP1 hyperphosphorylation retards this interaction, releasing eIF4E, promoting proliferation. Thus, based on the growing evidence for 4E-BP1 dysregulation in cancer, and the overlapping pathobiology of PKD and oncology, we developed the hypothesis that there is hyperphosphorylation of 4E-BP1 in *in vivo* and *in vitro* PKD models, supporting epithelial proliferation and cyst expansion.

Phosphorylation of 4E-BP1 (p4E-BP1) can be carried out by numerous kinases through 4E-BP1's two kinase recognition domains (KRDs), RAIP (15,16) and FEMDI (14). A wealth of evidence indicates that mTOR, through FEMDI (17), phosphorylates 4E-BP1 thereby serving as a major factor in releasing 4E-BP1 from eIF4E and thus promoting protein translation and proliferation (18–20). Mutation of essential residues within FEMDI (e.g. Phe to Ala, F113A) eliminates phosphorylation of 4E-BP1 by mTOR at Thr37 and Thr46 (21). We hypothesized that preventing mTOR from initiating phosphorylation of 4E-BP1 with FEMDI mutant, F113A, would reduce proliferation in hyperproliferative cystic epithelial cells. This mechanism has precedent, as both constitutively active 4E-BP1 and FEMDI mutation constructs are insensitive to insulin-mediated release of 4E-BP1 from eIF4E (14,16).

Thus, our aims were to characterize p4E-BP1 *in vivo* and *in vitro* models of PKD and to assess the effect of expressing 4E-BP1 KRD mutants in a clinically relevant rodent model, the *Pkd1*$^{RC/RC}$ mouse and the ADPKD patient-derived cystic epithelial cells.

It is known that mTORC1 controls mitochondrial activity and biogenesis through 4E-BP-dependent translational regulation (22). 4E-BPs mediated the stimulatory effect of mTORC1 on the translation of mitochondria-related mRNAs, mitochondrial respiration and biogenesis and ATP production *in vitro* and *in vivo* (22). At the molecular level, this was explained by preferential inhibition of translation of a subset of cellular mRNAs that encode for essential nucleus-encoded mitochondrial proteins including the components of complex V and TFAM (transcription factor a, mitochondrial). Also, 4E-BP1 regulates mitochondrial activity and biogenesis in skeletal muscle (23). Thus, a further aim of the study was to determine the effect of 4E-BP1 on mitochondrial activity and biogenesis in PKD models.

Results

Increased phosphoregulation of 4E-BP1 is present in mice, rats and patient-derived PKD models *in vivo* and *in vitro*

4E-BP1 has multiple phospho-sites (17), with a hierarchy of phosphorylation (I: Thr37/Thr46, II: Thr70 and III: Ser65) in order to release eIF4E. The initial phospho-event is thought to be at Thr37 and Thr46 and caused by numerous kinases (17). For this reason, we screened rodent models of ADPKD for the presence of the initial phospho-primed p4E-BP1 (Thr37/Thr46). In *Pkd1*$^{RC/RC}$ mice and Cy/+ rat renal cortical tissues, p4E-BP1 (Thr37/Thr46) was elevated in both non-cystic and cystic tissues in contrast to age-matched wild-type (WT) controls (Fig. 1A and B). To characterize p4E-BP1 in patient tissues, we screened ADPKD patient biopsies for p4E-BP1 species by immunohistochemistry (Fig. 1C). All samples were positive for Thr37/Thr46, Thr70 and Ser65 p4E-BP1. Lastly, p4E-BP1 was present and elevated in the PKD patient-derived renal epithelial immortalized cell line (9–12, *PKD1*$^{-/-}$) in contrast to the renal tubular epithelial control immortalized cell line (RCTE, *PKD1*$^{+/+}$) (Fig. 1D). Total 4E-BP1 was not dif-

ferent between groups (Fig. 1D). In line with this observation, and consistent with previously published data (24), a variety of kinases known to have the potential to phosphorylate 4E-BP1 were increased in the phosphorylated state in *PKD1*$^{-/-}$ in contrast to *PKD1*$^{+/+}$ cells, including ERK, mTOR and JNK (Supplementary Material, Fig. S1A). *PKD1*$^{-/-}$ cells also exhibited increased cleaved caspase-3 (Supplementary Material, Fig. S1B), Ki-67 positivity and metabolic correlate NADPH oxidoreductase activity (MTT), in contrast to *PKD1*$^{+/+}$ (Supplementary Material, Fig. S1C and D). Thus, p4E-BP1 is present and elevated in PKD rodent and patient renal tissues. Additionally, *in vitro PKD1*$^{-/-}$ cells exhibit hyperphosphorylated 4E-BP1 in the presence of multiple activated kinases, increased proliferation and increased metabolic activity.

Exogenous 4E-BP1 increases cyst burden

In order to determine the effect of phospho-4E-BP1 *in vivo*, we generated and delivered FEMDI, Phe to Ala, 4E-BP1^{F113A}-expressing vectors (Fig. 2A) to WT pups in an acute tolerability and bio-distribution experiment (Fig. 2B). All treated animals were aged to study termination without weight loss or obvious pathology. To determine the biodistribution of intraperitoneal administered vectors, AAV genomes were detected in cardiac, hepatic and renal whole tissues (Fig. 2C). Endogenous 4E-BP1 transcripts were quantified and shown to be unaffected by expression vectors (data not shown). Exogenous, AAV-mediated murine codon-optimized 4E-BP1^{F113A} transcripts (Fig. 2D) were detected in cardiac, renal and hepatic tissues of treated animals and not observed in littermates receiving control TdTomato expression vectors (Fig. 2D). Total cumulative 4E-BP1 expression in whole kidneys of treated and control animals confirmed elevated total 4E-BP1 expression with delivery of 4E-BP1^{F113A}, in contrast to littermate controls (Fig. 2E). In summary, acute exposure to 4E-BP1^{F113A} was well tolerated, associated with no morbidity or developmental pathology and resulted in detectable 4E-BP1^{F113A} transcripts and modestly augmented 4E-BP1 protein in the kidneys of treated mice in contrast to control vector-treated littermates.

To determine the effect of 4E-BP1 expression on cyst burden, *Pkd1*$^{RC/RC}$ were treated with AAV9-4E-BP1^{F113A} or AAV9-TdTomato (Fig. 3A) at post-natal (PN) Day 3 and aged to PN120 (Fig. 3B). As in the acute study, vector genomes were detected in cardiac, renal and hepatic tissues (Fig. 3C) at study termination. Further, 4E-BP1^{F113A} transcripts (Fig. 3D) were detected, and 4E-BP1 expression (Fig. 3E) was increased, relative to loading control vinculin in treated mice.

Unexpectedly, long-term exposure to 4E-BP1^{F113A} resulted in significantly worsened PKD burden in *Pkd1*$^{RC/RC}$, as indicated by fast imaging with steady-state procession (FISP) abdominal MRIs (Fig. 3F). Total kidney volume (TKV) and the percentage of cystic renal tissue were significantly increased, indicating exacerbated disease in association with 4E-BP1^{F113A} (Fig. 3G). Inversely, the percentage of remaining functional parenchyma was significantly reduced with 4E-BP1^{F113A} (Fig. 3G). Blood urea nitrogen (Fig. 3H) and serum creatinine (Fig. 3I) were not significantly altered by 4E-BP1^{F113A}. Examination of renal tissues by H&E staining revealed significant increases in both the number of cysts and the average cyst size in the kidneys of 4E-BP1^{F113A}-treated animals (Fig. 3J–L). Immunohistochemistry of renal sections demonstrated reduced TUNEL-positive cyst-lining cells (Fig. 3M) and elevated Bcl-2 expression in the whole kidney homogenates of 4E-BP1^{F113A}-treated animals in contrast to littermate controls (Fig. 3N).
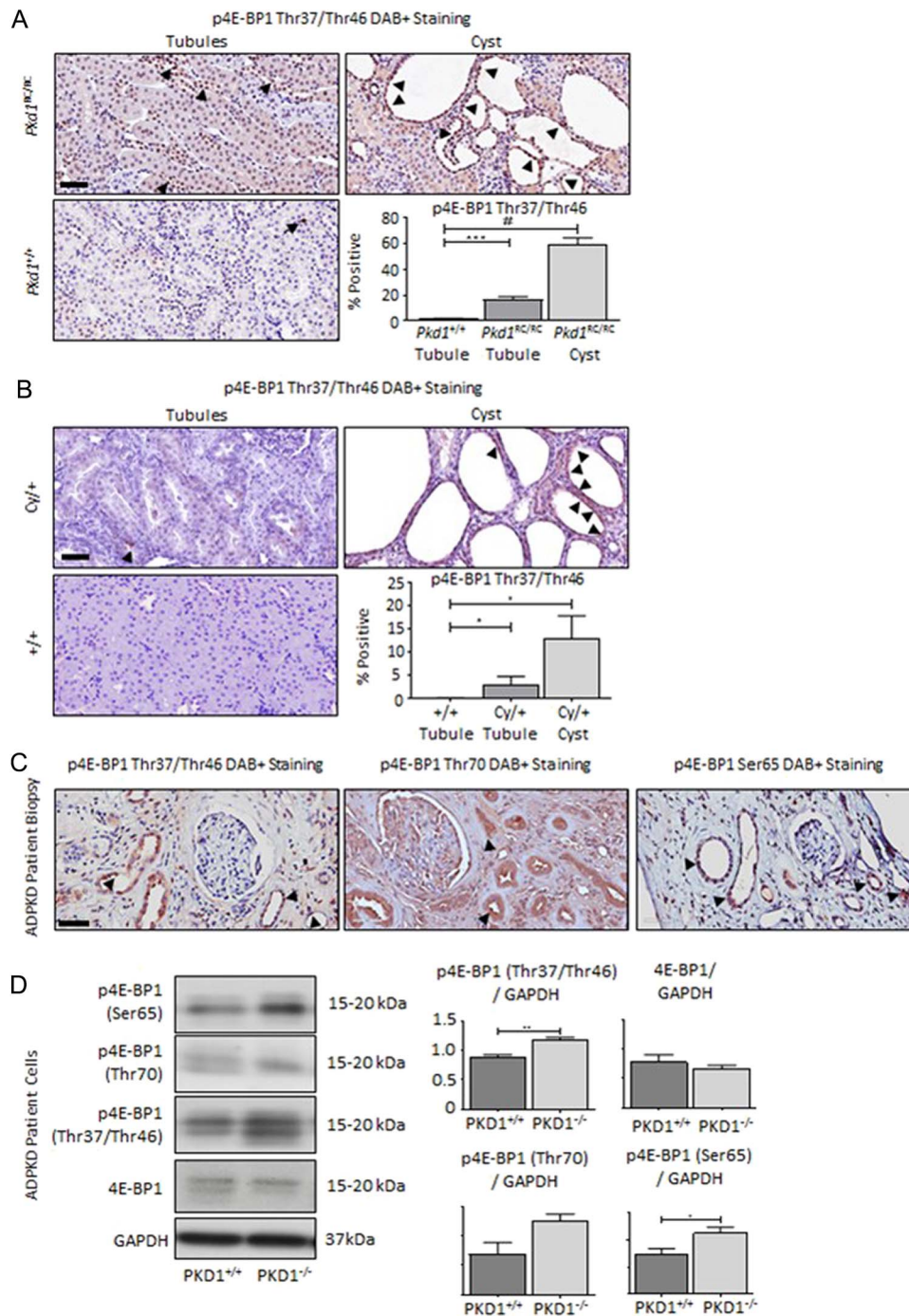
Figure 1. Increased phosphorylated 4E-BP1 in PKD rodent and patient tissues. (**A**) *Pkd1*$^{RC/RC}$ mice and (**B**) Cy/+ rats relative to age-matched strain controls (+/+) demonstrated increased p4E-BP1 (Thr37/46) in non-cystic tubules and stained positively in cells lining cysts. (**C**) End-stage renal biopsies indicated DAB positivity for p4E-BP1 (Thr37/Thr46, Thr70 and Ser65) by immunohistochemistry. Quantification is expressed as percent of cells staining positive per 100-μm^2 area. Black arrows indicate DAB+ staining. Scale bar = 50 μm (**D**) *PKD1*$^{-/-}$ cells exhibit increased expression of p4E-BP1 (Thr37/Thr46, Thr70 and Ser65) in contrast to the *PKD1*$^{+/+}$ renal epithelial cell line. Total 4E-BP1 was not different between groups. RDU, relative densitometry units. *N* = 4–5 per group. Multiple-group comparisons are performed using analysis of variance (ANOVA) with posttest according to Newman–Keuls. Single comparisons were made using Student's *T* test. A *P* value of < 0.05 was considered statistically significant. Values are expressed as the mean ± SEM. *$P < 0.05$, **$P < 0.01$, ***$P < 0.001$, #$P < 0.0001$.

To determine whether the 4E-BP1^{F113A} mutant had effects in other organs, cleaved caspase-3 (CC3), a marker of apoptosis, Bcl-2 and PCNA, a marker of proliferation, were measured in the heart and liver. In the liver, as in the kidney, there was a decrease in CC3 in the 4E-BP1^{F113A} -treated in contrast to control mice, but Bcl-2 that was increased in the kidney was decreased in the liver in the 4E-BP1^{F113A}-treated mice and PCNA was unchanged (Supplementary Material, Fig. S2A). In the heart, there were no changes in Bcl-2 or PCNA and CC3 was undetectable in 4E-BP1^{F113A}-treated in contrast to control mice (Supplementary Material, Fig. S2B).
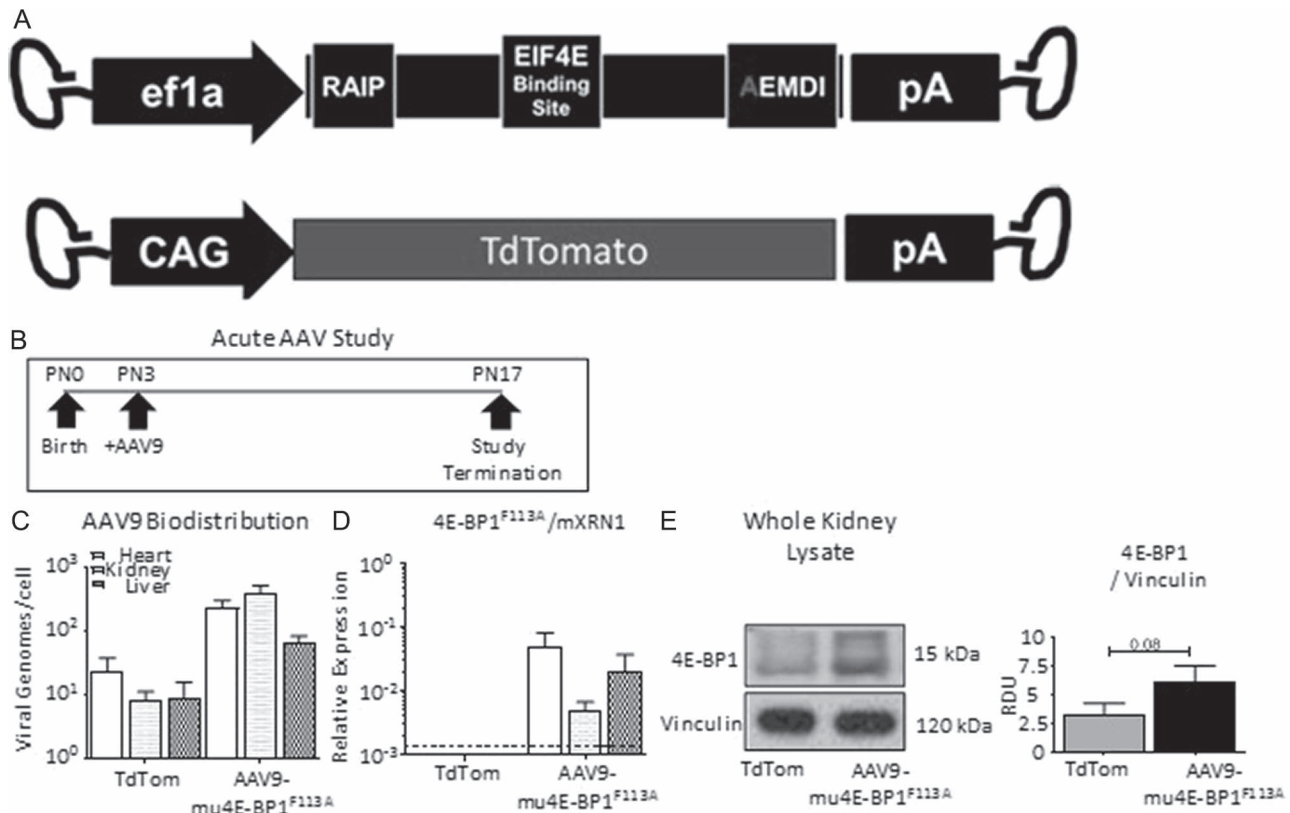
Figure 2. Acute exposure to 4E-BP1 FEMDI mutant *in vivo*. (**A**) Diagrams of AAV9-4E-BP1^{F113A} (F113A, $N = 12$) and AAV9-TdTomato (TdTom, $N = 3$) AAV vector genomes. (**B**) Study schematic. (**C**) Vector biodistribution in whole heart, kidney and liver homogenates. (**D**) Quantification of 4E-BP1^{F113A} expression in whole heart, kidney and liver homogenates. (**E**) Quantification and representative immunoblot of total 4E-BP1 protein in whole kidney homogenates corrected for by loading control vinculin. Single comparisons were made using Student's T test. Values are expressed as the mean ± SEM.

In summary, short-term exposure to 4E-BP1^{F113A} in WT mouse pups was found to be benign and resulted in vector genomes, vector-mediated 4E-BP1^{F113A} RNA and elevated 4E-BP1 protein within the kidneys of treated animals. Long-term studies in PKD animals achieved the same readouts: broad vector distribution, detectable vector-mediated RNA and elevated 4E-BP1 protein. However, long-term expression of 4E-BP1 FEMDI mutant, 4E-BP1^{F113A}, resulted in the worsening of PKD, a sizeable decline in the remaining functional parenchyma and elevated TKV. Increased disease burden was associated with increased cyst number and size, reduced TUNEL-positive cyst-lining cells and increased expression of the anti-apoptotic protein, Bcl-2, in whole kidneys of 4E-BP1^{F113A}-treated *Pkd1*$^{RC/RC}$ mice.

4E-BP1 ^{F113A} in *in vitro* ADPKD patient cell lines shifts cellular translation, increases proliferation and decreases apoptosis

Next, we examined the effect of HA-tagged 4E-BP1^{F113A} expression (Supplementary Material, Fig. S3A, HA-4E-BP1) in *PKD1*$^{+/+}$, *PKD1*$^{-/-}$ and two patient cyst-lining cells, Cyst 5 and Cyst 9. 4E-BP1^{F113A} expression resulted in both total and phosphorylated mTOR protein elevation (Fig. 4A) in the presence of 4E-BP1^{F113A} across genotype. However, the ratio of phosphorylated mTOR to total mTOR was not significantly elevated by densitometry (Fig. 4B). Further, a decrease in phosphorylated 4E-BP1 isoforms (Thr70, Thr37/Thr46 and Ser65) relative to total 4E-BP1 abundance was uniquely evident in PKD patient-derived cell lines with 4E-BP1^{F113A} expression (Fig. 4B). In addition, proliferation

marker, Ki-67, staining was significantly elevated in PKD patient-derived cell lines with 4E-BP1^{F113A} expression (Fig. 4C). Conversely, apoptosis marker, Apopxin, was significantly suppressed with 4E-BP1^{F113A} expression relative to control transduced *PKD1*$^{-/-}$, Cyst 5 and 9 cell lines (Fig. 4D). Apopxin staining in WT *PKD1*$^{+/+}$ was uninfluenced by 4E-BP1^{F113A}. Similarly, apoptosis indicated by Apopxin staining in PKD patient-derived cell lines trended to be elevated in contrast to *PKD1*$^{+/+}$. Anti-apoptotic protein Bcl-2 and phosphorylation of GSK-3β, a posttranslational modification associated with suppressed apoptosis (25,26), were both substantially augmented with 4E-BP1^{F113A} expression *in vitro* (Fig. 4E). There was an increase in both phospho and total S6K, confirming that mTOR activity was not increased (Fig. 4F).

These data indicate that 4E-BP1^{F113A} reduced the accumulation of different phosphorylated 4E-BP1 isoforms (relative to total 4E-BP1 expression) in PKD patient-derived cell lines. Further, 4E-BP1^{F113A} expression increased proliferation and substantially suppressed apoptosis signals in a genotype-dependent manner, mediating milder and largely insignificant changes to proliferation, and apoptosis in WT non-PKD cells, *PKD1*$^{+/+}$.

4E-BP1^{F113A} in *in vitro* disrupts NADPH oxidoreductase activity and increases mitochondrial superoxide production

To determine the mechanism through which 4E-BP1^{F113A} supported proliferation, we assessed NADPH oxidoreductase activity by MTT assay, a marker of cellular metabolism (27).
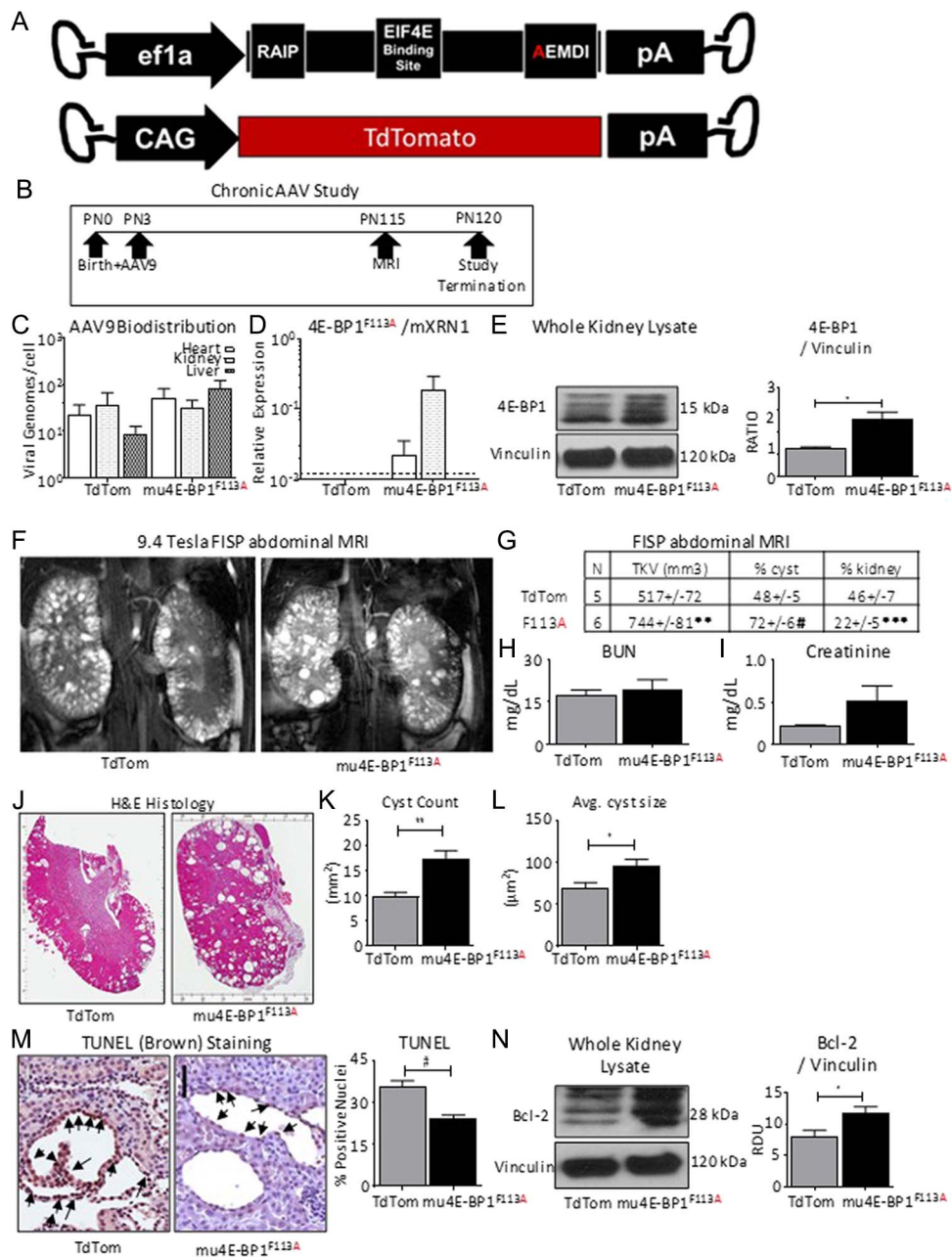
Figure 3. Chronic exposure to 4E-BP1 FEMDI mutant increases cyst burden *in vivo*. (**A**) Diagrams of AAV9-4E-BP1^F113A (F113A, $N = 6$) and AAV9-TdTomato (TdTom, $N = 5$). (**B**) Study schematic. (**C**) AAV biodistribution in whole heart, kidney and liver homogenates. (**D**) Quantification of 4E-BP1^F113A expression in whole heart, kidney and liver homogenates. (**E**) Quantification and representative immunoblot of total 4E-BP1 and loading control vinculin protein levels in whole kidney homogenates. (**F**) Representative FISP abdominal MRIs of 4E-BP1^F113A and TdTom treated *Pkd1*^RC/RC. (**G**) Quantification of total kidney volume (TKV), % of the kidney determined to be cystic by MRI (% cyst) or functional by MRI (% kidney). (**H**) Blood urea nitrogen (BUN), and (**I**) serum creatinine measurements of 4E-BP1^F113A (F113A, $N = 6$) and TdTomato (TdTom, $N = 5$) treated mice. (**J**) Representative hematoxylin & eosin (H&E) stained sections and (**K**) cystic indices quantified, such as Cyst count, and (**L**) average cyst size. (**M**) Immunohistochemistry staining of apoptosis marker, TUNEL, quantification specific to cells lining the cysts, and (**N**) immunoblotting of anti-apoptotic marker, Bcl-2, in whole kidney homogenates of treated and control *Pkd1*^RC/RC kidneys. Quantification of TUNEL is expressed as percent of nuclei staining positive per cyst. Black arrows indicate DAB+ staining. Scale bar = 50 μm. Single comparisons were made using Student's T test. Values are expressed as the mean ± SEM. *$P < 0.05$, **$P < 0.01$, ***$P < 0.001$, #$P < 0.0001$.

4E-BP1^F113A expression significantly suppressed NADPH flux in *PKD* patient-derived cell lines, *PKD1*^−/− and Cyst 5 (Fig. 5A). As suppressed NADPH oxidoreductase activity can be linked to decreased mitochondrial number or function (28), we quantified mitochondrial genomes. As anticipated, there were significantly decreased mitochondrial genomes present in *PKD1*^−/− cell lines relative to *PKD1*^+/+ cell lines, as previously demonstrated

(29). Secondly, 4E-BP1^F113A expression significantly increased mitochondrial biogenesis in PKD patient-derived cell lines (Fig. 5B), insignificantly augmenting the WT cell line, *PKD1*^+/+. Subsequently, we measured mitochondrial derived superoxide (O₂^−) production (MitoSOX), to assess oxidative stress secondary to mitochondrial function (30). MitoSOX measurements on *PKD1*^+/+, *PKD1*^−/− and Cyst 5 cell lines confirmed enhanced
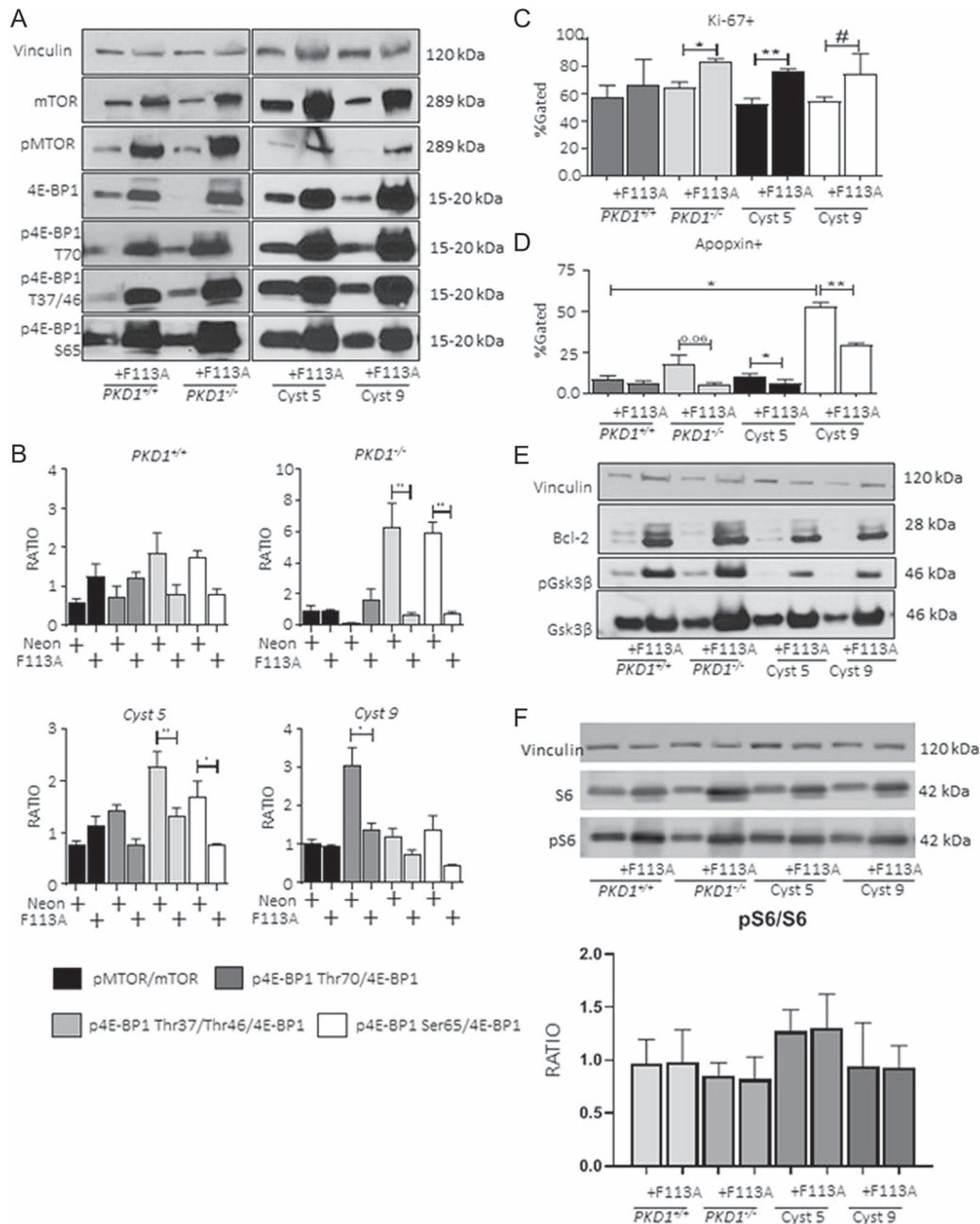
Figure 4. 4E-BP1^{F113A} *in vitro* promotes proliferation and retards apoptosis. PKD1$^{+/+}$, PKD1$^{-/-}$ and Human Cyst 5 and 9 were transduced with either control neon-expressing, or HA-tagged 4E-BP1^{F113A} constructs as described. (**A**) Loading control vinculin, total and phosphorylated mTOR and total and phosphorylated 4E-BP1 (Thr70, Thr37/Thr46 and Ser65) were detected and quantified (**B**) as the ratio of densitometry units for phosphorylated to total substrate abundance. (**C**) Proliferation marker (Ki-67), and (**D**) apoptosis marker (Apopxin) were assayed by flow cytometry. (**E**) Immunoblotting of anti-apoptotic proteins; Bcl-2, GSK3β (total, and phospho) were augmented in 4E-BP1^{F113A}-transduced cell lines. (**F**) Increase in both phospho and total S6K. Representative immunoblots reflect a minimum of six independent protein isolations from successive passages. Multiple comparisons were made using two-way ANOVA. Values are expressed as the mean ± SEM. *$P < 0.05$, **$P < 0.01$, ***$P < 0.001$, #$P < 0.0001$.

O$_2^-$ production in association with 4E-BP1^{F113A} expression (Fig. 5C). Lastly, we further interrogated the 4E-BP1^{F113A} *in vivo* study, specifically total kidney homogenates by proteomics, to determine if 4E-BP1^{F113A} affected metabolic pathways, as seen in the *in vitro* experiments (MTT, MitoSOX). A subset of kidneys from the chronic *Pkd1*$^{RC/RC}$ 4E-BP1^{F113A}-treated animals was submitted for proteomic analysis. The proteomic dataset generated revealed the top dysregulated proteins in

whole kidney homogenates of 4E-BP1^{F113A}-treated *Pkd1*$^{RC/RC}$ (F113A) to be enriched for mitochondrial proteins, relative to control treated (TdTom) littermates (Supplementary Material, Fig. S4A and B).

Immunoblot analysis of PKD1$^{+/+}$, PKD1$^{-/-}$ and two patient cyst-lining cells, Cyst 5 and Cyst 9, was performed for the top mitochondrial proteins that were increased in 4E-BP1^{F113A}-treated *Pkd1*$^{RC/RC}$ mouse kidneys. The mitochondrial proteins
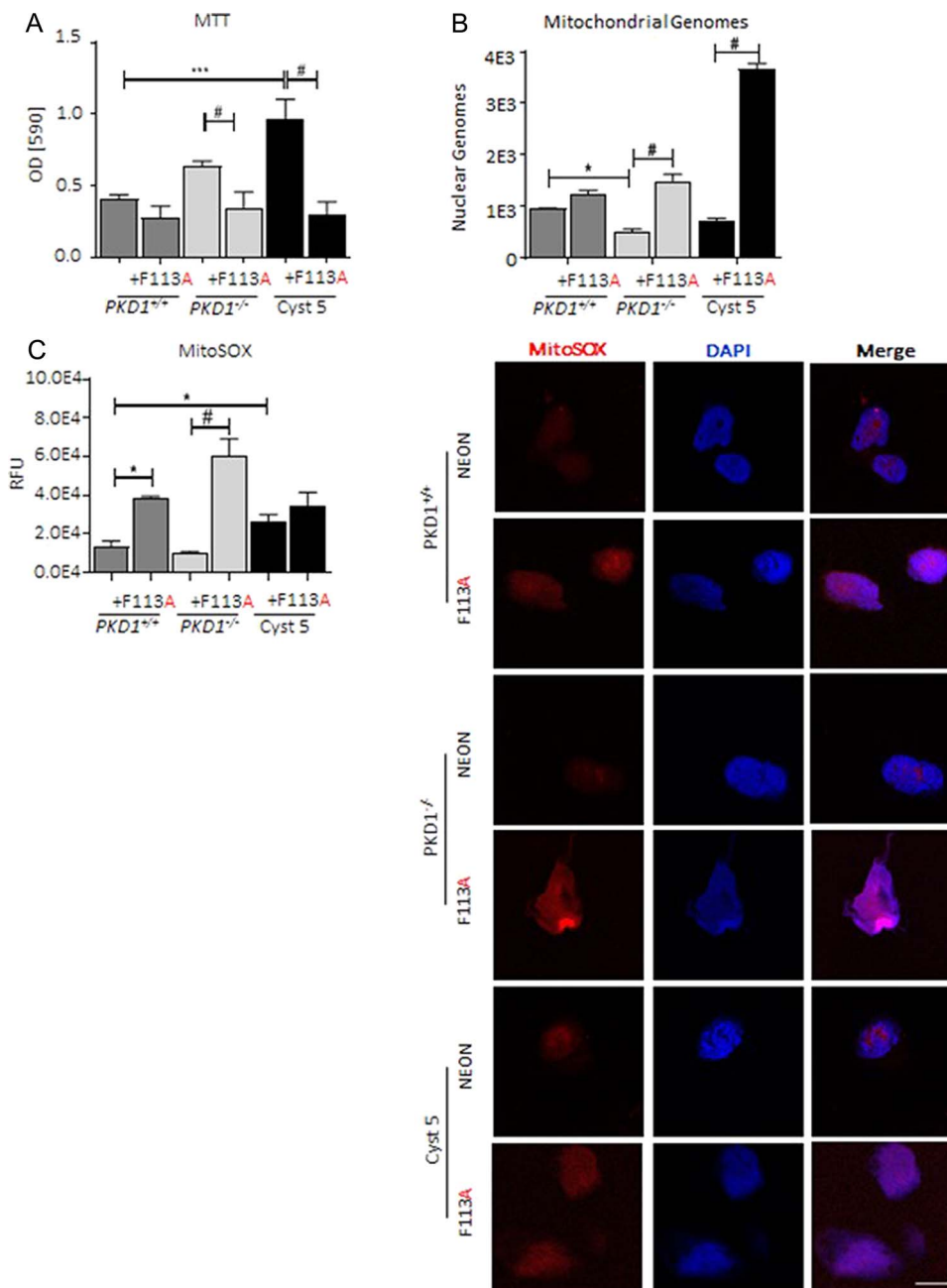
Figure 5. 4E-BP1[F113A] impairs cellular metabolism and increases mitochondrial stress *in vitro*. (**A**) MTT in control and FEMDI mutant 4E-BP1[F113A] transduced cell lines were measured in a minimum of three separate assays with each transduced cell line plated in replicates of 8. (**B**) Mitochondrial genomes were quantified by qPCR of 4E-BP1[F113A] and control transduced cell lines. Data graphed is mitochondrial encoded MT-TL1 DNA copy number, relative to nuclear encoded B2μGLBN DNA copy number. (**C**) Quantification and representative images of mitochondrial O_2^- (MitoSOX, Red, Nuclear co-stain, DAPI, Blue) in neon control and 4E-BP1[F113A]-transduced cell lines. Relative fluorescent unit (RFU) of MitoSOX staining. Scale bar (white): 20 μm. Multiple comparisons were made using two-way ANOVA. Values are expressed as the mean ± SEM. *$P < 0.05$, **$P < 0.01$, ***$P < 0.001$, #$P < 0.0001$.

that were increased in 4E-BP1 [F113A]-treated *Pkd1*[RC/RC] mouse kidneys (Supplementary Material, Fig. S4) were also increased in ADPKD patient-derived cells (Supplementary Material, Fig. S5).

These data indicate that 4E-BP1[F113A] expression in PKD cell lines impacts metabolic activity, enhances mitochondrial biogenesis and significantly increases mitochondrial-derived O_2^- production. Further, 4E-BP1[F113A] expression *in vivo* substantially increased PKD disease burden in association with substantially increased mitochondrial protein abundance within whole kidney homogenates, as demonstrated by the proteomics dataset.

mTOR does not drive proliferation or NADPH oxidoreductase activity in patient-derived cystic epithelial cells

The FEMDI motif, also known as TOS (mTOR recognition Sequence), is required for successful 4E-BP1-mTOR binding (16). To rule out mTOR as a mediator of 4E-BP1[F113A]-promoted proliferation, suppressed apoptosis and reduced NADPH oxidoreductase, cells were exposed to an mTOR inhibitor, sirolimus. Sirolimus reduced phosphorylation of mTOR and
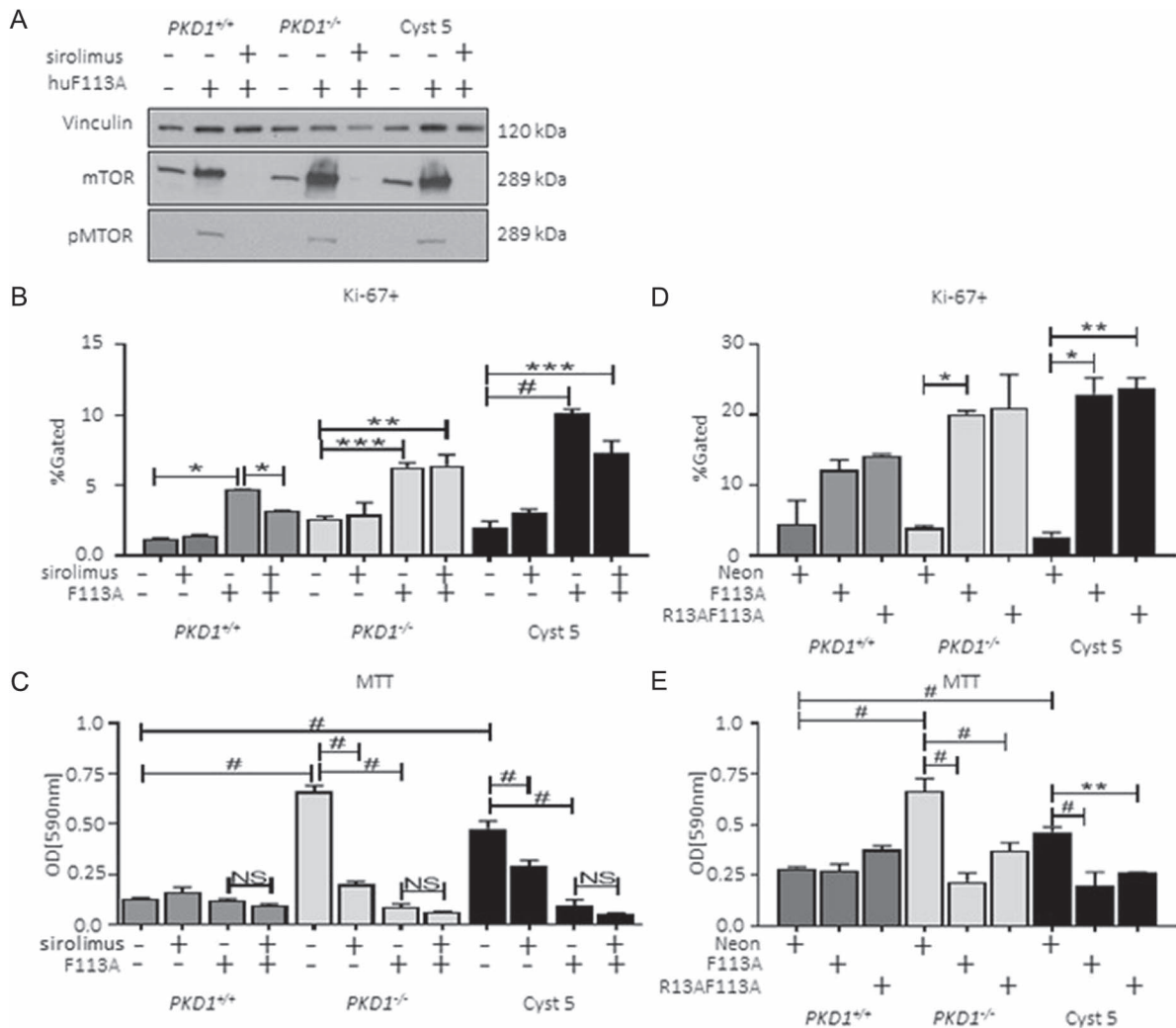
Figure 6. 4E-BP1 promoted proliferation and impaired cellular metabolism is kinase-independent in ADPKD patient-derived cystic epithelial cells. (**A**) 4E-BP1^{F113A} and control transduction cells were exposed to sirolimus and assayed by immunoblot for total and phosphorylated mTOR (Ser2448) and loading control vinculin. Under the same conditions (**B**) Ki-67+ and (**C**) MTT were assayed. Expression of pan-kinase blind 4E-BP1 (4E-BP1^{R13AF113A}) mirrored the results of 4E-BP1^{F113A}-transduced cell lines as demonstrated by (**D**) Ki-67+ and (**E**) MTT assays. MTT data is a minimum of three separate assays with each transduced cell line plated in replicates of 8. Flow data is a minimum of three independent experiments in duplicate. Multiple-group comparisons were performed using analysis of variance (ANOVA) with posttest according to Newman–Keuls. Values are expressed as the mean ± SEM. *$P < 0.05$, **$P < 0.01$, ***$P < 0.001$, #$P < 0.0001$.

total mTOR abundance (Fig. 6A) regardless of cell line genotype. Proliferation in PKD cell lines with 4E-BP1^{F113A} expression was insensitive to sirolimus treatment (Fig. 6B). Importantly, while mTOR activation and signaling was ablated, sirolimus was unable to rescue suppressed NADPH oxidoreductase activity, as assayed by MTT (Fig. 6C), in PKD patient-derived cells with 4E-BP1^{F113A} expression. These data demonstrate that 4E-BP1^{F113A} mediates an increase in proliferation marker, Ki-67, staining and suppresses NADPH oxidoreductase activity (MTT) independent of mTOR kinase activity in $PKD1^{-/-}$ cells.

As 4E-BP1^{F113A} maintains a functional RAIP motif, in order to rule out the involvement of 4E-BP1 regulation by RAIP-specific kinase activity, a pan-kinase-blind 4E-BP1 (4E-BP1^{R13AF113A}) was generated. 4E-BP1^{R13AF113A} expression in $PKD1^{+/+}$, $PKD1^{-/-}$ and Cyst 5 cell lines (Supplementary Material, Fig. S3B, HA-4E-BP1) resulted in elevated Ki-67 staining of PKD patient-derived cell lines (Fig. 6D) similar to 4E-BP1^{F113A} levels. Further, 4E-BP1^{R13AF113A} suppressed NADPH oxidoreductase activity similar to 4E-BP1^{F113A}, as assessed by MTT, relative to control transduction

cell lines (Fig. 6E). Again, exogenous 4E-BP1 construct-mediated changes were genotype-specific; WT $PKD1^{+/+}$ cells exhibited no significant augmentation to proliferation or metabolic activity in the presence of 4E-BP1^{R13AF113A} expression.

These data indicate that expression of 4E-BP1 constructs, with one or both KRDs mutated in $PKD1^{-/-}$ patient-derived cyst-lining cell lines, increases Ki-67 staining and suppresses NADPH oxidoreductase activity. Therefore, 4E-BP1, independent of kinase regulation, stimulates proliferation and suppresses apoptosis signaling in PKD renal epithelial cell lines.

4E-BP1 suppression reduces proliferation signals, NADPH oxidoreductase activity dysregulation, and mitochondrial superoxide production in patient-derived cystic epithelial cells

We determined the effect of reduced endogenous 4E-BP1 expression in $PKD1^{-/-}$ and $PKD1^{+/+}$ cells. shRNA targeting
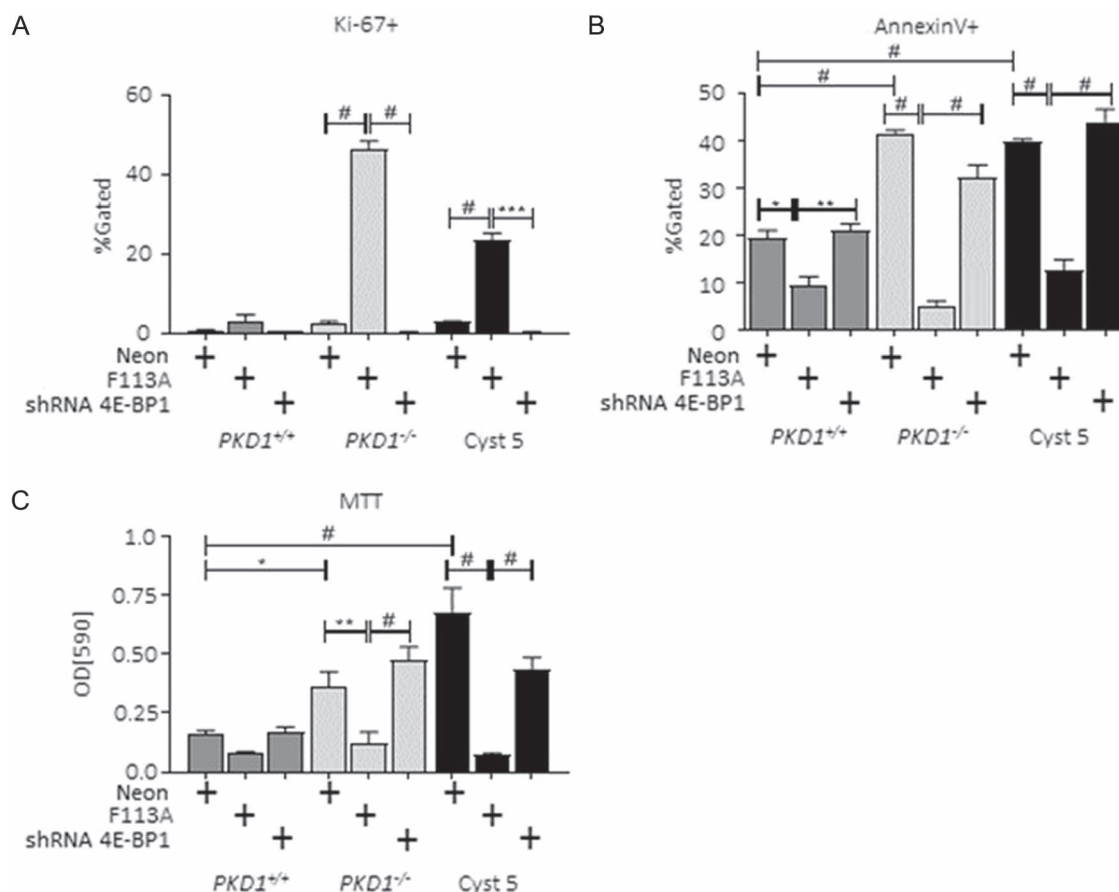
Figure 7. Reduced 4E-BP1 expression restores cellular metabolism, suppresses proliferation and restores apoptosis signaling in ADPKD *in vitro* models. $PKD1^{+/+}$, $PKD1^{-/-}$ and Human Cyst 5 were transduced with 4E-BP1 targeting shRNA. (**A**) Proliferation marker, Ki-67+, (**B**) apoptosis marker, Annexin V+, and (**C**) MTT assays were performed as described. Flow and luciferase expression data was generated in a minimum of three experiments. Multiple-group comparisons are performed using ANOVA with posttest according to Newman–Keuls. Values are expressed as the mean ± SEM. *$P < 0.05$, **$P < 0.01$, ***$P < 0.001$, #$P < 0.0001$. Not significant, NS.

4E-BP1 reduced total protein expression relative to control-transduced cell lines (Supplementary Material Fig. S3C, 4E-BP1^{shRNA}). Proliferation marker, Ki-67, staining was significantly reduced (Fig. 7A), and apoptosis marker, Annexin V (Fig. 7B), was elevated in PKD patient cyst-lining cell-derived lines ($PKD1^{-/-}$ and Cyst 5) transduced with 4E-BP1^{shRNA} relative to 4E-BP1^{F113A} transduction. Further, NADPH oxidoreductase activity, as assessed by MTT, was restored in 4E-BP1^{shRNA} PKD cell lines $PKD1^{-/-}$ and Cyst 5 (Fig. 7C).

Relative to 4E-BP1^{F113A}-transduced cell lines, 4E-BP1^{shRNA} significantly reduced mitochondrial O_2^- production (Fig. 8A) from the elevated production present in 4E-BP1^{F113A}-transduced cell lines. Further, 4E-BP1^{shRNA} restored the number of mitochondria present in transduced cells, relative to control transduction cell lines, as quantified by mitochondrial protein ACAA2 in $PKD1^{-/-}$ and $PKD1^{+/+}$ (Fig. 8B).

These data indicate that PKD cyst-lining cells may have a narrow range of tolerating 4E-BP1 expression, influencing proliferation, apoptosis, mitochondrial function and metabolic processes.

eIF4e suppression reduces NADPH oxidoreductase activity dysregulation and decreases protein synthesis in $PKD1^{-/-}$ cells

We determined the effect of reduced endogenous eIF4e expression in $PKD1^{-/-}$ cells. The siRNA targeting eIF4e reduced eIF4e protein expression (Supplementary Material, Fig. S6). The reduced NADPH oxidoreductase activity, as assessed by MTT, which was seen in 4E-BP1^{F113A}-transduced cell lines was restored in PKD cell lines treated with the eIF4e siRNA (Supplementary Material, Fig. S7).

Protein synthesis was increased in $PKD1^{-/-}$ cells in contrast to $PKD^{+/+}$ cells (Fig. 9). Both the 4E-BP1^{F113A} and the eIF4e siRNA resulted in a significant decrease in protein synthesis in $PKD1^{-/-}$ cells (Fig. 9).

Discussion

There is a relationship between polycystin1/2, mTOR and 4E-BP1. The carboxy terminal tail of PC-1 regulates mTOR signaling by altering the subcellular localization of tuberous sclerosis complex 2 (TSC2) tumor suppressor, a gatekeeper of mTOR activity, and deficiency of PC1 has been shown to activate mTOR (31). Thus, PC1 controls the mTOR/S6/4E-BP1 pathway in a TSC-2-dependent manner (32). Overexpression of PC1 in renal epithelial cells downregulates mTOR and decreases phosphorylation of 4E-BP1 (32). In Pkd1$^{-/-}$, but not pkd2$^{-/-}$ mouse embryonic fibroblasts (MEFs), there is upregulation of mTOR and phosphorylation of 4E-BP1 (32). Thus, a mutation in the Pkd1 gene would be expected to increase phosphorylation of 4E-BP1 as was seen in the *in vivo* and *in vitro* Pkd1 knockout models in this study.
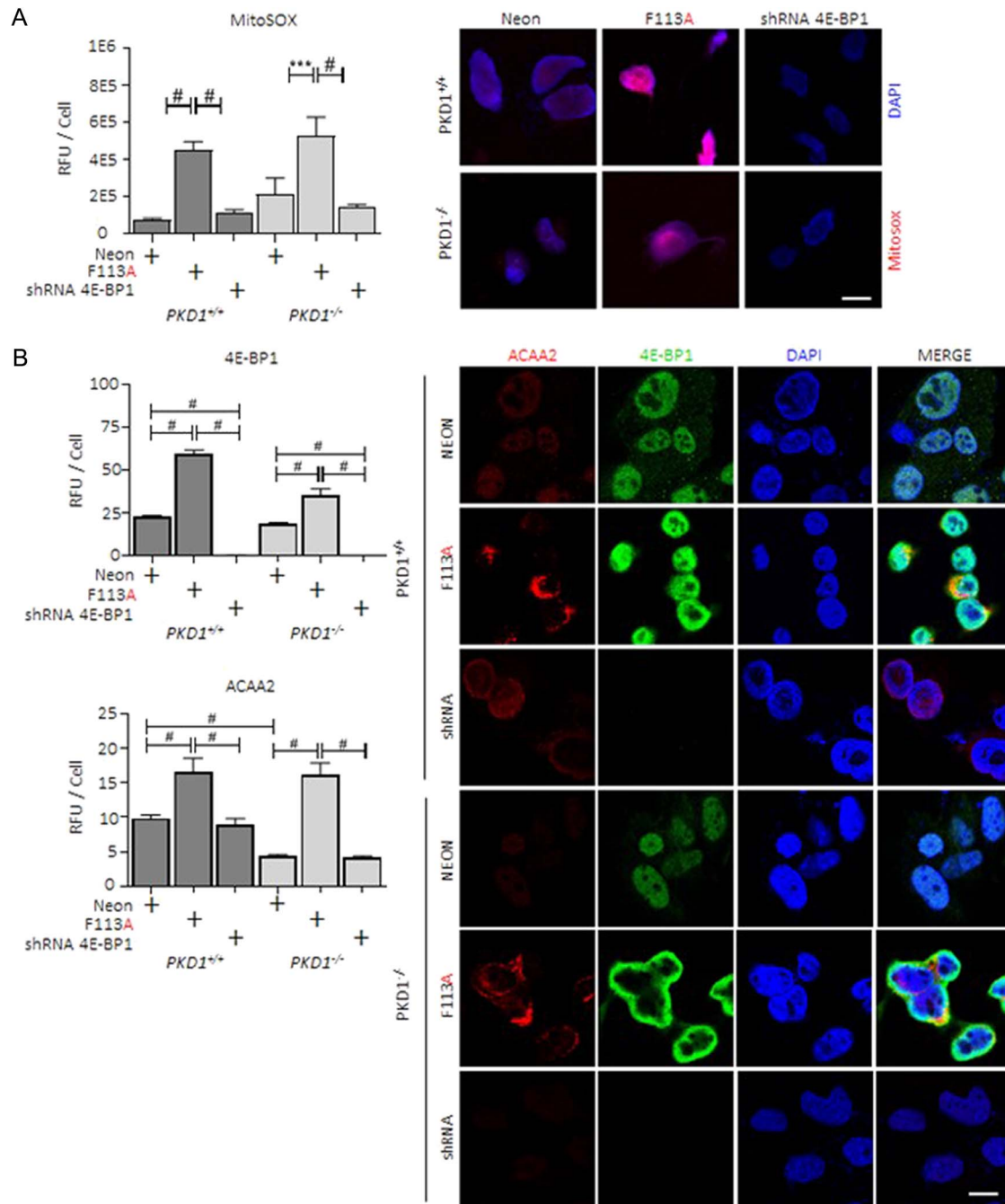
Figure 8. Reduced 4E-BP1 expression reduces mitochondrial superoxide production and mitochondrial biogenesis in ADPKD *in vitro* models. $PKD1^{+/+}$, $PKD1^{-/-}$ and Human Cyst 5 were transduced with 4E-BP1 targeting shRNA as described. (**A**) Mitochondrial O_2^- production (MitoSOX, Red, Nuclear co-stain DAPI, Blue) and (**B**) mitochondria quantification (ACAA2, Red; 4E-BP1, Green; Nuclear co-stain DAPI, Blue) were determined in neon, 4E-BP1^{F113A} and 4E-BP1^{shRNA}-transduced cell lines. Relative fluorescent unit (RFU). Scale bar (white): 20 μm. MitoSOX data was generated in a minimum of three experiments. Multiple-group comparisons are performed ANOVA with posttest according to Newman–Keuls. Values are expressed as the mean ± SEM. *$P < 0.05$, **$P < 0.01$, ***$P < 0.001$, #$P < 0.0001$. Not significant, NS.

The principal function of 4E-BP1 is translational repression, and loss of repression through hyperphosphorylation can push cells into an oncogenic and pro-proliferative phenotype (19). The demonstrated involvement of dysregulated 4E-BP1 in tumorigenesis, and the striking similarities between the pathobiology of cancer and ADPKD, informed the study hypothesis. Briefly, we hypothesized that increasing the pool of hypophosphorylated 4E-BP1 would impair cystic epithelial proliferation and cyst expansion. 4E-BP1 has two KRDs, RAIP and FEMDI. A wealth

of evidence indicates that mTOR, through the FEMDI motif (16), is a major factor in phospho-priming 4E-BP1 at Thr37 and Thr46. Phospho-priming and subsequent phosphorylation of 4E-BP1 causes release of 4E-BP1 from eIF4E (17) and thus promotes translation and proliferation. Further, phosphorylation at Thr46 has been shown to be sufficient in preventing eIF4E-4E-BP1 binding (33). Mutation of the essential Phe residue impairs the interaction of 4E-BP1 with mTOR and therefore eliminates the phospho-priming of 4E-BP1 (21). We hypothesized that
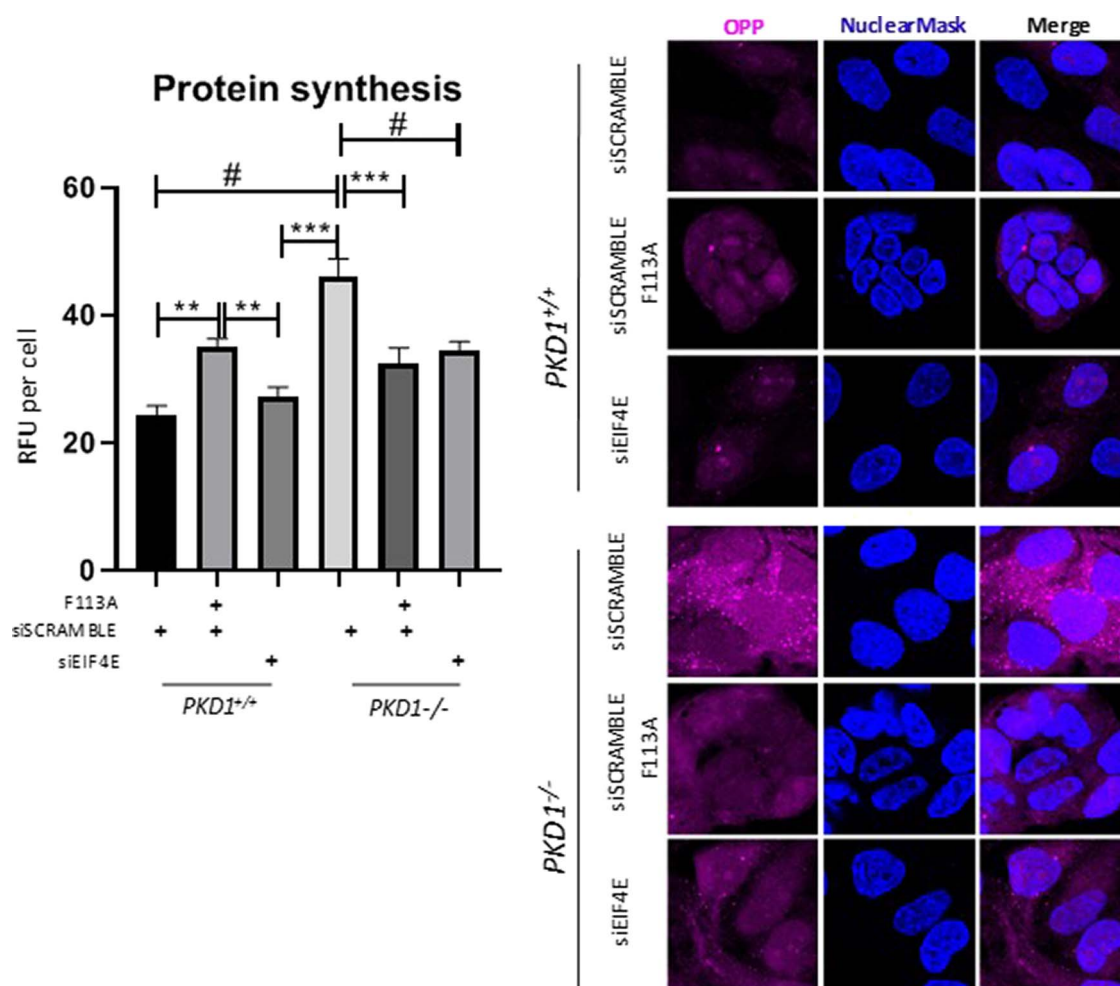
Figure 9. Protein synthesis was increased in $PKD1^{-/-}$ cells in contrast to $PKD1^{+/+}$ cells. Both the 4E-BP1^{F113A} and the eIF4e siRNA resulted in a significant decrease in protein synthesis in $PKD1^{-/-}$ cells. $PKD1^{+/+}$ and $PKD1^{-/-}$ cells were transduced with the 4E-BP1^{F113A} mutant or the eIF4e siRNA. Protein synthesis was measured using O-propargyl-puromycin (OPP)-based protein synthesis assay kit as described in the Methods section. Protein synthesis (OPP, purple; Nuclear co-stain DAPI, Blue) was determined in control (siScramble), 4E-BP1^{F113A} and eIF4e siRNA-transduced cell lines. Relative fluorescent unit (RFU). Multiple-group comparisons are performed ANOVA with posttest according to Newman–Keuls. Values are expressed as the mean ± SEM. $**P < 0.01$, $***P < 0.001$, $\#P < 0.0001$.

in PKD, expression of the FEMDI mutant, 4E-BP1^{F113A}, would therefore create an excess pool of 4E-BP1 in the cell, unable to be phospho-primed, and thus staving off decreased eIF4E binding. Further, by increasing the population of hypophosphorylated 4E-BP1, we hypothesized that the FEMDI mutant would suppress proliferation in cystic epithelial cells as has been shown in cancer (14,16).

We found that acute delivery of FEMDI mutant 4E-BP1^{F113A} in WT mouse pups was benign and resulted in detectable 4E-BP1^{F113A} RNA and elevated total 4E-BP1 protein. However, long-term 4E-BP1^{F113A} expression in $Pkd1^{RC/RC}$ resulted in worsened cyst burden. Aggravated disease progression was associated with reduced apoptosis signals (decreased TUNEL staining and increased Bcl-2 expression) and an enrichment in the kidney of dysregulated mitochondrial proteins, as revealed by proteomics (Supplementary Fig. S4A and B).

To determine the mechanism of how 4E-BP1 aggravated PKD *in vivo*, we performed *in vitro* studies expressing the FEMDI mutant, 4E-BP1^{F113A}. *In vitro*, 4E-BP1^{F113A} suppressed apoptosis and increased anti-apoptosis, Bcl-2, signaling.

In addition to supporting suppressed apoptosis signaling, 4E-BP1^{F113A} increased the expression of mTOR. Further, the increase

in phospho activation of mTOR with 4E-BP1^{F113A} transduction *in vitro* did not reach statistical significance. It is known that repressed protein synthesis can rapidly stimulate mTOR activation by a reduction in the cellular abundance of mTOR repressor proteins, such as tuberous sclerosis complex subunit 1 or 2 (Tsc1/2) (34) or Regulated in development and DNA damage response 1 (REDD1) expression (35).

In summary, we found that *in vitro* 4E-BP1^{F113A} transduction suppressed apoptosis and increased translation of mTOR and Bcl-2. Expression of FEMDI mutant, 4E-BP1^{F113A} increased the total abundance of 4E-BP1 detected *in vivo* and *in vitro* as anticipated.

Proteomic analysis of kidneys of $Pkd1^{RC/RC}$ 4E-BP1^{F113A}-treated animals revealed an enrichment of mitochondrial proteins (Supplementary Fig. S4A and B). *In vitro* 4E-BP1^{F113A} increased mitochondrial biogenesis and mitochondrial superoxide (O$_2^-$) production and increased the same mitochondrial proteins as seen on the proteomic analysis of $Pkd1^{RC/RC}$ 4E-BP1^{F113A}-treated animals. One explanation for the increase in mitochondrial biogenesis and O$_2^-$ production may be based on the mechanics of mitochondrial respiration. Specifically, 4E-BP1^{F113A} may have selectively increased the translation of mRNAs encoding compo-
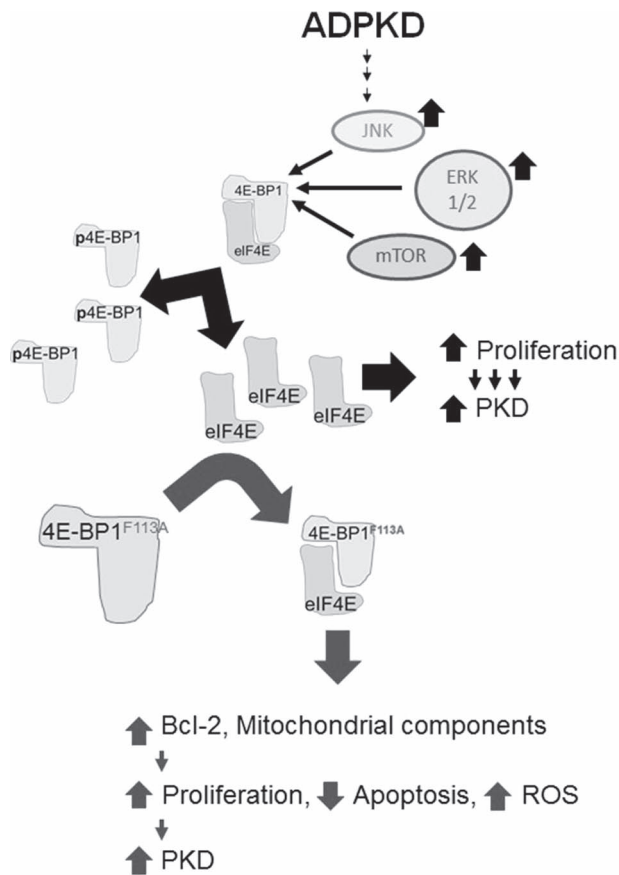
Figure 10. Summary slide. In PKD mouse, rat and human *in vitro* and *in vivo* models, regardless of precipitating genetic mutation, there is an increase in phosphorylated 4E-BP1. Excess phosphorylated 4E-BP1 increases the cellular bioavailability of eIF4E supporting hyperproliferation, and ultimately PKD progression. Expression of constitutively active FEMDI mutant 4E-BP1 decreased phosphorylated 4E-BP1 *in vivo* and *in vitro*. *In vitro*, exogenous 4E-BP1 expression resulted in hyperproliferative human ADPKD cyst-lining epithelial cell lines, increased anti-apoptotic Bcl-2 protein, suppressed apoptotic signals, increased O_2^- production and increased mitochondrial proteins. *In vivo*, there was worsening of PKD.

nents of complex V (such as Atp5f1, Supplementary Figs S4B and S5), or components of the mitochondrial respiratory chain (such as pyruvate kinase (36) and Sardh (37), Supplementary Figs S4B and S5) or global mitochondrial regulator TFAM (transcription factor A, mitochondrial) which in turn promotes the transcription of mRNAs responsible for (i) mitochondrial DNA replication and transcription (38) and (ii) mitochondrial ribosomal proteins (22). To this point, 4E-BPs have been shown to be major mediators of TFAM mRNA translation (22). The preferential synthesis of mitochondrial structural and functional proteins would therefore support the observations seen both *in vitro* and *in vivo* in datasets of increased biogenesis and increased mitochondrial O_2^- production, as a by-product of increased mitochondrial respiration.

While mTOR activity is well-known to be associated with increased proliferation, it is unlikely that mTOR or kinases endemic to cyst-derived cell lines are responsible for *in vitro* pro-proliferative phenotype, or *in vivo* enhanced cyst burden. This is based on the proliferative read-outs of our studies with (i) sirolimus-treated single KRD mutant 4E-BP1^{F113A} and (ii) transduction with double KRD mutant 4E-BP1^{R13AF113A}. We found

that sirolimus successfully reduced the phosphorylation of mTOR affected by 4E-BP1^{F113A} transduction. However, sirolimus was not able to substantially reduce proliferation in PKD cell lines in contrast to 4E-BP1^{F113A} transduction. Further, we performed studies with the pan-kinase blind 4E-BP1^{R13AF113A} transduced cell lines. As 4E-BP1^{R13AF113A} has no functional KRD, the resulting phenotype (increased proliferation, decreased metabolic activity) is kinase-independent and stems from excess 4E-BP1.

Importantly, both 4E-BP1 constructs, 4E-BP1^{F113A} and 4E-BP1^{R13AF113A}, exhibited suppressed NADPH oxidoreductase activity *in vitro*, a correlate for suppressed cellular metabolic activity. Reactive oxygen species (ROS), such as O_2^-, are produced as a consequence of normal mitochondrial respiration. However, in surplus, ROS and oxidative stress are considered driving forces for cancer development and progression (39,40). To this point, increased ROS has been linked to various metabolic stresses (41). Further, increased ROS production in non-polarized oncogenic epithelial cells enhances proliferation (42,43). We found that 4E-BP1 transduction resulted in an increase in ROS production, an increase in proliferation and a suppression of NADPH oxidoreductase activity, and conversely, these effects were reversed by reduced 4E-BP1 expression. As mitochondria lie at the nexus of the majority of biosynthetic pathways producing ROS and regulating proliferation (44), it is possible that 4E-BP1-enhanced mitochondrial biogenesis and respiration mediate both the suppression of cellular metabolic activity and enhanced cellular proliferation signaling in cells with increased expression of 4E-BP1.

Finally, we determined the effect of reduced 4E-BP1 expression in PKD patient cells. Reduced expression of 4E-BP1 in PKD patient cell lines resulted in an increase in apoptotic signals, suppressed proliferation, improved NADPH oxidoreductase activity and reduction in mitochondria and mitochondrial derived O_2^- production relative to 4E-BP1^{F113A} transduction. 4E-BP1 is implicated in the regulation of both metabolic and mitochondrial function in both *Drosophila* and mammals (45). In *Drosophila*, knockout of 4E-BP1 reduced mitochondrial Complex I activity (46). In mammals, Eif4ebp1$^{-/-}$ mice display an increase in metabolic rate, relative to Eif4ebp1$^{+/+}$ mice, demonstrating 4E-BP1 as a regulator of metabolism in mammals (47). Additionally, in prostate cancer, genetic deletion of 4E-BP1 significantly decreases proliferation and increases hypoxia-induced cell death, demonstrating the essential role of 4E-BP1 in cancer metabolism (48). Lastly, transgenic mice crossbred for cardiac-specific knockout of mTOR and whole-body knockout of 4E-BP1 (αMHC-MCM/*Mtor*$^{fl/fl}$/4E-BP1-KO) exhibited improved cardiac outcomes and survival in a heart failure model (49). RapaLink-1, a third-generation mTOR inhibitor, has demonstrated the most effective inhibition of p4E-BP1 in contrast to previous mTOR inhibitors (50). Thus, in the future, genetic or pharmacological studies with increased targeting of 4E-BP1 in PKD could potentially decrease proliferation, increase apoptosis and slow cyst growth.

PKD is a disease known for being driven by abnormal epithelial proliferation (6) and apoptosis (51). Mitochondrial abnormalities are known to facilitate cyst formation in ADPKD (29). In our *in vitro* studies, constitutively active 4E-BP1 suppressed apoptosis, increased proliferation, stimulated mitochondrial biogenesis and augmented superoxide production uniquely in a PKD genotype, largely leaving non-PKD cell lines uninfluenced. *In vivo*, constitutively active 4E-BP1 resulted in mitochondrial dysregulation and *worsened PKD disease*. Both *in vitro* and *in vivo*, the 4E-BP1^{F113A} mutant resulted in increased anti-apoptotic Bcl-

2 and an increase in mitochondrial proteins. These findings provide important insights into the role of 4E-BP1, Bcl-2 and mitochondrial proteins in PKD (Fig. 10).

In summary, we have provided the first evidence that 4E-BP1, independent of kinase regulation, in PKD patient-derived cells promotes mitochondrial biogenesis and $O_2{}^-$ production, which leads to the pro-survival phenotype observed (increased proliferation, suppressed apoptosis). These effects were largely insignificant in WT, non-PKD-derived renal epithelial cells. Our study provides the molecular framework behind the premise supporting future studies aimed at developing interventional approaches exploiting 4E-BP1 expression in PKD.

Materials and Methods

In vitro

Human primary immortalized cells and previously characterized cell lines, normal renal cortical tubular epithelium (RCTE, *PKD1*$^{+/+}$) and ADPKD cyst-lining epithelium (9–12, *PKD1*$^{-/-}$) immortalized with ori-adeno-SV40 viruses were cultured as previously described (52). Primary isolates from patients, known as Cyst 5 and 9, were a generous gift from Dr Woodward, Baltimore PKD Center. Cyst 5 and 9 isolates were received, recovered and immortalized with lentivectors expressing the large and small T antigens (SV40). Lentivectors were produced by standard triple transfection (Mirus) in 293Ts (generous gift from Dr James Morrison, UC Denver) and 0.45 μm filtered as previously described (53). Cell lines were transduced in six-well plates, with the following vectors: LV-EGFP:T2A:Puro-EF1A-3xHA CO-HU-4E-BP1R13AF113A, LV-mCherry:T2A:Puro-EF1A-3xHA CO-HU-4E-BP1F113A, LV-Puro-CBh-mNeonGreen, pLKO.1 eIF4EBP1 MISSION shRNA TRCN40203, Clone ID: NM_004095.2–489s1c1 (Sigma). Fluorescent protein, mCherry, eGFP or Neon expression was confirmed, and cells were expanded under 0.5–1.0 μg/mL puromycin selection. eIF4e si RNA studies: cell lines were transfected in six-well plates with a eIF4e siRNA from Santa Cruz Biotechnology (sc-35284) or a control siRNA that contains a scrambled sequence that does not lead to the specific degradation of any known cellular mRNA.(sc-37007) as described by the manufacturer. Absence of eIF4e protein was confirmed on immunofluorescence staining (Supplementary Material, Fig. S6). MTT to assay metabolic activity was performed as per manufacturer's instruction; briefly, 5000 cells were plated per well of a 96-well plate and then assayed for 3-[4,5-dimethyl-thiazol-2-yl]-2,5-diphenyl-tetrazolium bromide reduction. Optical density (OD) measurements were taken at 590 nm and the data graphed. Flow cytometry analysis of samples (Ki-67+, Annexin V+, Apopxin+) assays were carried out as per flow core and product protocols. Briefly, *in vitro* samples were harvested, washed with PBS, exposed to a binding buffer (0.1 M Hepes (pH 7.4), 1.4 M NaCl and 25 mM CaCl$_2$ solution), stained for membrane extracellular proteins (Annexin V+, Apopxin+), washed (400×g 5 min), fixed (2% PFA, 2% FBS), permeabilized (0.01% Triton-X), probed for intracellular proteins (Ki-67+), washed and resuspended in FACS buffer (2% FBS, 0.1% NaN$_3$, 1× PBS) until samples were run by The Rocky Mountain Regional VA Medical Center Flow Core. Mitochondrial and nuclear DNA quantitation: DNA was isolated (Qiagen), quantified by NanoDrop and assayed with RT^2 SYBR Green RT-PCR, as per manufacturer's guidelines, using primers against (Human) mitochondrial encoded MT-TL1 FWD CAC CCA AGA ACA GGG TTT GT, REV: TGG CCA TGG GTA TGT TGT TA and (Human) Nuclear encoded B2μGLBN (54), FWD: TGC TGT CTC

CAT GTT TGA TGT ATC T, REV: TCT CTG CTC CCC ACC TCT AAG T. Immunofluorescence protocol: Cells were plated in a four-well staining chamber at 100000 cells per well and allowed to adhere overnight. The following day, the cells were fixed in 4% paraformaldehyde, washed three times in PBS for 5 min each and incubated in blocking/permeabilization solution (0.1 M glycine, 5% bovine serum albumin, 0.1% Triton X-100 in PBS) for 1 h at room temperature. Next, the cells were incubated in primary antibodies ACAA2 (1:100, Abcam #ab128911) and 4E-BP1 (1:50, Thermo Fisher #AHO1382) overnight at 4°C. The next morning, the primary antibody was decanted, and the cells were washed three times in PBS for 5 min each. The cells were incubated in secondary antibodies Alexa Fluor555-conjugated anti-rabbit (11 000, Thermo Fisher #A-21428) and Alexa Fluor488-conjugated anti-mouse (11 000, Thermo Fisher #R37120) for 1 h at room temperature in the dark. The cells were washed 3 times in PBS for 5 min each. The slides were then cover-slipped with DAPI mounting media. Cells were imaged using a Zeiss 780 confocal scanning microscope. MitoSOX: cells were grown in four-well chamber slides to reach 90% confluency. The cells were washed with Hank's balanced salt solution (HBSS) once before adding 5 μm MitoSOX reagent. The cells were then incubated at 37°C for 10 min and then washed three times with warm HBSS. The cells were cover-slipped with DAPI mounting media and immediately analyzed for fluorescence. A Zeiss 780 confocal microscope was used to take at least three images of each cell type. One to five cells were quantified for red fluorescence per image using ImageJ. Protein synthesis was measured using the Click-iT® Plus O-propargyl-puromycin (OPP) protein synthesis assay kit as described by the manufacturer (Molecular Probes by Life Technologies Corporation, Catalog no. C10458).

In vivo

Renal tissues for histology were obtained from our colony: briefly, 90-day male Han:SPRD+/+ and Cy/+ rats, 120-day male and female *Pkd1*$^{+/+}$ and *Pkd1*$^{RC/RC}$ (for IHC quantification, $n > 10$ per genotype). Blinded (unknown age, sex, comorbidities) ADPKD ESRD patient ($n > 10$) paraffin-embedded tissues were obtained from the University of Denver, AMC PKD program (Dr Gitomer/Hopp). All mouse studies were carried out in the C57BL/6 strain. *Pkd1*$^{RC/RC}$ mice have a hypomorphic *Pkd1* gene mutation orthologous to PKD patient disease variant, *PKD1* p. R3277C (*Pkd1*$^{RC/RC}$) (55,56). Acute study: AAV vectors (AAV2-EF1A-CO-MU-4E-BP1F113A-pA and AAV2-CAG-TdTomato-pA) were produced by standard triple transfection (Mirus) in 293Ts and purified and titered as previously described (53,57,58). 1E9 AAV vectors were administered by intraperitoneal (IP) injection into three litters (15 total pups) of C57BL/6 pups at PN3. Animals were euthanized at PN17. Chronic study: 11 animals from four litters of *Pkd1*$^{RC/RC}$ pups were administered AAV vectors by IP on PN3, weaned at PN21 and aged to 120 days. Animals received FISP MRI measurements by UC Denver Small animal imaging core and euthanized, and tissues harvested. At study termination, blood urea nitrogen (BUN) was measured with a BioAssay Systems Urea Assay Kit (Hayward, CA, USA) according to manufacturer's instructions (DIUR-100). Serum creatinine was measured with HPLC tandem mass spectrometry (Applied Biosystems 3200 Qtrap). [^{2}H3] and creatinine were detected in multiple reaction-monitoring mode, examining transitions of m/z from 114 to 44.2 and from 117 to 47.2, respectively. DNA and RNA isolation of *in vivo* samples, specifically cardiac, renal and hepatic tissues, was carried out as per manufacturers'

protocols (Qiagen). qPCR assays were followed SYBR-based quantitative PCR protocol as detailed by Sigma-Aldrich. Briefly, 1 µg of RNA was synthesized into cDNA using cDNA synthesis kit (Quantabio), 2 µL of cDNA, 5 µM of forward and reverse primer and 7.5 µL 2× SYBR qPCR master mix were assayed per well of a 96-well plate. Samples were assayed in triplicate and assayed from each study animal. Cycling parameters included 10 min at 95°C, followed by 40 cycles of 94°C for 15 s, and 55°C for 30 s, with a terminal 4°C hold. Proteomics: kidneys were harvested at study termination by necropsy, snap-frozen, milled and lyophilized. Approximately 5 mg of each sample was subjected to sequential protein extraction resulting in a cellular and soluble ECM fraction as previously described (https://www.ncbi.nlm.nih.gov/pubmed/27693690). All fractions were reduced, alkylated and enzymatically digested with trypsin utilizing a filter-aided sample preparation protocol (https://www.ncbi.nlm.nih.gov/pubmed/28971683). Liquid chromatography tandem mass spectrometry (LC-MS/MS) was performed on a Thermo nanoEasy LC II coupled to a Q Exactive HF. MS acquisition parameters are detailed previously (https://www.ncbi.nlm.nih.gov/pubmed/30312994). Raw files were searched with Proteome Discoverer 2.2 against the *Mus musculus* uniprotKB database in Mascot. Precursor mass tolerance was set to $+/- 10$ ppm and MS/MS fragment ion tolerance of $+/- 25$ ppm. Trypsin specificity was selected allowing for one missed cleavage. Variable modifications include Met oxidation, proline hydroxylation, protein N-terminal acetylation, peptide N-terminal pyroglutamic acid formation and a fixed modification of Cys carbamidomethylation. Search results were visualized using MetaboAnalyst v4.0 (https://www.ncbi.nlm.nih.gov/pubmed/29955821). Immunoblot analysis: protein was isolated from cells and tissues using RIPA and a protease/phosphatase inhibitor cocktail. Homogenates were centrifuged, and supernatant was taken for protein analysis. Protein was quantified with Bio-Rad (Hercules, CA, USA) DC Protein Assay kit as described by the manufacturer. Samples were mixed with Laemmli Sample Buffer and boiled for 5 min. Samples were run on 4–20% precast polyacrylamide gels. Proteins were then transferred to PVDF membranes, blocked with 2.5% milk and probed with antibodies listed in Supplementary Material, Table S1. Blots were developed by chemiluminescence and analyzed for densitometry using ImageJ. Immunohistochemistry protocol: tissue sections were deparaffinized and rehydrated, then antigen unmasking was performed in sodium citrate buffer (pH 6.0) for 25 min at 100°C. After rinsing sections for 10 min in cold tap water, endogenous peroxidase activity was blocked by immersing the sections in 3% hydrogen peroxide for 10 min, followed by a 5-min rinse in deionized water. Blocking was performed using Vectastain® Elite® ABC Kit blocking serum for 30 min at room temperature. The primary antibodies were diluted in Tris-buffered saline with Tween 20 (TBST) as indicated in Supplementary Material, Table S1, and the sections were incubated overnight at 4°C in a humidified chamber. Immunoreactions were detected using the Vectastain standard protocol with 3,3′-diaminobenzidine tetrahydrochloride hydrate (DAB) counterstained with hematoxylin. Slides were subsequently dipped one to three times in 0.3% acid alcohol to lighten hematoxylin staining, then dehydrated and mounted. TUNEL staining was performed on tissue sections using a Promega DeadEnd™ Colorimetric Apoptosis Detection System Kit following the manufacturer's instructions. Quantitation of PCNA and TUNEL staining: the number of positive staining cells were counted using the Aperio ImageScope, Leica Biosystems, by an observer blinded to the treatment modality. Non-cystic tubules were defined as

tubules less than 50 µm diameter. Fifteen to 20 fields of view (40× magnification) devoid of cysts in the cortex per sample were randomly selected for non-cystic quantitation. To avoid sensitivity and selection artifacts between non-cystic tubules and dilated possibly pre-cystic tubules, as well as potential changes in tubular epithelium lining massive cysts, positive nuclei were counted in cysts of approximately 100–200 µm diameter. Fifty to 75 cysts in the cortex per tissue section were randomly selected for analysis.

Statistics

Multiple-group comparisons were performed using analysis of variance (ANOVA) with posttest according to Newman–Keuls. Single comparisons were made using Student's *T* test. A *P* value of <0.05 was considered statistically significant. Values are expressed as the mean $\pm$ SEM.

Study approval

All experiments were conducted with adherence to the National Institutes of Health Guide for the Care and Use of Laboratory Animals. The animal protocol was approved by the Animal Care and Use Committee of the University of Colorado at Denver. Mice were maintained on a standard diet, and water was freely available. As published, no difference was seen between male and female *Pkd1*^RC/RC in disease presentation; therefore, all study animals were included in statistical analyses.

Supplementary Material

Supplementary Material is available at *HMG* online.

References

1. Wilson, P.D. (2004) Polycystic kidney disease: new understanding in the pathogenesis. *Int J Biochem Cell Biol*, **36**(10), 1868–1873.
2. Hanahan, D. and Weinberg, R.A. (2011) Hallmarks of cancer: the next generation. *Cell*, **144**(5), 646–674.
3. Wallace, D.P., White, C., Savinkova, L., Nivens, E., Reif, G.A., Pinto, C.S., Raman, A., Parnell, S.C., Conway, S.J. and Fields, T.A. (2014) Periostin promotes renal cyst growth and interstitial fibrosis in polycystic kidney disease. *Kidney Int*, **85**(4), 845–854.

4. Parker, E., Newby, L.J., Sharpe, C.C., Rossetti, S., Streets, A.J., Harris, P.C., O'Hare, M.J. and Ong, A.C. (2007) Hyperproliferation of PKD1 cystic cells is induced by insulin-like growth factor-1 activation of the Ras/Raf signalling system. *Kidney Int*, **72**(2), 157–165.

5. Goilav, B. (2011) Apoptosis in polycystic kidney disease. *Biochim Biophys Acta*, **1812**(10), 1272–1280.

6. Nishio, S., Hatano, M., Nagata, M., Horie, S., Koike, T., Tokuhisa, T. and Mochizuki, T. (2005) Pkd1 regulates immortalized proliferation of renal tubular epithelial cells through p53 induction and JNK activation. *J Clin Invest*, **115**(4), 910–918.

7. Rowe, I., Chiaravalli, M., Mannella, V., Ulisse, V., Quilici, G., Pema, M., Song, X.W., Xu, H., Mari, S., Qian, F. *et al.* (2013) Defective glucose metabolism in polycystic kidney disease identifies a new therapeutic strategy. *Nat Med*, **19**(4), 488–493.

8. Mao, Z., Xie, G. and Ong, A.C. (2015) Metabolic abnormalities in autosomal dominant polycystic kidney disease. *Nephrol Dial Transplant*, **30**(2), 197–203.

9. Shibazaki, S., Yu, Z., Nishio, S., Tian, X., Thomson, R.B., Mitobe, M., Louvi, A., Velazquez, H., Ishibe, S., Cantley, L.G. *et al.* (2008) Cyst formation and activation of the extracellular regulated kinase pathway after kidney specific inactivation of Pkd1. *Hum Mol Genet*, **17**(11), 1505–1516.

10. Rousseau, D., Gingras, A.C., Pause, A. and Sonenberg, N. (1996) The eIF4E-binding proteins 1 and 2 are negative regulators of cell growth. *Oncogene*, **13**(11), 2415–2420.

11. Dowling, R.J., Topisirovic, I., Alain, T., Bidinosti, M., Fonseca, B.D., Petroulakis, E., Wang, X., Larsson, O., Selvaraj, A., Liu, Y. *et al.* (2010) mTORC1-mediated cell proliferation, but not cell growth, controlled by the 4E-BPs. *Science*, **328**(5982), 1172–1176.

12. Jiang, H., Coleman, J., Miskimins, R. and Miskimins, W.K. (2003) Expression of constitutively active 4EBP-1 enhances p27Kip1 expression and inhibits proliferation of MCF7 breast cancer cells. *Cancer Cell Int*, **3**(1), 2.

13. So, L., Lee, J., Palafox, M., Mallya, S., Woxland, C.G., Arguello, M., Truitt, M.L., Sonenberg, N., Ruggero, D. and Fruman, D.A. (2016) The 4E-BP-eIF4E axis promotes rapamycin-sensitive growth and proliferation in lymphocytes. *Sci Signal*, **9**(430), ra57.

14. Schalm, S.S., Fingar, D.C., Sabatini, D.M. and Blenis, J. (2003) TOS motif-mediated raptor binding regulates 4E-BP1 multisite phosphorylation and function. *Curr Biol*, **13**(10), 797–806.

15. Tee, A.R. and Proud, C.G. (2002) Caspase cleavage of initiation factor 4E-binding protein 1 yields a dominant inhibitor of cap-dependent translation and reveals a novel regulatory motif. *Mol Cell Biol*, **22**(6), 1674–1683.

16. Beugnet, A., Wang, X. and Proud, C.G. (2003) Target of rapamycin (TOR)-signaling and RAIP motifs play distinct roles in the mammalian TOR-dependent phosphorylation of initiation factor 4E-binding protein 1. *J Biol Chem*, **278**(42), 40717–40722.

17. Gingras, A.C., Raught, B., Gygi, S.P., Niedzwiecka, A., Miron, M., Burley, S.K., Polakiewicz, R.D., Wyslouch-Cieszynska, A., Aebersold, R. and Sonenberg, N. (2001) Hierarchical phosphorylation of the translation inhibitor 4E-BP1. *Genes Dev*, **15**(21), 2852–2864.

18. Showkat, M., Beigh, M.A. and Andrabi, K.I. (2014) mTOR signaling in protein translation regulation: implications in cancer genesis and therapeutic interventions. *Mol Biol Int*, **2014**, 686984.

19. Qin, X., Jiang, B. and Zhang, Y. (2016) 4E-BP1, a multifactor regulated multifunctional protein. *Cell Cycle*, **15**(6), 781–786.

20. Josse, L., Xie, J., Proud, C.G. and Smales, C.M. (2016) mTORC1 signalling and eIF4E/4E-BP1 translation initiation factor stoichiometry influence recombinant protein productivity from GS-CHOK1 cells. *Biochem J*, **473**(24), 4651–4664.

21. Schalm, S.S. and Blenis, J. (2002) Identification of a conserved motif required for mTOR signaling. *Curr Biol*, **12**(8), 632–639.

22. Morita, M., Gravel, S.P., Chenard, V., Sikstrom, K., Zheng, L., Alain, T., Gandin, V., Avizonis, D., Arguello, M., Zakaria, C. *et al.* (2013) mTORC1 controls mitochondrial activity and biogenesis through 4E-BP-dependent translational regulation. *Cell Metab*, **18**(5), 698–711.

23. Tsai, S., Sitzmann, J.M., Dastidar, S.G., Rodriguez, A.A., Vu, S.L., McDonald, C.E., Academia, E.C., O'Leary, M.N., Ashe, T.D., La Spada, A.R. *et al.* (2015) Muscle-specific 4E-BP1 signaling activation improves metabolic parameters during aging and obesity. *J Clin Invest*, **125**(8), 2952–2964.

24. de Stephanis, L., Bonon, A., Varani, K., Lanza, G., Gafa, R., Pinton, P., Pema, M., Somlo, S., Boletta, A. and Aguiari, G. (2017) Double inhibition of cAMP and mTOR signalling may potentiate the reduction of cell growth in ADPKD cells. *Clin Exp Nephrol*, **21**(2), 203–211.

25. Yin, H., Chao, L. and Chao, J. (2004) Adrenomedullin protects against myocardial apoptosis after ischemia/reperfusion through activation of Akt-GSK signaling. *Hypertension*, **43**(1), 109–116.

26. Mokhtari, B., Badalzadeh, R., Alihemmati, A. and Mohammadi, M. (2015) Phosphorylation of GSK-3beta and reduction of apoptosis as targets of troxerutin effect on reperfusion injury of diabetic myocardium. *Eur J Pharmacol*, **765**, 316–321.

27. Dias, N., Nicolau, A., Carvalho, G.S., Mota, M. and Lima, N. (1999) Miniaturization and application of the MTT assay to evaluate metabolic activity of protozoa in the presence of toxicants. *J Basic Microbiol*, **39**(2), 103–108.

28. Powelka, A.M., Seth, A., Virbasius, J.V., Kiskinis, E., Nicoloro, S.M., Guilherme, A., Tang, X., Straubhaar, J., Cherniack, A.D., Parker, M.G. *et al.* (2006) Suppression of oxidative metabolism and mitochondrial biogenesis by the transcriptional corepressor RIP140 in mouse adipocytes. *J Clin Invest*, **116**(1), 125–136.

29. Ishimoto, Y., Inagi, R., Yoshihara, D., Kugita, M., Nagao, S., Shimizu, A., Takeda, N., Wake, M., Honda, K., Zhou, J. *et al.* (2017) Mitochondrial abnormality facilitates cyst formation in autosomal dominant polycystic kidney disease. *Mol Cell Biol*.

30. Dikalov, S.I. and Harrison, D.G. (2014) Methods for detection of mitochondrial and cellular reactive oxygen species. *Antioxid Redox Signal*, **20**(2), 372–382.

31. Dere, R., Wilson, P.D., Sandford, R.N. and Walker, C.L. (2010) Carboxy terminal tail of polycystin-1 regulates localization of TSC2 to repress mTOR. *PLoS One*, **5**(2), e9239.

32. Distefano, G., Boca, M., Rowe, I., Wodarczyk, C., Ma, L., Piontek, K.B., Germino, G.G., Pandolfi, P.P. and Boletta, A. (2009) Polycystin-1 regulates extracellular signal-regulated kinase-dependent phosphorylation of tuberin to control cell size through mTOR and its downstream effectors S6K and 4EBP1. *Mol Cell Biol*, **29**(9), 2359–2371.

33. Livingstone, M. and Bidinosti, M. (2012) Rapamycin-insensitive mTORC1 activity controls eIF4E:4E-BP1 binding. *F1000Res*, **1**, 4.

34. Zhang, H., Cicchetti, G., Onda, H., Koon, H.B., Asrican, K., Bajraszewski, N., Vazquez, F., Carpenter, C.L. and Kwiatkowski, D.J. (2003) Loss of Tsc1/Tsc2 activates mTOR

and disrupts PI3K-Akt signaling through downregulation of PDGFR. *J Clin Invest*, **112**(8), 1223–1233.

35. Kimball, S.R., Do, A.N., Kutzler, L., Cavener, D.R. and Jefferson, L.S. (2008) Rapid turnover of the mTOR complex 1 (mTORC1) repressor REDD1 and activation of mTORC1 signaling following inhibition of protein synthesis. *J Biol Chem*, **283**(6), 3465–3475.

36. Chiavarina, B., Whitaker-Menezes, D., Martinez-Outschoorn, U.E., Witkiewicz, A.K., Birbe, R., Howell, A., Pestell, R.G., Smith, J., Daniel, R., Sotgia, F. *et al.* (2011) Pyruvate kinase expression (PKM1 and PKM2) in cancer-associated fibroblasts drives stromal nutrient production and tumor growth. *Cancer Biol Ther*, **12**(12), 1101–1113.

37. Hoskins, D.D. and Mackenzie, C.G. (1961) Solubilization and electron transfer flavoprtein requirement of mitochondrial sarcosine dehydrogenase and dimethylglycine dehydrogenase. *J Biol Chem*, **236**, 177–183.

38. Bonawitz, N.D., Clayton, D.A. and Shadel, G.S. (2006) Initiation and beyond: multiple functions of the human mitochondrial transcription machinery. *Mol Cell*, **24**(6), 813–825.

39. Cairns, R.A., Harris, I.S. and Mak, T.W. (2011) Regulation of cancer cell metabolism. *Nat Rev Cancer*, **11**(2), 85–95.

40. Kamp, D.W., Shacter, E. and Weitzman, S.A. (2011) Chronic inflammation and cancer: the role of the mitochondria. *Oncology (Williston Park)*, **25**(5), 400–410 413.

41. Liemburg-Apers, D.C., Willems, P.H., Koopman, W.J. and Grefte, S. (2015) Interactions between mitochondrial reactive oxygen species and cellular glucose metabolism. *Arch Toxicol*, **89**(8), 1209–1226.

42. Moreno-Sanchez, R., Rodriguez-Enriquez, S., Marin-Hernandez, A. and Saavedra, E. (2007) Energy metabolism in tumor cells. *FEBS J*, **274**(6), 1393–1418.

43. Liou, G.Y. and Storz, P. (2010) Reactive oxygen species in cancer. *Free Radic Res*, **44**(5), 479–496.

44. Antico Arciuch, V.G., Elguero, M.E., Poderoso, J.J. and Carreras, M.C. (2012) Mitochondrial regulation of cell cycle and proliferation. *Antioxid Redox Signal*, **16**(10), 1150–1180.

45. Goo, C.K., Lim, H.Y., Ho, Q.S., Too, H.P., Clement, M.V. and Wong, K.P. (2012) PTEN/Akt signaling controls mitochondrial respiratory capacity through 4E-BP1. *PLoS One*, **7**(9), e45806.

46. Zid, B.M., Rogers, A.N., Katewa, S.D., Vargas, M.A., Kolipinski, M.C., Lu, T.A., Benzer, S. and Kapahi, P. (2009) 4E-BP extends lifespan upon dietary restriction by enhancing mitochondrial activity in Drosophila. *Cell*, **139**(1), 149–160.

47. Tsukiyama-Kohara, K., Poulin, F., Kohara, M., DeMaria, C.T., Cheng, A., Wu, Z., Gingras, A.-C., Katsume, A., Elchebly, M., Spiegelman, B.M. *et al.* (2001) Adipose tissue reduction in mice lacking the translational inhibitor 4E-BP1. *Nature Medicine*, **7**, 1128.

48. Ding, M., Van der Kwast, T.H., Vellanki, R.N., Foltz, W.D., McKee, T.D., Sonenberg, N., Pandolfi, P.P., Koritzinsky, M. and Wouters, B.G. (2018) The mTOR targets 4E-BP1/2 restrain tumor growth and promote hypoxia tolerance in PTEN-driven prostate cancer. *Mol Cancer Res*, **16**(4), 682–695.

49. Zhang, D., Contu, R., Latronico, M.V., Zhang, J., Rizzi, R., Catalucci, D., Miyamoto, S., Huang, K., Ceci, M., Gu, Y. *et al.* (2010) MTORC1 regulates cardiac function and myocyte survival through 4E-BP1 inhibition in mice. *J Clin Invest*, **120**(8), 2805–2816.

50. Fan, Q., Aksoy, O., Wong, R.A., Ilkhanizadeh, S., Novotny, C.J., Gustafson, W.C., Truong, A.Y., Cayanan, G., Simonds, E.F., Haas-Kogan, D. *et al.* (2017) A kinase inhibitor targeted to mTORC1 drives regression in glioblastoma. *Cancer Cell*, **31**(3), 424–435.

51. Edelstein, C.L. (2005) What is the role of tubular epithelial cell apoptosis in polycystic kidney disease (PKD)? *Cell Cycle*, **4**(11), 1550–1554.

52. Loghman-Adham, M., Nauli, S.M., Soto, C.E., Kariuki, B. and Zhou, J. (2003) Immortalized epithelial cells from human autosomal dominant polycystic kidney cysts. *Am J Physiol Renal Physiol*, **285**(3), F397–F412.

53. Holditch, S.J., Schreiber, C.A., Harris, P.C., LaRusso, N.F., Ramirez-Alvarado, M., Cataliotti, A., Torres, V.E. and Ikeda, Y. (2017) B-type natriuretic peptide overexpression ameliorates hepatorenal fibrocystic disease in a rat model of polycystic kidney disease. *Kidney Int*, **92**(3), 657–668.

54. Rooney, J.P., Ryde, I.T., Sanders, L.H., Howlett, E.H., Colton, M.D., Germ, K.E., Mayer, G.D., Greenamyre, J.T. and Meyer, J.N. (2015) PCR based determination of mitochondrial DNA copy number in multiple species. *Methods Mol Biol*, **1241**, 23–38.

55. Hopp, K., Hommerding, C.J., Wang, X., Ye, H., Harris, P.C. and Torres, V.E. (2015) Tolvaptan plus pasireotide shows enhanced efficacy in a PKD1 model. *J Am Soc Nephrol*, **26**(1), 39–47.

56. Hopp, K., Ward, C.J., Hommerding, C.J., Nasr, S.H., Tuan, H.F., Gainullin, V.G., Rossetti, S., Torres, V.E. and Harris, P.C. (2012) Functional polycystin-1 dosage governs autosomal dominant polycystic kidney disease severity. *J Clin Invest*, **122**(11), 4257–4273.

57. Holditch SJ, Schreiber CA, Nini R, Tonne JM, Peng KW, Geurts A, Jacob HJ, Burnett JC, Cataliotti A, Ikeda Y: B-type natriuretic peptide deletion leads to progressive hypertension, associated organ damage, and reduced survival: novel model for human hypertension. *Hypertension* 2015, **66**(1): 199–210.

58. Holditch, S.J., Schreiber, C.A., Burnett, J.C. and Ikeda, Y. (2016) Arterial remodeling in B-type natriuretic peptide Knock-out females. *Sci Rep*, **6**, 25623.

ELSEVIER
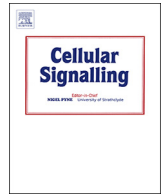
Apoptosis and autophagy in polycystic kidney disease (PKD)

Kristen L. Nowak, Charles L. Edelstein*

Division of Renal Diseases and Hypertension, Univ. of Colorado Anschutz Medical Campus, Aurora, CO, USA

ARTICLE INFO

ABSTRACT

Apoptosis in the cystic epithelium is observed in most rodent models of polycystic kidney disease (PKD) and in human autosomal dominant PKD (ADPKD). Apoptosis inhibition decreases cyst growth, whereas induction of apoptosis in the kidney of Bcl-2 deficient mice increases proliferation of the tubular epithelium and subsequent cyst formation. However, alternative evidence indicates that both induction of apoptosis as well as increased overall rates of apoptosis are associated with decreased cyst growth. Autophagic flux is suppressed in cell, zebra fish and mouse models of PKD and suppressed autophagy is known to be associated with increased apoptosis. There may be a link between apoptosis and autophagy in PKD. The mammalian target of rapamycin (mTOR), B-cell lymphoma 2 (Bcl-2) and caspase pathways that are known to be dysregulated in PKD, are also known to regulate both autophagy and apoptosis. Induction of autophagy in cell and zebrafish models of PKD results in suppression of apoptosis and reduced cyst growth supporting the hypothesis autophagy induction may have a therapeutic role in decreasing cyst growth, perhaps by decreasing apoptosis and proliferation in PKD. Future research is needed to evaluate the effects of direct autophagy inducers on apoptosis in rodent PKD models, as well as the cause and effect relationship between autophagy, apoptosis and cyst growth in PKD.

1. Introduction

ADPKD is the commonest life threatening hereditary disease often resulting in end stage kidney disease requiring dialysis and kidney transplantation [1]. Most ADPKD is caused by a mutation in either the Pkd1 gene (85% of cases) or the Pkd2 gene [2]. There are a multitude of signaling pathways that are either increased or decreased in PKD [3] [4] [5] [6]. Abnormal cross-talk between intracellular calcium and cAMP signaling is likely one of the first effects of PKD mutations and can result in increased proliferation of the tubular cells lining the cyst [3]. Protein kinase A-induced phosphorylation of cystic fibrosis transmembrane conductance regulator (CFTR) allows chloride and fluid secretion into the cysts and increases cyst growth [3]. Mammalian target of rapamycin (mTOR), that plays a role in both autophagy and apoptosis signaling, is increased in PKD kidneys [7]. mTOR inhibitors that protect against cyst growth in animal models [7] [8] are known to affect both autophagy and apoptosis. The Bcl-2 family of proteins that is dyregulated in PKD [9] [10] [11] also plays an important role in both apoptosis and autophagy signaling. Caspases, the major mediators of

apoptosis that can also affect autophagy are increased in PKD kidneys [12] [9] [13] [14]. Studies in Pkd1$^{-/-}$ cells [15], Pkd1$^{-/-}$ zebrafish [16] and mouse models of PKD [17] [18] [19] suggest that there may be a disturbance in the balance between tubular cell proliferation, apoptosis, and autophagy in PKD. This review will focus on the role of tubular cell apoptosis and autophagy in cyst growth in PKD and explore the possible interactions between apoptosis and autophagy in PKD.

2. Apoptosis

Apoptosis is a process of programmed cell death characterized by volume reduction, cell surface blebbing, chromatin condensation, internucleosomal cleavage of DNA, and formation of apoptotic bodies [20] [21] [22]. Apoptotic cells are quickly phagocytosed by macrophages to prevent the release of intracellular components and inflammatory factors, resulting in "clean" cell death. Lockshin & Williams [23] originally defined programmed cell death in the context of insect development. Subsequently, Kerr et al. noticed by ultrastructural analysis two morphologically different types of cell death in humans:

Table 1
Apoptosis of tubular cells lining the cyst is seen in most rodent models of PKD and in human PKD kidneys. Oak Ridge polycystic kidney (orpk), post natal (PN), Not applicable (NA)

Model	Inheritance	Gene	Characteristics	Ref
Male Han:SPRD rat	ADPKD	Anks6	Doubling kidney size and kidney failure by 8 wks of age. Apoptosis in cystic and non cystic tubules. Hypertension, anemia, ESRD	[12] [51]
pck rat	ADPKD	Pkhd1	Cysts in kidney and liver at 1 yr of age. Apoptosis in cystic and non cystic tubules.	[169]
C57Bl6 PKD1$^{RC/RC}$	ADPKD	Pkd1	Hypomorphic PKD1 gene knockout matching a human disease variant. Renal failure at 70 d of age. Apoptosis in cystic and non cystic tubules.	[37]
Pkd1$^{nl/nl}$ mice	ADPKD	Pkd1	Apoptosis induced in cystic epithelium by smac-mimetic	[90]
PKD2$^{WS25-/-}$ mice	ADPKD	Pkd2	PKD and renal failure at 16 wks of age. Apoptosis in cystic epithelium and caspase-3 activity not affected by sirolimus.	[33]
orpk mouse	ARPKD	Ift88^{Tg737Rpw}	Ciliary defect model of ARPKD. Sirolimus increases apoptosis in cystic epithelial cells.	[8]
C57Bl6 jck mouse	ARPKD	Nphp9	Mutated gene product in primary cilia affects normal expression of PC1/2. High rate of epithelial cell proliferation and apoptosis in cystic epithelium	[170]
cpk mouse	ARPKD	Cys1	Lifespan 4-6 weeks. Apoptosis of tubular and interstitial cells. Deletion of caspase-3 gene increases lifespan.	[14]
pcy mouse	ADPKD	Nphp3	Orthologous to adolescent nephronophthisis. Apoptotic DNA fragmentation evident in preuremic kidneys.	[27]
SBM mice	ADPKD	c-myc	Overexpression of c-myc. Tubular apoptosis increased 3-9 -fold over controls.	[95] [104] [96]
AP-2 β$^{-/-}$knockout mice	NA	AP-2 β	Mice lack transcription factor AP-2 β die at PN day 1-2 from PKD. Enhanced apoptotic cell death of renal epithelial cells.	[171]
Bcl-2$^{-/-}$ mice	NA	Bcl-2	Knockout of anti-apoptotic Bcl-2. Fulminant lymphoid apoptosis, polycystic kidneys, and hypopigmented hair. Apoptosis in kidney interstitium.	[50]
Dysplastic human renal disease	NA	NA	Cell death prominent in undifferentiated cells around dysplastic tubules and occasionally cystic epithelia	[172]
Human kidneys	ADPKD	Pkd1/2	Apoptotic cells in glomeruli, cyst walls, cystic and noncystic tubules regardless of renal function	[27]
Human kidneys	ARPKD	Pkhd1	Apoptosis more prevalent in human ARPKD kidneys than in age-matched normal kidneys	[911] [173]

apoptosis and necrosis [24]. In necrosis, the cells swell, plasma membranes rupture, and cellular components are released. In apoptosis, the cells shrink with intact plasma membranes, and nuclei are condensed and fragmented. As apoptosis was discovered to be mediated by gene products, it was termed as being programmed. Thus, the term programmed cell death has been used in the context of apoptosis. It should be noted that cell death with a necrotic morphology that occurs during inflammation or infection can also be programmed or regulated by gene products, and is categorized as necroptosis and pyroptosis [25] [26].

3. Apoptosis in PKD

Apoptosis in the tubular epithelial cells lining the cyst and/or non-cystic tubular epithelium in PKD kidneys is observed in most rodent models of PKD, regardless of the genetic defect (Table 1).

Apoptosis has also been detected in human ADPKD kidneys compared to normal kidneys, regardless of renal function [27] (Table 1). Specifically, apoptosis is evident in normal non cystic tubular epithelium in human polycystic kidneys from non-uremic ADPKD patients [27].

As apoptosis in renal tubular epithelium is detected in most models of PKD resulting from differing gene defects, it is unlikely that the Pkd1 or Pkd2 gene defect directly causes apoptosis.

mTOR, which exists in association with two different complexes, mTORC1 and mTORC2, may provide the link between cyst growth and apoptosis in diverse models of PKD [28] [29]. mTORC1 consists of mTOR and regulatory associated protein of mTOR (Raptor), while mTORC2 consists of mTOR and rapamycin-independent companion of mTOR (Rictor) [29]. mTOR is known to regulate apoptosis and proliferation [30]. Increased mTOR signaling is an almost universal phenomenon in PKD kidneys from different gene defects. Increased mTORC1 signaling has been observed in many rodent models of PKD [12] [31] [32] [8] [33] and in human ARPKD kidneys [34] [35]. Both mTORC1 and 2 signaling are increased in mouse models of PKD [36] [37]. The effects of mTORC1/2 inhibition on apoptosis in PKD models will be discussed later in this review.

4. Pathways of caspase-mediated apoptosis in PKD

A family of cysteine proteases, known as caspases, are the major mediators of apoptosis. The caspase pathways that are centrally important in apoptosis involve the "initiator" caspases-8 and -9 and the "executioner" caspases-3 and -7 [38] [39] [40]. Caspase-3 plays a crucial and extensively studied role in the promotion of apoptosis [41] [42] [43]. Caspase-3 terminates contacts with surrounding cells, reorganizes the cytoskeleton, shuts down DNA replication, interrupts splicing, destroys DNA, disrupts the nuclear structure, marks the cell for phagocytosis, and disintegrates the cell into apoptotic bodies [44] [45].

There are two major pathways of caspase-mediated apoptosis [39][20]. In the mitochondrial or "intrinsic" pathway, stress-induced signals act via Bcl-2 proteins to promote cytochrome c release from mitochondria [46] [47]. Cytochrome c binds to the cytosolic protein Apaf-1 to facilitate the formation of an apoptosome. Once formed, the apoptosome can then recruit and activate caspase-9, that can in turn activate caspase-3. In support of a role of the Bcl-2 protein family in PKD, Bcl-2 deficient mice have increased apoptosis and die from severe PKD [48] [49] [50]. Activation of caspase-3 and dysregulation of the balance between pro- and anti-apoptotic Bcl-2 family members, specifically a downregulation of anti-apoptotic Bcl-X$_L$, correlates with increased apoptosis in polycystic Han:SPRD rat kidneys [9]. In Han:SPRD rat kidneys, the pro form of caspase-9, cytochrome c release into the cytosol, and caspase-2 protein and activity are increased, demonstrating involvement of the intrinsic pathway [51]. In the "extrinsic" pathway, the binding of a ligand to its death receptor recruits an adaptor protein that in turn recruits and activates procaspase-8, which subsequently activates caspase-3 [52]. The proform of caspase-8 is also

Table 2
Effects of treatments on apoptosis/autophagy and PKD.

Treatment	In vivo model	Effect on apoptosis	Effect on autophagy	Effect on PKD	Ref
Cell cycle inhibitor, roscovitine	jck, cpk mice	Decreased	ND	Long-lasting arrest of cystogenesis	[58] [59].
Hydroxyestradiol (2-OHE)	Han: SPRD rat	Decreased	ND	Decreased cyst growth	[61].
GlcCer synthase inhibitor, Genz-123346	jck and pcy mice	Decreased	ND.	Decreased cyst growth	[62]
Immunodepletion of CD8 + T cells	C57BL/6 Pkd1 RC/RC mice	Decreased	ND	Worsening	[63]
Caspase inhibitor, IDN-8050	Han:SPRD rat	Decreased apoptosis and proliferation	ND	Decreased cyst growth	[12]
MIF inhibitor ISO-1	Pkd1-/- mice	Increased	ND	Delays cyst growth	[67]
High dose sirolimus	Pkd1-/-, orpk mice	Increased	ND	Decreased cyst growth	[8] [69] [70]
Low dose sirolimus	Pkd2 WS25/- mice	No effect	ND	Decreased cyst growth	[33]
mTOR kinase inhibitor, torin-2	Pkd1 RC/RC mice	Increased	ND	Decreased cyst growth	[37]
mTOR kinase inhibitor, PP242	Han:SPRD rat	No effect	ND	Decreased cyst growth	[71]
mTOR ASO	Pkd2 WS25/- mice	Decreased	ND	Decreased cyst growth	[36].
Smac-mimetic	Pkd1-/- mice	Increased TNF-α-dependent apoptosis	ND	Delays cyst growth	[90]
Bafilomycin	cpk mice	ND	Decreased	ND	[17]
Autophagy inducer: Trehalose	Hypomorphic Pkd1-/- mice	ND	No effect on suppressed autophagy	No effect	[18]
Caloric restriction mimetic, 2DG	Pkd1-/- mice	ND	ND	Delays cyst growth	[160] [161] [15]
Saikosaponin-d (SSd), a SERCA inhibitor	UCL93, OX161 ADPKD cells. MDCK cells	ND	Increased	Decreased	[164]
Glucose deprivation	Pkd1-/- cells	Increased	Decreased. Rescued by sirolimus	ND	[15]
Autophagy activators: Beclin-1, sirolimus, carbamazepine and minoxidil	Zebrafish pkd1a mutants	Decreased	Increased	Decreased cysts	[16]
Metformin	Zebrafish pkd2 mutants	ND	Increased	Decreased cysts	[118]
HDACi, Trichostatin A	Pkd1-/- cells	ND	Increased	Prevents cyst formation	[165]

Not determined (ND), glucosylceramine (GlcCer), antisense oligonucleotide (ASO), macrophage migration inhibitory factor (MIF-1), 2-deoxy-glucose (2DG), second mitochondria-derived activator of caspase (Smac), Madin-Darby canine kidney cells (MDCK), Sarcoplasmic/endoplasmic reticulum Ca2 + ATPase pump (SERCA).

increased in PKD, demonstrating involvement of the extrinsic pathway [51]. No differences in Fas ligand (FasL) mRNA are observed, suggesting that the extrinsic pathway is independent of the death receptor ligand, FasL [51].

5. Relationship between apoptosis and cyst growth in PKD

Apoptosis may be causally linked to the development of renal cystic disease. For example, apoptosis is essential for Madin-Darby canine kidney (MDCK) cell cyst cavitation in collagen type 1 matrix. Cystogenesis in this system is inhibited by overexpression of the anti-apoptotic gene, Bcl-2 [53]. In a novel cell culture system for studying how PKD1 regulates apoptosis, proliferation and cyst formation, expression of human PKD1 in MDCK cells slows their growth and protects them from apoptosis [54]. MDCK cells expressing PKD1 also spontaneously form branching tubules, while control cells form simple cysts. Thus, PKD1 may function to regulate both apoptosis and proliferation pathways, allowing cells to enter a differentiation pathway that results in tubule formation. Collectively, this provides evidence that polycystin-1 (PC-1) may inhibit apoptosis, and confirms that increased apoptosis is associated with cyst formation in MDCK cells. Similarly, inhibition of fibrocystin (the gene product of PKHD1 that is responsible for autosomal recessive PKD) by short hairpin RNA inhibition in inner medullary collecting duct cells disrupts normal tubulomorphogenesis and results in increased apoptosis and proliferation [55].

Y528C and R1942H are two missense mutations that have been identified from a PKD1-affected individual. MDCK cells expressing the Y528C variant form cysts in culture and display increased rates of growth and apoptosis compared to MDCK cells stably expressing the wild-type [56]. The protein product of PKD1 (PC-1) is a large transmembrane protein with a short intracellular C terminus that interacts with numerous signaling molecules, including Galpha(12). G12/G13 alpha subunits are alpha subunits of heterotrimeric G proteins. MDCK cells can increase apoptosis via Galpha(12) stimulation of JNK and degradation of the anti-apoptotic protein Bcl-2, with PC1 expression levels determining the activity of the JNK/Bcl-2 apoptosis pathway [57]. Thus, there appears to be a causal relationship between apoptosis, proliferation and cyst formation. In summary, most (but not all) *in vitro* studies in PKD cells support that increased levels of apoptosis are associated with formation and growth of cysts. Next, the effect of therapies that decrease cyst growth *in vivo* on apoptosis will be discussed.

6. The effect of therapies that decrease cyst growth on apoptosis in vivo (Table 2)

Therapies that decrease cyst growth in PKD have variable effects on apoptosis. Some therapies that decrease cyst growth also decrease apoptosis. The cell cycle inhibitor roscovitine results in long-lasting arrest of cystogenesis, along with decreased apoptosis [58] [59]. Erb-b2 receptor tyrosine kinase 4 (ErbB4) is a receptor tyrosine kinase and member of the epidermal growth factor receptor family that is highly expressed in cystic kidneys. In cpk mice, ErbB4 deletion results in accelerated cyst progression, renal function deterioration, increased cell proliferation in the cyst-lining epithelial cells, and significantly more apoptotic cells. This is associated with decreased levels of cyclin D1, increased levels of p21, p27, and cleaved caspase 3, suggesting that decreased cell cycle progression may contribute to apoptosis [60]. Similarly, in Han:SPRD rats treated with 2-hydroxyestradiol (2-OHE), the resultant decrease in cyst growth and preservation of kidney function is associated with suppression of proliferation, apoptosis, and markers of angiogenesis [61]. Sphingolipids and glycosphingolipids are emerging as major regulators of proliferation, apoptosis, and activation of growth regulatory pathways. Blockade of glucosylceramide (GlcCer; a glycosphingolipid) accumulation with the GlcCer synthase inhibitor Genz-123346 effectively inhibits cystogenesis in Pkd1 conditional knockout mice and jck and pcy mouse models of nephronophthisis [62].

Mechanism-of-action studies suggest that GlcCer synthase inhibition results in effective cell cycle arrest and inhibition of the Akt-mTOR pathway, ultimately leading to decreased apoptosis and mitogenic signaling [62]. Of note, enrollment in a phase II/III trial in adults with ADPKD evaluating the efficacy of Venglustat, which reduces accumulation of GlcCer, is ongoing (NCT03523728).

In contrast, some therapies that decrease cyst growth can increase apoptosis; likewise, worsening ADPKD may associate with reduced apoptosis. Immunodepletion of CD8+ T cells from one to three months in C57Bl/6 Pkd1$^{RC/RC}$ mice results in worsening of ADPKD pathology, decreased apoptosis, and increased proliferation compared to IgG-control, consistent with a reno-protective role of CD8+ T cells [63]. microRNAs (miRNAs) are short noncoding RNAs that function as sequence-specific inhibitors of gene expression [64]. The miR-17 family and miR-21 are both upregulated in kidney cysts and promote ADPKD progression in mouse models. miR-21 represses proapoptotic genes and thus inhibits cyst apoptosis and promotes PKD progression [65]. Overexpression of exogenous kidney-specific neutrophil gelatinase-associated lipocalin (Ngal) attenuates progressive cyst development and prolongs lifespan in a murine model of PKD, which is associated with reductions in interstitial fibrosis and proliferation and augmented apoptosis [66]. Macrophage migration inhibitory factor (MIF) is another important regulator of cyst growth in ADPKD. MIF is upregulated in cyst-lining epithelial cells in PC-1-deficient murine kidneys and accumulates in cyst fluid of human ADPKD kidneys [67]. MIF regulates cystic renal epithelial cell apoptosis through p53-dependent signaling. MIF deletion or pharmacologic inhibition of MIF delays cyst growth and increases p53-dependent apoptosis in multiple murine ADPKD models [67].

Sirolimus is an autophagy inducer, but its effects on apoptosis in PKD are complex [68]. The effect of sirolimus on apoptosis in PKD may be determined by the dose. High-dose sirolimus increases apoptosis of cyst lining epithelium in PKD [8] [69] [70]. However, low-dose sirolimus may also result in effective blockade of PKD without an effect on apoptosis [33]. Thus, an appropriate therapeutic dose of sirolimus may not have an effect on apoptosis in PKD. Furthermore, the effect of mTOR inhibitors on apoptosis may depend on whether there is dual blockade of both mTORC1 and 2. The mTOR kinase inhibitor, torin-2, decreases PKD severity and improves kidney function in the Pkd1$^{RC/RC}$ mouse model of PKD [37]. Torin-2 decreases proliferation and increases apoptosis in cells lining the cysts in these mice [37]. However, in Han:SPRD rats with PKD, the mTOR kinase inhibitor PP242, which inhibits both mTORC1 and 2, has no effect on caspase-3 activity, TUNEL positive or active caspase-3-positive tubular cells, despite significantly reducing kidney enlargement, cyst density, blood urea nitrogen, and proliferation in cells lining the cysts and non-cystic tubules [71]. Finally, an mTOR anti-sense oligonucleotide (ASO) that blocks both mTORC1 and 2, decreases PKD severity in mice with a targeted mutation in Pkd2, which is associated with a significant decrease in proliferation and apoptosis of tubular epithelial cells [36]. Thus, blockade of both mTORC1 and 2 does not have a consistent effect on apoptosis in the cells lining the cysts in the PKD kidney.

Differences in apoptosis observeed in *in vivo* studies may be due to different methods used to detect apoptosis *in vivo*. Numerous studies simply count TUNEL-positive cells in an automated fashion. However, the gold-standard is to count cells that have morphologic criteria of apoptosis that include cellular rounding and shrinkage, nuclear chromatin compaction, and formation of apoptotic bodies [72]. Morphology is the gold-standard for detection of apoptosis and TUNEL staining fails to discriminate between proximal tubule apoptosis and necrosis, particularly *in vivo* in the kidney, and it grossly overestimates proximal tubule apoptosis in the kidney [73] [72] [74] [75] [76]. This is especially true in cystic tubular epithelial cells that may have injury that can cause necrosis [77]. For these reasons, the number of TUNEL–stained nuclei that also demonstrate the morphological features of apoptosis should be also be quantitated.

With this background, studies have been performed to determine the effect of direct apoptosis inhibition or apoptosis induction on tubular cell proliferation, cyst formation, kidney size, and kidney function in PKD.

7. Caspase inhibition in PKD

Caspases are attractive potential targets for treatment of diseases because of their central role in apoptosis and the appealing prospect of small-molecule inhibitor therapy [78]. In animal models, caspase inhibitors decrease ischemia-perfusion injury in heart [79] [80], liver [81] and kidney [82] [83]. The pan-caspase inhibitor IDN-1965 improves cardiac function and decreases mortality in mouse cardiomyopathy [84] and reduces apoptosis of sinusoidal endothelial cells during liver preservation injury [85]. The pan-caspase inhibitor IDN-6556 decreases liver enzyme elevations in patients with hepatic dysfunction [86]. Of note, the orally active caspase inhibitor, Emricasan, is currently being tested in multiple clinical trials conducted in patients with liver disease [87] (see clinicaltrials.gov).

Early evidence in rodents suggests that caspase inhibitors may also be an attractive therapy to slow PKD progression. Three-week old heterozygous and littermate control Han:SPRD male rats treated with the caspase inhibitor, IDN-8050 (10 mg/kg/d) via a minipump for 5 weeks, have a 44% reduction in kidney enlargement, a 29% reduction in cyst volume density, and attenuated increase in BUN, as compared to vehicle [12]. IDN-8050-treatment additionally reduces the number of proliferating cell nuclear antigen (PCNA) positive tubular cells and apoptotic tubular cells in non-cystic and cystic tubules. Collectively, this indicates that in a rat model of PKD, caspase-inhibition with IDN-8050: 1) decreases apoptosis and proliferation in cystic and non-cystic tubules, 2) inhibits renal enlargement and cystogenesis, and 3) attenuates the loss of kidney function. These findings will require confirmation in other animal models of PKD prior to translation to clinical trials in humans with ADPKD.

Mice with caspase-3 gene deletion have been crossed with mice harboring the congenital polycystic kidney (cpk) mutation to generate double-mutant mice [14]. Homozygous caspase-3 (cpk;casp3$^{-/-}$ mice) live nearly four-times longer than littermate control cpk mice, and heterozygous (cpk;casp3$^{+/-}$ mice) live significantly longer than controls. In addition, kidney weight, relative to body weight, is significantly lower in the cpk;casp3$^{-/-}$ mice than in the cpk and cpk;casp3$^{+/-}$ mice. However, despite deletion of caspase-3, apoptosis occurs and cysts form; therefore, alternative pathways of apoptosis in cystic kidneys have been investigated. Caspase-7 is up-regulated and the anti-apoptotic protein Bcl-2 is down-regulated in cpk, cpk;casp3$^{+/-}$, and cpk;casp3$^{-/-}$ mice compared with wild-type controls. In summary, homozygous deletion of caspase-3 markedly prolongs survival of cpk mice, but a caspase-7-mediated pathway may compensate for the deficiency of functional caspase-3 [14]. These findings suggest that pan-caspase inhibition may have a greater therapeutic effect than selective caspase inhibition in PKD.

8. Apoptosis induction in PKD

The mitochondrial protein Smac promotes caspase activation in the cytochrome c/Apaf-1/caspase-9 pathway by binding to inhibitor of apoptosis proteins and removing their inhibitory activity [88]. While Smac is normally a mitochondrial protein, it is released into the cytosol when cells undergo apoptosis [89]. Overexpression of Smac increases cells' sensitivity to apoptotic stimuli. *In vitro*, a Smac-mimetic and co-treatment with tumor necrosis factor-α (TNF-α) augments the formation and activation of the receptor-interacting serine/threonine-protein kinase 1-dependent death complex and the degradation and cleavage of the caspase-8 inhibitor FLIP. This results in death in Pkd1 mutant epithelial cells, with no effect on normal renal epithelial cells [90]. *In vitro*, a Smac-mimetic selectively induces TNF-α-dependent cystic renal

epithelial cell death and delays cyst formation [90]. Similarly, treatment with a Smac-mimetic slows cyst growth and kidney enlargement, as well as preserves renal function in two genetic strains of mice with Pkd1 mutations, without affecting proliferation.

How do we reconcile the seeming contradiction that both apoptosis inhibition and apoptosis induction can lessen cyst growth? Whether apoptosis promotes or retards cyst growth is confounded by factors such as differing rodent models of PKD with differing mutations, early-versus late-disease, and apoptosis in cysts versus apoptosis limited to non-cystic tubules and interstitial cells [91]. It is possible that apoptosis inhibition and apoptosis induction decrease cyst growth by very different mechanisms that can act independently. Under certain conditions, enhanced apoptosis may preserve renal structure by eliminating mural cells from cysts that otherwise would expand endlessly without having an effect on proliferation [90]. Likewise, apoptosis inhibition can decrease proliferation of cystic epithelial cells that is crucial for growth of the cyst [12].

9. Apoptosis may be causally linked to proliferation and the development of cysts

Abnormal proliferation in tubular epithelial cells plays a crucial role in cyst development and/or growth in PKD [92] [2,93] and apoptosis may be causally linked to these processes. Convincing evidence indicates that increased tubular cell proliferation is accompanied by tubular apoptosis in PKD, and apoptosis and proliferation are directly related [94] [95] [50] [96] [97]. A massive increase in both apoptosis and proliferation is observed in both SBM mice that overexpress c-myc and Bcl-2 deficient mouse models of cystic disease [95] [50]. In fact, increased apoptosis and proliferation occur early in the course of the disease and precede cystogenesis in SBM mice [95]. In Han:SPRD rats fed soy protein, the improved renal function and decreased cyst formation is accompanied by decreases in both tubular cell proliferation and apoptosis [97][34]. Also, mice deficient in the pro-apoptotic Bcl-2 gene have hyperproliferation as well as apoptosis that accompanies renal cysts [50,98] [48]. Kidneys from patients with ADPKD have high levels of apoptosis as well as cellular proliferation [27] [99]. Thus, epithelial cell apoptosis and proliferation are dysregulated in ADPKD and may represent a general mechanism for cyst growth and tissue remodeling [94] [2] [100].

The precise pathways that link apoptosis and proliferation in PKD remain to be determined. However, a common pathway of apoptosis and proliferation may involve adhesion-dependent control of apoptosis and overexpression of the proto-oncogene c-myc. Changes in cell shape and loss of cell to cell adhesion during apoptosis may stimulate surrounding cells to proliferate [101] [102]. Theoretically, in PKD loss of tubular cells by apoptosis may initiate proliferation of neighboring tubular cells. In this case, both apoptosis and proliferation would be observed in the same cyst and caspase inhibition would attenuate both of these processes. Overexpression of c-myc is thought to play a role in the dysregulation of both proliferation and apoptosis in ADPKD. Mice overexpressing c-myc (also known as SBM mice) develop PKD concomitant with massively increased apoptosis and proliferation [103,104]. Renal c-myc expression is also increased in the Han:SPRD rat model of ADPKD [105]. The pathway of c-myc-induced apoptosis is thought to be mediated by the "initiator" caspase-9 [106] and the "executioner" caspase-3 [107] [108]. A novel Ste20-related kinase (SLK) is cleaved and activated by caspase-3 during c-myc-induced apoptosis [109]. In human ADPKD, a large increase in c-myc expression is associated with both tubular cell proliferation and apoptosis [96] [110] [111] [94]. Thus, caspase inhibition may have therapeutic relevance by impeding a common pathway for both apoptosis and proliferation, resulting in reduced cyst formation.

With caspase inhibition, it is important to consider that apoptosis in ADPKD may be a double-edged sword [112]. While increased apoptosis may result in increased proliferation, cyst growth, and deterioration of

renal function in PKD, apoptosis may also be a defense against oxidative or other forms of DNA damage and thus reduce the risk of neoplastic transformation. In this regard, the simultaneous induction of cell proliferation and apoptosis has been regarded as a safeguard against neoplastic transformation. However, cancer-prone mice treated with the caspase inhibitor IDN-8050 (Emricasan) from a young age have no detectable deliterious effects, including no evidence of treatment-related tumor formation or carcionogenicity [113]. Emricasan does not affect apoptosis in normal healthy cells, and as noted previously, it is currently being tested in multiple Phase 3 clinical trials, without reports of carcinogenicity (see clinicaltrials.gov). So it is unlikely that caspase inhibition would result in tumor development in PKD kidneys.

10. Summary on apoptosis

There is abundant evidence that apoptosis plays a causal role in cyst formation: 1) induction of apoptosis in tubular cells in culture results in cyst formation; 2) tubular epithelial cell apoptosis occurs in most animal models of PKD and in kidneys from humans with ADPKD; 3) both apoptosis and proliferation occur in non-cystic as well as cystic epithelial cells early in the course of PKD; 4) caspase inhibition results in less apoptosis and proliferation in the tubular epithelium, with attenuation of cyst formation and kidney failure.

11. Autophagy

Autophagy is a process that occurs in all eukaryotic cells to keeps cells alive under stressful conditions [114]. In autophagy, damaged organelles are sequestered into double-membraned autophagosomes that subsequently fuse with lysosomes to deliver their cargoes for degradation and recycling. Autophagy received prominence in 2016 when the Nobel Prize in Physiology or Medicine was awarded to Dr. Yoshinori Ohsumi for "discoveries of the mechanisms for autophagy." It is now known that there are 3 major forms of autophagy: macroautophagy, microautophagy and chaperone—mediated autophagy (CMA) [26]: 1) Macroautophagy is the best characterized variant of autophagy, that occurs in all eukaryotic cells and involves the sequestration of cytoplasmic components in double-membraned autophagosomes that subsequently fuse with lysosomes, where the cargo e.g. damaged organelles is delivered for degradation and recycling; 2) Microautophagy, or endosomal microautophagy, is a form of autophagy where cytoplasmic cargo destined for degradation is taken up by the vacuole via direct membrane invagination; 3) Chaperone-mediated autophagy (CMA) involves the direct delivery of cytosolic proteins targeted for degradation to the lysosome. The characteristic feature of CMA is that neither vesicles nor membrane invaginations are required for substrate delivery to lysosomes, and substrates reach the lysosomal lumen via a protein-translocation complex at the lysosomal membrane. Other forms of autophagy target mitochondria (mitophagy), peroxisomes (pexophagy), endoplasmic reticulum (reticulophagy), protein aggregates (aggrephagy), lipid droplets (lipophagy), and inactive proteasomes (proteaphagy).

Autophagic flux is the most well accepted measure of the state of autophagy. For example, increased autophagosomes may be used to characterize systems of either increased autophagosome production or decreased autophagosome clearance by the lysosome, two dissimilar cellular responses [115,116]. According to the 2016 Guidelines for the use and interpretation of assays for monitoring autophagy, if the basal increase in microtubule-associate protein 1A/1B-light chain 3-II (LC3-II; a central protein in the autophagy pathway) is due to increased autophagosome production, then it is expected that lysosomal inhibition will further increase LC3-II [116]. Alternatively, if the increase in LC3-II is due to a block in autophagosome-lysosome fusion or a defect in lysosome function, then lysosomal inhibition would not affect LC3-II expression. The measurement of autophagic flux requires the measurement of autophagosomes (e.g., LC3-II, a marker of

autophagosomes), in the presence and absence of lysosomal inhibition. Autophagic flux, measured as described above, is decreased in the cpk mouse model of ARPKD [17].

Autophagy was originally characterized as a hormonal and starvation response. It is now known that autophagy has a broad role in biology, including organelle remodeling, protein and organelle quality control, prevention of genotoxic stress, tumor suppression, pathogen elimination, regulation of immunity and inflammation, maternal DNA inheritance, metabolism, and cellular survival [117]. While autophagy is usually a degradative pathway, it also plays a role in biosynthetic and secretory processes. As autophagy is critical to many essential cellular functions, it is not surprising that defects in autophagy have been implicated in a variety of diseases [16,17,19,118–121]. Autophagy is crucial in maintaining cell and organ homeostasis, protecting against disease, and promoting recovery after injury [122], particularly in the kidneys. There is accumulating evidence that autophagy may be dysregulated in kidney disease and injury. Acute kidney injury, induced by either cisplatin or ischemia, has been hypothesized to upregulate autophagy as a recovery mechanism [123–126]. Autophagy enhancement benefits mice with cisplatin-induced acute kidney injury, and autophagy inhibition exacerbates injury in this model [124]. Further, autophagy is important for maintaining podocyte proteostasis in aging mice [127]. Autophagy also has implications as a stress response during kidney transplant injury, with opposing effects resulting from immunosuppressive drugs or ischemic stresses [119].

12. Autophagy in PKD

Autophagy research in PKD is in its infancy, but there are reasons to believe that autophagy may be dysregulated in the PKD kidney and specifically that autophagy may be supressed in PKD. Autophagic flux is suppressed in ADPKD as evidenced by studies in PKD1$^{-/-}$ cells, Pkd1$^{-/-}$ zebrafish and rodent models of PKD.

12.1. In vitro models

In human Pkd1$^{-/-}$ cells, there is an attenuated increase in LC3-II expression after bafilomycin A1 (BafA1) treatment demonstrating decreased autophagic flux [16]. Additionally, by immunofluorescence, the number of both autophagosomes and autolysosomes in PKD1$^{-/-}$ cells is significantly lower, and the number of autophagosomes fails to be upregulated in response to BafA1 treatment, suggesting inadequate autophagosome formation and diminished autophagosome-lysosome fusion. Autophagy impairment accounts for a weakened ability to remove protein aggregates, as PKD1$^{-/-}$ cells accumulate more aggregates in the absence of any stress and also break down MG132-induced protein aggregation less efficiently. Mouse Pkd1$^{-/-}$ cells show a similar deficiency in the clearance of protein aggregates [16]. Zebrafish mutants for pkd1a develop mTOR activation, impaired autophagic flux and cystic kidneys [16].

12.2. In vivo models

Dysregulated autophagy has also been described in rodent models of PKD. Autophagic vacuoles in the cells surrounding cysts have been described in polycystic kidneys in the Han:SPRD rat [17]. By electron microscopy, features suggestive of autophagy-like autophagosomes, mitophagy, and autolysosomes are observed in both wild-type and PKD kidneys [17]. Specific to the Han:SPRD rat, autophagosomes are found by electron microscopy in the tubular cells lining the cysts. LC3 staining by immunofluorescence is also present in the tubular epithelial cells lining the cysts. Autophagic flux is also dysregulated in the cpk mouse model of ARPKD [17]. LC3-II expression is increased in PKD kidneys of cpk mice as compared to wild-type kidneys. Additionally, *in vivo* treatment with the lysosomal inhibitor BafA1 increases LC3-II expression in the kidneys of wild-type mice. In contrast, BafA1 has no effect on
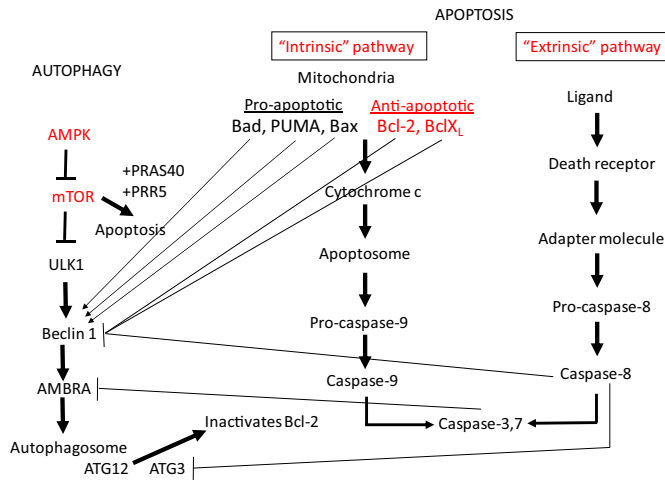
Figure 1. Molecular pathways involved in PKD, autophagy and apoptosis. Autophagy and apoptosis are intimately related. Pathways known to be activated in PKD are shown in red. The mTOR pathway that inhibits autophagy is activated in PKD [28]. There is cross talk between mTOR pathway of autophagy and the apoptosis pathways [129]. Bcl-2 is a central regulator of autophagy and apoptosis and functions by interacting with Beclin-1 and inhibiting autophagy. The pro-apoptotic mitochondrial protein, Bad, disrupts the interaction between Bcl-2 and Beclin-1 to induce autophagy. The pro-apoptotic protein, PUMA, a p53-inducible BH3-only protein, triggers mitochondrial-specific autophagy. Activation of caspase-3 and dysregulation of the balance between pro- and anti-apoptotic Bcl-2 family members, specifically a down-regulation of anti-apoptotic Bcl-xL, has been shown in PKD [9] and Bcl-2 downregulation worsens PKD [10]. Caspases activated during apoptosis can cleave and inactivate Beclin-1. Ambra-1, a key molecule that promotes the initial steps of autophagy, is irreversibly cleaved by both calpains and caspases. During apoptosis, Atg3 is cleaved by caspase 8 and cleaved Atg3 inhibits autophagy. Autophagy is inhibited by caspase-8-mediated cleavage of Beclin-1 [174]. The intrinsic and extrinsic pathways of caspase activation in apoptosis are activated in PKD [51]. In addition to the role that apoptosis-related proteins play in modulating autophagy, many autophagic proteins can induce apoptosis. mTOR forms a complex with PRAS40 and PRR5-like proteins to induce apoptosis. Activation of AMPK is known to inhibit mTOR and induce autophagy. AMPK activation with metformin is protective in PKD [152] but the effect of metformin on autophagy and apoptosis in PKD is not known. Atg12 increases mitochondrial apoptosis by directly binding to and inactivating Bcl-2. PKD mice have a significantly lower renal mRNA expression of Atg12 and other autophagy-related genes, Atg3, beclin1 and p62, [18].

Abbreviations: B-cell lymphoma 2 (Bcl-2), B-cell lymphoma-extra large (Bcl-xL), p53 upregulated modulator of apoptosis (PUMA), proline-rich Akt substrate of 40 kDa (PRAS40), PRoline-Rich protein 5 (PRR5), activating molecule in Beclin1-regulated autophagy protein-1 (Ambra-1), 5' AMP-activated protein kinase (AMPK).

LC3-II in the polycystic kidneys of cpk mice, suggesting a defect in autophagic flux in PKD resulting from impaired autophagosome-lysosme fusion and degradation. In a Pkd1-hypomorphic mouse model (Pkdd1 miRNA transgenic mice) there is a significantly lower renal mRNA expression of autophagy-related genes, including Atg12, Atg3, beclin1, and p62, compared with wild-type control mice [18]. Collectively, these results suggest a modifying effect of ADPKD on autophagy and establish autophagy activation as a potential novel therapy for ADPKD [128].

13. Interactions between apoptosis and autophagy in PKD

There is cross talk between mTOR pathway of autophagy and the apoptosis pathways [129] (Figure 1). The mTOR pathway that inhibits autophagy is activated in PKD [28]. The intrinsic and extrinsic pathways of apoptosis are activated in PKD [51]. Many of the signals that regulate apoptosis in PKD also regulate autophagy, for example, the

Bcl-2 family of proteins and caspases [130] [131] [132] [133] [134]. The relationship between apoptosis and autophagy is complex, depending on the type of cell and the nature and timing of the injury [133]. For example, increased autophagy may result in a delay of apoptosis [135] [136] [137] and genetic deletion of crucial autophagy proteins increases apoptotic cell death [138]. Autophagy is closely related to apoptosis, a process that is dysregulated in PKD. PKD kidneys have a significantly lower renal expression of autophagy-related genes, including Atg12, Atg3, beclin1, and p62, compared with wild-type control mice [166]. Inhibition of autophagy by knocking down the essential autophagy protein Atg5 promotes cystogenesis and specific induction of autophagy inhibits apoptosis [16]. Thus, it could be hypothesized that suppressed autophagy in PKD may be associated with increased apoptosis and cyst growth.

The hypothesis that autophagy suppression may contribute to cyst formation and growth is based on studies that many of the agents that protect against PKD, such as mTOR inhibitors, cyclin-dependent kinase inhibitors, caspase inhibitors, tyrosine kinase inhibitors, metformin, curcumin, and triptolide, affect both autophagy and apoptosis. Discussion of the effect of these agents on autophagy and apoptosis will be divided into agents that have been used in human studies, agents that have shown positive effects on PKD in animals and represent potential new therapies for PKD and in vitro studies.

13.1. Human studies

The mTOR inhibitors sirolimus and everolimus have been used in patients with ADPKD [139] [140]. The effect of mTOR inhibitors on PKD in humans was disappointing most likely related factors like dosage, side effects and penetration of mTOR inhibitors into the polycystic kidney [141]. mTOR is the major regulator of autophagy. mTOR activation inhibits autophagy, while mTOR inhibitors induce autophagy. With present technology, the effect of mTOR inhibitors on autophagy in human kidneys would be near impossible to determine.

13.2. Rodent studies

The effects of treatments on apoptosis/autophagy and PKD in *in vivo* models of PKD is shown in Table 2. There are autophagy inducers that have shown positive effects on PKD in animals and represent potential new therapies for PKD. mTOR inhibitors that induce autophagy can protect against PKD in rat and mouse models with variable effects to either increase or decrease apoptosis depending on the dose of mTOR inhibitor and PKD model [7] [69]. The traditional Chinese medicine, triptolide, which affects Ca^{2+} signaling as well as autophagy and apoptosis, protects against PKD [142] [143]. Curcumin, a hydrophobic polyphenol compound extracted from the spice turmeric, is an autophagy inducer [144]. Curcumin inhibits cystogenesis in Pkd-1 knockout mice by inhibiting signal transducers and activator of transcription 3 (STAT3), which play a major role in the regulation of autophagy [145] [146] [147] [148] [149]. Of note, an ongoing randomized controlled trial is evaluating the efficacy of curcumin supplementation in children and young adults with ADPKD (NCT02494141). The cyclin-dependent kinase inhibitor, Roscovitine [59], a dual Src and tyrosine kinase inhibitor, and epidermal growth factor receptor (EGFR) tyrosine kinase inhibition, all known autophagy inducers, also ameliorates PKD in rodent models [150] [151]. While roscovitine decreased apoptosis in PKD, the effect on autophagy was not determined [59]. The adenosine monophosphate-activated protein kinase (AMPK) inhibitor, metformin, a known autophagy inducer, also slows cyst growth in mouse models of PKD [152] [153,154]. However, the effects of metformin on autophagic flux, mitophagy, or apoptosis in PKD were not described.

Trehalose is a natural, nonreducing disaccharide that has been shown to enhance autophagy independent of mTOR [155]. In a *Pkd1*-hypomorphic mouse model, renal mRNA expression of autophagy-related genes, including *atg5, atg12, ulk1, beclin1*, and *p62* are reduced

and there is positive staining for the p62 protein in cystic lining cells, indicating impaired degradation by the autophagy-lysosome pathway [18]. However, trehalose treatment does not affect autophagy signaling, nor does it reduce kidney cysts or improve kidney function *in this model*, suggesting that treholose supplementation is not a candidate to slow PKD progression.

Lifestyle interventions may also modulate autophagy in PKD. Fasting inhibits the mTOR pathway and stimulates autophagy to remove damaged molecules and organelles, including in the kidney [156]. Thirty-percent caloric restriction for two weeks prior to ischemia reperfusion injury in a rodent model improves renal function, which may be mediated by increased autophagy [157]. More recently, the effects of caloric restriction and agents targeting metabolic pathways on autophagy have been evaluated in rodent of models of PKD. Mild-to-moderate caloric restriction resulted in a decrease in cleaved caspase-3, a marker of apoptosis, but autophagy was not measured [158]. Mild food restriction decreased PKD associated with no change in LC3-II, a marker of autophagosomes, but not a marker of true autophagic flux [159]. In this study, apoptosis was not determined. The caloric restriction mimetic, 2-deoxy-glucose (2DG) [160] [161] [15] also protects against PKD, however the effect of 2DG on apoptosis or autophagy was not determined in the PKD kidney.

Notably, overweight, and particularly obesity, are strong independent predictors of more rapid kidney growth, as well as kidney function decline in adults with early-stage ADPKD [162]. Of relevance to this obervation, mouse models of deficient autophagic competence exhibit significantly greater weight gain in response to metabolic challenge, suggesting an intimate link between autophagy and obesity [163]. An ongoing clinical trial (NCT03342742) is evaluating the feasibility of two weight loss interventions in adults with ADPKD who are oveweight or obese (daily caloric restriction and intermittent fasting); these diets may influence disease progression via weight loss and/or periods of fasting, both of which are tied to autophagy.

In summary, while many potential autophagy inducers are potential therapies for PKD, the role of autophagy induction in the protection against PKD is not known. mTOR inhibitors that protect against PKD have variable effects on apoptosis, but autophagy was not determined in mTOR inhibition studies (Table 2). The effect of potential autophagy inducers on both apoptosis and autophagy has not been systematically studied in preclinical studies of PKD.

13.3. In vitro studies

The effects of treatments on apoptosis/autophagy and PKD in *in vitro* models of PKD is shown in Table 2. Saikosaponin-d (SSd), a sarcoplasmic/endoplasmic reticulum Ca^{2+} ATPase pump (SERCA) inhibitor, may suppress proliferation in ADPKD cells by up-regulating autophagy [164]. SSd results in the accumulation of intracellular calcium, activation of the calcium/calmodulin-dependent protein kinase β (CaMKKβ)-AMPK signaling cascade, inhibition of mTOR signaling, and induction of autophagy. Notably, treatment with an autophagy inhibitor (3-methyladenine), AMPK inhibitor (Compound C), CaMKKβ inhibitor (STO-609), or an intracellular calcium chelator (BAPTA/AM) reduces autophagy puncta formation mediated by SSd. Thus, SERCA may represent a new autophagy target in ADPKD. Likewise, histone deacetylase inhibitors (HDACi) have therapeutic effects in *in vitro* models of ADPKD. Treatment with trichostatin A, a specific HDACi, prevents cyst formation in Pkd1$^{-/-}$ cells and also stimulates autophagy, suggesting a role for autophagy in slowing cyst growth with HDACi [165]. However, in these two studies, the effects of SSd or trichostatin on apoptosis was not determined.

Studies in Pkd1$^{-/-}$ zebrafish and Pkd1$^{-/-}$ cell models have shown consistent relationship between apoptosis and autophagy. Evidence from a zebrafish model of PKD implicates autophagy in cystogenesis [16]. Zebrafish mutants for pkd1a develop cystic kidneys and mTOR activation, suggesting a conserved ADPKD model. Further assessment of

the pkd1a mutants reveals impaired autophagic flux and increased apoptosis. Inhibition of autophagy by knocking down the core autophagy protein Atg5 promotes cystogenesis. Activation of autophagy using a specific inducer Beclin-1 peptide results in a decrease in apoptosis and ameliorates cysts in this model. Additionally, treatment with both mTOR-dependent (sirolimus) and mTOR-independent (carbamazepine and minoxidil) autophagy activators, markedly attenuate cyst formation.

There appears to be an important connection between the Pkd1 gene, apoptosis, and autophagy. Pkd1$^{+/+}$ cells deprived of glucose activated cell autophagy to survive; however, two different Pkd1$^{-/-}$ cell lines fail to activate autophagy, but instead increase apoptotic rates [15]. The effect is in part dependent on mTORC1, as treatment with sirolimus partially restores autophagy and decreases apoptosis in Pkd1$^{-/-}$ cells. This is the first direct evidence of a connection between the Pkd1 gene, apoptosis, and autophagy.

Metformin also reduces cyst formation in a zebrafish model of polycystin-2 deficiency, in part via modulation of autophagy [118]. In this model, metformin inhibits pronephric cyst formation by 42–61% compared to untreated controls. Metformin also reduces the number of proliferating cells in the pronephric ducts, increases the phosphorylation of adenosine monophosphate-activated protein kinase (AMPK), and enhances autophagy in the pronephros. In this study, the effect of autophagy induction with metformin on apoptosis was not determined.

In summary, the lack of autophagy and increased apoptosis in Pkd1$^{-/-}$ zebrafish and Pkd1$^{-/-}$ cells and the effect of autophagy inducers to increase autophagy and decrease apoptosis in these cells supports the hypothesis that a lack of autophagy and increased apoptosis are central features of PKD and may explain why drugs or lifestyle interventions that induce autophagy and inhibit apoptosis may have therapeutic value in PKD.

14. Autophagy inhibition in the polycystic liver

Contrary to the hypothesis that increasing autophagy will slow PKD, autophagy appears to be increased in polycystic liver disease (PLD) cholangiocytes and contribute to hepatic cystogenis [166]. PLD cholangiocytes have increased number and size of autophagosomes, lysosomes, and autolysosomes both *in vitro* and *in vivo*, overexpress autophagy-related proteins (Atg5, Beclin1, Atg7, and LC3), and have enhanced autophagic flux. Molecular and pharmacologic interventions to inhibit autophagy with ATG7 small interfering RNA, BafA1, or hydroxychloroquine, reduce proliferation of PLD cholangiocytes and growth of hepatic cysts. Hydroxychloroquine also efficiently inhibits hepatic cystogenesis in the pck rat. In contrast, autophagy inhibition using siRNA against LC3 and the inhibitor 3-methyladenine significantly increase the cell proliferative activity of pck rat cholangiocytes treated with NVP-BEZ235, a combined PI3K, mTORC1/2 inhibitor [167]. *In vivo*, NVP-BEZ235 treatment attenuates cystic dilatation of the intrahepatic bile ducts, without affecting renal cyst development. Finally, knockdown of hepatocystin, a gene implicated in autosomal dominant PLD, results in an autophagy a defect that can be rescued by ectopic expression of wild-type hepatocystin [168]. The pathogenesis of PLD is different from PKD [4]; for example, growth of liver compared to kidney cysts is very estrogen dependent [4], and this may influence the role of autophagy in the polycystic liver versus the polycystic kidney. However, in pursuing autophagy inducers as a potential therapeutic option to treat PKD, it will be important to also determine whether there is an adverse effect on PLD.

15. Summary

Apoptosis is present in the cells lining cysts in most rodent models of PKD and in human PKD kidneys. Inhibition of apoptosis using caspase inhibitors, knockout of apoptosis in PKD mice, as well as apoptosis induction using a SMAC-mimetic can all protect against PKD,

highlighting the complex nature of the role of apoptosis in cyst growth. Increased proliferation of the cells lining the cyst is a major factor in cyst growth. Highlighting the connection between apoptosis and proliferation in PKD, both proliferation and apoptosis are hugely increased in the SBM mouse, a unique transgenic model of PKD induced by the dysregulated expression of c-myc in renal tissue. Apoptosis is likely closely related to dysregulated autophagy in PKD. Pkd1$^{-/-}$ zebrafish, Pkd1$^{-/-}$ cells, and some PKD mouse models demonstrate both increased apoptosis and suppressed autophagy in the kidney. Autophagy induction directly leads to decreased apoptosis and protection against PKD in zebrafish models. Autophagy induction directly leads to decreased apoptosis in Pkd1$^{-/-}$ cells suggesting a direct connection between apoptosis and autophagy in PKD. However, mTOR inhibitors, that are known autophagy inducers, have a variable effect on apoptosis depending on dose and PKD model. In conclusion, autophagy is suppressed in *in vitro* and *in vivo* PKD models and autophagy induction may have a therapeutic role in decreasing cyst growth, perhaps by decreasing apoptosis and proliferation. In the future, direct autophagy inducers should be evaluated in rodent PKD models, and the cause and effect relationship between autophagy, apoptosis and cyst growth in PKD should be tested via autophagy knockout in PKD kidneys.

Funding

Credit Author Statement

Charles Edelstein: Conceptualization, Writing-original draft preparation, Writing-review and editing, supervision, Funding acquisition. Kristen Nowak: Writing-review and editing.

References

[1] G.M. Fick, P.A. Gabow, Natural history of autosomal dominant polycystic kidney disease, Annu. Rev. Med. 45 (1994) 23–29.

[2] P.D. Wilson, Polycystic kidney disease, N. Engl. J. Med. 350 (2) (2004) 151–164.

[3] C. Antignac, J.P. Calvet, G.G. Germino, J.J. Grantham, L.M. Guay-Woodford, P.C. Harris, F. Hildebrandt, D.J. Peters, S. Somlo, V.E. Torres, et al., The future of polycystic kidney disease research-as seen by the 12 Kaplan Awardees, J. Am. Soc. Nephrol. 26 (9) (2015 Sep) 2081–2095.

[4] F.A. Belibi, C.L. Edelstein, Novel targets for the treatment of autosomal dominant polycystic kidney disease, Expert Opin. Investig. Drugs 19 (3) (2010) 315–328.

[5] V.E. Torres, P.C. Harris, Autosomal dominant polycystic kidney disease: the last 3 years, Kidney Int. 76 (2) (2009) 149–168.

[6] G. Wu, S. Somlo, Molecular genetics and mechanism of autosomal dominant polycystic kidney disease, Mol. Genet. Metab. 69 (1) (2000) 1–15.

[7] Y. Tao, J. Kim, R.W. Schrier, C.L. Edelstein, Rapamycin markedly slows disease progression in a rat model of polycystic kidney disease(PKD), J. Am. Soc. Nephrol. 16 (2005) 46–51.

[8] J.M. Shillingford, N.S. Murcia, C.H. Larson, S.H. Low, R. Hedgepeth, N. Brown, C.A. Flask, A.C. Novick, D.A. Goldfarb, A. Kramer-Zucker, et al., The mTOR pathway is regulated by polycystin-1, and its inhibition reverses renal cystogenesis in polycystic kidney disease, Proc. Natl. Acad. Sci. U. S. A. 103 (14) (2006) 5466–5471.

[9] T. Ecder, V.Y. Melnikov, M. Stanley, D. Korular, M.S. Lucia, R.W. Schrier, C.L. Edelstein, Caspases, Bcl-2 proteins and apoptosis in autosomal-dominant polycystic kidney disease, Kidney Int. 61 (4) (2002) 1220–1230.

[10] L. Duplomb, N. Droin, O. Bouchot, C. Thauvin-Robinet, A.L. Bruel, J. Thevenon, P. Callier, G. Meurice, N. Pata-Merci, R. Loffroy, et al., A constitutive BCL2 down-regulation aggravates the phenotype of PKD1-mutant-induced polycystic kidney disease, Hum. Mol. Genet. 26 (23) (2017) 4680–4688.

[11] S.J.B.C. Holditch, D. Atwood, S.E. Brown, A.M. Lombardi, K.N. Nguyen, R.C. Hill, M. Lanaspa, K. Hopp, M. Weiser-Evans, C.L. Edelstein, The consequences of increased 4E-BP1 in polycystic kidney disease, Hum. Mol. Genet. (2019) In Press.

[12] Y. Tao, J. Kim, S. Faubel, J.C. Wu, S.A. Falk, R.W. Schrier, C.L. Edelstein, Caspase inhibition reduces tubular apoptosis and proliferation and slows disease progression in polycystic kidney disease(PKD), Proc. Natl. Acad. Sci. USA 102 (19) (2005) 6954–6959.

[13] S.M. Ali, V.Y. Wong, K. Kikly, T.A. Fredrickson, P.M. Keller, W.E. DeWolf Jr., D. Lee, D.P. Brooks, Apoptosis in polycystic kidney disease: involvement of caspases, Am. J. Physiol. Regul. Integr. Comp. Physiol. 278 (3) (2000) R763–R769.

[14] Y. Tao, I. Zafar, J. Kim, R.W. Schrier, C.L. Edelstein, Deletion of the caspase-3 gene

[15] I. Rowe, M. Chiaravalli, V. Mannella, V. Ulisse, G. Quilici, M. Pema, X.W. Song, H. Xu, S. Mari, F. Qian, et al., Defective glucose metabolism in polycystic kidney disease identifies a new therapeutic strategy, Nat. Med. 19 (4) (2013) 488–493.

[16] P. Zhu, C.J. Sieben, X. Xu, P.C. Harris, X. Lin, Autophagy activators suppress cystogenesis in an autosomal dominant polycystic kidney disease model, Hum. Mol. Genet. 26 (1) (2017) 158–172.

[17] F. Belibi, I. Zafar, K. Ravichandran, A.B. Segvic, A. Jani, D.G. Ljubanovic, C.L. Edelstein, Hypoxia-inducible factor-1alpha (HIF-1alpha) and autophagy in polycystic kidney disease (PKD), Am. J. Physiol. Renal Physiol. 300 (5) (2011) F1235–F1243.

[18] L.F. Chou, Y.L. Cheng, C.Y. Hsieh, C.Y. Lin, H.Y. Yang, Y.C. Chen, C.C. Hung, Y.C. Tian, C.W. Yang, M.Y. Chang, Effect of trehalose supplementation on autophagy and cystogenesis in a mouse model of polycystic kidney disease, Nutrients 11 (1) (2018).

[19] K. Ravichandran, C.L. Edelstein, Polycystic kidney disease: a case of suppressed autophagy? Semin. Nephrol. 34 (1) (2014) 27–33.

[20] C.M. Sorenson, Life, death and kidneys: regulation of renal programmed cell death, Curr. Opin. Nephrol. Hypertens. 7 (1) (1998) 5–12.

[21] J. Savill, Apoptosis and the kidney [editorial], J. Am. Soc. Nephrol. 5 (1) (1994) 12–21.

[22] M.R. Hammerman, Renal programmed cell death and the treatment of renal disease [editorial], Curr. Opin. Nephrol. Hypertens. 7 (1) (1998) 1–3.

[23] R.A. Lockshin, Early work on apoptosis, an interview with Richard Lockshin, Cell Death Differ. 15 (7) (2008) 1091–1095.

[24] J.F. Kerr, A.H. Wyllie, A.R. Currie, Apoptosis: a basic biological phenomenon with wide-ranging implications in tissue kinetics, Br. J. Cancer 26 (4) (1972) 239–257.

[25] L. Galluzzi, I. Vitale, S.A. Aaronson, J.M. Abrams, D. Adam, P. Agostinis, E.S. Alnemri, L. Altucci, I. Amelio, D.W. Andrews, et al., Molecular mechanisms of cell death: recommendations of the Nomenclature Committee on Cell Death 2018, Cell Death Differ. 25 (3) (2018) 486–541.

[26] L. Galluzzi, E.H. Baehrecke, A. Ballabio, P. Boya, J.M. Bravo-San Pedro, F. Cecconi, A.M. Choi, C.T. Chu, P. Codogno, M.I. Colombo, et al., Molecular definitions of autophagy and related processes, EMBO J. 36 (13) (2017) 1811–1836.

[27] D. Woo, Apoptosis and loss of renal tissue in polycystic kidney diseases, N. Engl. J. Med. 333 (1) (1995) 18–25.

[28] C.L. Edelstein, Mammalian target of rapamycin and caspase inhibitors in polycystic kidney disease, Clin. J. Am. Soc. Nephrol. 3 (4) (2008) 1219–1226.

[29] R.A. Saxton, D.M. Sabatini, mTOR signaling in growth, metabolism, and disease, Cell 168 (6) (2017) 960–976.

[30] B. Ravikumar, Z. Berger, C. Vacher, C.J. O'Kane, D.C. Rubinsztein, Rapamycin pretreatment protects against apoptosis, Hum. Mol. Genet. 15 (7) (2006) 1209–1216.

[31] P.R. Wahl, A.L. Serra, M. Le Hir, K.D. Molle, M.N. Hall, R.P. Wuthrich, Inhibition of mTOR with sirolimus slows disease progression in Han:SPRD rats with autosomal dominant polycystic kidney disease (ADPKD), Nephrol. Dial. Transplant. 21 (3) (2006) 598–604.

[32] M. Wu, P.R. Wahl, M. Le Hir, Y. Wackerle-Men, R.P. Wuthrich, A.L. Serra, Everolimus retards cyst growth and preserves kidney function in a rodent model for polycystic kidney disease, Kidney Blood Press. Res. 30 (4) (2007) 253–259.

[33] I. Zafar, K. Ravichandran, F.A. Belibi, R.B. Doctor, C.L. Edelstein, Sirolimus attenuates disease progression in an orthologous mouse model of human autosomal dominant polycystic kidney disease, Kidney Int. 78 (8) (2010) 754–761.

[34] J.U. Becker, A.O. Saez, X. Zerres, O. Witzke, P.F. Hoyer, K.W. Schmid, A. Kribben, C. Bergmann, J. Nurnberger, The mTOR pathway is activated in human auto-somal-recessive polycystic kidney disease, Kidney Blood Press. Res. 33 (2) (2010) 129–138.

[35] D.C. Fischer, U. Jacoby, L. Pape, C.J. Ward, E. Kuwertz-Broeking, C. Renken, H. Nizze, U. Querfeld, B. Rudolph, D.E. Mueller-Wiefel, et al., Activation of the AKT/mTOR pathway in autosomal recessive polycystic kidney disease (ARPKD), Nephrol. Dial. Transplant. 24 (6) (2009) 1819–1827.

[36] K. Ravichandran, I. Zafar, Z. He, R.B. Doctor, R. Moldovan, A.E. Mullick, C.L. Edelstein, An mTOR anti-sense oligonucleotide decreases polycystic kidney disease in mice with a targeted mutation in Pkd2, Hum. Mol. Genet. 23 (18) (2014) 4919–4931.

[37] S.J. Holditch, C.N. Brown, D.J. Atwood, A.M. Lombardi, K.N. Nguyen, H.W. Toll, K. Hopp, C.L. Edelstein, A study of sirolimus and an mTOR kinase inhibitor (TORKi) in a hypomorphic Pkd1 mouse model of autosomal dominant polycystic kidney disease (ADPKD), Am. J. Physiol. Renal Physiol. 317 (1) (2019 Jul 1) F187–F196.

[38] D.R. Green, Apoptotic pathways: the roads to ruin, Cell 94 (1998) 695–698.

[39] D.R. Green, Apoptotic pathways: paper wraps stone blunts scissors, Cell 102 (2000) 1–4.

[40] D.R. Green, J.C. Reed, Mitochondria and apoptosis, Science 281 (5381) (1998) 1309–1312.

[41] M. Barinaga, Cell suicide:by ICE, not fire, Science 263 (1994) 754–756.

[42] M. Barinaga, Death by dozens of cuts, Science 280 (1998) 32–34.

[43] D.W. Nicholson, A. Ali, N.A. Thornberry, J.P. Vaillancourt, C.K. Ding, M. Gallant, Y. Gareau, P.R. Griffin, M. Labelle, Y.A. Lazebnik, Identification and inhibition of the ICE/CED-3 protease neccessary for mammalian apoptosis, Nature 376 (1995) 37–43.

[44] G.S. Salvesen, V.M. Dixit, Caspases: intracellular signaling by proteolysis, Cell 91 (4) (1997) 443–446.

[45] A. Fraser, G. Evan, A license to kill, Cell 85 (1996) 781–784.

[46] J.M. Adams, S. Cory, The Bcl-2 protein family: arbiters of cell survival, Science 281 (5381) (1998) 1322–1326.

[47] S.J. Korsmeyer, BCL-2 gene family and the regulation of programmed cell death, Cancer Res. 59 (1999) 1693s–1700s.

[48] K. Nakayama, K. Nakayama, I. Negishi, K. Kuida, H. Sawa, D.Y. Loh, Targeted disruption of Bcl-2 alpha beta in mice: occurrence of gray hair, polycystic kidney disease, and lymphocytopenia, Proc. Natl. Acad. Sci. U. S. A. 91 (9) (1994) 3700–3704.

[49] S. Kamada, A. Shimono, Y. Shinto, T. Tsujimura, T. Takahashi, T. Noda, Y. Kitamura, H. Kondoh, Y. Tsujimoto, bcl-2 deficiency in mice leads to pleiotropic abnormalities: accelerated lymphoid cell death in thymus and spleen, polycystic kidney, hair hypopigmentation, and distorted small intestine, Cancer Res. 55 (2) (1995) 354–359.

[50] D.J. Veis, C.M. Sorenson, J.R. Shutter, S.J. Korsmeyer, Bcl-2-deficient mice demonstrate fulminant lymphoid apoptosis, polycystic kidneys, and hypopigmented hair, Cell 75 (2) (1993) 229–240.

[51] Y. Tao, J. Kim, S. M, Z. He, S.G. Faubel, R.W. Schrier, C.L. Edelstein, Pathways of caspase-mediated apoptosis in autosomal dominant polycystic kidney disease (ADPKD), Kidney Int. 67 (3) (2004) 909–919.

[52] A. Ashkenazi, V.M. Dixit, Death receptors: signaling and modulation, Science 281 (1998) 1305–1308.

[53] H.H. Lin, T.P. Yang, S.T. Jiang, H.Y. Yang, M.J. Tang, Bcl-2 overexpression prevents apoptosis-induced Madin-Darby canine kidney simple epithelial cyst formation, Kidney Int. 55 (1) (1999) 168–178.

[54] A. Boletta, F. Qian, L.F. Onuchic, A.K. Bhunia, B. Phakdeekitcharoen, K. Hanaoka, W. Guggino, L. Monaco, G.G. Germino, Polycystin-1, the gene product of PKD1, induces resistance to apoptosis and spontaneous tubulogenesis in MDCK cells, Mol. Cell 6 (5) (2000) 1267–1273.

[55] W. Mai, D. Chen, T. Ding, I. Kim, S. Park, S.Y. Cho, J.S. Chu, D. Liang, N. Wang, D. Wu, et al., Inhibition of Pkhd1 impairs tubulomorphogenesis of cultured IMCD cells, Mol. Biol. Cell 16 (9) (2005) 4398–4409.

[56] Y. Pei, Z. Lan, K. Wang, M. Garcia-Gonzalez, N. He, E. Dicks, P. Parfrey, G. Germino, T. Watnick, A missense mutation in PKD1 attenuates the severity of renal disease, Kidney Int. 81 (4) (2012) 412–417.

[57] W. Yu, T. Kong, S. Beaudry, M. Tran, H. Negoro, V. Yanamadala, B.M. Denker, Polycystin-1 protein level determines activity of the Galpha12/JNK apoptosis pathway, J. Biol. Chem. 285 (14) (2010) 10243–10251.

[58] N.O. Bukanov, S.E. Moreno, T.A. Natoli, K.A. Rogers, L.A. Smith, S.R. Ledbetter, N. Oumata, H. Galons, L. Meijer, O. Ibraghimov-Beskrovnaya, CDK inhibitors R-roscovitine and S-CR8 effectively block renal and hepatic cystogenesis in an orthologous model of ADPKD, Cell Cycle 11 (21) (2012) 4040–4046.

[59] N.O. Bukanov, L.A. Smith, K.W. Klinger, S.R. Ledbetter, O. Ibraghimov-Beskrovnaya, Long lasting arrest of murine polycystic kidney disease with CDK inhibitor roscovitine, Nature 444 (7121) (2006) 949–952.

[60] F. Zeng, T. Miyazawa, L.A. Kloepfer, R.C. Harris, Deletion of ErbB4 accelerates polycystic kidney disease progression in cpk mice, Kidney Int. 86 (3) (2014) 538–547.

[61] S. Anderson, T.T. Oyama, J.N. Lindsley, W.E. Schutzer, D.R. Beard, V.H. Gattone, R. Komers, 2-Hydroxyestradiol slows progression of experimental polycystic kidney disease, Am. J. Physiol. Renal Physiol. 302 (5) (2012) F636–F645.

[62] T.A. Natoli, L.A. Smith, K.A. Rogers, B. Wang, S. Komarnitsky, Y. Budman, A. Belenky, N.O. Bukanov, W.R. Dackowski, H. Husson, et al., Inhibition of glucosylceramide accumulation results in effective blockade of polycystic kidney disease in mouse models, Nat. Med. 16 (7) (2010) 788–792.

[63] E.K. Kleczko, K.H. Marsh, L.C. Tyler, S.B. Furgeson, B.L. Bullock, C.J. Altmann, M. Miyazaki, B.Y. Gitomer, P.C. Harris, M.C.M. Weiser-Evans, et al., CD8(+) T cells modulate autosomal dominant polycystic kidney disease progression, Kidney Int. 94 (6) (2018) 1127–1140.

[64] C.G. Lee, J.G. Kim, H.J. Kim, H.K. Kwon, I.J. Cho, D.W. Choi, W.H. Lee, W.D. Kim, S.J. Hwang, S. Choi, et al., Discovery of an integrative network of microRNAs and transcriptomics changes for acute kidney injury, Kidney Int. 86 (5) (2014) 943–953.

[65] M. Yheskel, V. Patel, Therapeutic microRNAs in polycystic kidney disease, Curr. Opin. Nephrol. Hypertens. 26 (4) (2017) 282–289.

[66] E. Wang, Y.Y. Chiou, W.Y. Jeng, H.K. Lin, H.H. Lin, H.J. Chin, C.K. Leo Wang, S.S. Yu, S.C. Tsai, C.Y. Chiang, et al., Overexpression of exogenous kidney-specific Ngal attenuates progressive cyst development and prolongs lifespan in a murine model of polycystic kidney disease, Kidney Int. 91 (2) (2017) 412–422.

[67] L. Chen, X. Zhou, L.X. Fan, Y. Yao, K.I. Swenson-Fields, M. Gadjeva, D.P. Wallace, D.J. Peters, A. Yu, J.J. Grantham, et al., Macrophage migration inhibitory factor promotes cyst growth in polycystic kidney disease, J. Clin. Invest. 125 (6) (2015) 2399–2412.

[68] N. Carayol, E. Vakana, A. Sassano, S. Kaur, D.J. Goussetis, H. Glaser, B.J. Druker, N.J. Donato, J.K. Altman, S. Barr, et al., Critical roles for mTORC2- and rapamycin-insensitive mTORC1-complexes in growth and survival of BCR-ABL-expressing leukemic cells, Proc. Natl. Acad. Sci. U. S. A. 107 (28) (2010) 12469–12474.

[69] J.M. Shillingford, K.B. Piontek, G.G. Germino, T. Weimbs, Rapamycin ameliorates PKD resulting from conditional inactivation of Pkd1, J. Am. Soc. Nephrol. 21 (3) (2010) 489–497.

[70] J.M. Shillingford, C.P. Leamon, I.R. Vlahov, T. Weimbs, Folate-conjugated rapamycin slows progression of polycystic kidney disease, J. Am. Soc. Nephrol. 23 (10) (2012) 1674–1681.

[71] K. Ravichandran, I. Zafar, A. Ozkok, C.L. Edelstein, An mTOR kinase inhibitor slows disease progression in a rat model of polycystic kidney disease (PKD), Nephrol. Dial. Transplant. 30 (1) (2014) 45–53.

[72] G. Gobe, D. Willgoss, N. Hogg, E. Schoch, Z. Endre, Cell survival or death in renal tubular epithelium after ischemia- reperfusion injury, Kidney Int. 56 (4) (1999) 1299–1304.

[73] G. Gobe, X.J. Zhang, L. Cuttle, B. Pat, D. Willgoss, J. Hancock, R. Barnard, R.B. Endre, Bcl-2 genes and growth factors in the pathology of ischaemic acute renal failure, Immunol. Cell Biol. 77 (3) (1999) 279–286.

[74] A. L, V. JM, S. R, How cells die counts, Am. J. Kidney Dis. 36 (2000) 662–668.

[75] B. Grasl-Kraupp, B. Ruttkay-Nedecky, H. Koudelka, K. Bukowska, W. Bursch, R. Schulte-Hermann, In situ detection of fragmented DNA (TUNEL assay) fails to discriminate among apoptosis, necrosis, and autolytic cell death: a cautionary note, Hepatology 21 (5) (1995) 1465–1468.

[76] G. Gobe, X.J. Zhang, D.A. Willgoss, E. Schoch, N.A. Hogg, Z.H. Endre, Relationship between expression of Bcl-2 genes and growth factors in ischemic acute renal failure in the rat, J. Am. Soc. Nephrol. 11 (3) (2000) 454–467.

[77] T. Weimbs, Regulation of mTOR by polycystin-1: is polycystic kidney disease a case of futile repair? Cell Cycle 5 (21) (2006) 2425–2429.

[78] M.B. Boxer, A.M. Quinn, M. Shen, A. Jadhav, W. Leister, A. Simeonov, D.S. Auld, C.J. Thomas, A highly potent and selective caspase 1 inhibitor that utilizes a key 3-cyanopropanoic acid moiety, ChemMedChem 5 (5) (2010) 730–738.

[79] J.G. Chapman, W.P. Magee, H.A. Stukenbrok, G.E. Beckius, A.J. Milici, W.R. Tracey, A novel nonpeptidic caspase-3/7 inhibitor, (S)-(+)-5-[1-(2-methoxymethylpyrrolidinyl)sulfonyl]isatin reduces myocardial ischemic injury, Eur. J. Pharmacol. 456 (1–3) (2002) 59–68.

[80] A. Abbate, G.G. Biondi-Zoccai, A. Baldi, Pathophysiologic role of myocardial apoptosis in post-infarction left ventricular remodeling, J. Cell. Physiol. 193 (2) (2002) 145–153.

[81] R. Cursio, J. Gugenheim, J.E. Ricci, D. Crenesse, P. Rostagno, L. Maulon, M.C. Saint-Paul, B. Ferrua, A.P. Auberger, A caspase inhibitor fully protects rats against lethal normothermic liver ischemia by inhibition of liver apoptosis, FASEB J. 13 (2) (1999) 253–261.

[82] V.Y. Melnikov, S.G. Faubel, B. S, M.S. Lucia, D. Ljubanovic, C.L. Edelstein, Neutrophil-independent mechanisms of caspase-1- and IL-18-mediated ischemic acute tubular necrosis in mice, J. Clin. Invest. 110 (2002) 1083–1091.

[83] S. Faubel, C.L. Edelstein, Caspases as drug targets in ischemic organ injury, Curr. Drug Targets Immune Endocr. Metabol. Disord. 5 (3) (2005) 269–287.

[84] Y. Hayakawa, M. Chandra, W. Miao, J. Shirani, J.H. Brown, G.W. Dorn, R.C. Armstrong, R.N. Kitsis, Inhibition of cardiac myocyte apoptosis improves cardiac function and abolishes mortality in the peripartum cardiomyopathy of Galpha(q) transgenic mice, Circulation 108 (24) (2003) 3036–3041.

[85] S. Natori, H. Higuchi, P. Contreras, G.J. Gores, The caspase inhibitor IDN-6556 prevents caspase activation and apoptosis in sinusoidal endothelial cells during liver preservation injury, Liver Transpl. 9 (3) (2003) 278–284.

[86] A. Canbay, A. Feldstein, E. Baskin-Bey, S.F. Bronk, G.J. Gores, The caspase inhibitor IDN-6556 attenuates hepatic injury and fibrosis in the bile duct ligated mouse, J. Pharmacol. Exp. Therap. 308 (3) (2004) 1191–1196.

[87] K.L. Valentino, M. Gutierrez, R. Sanchez, M.J. Winship, D.A. Shapiro, First clinical trial of a novel caspase inhibitor: anti-apoptotic caspase inhibitor, IDN-6556, improves liver enzymes, Int. J. Clin. Pharmacol. Ther. 41 (10) (2003) 441–449.

[88] C. Du, M. Fang, Y. Li, L. Li, X. Wang, Smac, a mitochondrial protein that promotes cytochrome c-dependent caspase activation by eliminating IAP inhibition, Cell 102 (2000) 33–42.

[89] S.M. Srinivasula, P. Datta, X.J. Fan, T. Fernandes-Alnemri, Z. Huang, E.S. Alnemri, Molecular determinants of the caspase-promoting activity of Smac/DIABLO and its role in the death receptor pathway, J. Biol. Chem. 275 (46) (2000) 36152–36157.

[90] L.X. Fan, X. Zhou, W.E. Sweeney Jr., D.P. Wallace, E.D. Avner, J.J. Grantham, X. Li, Smac-mimetic-induced epithelial cell death reduces the growth of renal cysts, J. Am. Soc. Nephrol. 24 (12) (2013) 2010–2022.

[91] B. Goilav, Apoptosis in polycystic kidney disease, Biochim. Biophys. Acta 1812 (10) (2011) 1272–1280.

[92] N.S. Murcia, W.E. Sweeney Jr., E.D. Avner, New insights into the molecular pathophysiology of polycystic kidney disease, Kidney Int. 55 (4) (1999) 1187–1197.

[93] S. Ibrahim, Increased apoptosis and proliferative capacity are early events in cyst formation in autosomal-dominant, polycystic kidney disease, Sci. World J. 7 (2007) 1757–1767.

[94] J. Lanoix, V. D'Agati, M. Szabolcs, M. Trudel, Dysregulation of cellular proliferation and apoptosis mediates human autosomal dominant polycystic kidney disease (ADPKD), Oncogene 13 (6) (1996) 1153–1160.

[95] M. Trudel, L. Barisoni, J. Lanoix, V. D'Agati, Polycystic kidney disease in SBM transgenic mice: role of c-myc in disease induction and progression, Am. J. Pathol. 152 (1) (1998) 219–229.

[96] M. Trudel, J. Lanoix, L. Barisoni, M.J. Blouin, C. L'Italien, V. D'Agati, C-myc-induced apoptosis in polycystic kidney disease is Bcl-2 and p53 independent, J. Exp. Med. 186 (11) (1997) 1873–1884.

[97] M.R. Ogborn, N. Bankovic-Calic, C. Shoesmith, R. Buist, J. Peeling, Soy protein modification of rat polycystic kidney disease, Am. J. Physiol. 274 (3 Pt 2) (1998) F541–F549.

[98] C.M. Sorenson, B.J. Padanilam, M.R. Hammerman, Abnormal postpartum renal development and cystogenesis in the bcl-2 (-/-) mouse, Am. J. Physiol. 271 (1 Pt 2) (1996) F184–F193.

[99] D. Woo, Loss of renal function in polycystic kidney diseases is a result of apoptosis, J. Am. Soc. Nephrol. 4 (1993) 268.

[100] M.R. Wilson, Apoptosis: unmasking the executioner, Cell Death Differ. 5 (8) (1998) 646–652.

[101] C.S. Chen, M. Mrksich, S. Huang, G.M. Whitesides, D.E. Ingber, Geometric control of cell life and death, Science 276 (1997) 1425–1429.

[102] A. Tsuboi, S. Ohsawa, D. Umetsu, Y. Sando, E. Kuranaga, T. Igaki, K. Fujimoto, Competition for space is controlled by apoptosis-induced change of local epithelial topology, Curr. Biol. 28 (13) (2018) 2115–2128 e2115.

[103] M. Couillard, R. Guillaume, N. Tanji, V. D'Agati, M. Trudel, c-myc-induced apoptosis in polycystic kidney disease is independent of FasL/Fas interaction, Cancer Res. 62 (8) (2002) 2210–2214.

[104] M. Trudel, V. D'Agati, F. Costantini, C-myc as an inducer of polycystic kidney disease in transgenic mice, Kidney Int. 39 (4) (1991) 665–671.

[105] B.D. Cowley Jr., S. Gudapaty, A.L. Kraybill, B.D. Barash, M.A. Harding, J.P. Calvet, V.H. Gattone 2d, Autosomal-dominant polycystic kidney disease in the rat, Kidney Int. 43 (3) (1993) 522–534.

[106] M.S. Soengas, R.M. Alarcon, H. Yoshida, A.J. Giaccia, R. Hakem, T.W. Mak, S.W. Lowe, Apaf-1 and caspase-9 in p53-dependent apoptosis and tumor inhibition, Science 284 (5411) (1999) 156–159.

[107] A. Kangas, D.W. Nicholson, E. Hottla, Involvement of CPP32/caspase-3 in c-myc-induced apoptosis, Oncogene 16 (1998) 387–398.

[108] T. Mochizuki, C. Kitanaka, K. Noguchi, A. Sugiyama, S. Kagaya, S. Chi, A. Asai, Y. Kuchino, Pim-1 kinase stimulates c-myc-mediated death signaling upstream of caspase-3 (CPP32)-like protease activation, Oncogene 15 (1997) 1471–1480.

[109] L.A. Sabourin, P. Seale, J. Wagner, M.A. Rudnicki, Caspase-3 cleavage of the Ste20-related kinase SLk releases and activates an apoptosis -inducing kinase domain and an actin-disassembling region, Mol. Cell. Biol. 20 (2000) 684–696.

[110] H. Husson, P. Manavalan, V.R. Akmaev, R.J. Russo, B. Cook, B. Richards, D. Barberio, D. Liu, X. Cao, G.M. Landes, et al., New insights into ADPKD molecular pathways using combination of SAGE and microarray technologies, Genomics 84 (3) (2004) 497–510.

[111] X. Song, G.V. Di, N. He, K. Wang, A. Ingram, N.D. Rosenblum, Y. Pei, Systems biology of autosomal dominant polycystic kidney disease (ADPKD): computational identification of gene expression pathways and integrated regulatory networks, Hum. Mol. Genet. 18 (13) (2009) 2328–2343.

[112] V.E. Torres, Apoptosis in cystogenesis: hands on or hands off? Kidney Int. 55 (1) (1999) 334–335.

[113] R.H. Elbekai, M.G. Paranjpe, P.C. Contreras, A. Spada, Carcinogenicity assessment of the pan-caspase inhibitor, emricasan, in Tg.rasH2 mice, Regul. Toxicol. Pharmacol. 72 (2) (2015) 169–178.

[114] B. Levine, G. Kroemer, Autophagy in the pathogenesis of disease, Cell 132 (1) (2008) 27–42.

[115] B. Loos, A. du Toit, J.H. Hofmeyr, Defining and measuring autophagosome flux-concept and reality, Autophagy 10 (11) (2014) 2087–2096.

[116] D.J. Klionsky, K. Abdelmohsen, A. Abe, M.J. Abedin, H. Abeliovich, A. Acevedo Arozena, H. Adachi, C.M. Adams, P.D. Adams, K. Adeli, et al., Guidelines for the use and interpretation of assays for monitoring autophagy (3rd edition), Autophagy 12 (1) (2016) 1–222.

[117] B. Levine, D.J. Klionsky, Autophagy wins the 2016 Nobel Prize in Physiology or Medicine: breakthroughs in baker's yeast fuel advances in biomedical research, Proc. Natl. Acad. Sci. U. S. A. 114 (2) (2017) 201–205.

[118] M.Y. Chang, T.L. Ma, C.C. Hung, Y.C. Tian, Y.C. Chen, C.W. Yang, Y.C. Cheng, Metformin inhibits cyst formation in a zebrafish model of polycystin-2 deficiency, Sci. Rep. 7 (1) (2017) 7161.

[119] T.B. Huber, C.L. Edelstein, B. Hartleben, K. Inoki, M. Jiang, D. Koya, S. Kume, W. Lieberthal, A. Nallet, A. Quiroga, et al., Emerging role of autophagy in kidney function, diseases and aging, Autophagy 8 (7) (2012) 1009–1031.

[120] H.A. Bustamante, A.E. Gonzalez, C. Cerda-Troncoso, R. Shaughnessy, C. Otth, A. Soza, P.V. Burgos, Interplay between the autophagy-lysosomal pathway and the ubiquitin-proteasome system: a target for therapeutic development in Alzheimer's disease, Front. Cell. Neurosci. 12 (2018) 126.

[121] Y. Sun, X. Yao, Q.J. Zhang, M. Zhu, Z.P. Liu, B. Ci, Y. Xie, D. Carlson, B.A. Rothermel, Y. Sun, et al., Beclin-1-dependent autophagy protects the heart during sepsis, Circulation 138 (20) (2018 Nov 13) 2247–2262.

[122] A. Sureshbabu, S.W. Ryter, M.E. Choi, Oxidative stress and autophagy: crucial modulators of kidney injury, Redox Biol. 4 (2015) 208–214.

[123] S. Liu, B. Hartleben, O. Kretz, T. Wiech, P. Igarashi, N. Mizushima, G. Walz, T.B. Huber, Autophagy plays a critical role in kidney tubule maintenance, aging and ischemia-reperfusion injury, Autophagy 8 (5) (2012) 826–837.

[124] M. Jiang, Q. Wei, G. Dong, M. Komatsu, Y. Su, Z. Dong, Autophagy in proximal tubules protects against acute kidney injury, Kidney Int. 82 (12) (2012) 1271–1283.

[125] C.T. Chien, S.K. Shyue, M.K. Lai, Bcl-xL augmentation potentially reduces ischemia/reperfusion induced proximal and distal tubular apoptosis and autophagy, Transplantation 84 (9) (2007) 1183–1190.

[126] S. Periyasamy-Thandavan, M. Jiang, Q. Wei, R. Smith, X.M. Yin, Z. Dong, Autophagy is cytoprotective during cisplatin injury of renal proximal tubular cells, Kidney Int. 74 (5) (2008) 631–640.

[127] B. Hartleben, M. Godel, C. Meyer-Schwesinger, S. Liu, T. Ulrich, S. Kobler, T. Wiech, F. Grahammer, S.J. Arnold, M.T. Lindenmeyer, et al., Autophagy influences glomerular disease susceptibility and maintains podocyte homeostasis in aging mice, J. Clin. Invest. 120 (4) (2010) 1084–1096.

[128] A. Aguilar, Polycystic kidney disease: autophagy boost to treat ADPKD? Nat. Rev. Nephrol. 13 (3) (2017) 134.

[129] S. Mukhopadhyay, P.K. Panda, N. Sinha, D.N. Das, S.K. Bhutia, Autophagy and apoptosis: where do they meet? Apoptosis 19 (4) (2014) 555–566.

[130] F. Zhou, Y. Yang, D. Xing, Bcl-2 and Bcl-xL play important roles in the crosstalk between autophagy and apoptosis, FEBS J. 278 (3) (2011) 403–413.

[131] S. Shimizu, T. Kanaseki, N. Mizushima, T. Mizuta, S. Arakawa-Kobayashi, C.B. Thompson, Y. Tsujimoto, Role of Bcl-2 family proteins in a non-apoptotic programmed cell death dependent on autophagy genes, Nat. Cell Biol. 6 (12) (2004) 1221–1228.

[132] J. Song, X. Zhao, Y. Feng, S. Xu, Y. Zhang, L. Wei, Involvement of proapoptotic genes in autophagic cell death induced by irradiation, Cell Death Dis. 3 (2017)

[133] V. Giansanti, A. Torriglia, A.I. Scovassi, Conversation between apoptosis and autophagy: "Is it your turn or mine?", Apoptosis 16 (4) (2011) 321–333.

[134] L. Yu, A. Alva, H. Su, P. Dutt, E. Freundt, S. Welsh, E.H. Baehrecke, M.J. Lenardo, Regulation of an ATG7-beclin 1 program of autophagic cell death by caspase-8, Science 304 (5676) (2004) 1500–1502.

[135] G.P. Kaushal, V. Kaushal, C. Herzog, C. Yang, Autophagy delays apoptosis in renal tubular epithelial cells in cisplatin cytotoxicity, Autophagy 4 (5) (2008) 710–712.

[136] G. Kroemer, B. Levine, Autophagic cell death: the story of a misnomer, Nat. Rev. Mol. Cell Biol. 9 (12) (2008) 1004–1010.

[137] M.C. Maiuri, E. Zalckvar, A. Kimchi, G. Kroemer, Self-eating and self-killing: crosstalk between autophagy and apoptosis, Nat. Rev. Mol. Cell Biol. 8 (9) (2007) 741–752.

[138] R.S. Hotchkiss, A. Strasser, J.E. McDunn, P.E. Swanson, Cell death, N. Engl. J. Med. 361 (16) (2009) 1570–1583.

[139] G. Walz, K. Budde, M. Mannaa, J. Nurnberger, C. Wanner, C. Sommerer, U. Kunzendorf, B. Banas, W.H. Horl, N. Obermuller, et al., Everolimus in patients with autosomal dominant polycystic kidney disease, New Engl. J. Med. 363 (9) (2010) 830–840.

[140] A.L. Serra, D. Poster, A.D. Kistler, F. Krauer, S. Raina, J. Young, K.M. Rentsch, K.S. Spanaus, O. Senn, P. Kristanto, et al., Sirolimus and kidney growth in autosomal dominant polycystic kidney disease, New Engl. J. Med. 363 (9) (2010) 820–829.

[141] T. Watnick, G.G. Germino, mTOR inhibitors in polycystic kidney disease, New Engl. J. Med. 363 (9) (2010) 879–881.

[142] S.J. Leuenroth, D. Okuhara, J.D. Shotwell, G.S. Markowitz, Z. Yu, S. Somlo, C.M. Crews, Triptolide is a traditional Chinese medicine-derived inhibitor of polycystic kidney disease, Proc. Natl. Acad. Sci. U. S. A. 104 (11) (2007) 4389–4394.

[143] S.J. Leuenroth, N. Bencivenga, P. Igarashi, S. Somlo, C.M. Crews, Triptolide reduces cystogenesis in a model of ADPKD, J. Am. Soc. Nephrol. 19 (9) (2008) 1659–1662.

[144] A. Shakeri, A.F.G. Cicero, Y. Panahi, M. Mohajeri, A. Sahebkar, Curcumin: a naturally occurring autophagy modulator, J. Cell. Physiol. 234 (5) (2019) 5643–5654.

[145] W.N. Leonhard, W.A. van der, Z. Novalic, S.J. Kunnen, R.T. Gansevoort, M.H. Breuning, E. de Heer, D.J. Peters, Curcumin inhibits cystogenesis by simultaneous interference of multiple signaling pathways: in vivo evidence from a Pkd1-deletion model, Am. J. Physiol. Renal Physiol. 300 (5) (2011 May) F1193–F1202.

[146] J. Han, X.Y. Pan, Y. Xu, Y. Xiao, Y. An, L. Tie, Y. Pan, X.J. Li, Curcumin induces autophagy to protect vascular endothelial cell survival from oxidative stress damage, Autophagy 8 (5) (2012) 812–825.

[147] Y. Cheng, X. Ren, Y. Zhang, Y. Shan, K.J. Huber-Keener, L. Zhang, S.R. Kimball, H. Harvey, L.S. Jefferson, J.M. Yang, Integrated regulation of autophagy and apoptosis by EEF2K controls cellular fate and modulates the efficacy of curcumin and velcade against tumor cells, Autophagy 9 (2) (2013) 208–219.

[148] J.J. Talbot, J.M. Shillingford, S. Vasanth, N. Doerr, S. Mukherjee, M.T. Kinter, T. Watnick, T. Weimbs, Polycystin-1 regulates STAT activity by a dual mechanism, Proc. Natl. Acad. Sci. U. S. A. 108 (19) (2011) 7985–7990.

[149] F. Pietrocola, V. Izzo, M. Niso-Santano, E. Vacchelli, L. Galluzzi, M.C. Maiuri, G. Kroemer, Regulation of autophagy by stress-responsive transcription factors, Semin. Cancer Biol. 23 (5) (2013 Oct) 310–322 E pub ahead of print.

[150] B. Chandrasekar, J.B. Smith, G.L. Freeman, Ischemia-reperfusion of rat myocardium activates nuclear factor-KappaB and induces neutrophil infiltration via lipopolysaccharide-induced CXC chemokine, Circulation 103 (18) (2001) 2296–2302.

[151] W.E. Sweeney Jr., R.O. von Vigier, P. Frost, E.D. Avner, Src inhibition ameliorates polycystic kidney disease, J. Am. Soc. Nephrol. 19 (7) (2008) 1331–1341.

[152] V. Takiar, S. Nishio, P. Seo-Mayer, J.D. King Jr., H. Li, L. Zhang, A. Karihaloo, K.R. Hallows, S. Somlo, M.J. Caplan, Activating AMP-activated protein kinase (AMPK) slows renal cystogenesis, Proc. Natl. Acad. Sci. U. S. A. 108 (6) (2011) 2462–2467.

[153] M. Hoyer-Hansen, M. Jaattela, AMP-activated protein kinase: a universal regulator of autophagy? Autophagy 3 (4) (2007) 381–383. Aug.

[154] Z. Xie, K. Lau, B. Eby, P. Lozano, C. He, B. Pennington, H. Li, S. Rathi, Y. Dong, R. Tian, et al., Improvement of cardiac functions by chronic metformin treatment is associated with enhanced cardiac autophagy in diabetic OVE26 mice, Diabetes 60 (6) (2011) 1770–1778.

[155] S.S. Seshia, J.Y. Yager, B. Johnston, P. Haese, Inter-observer agreement in assessing comatose children, Can. J. Neurol. Sci. 18 (4) (1991) 472–475.

[156] S. Kume, T. Uzu, K. Horiike, M. Chin-Kanasaki, K. Isshiki, S. Araki, T. Sugimoto, M. Haneda, A. Kashiwagi, D. Koya, Calorie restriction enhances cell adaptation to hypoxia through Sirt1-dependent mitochondrial autophagy in mouse aged kidney, J. Clin. Invest. 120 (4) (2010) 1043–1055.

[157] J. Lempiainen, P. Finckenberg, E.E. Mervaala, S. Sankari, J. Levijoki, E.M. Mervaala, Caloric restriction ameliorates kidney ischaemia/reperfusion injury through PGC-1alpha-eNOS pathway and enhanced autophagy, Acta Physiol. (Oxf.) 208 (4) (2013) 410–421.

[158] G. Warner, K.Z. Hein, V. Nin, M. Edwards, C.C. Chini, K. Hopp, P.C. Harris, V.E. Torres, E.N. Chini, Food restriction ameliorates the development of polycystic kidney disease, J. Am. Soc. Nephrol. 27 (5) (2016 May) 1437–1447.

[159] K.R. Kipp, M. Rezaei, L. Lin, E.C. Dewey, T. Weimbs, A mild reduction of food intake slows disease progression in an orthologous mouse model of polycystic kidney disease, Am. J. Physiol. Renal Physiol. 310 (8) (2016 Apr 15) F726–F731 ajprenal.

[160] M. Chiaravalli, I. Rowe, V. Mannella, G. Quilici, T. Canu, V. Bianchi, A. Gurgone, S. Antunes, P. D'Adamo, A. Esposito, et al., 2-Deoxy-d-glucose ameliorates PKD progression, J. Am. Soc. Nephrol. 27 (7) (2016 Jul) 1958–1969.

[161] A. Kraus, G. Schley, K. Kunzelmann, R. Schreiber, D.J. Peters, R. Stadler, K.U. Eckardt, B. Buchholz, Glucose promotes secretion-dependent renal cyst growth, J. Mol. Med. (Berl) 94 (1) (2016 Jan) 107–117.

[162] K.L. Nowak, Z. You, B. Gitomer, G. Brosnahan, V.E. Torres, A.B. Chapman, R.D. Perrone, T.I. Steinman, K.Z. Abebe, F.F. Rahbari-Oskoui, et al., Overweight and obesity are predictors of progression in early autosomal dominant polycystic kidney disease, J. Am. Soc. Nephrol. 29 (2) (2018) 571–578.

[163] A.F. Fernandez, C. Barcena, G.G. Martinez-Garcia, I. Tamargo-Gomez, M.F. Suarez, F. Pietrocola, F. Castoldi, L. Esteban, E. Sierra-Filardi, P. Boya, et al., Autophagy counteracts weight gain, lipotoxicity and pancreatic beta-cell death upon hypercaloric pro-diabetic regimens, Cell Death Dis. 8 (8) (2017) e2970.

[164] W. Shi, D. Xu, J. Gu, C. Xue, B. Yang, L. Fu, S. Song, D. Liu, W. Zhou, J. Lv, et al., Saikosaponin-d inhibits proliferation by up-regulating autophagy via the CaMKKbeta-AMPK-mTOR pathway in ADPKD cells, Mol. Cell. Biochem. 449 (1–2) (2018) 219–226.

[165] L. Sun, C. Hu, X. Zhang, Histone deacetylase inhibitors reduce cysts by activating autophagy in polycystic kidney disease, Kidney Dis. (Basel) 5 (3) (2019) 163–172.

[166] A.I. Masyuk, T.V. Masyuk, M.J. Lorenzo Pisarello, J.F. Ding, L. Loarca, B.Q. Huang, N.F. LaRusso, Cholangiocyte autophagy contributes to hepatic cystogenesis in polycystic liver disease and represents a potential therapeutic target, Hepatology 67 (3) (2018) 1088–1108.

[167] X.S. Ren, Y. Sato, K. Harada, M. Sasaki, S. Furubo, J.Y. Song, Y. Nakanuma, Activation of the PI3K/mTOR pathway is involved in cystic proliferation of cholangiocytes of the PCK rat, PLoS One 9 (1) (2014) e87660.

[168] J. Yang, Y. Zhao, K. Ma, F.J. Jiang, W. Liao, P. Zhang, J. Zhou, B. Tu, L. Wang, H.H. Kampinga, et al., Deficiency of hepatocystin induces autophagy through an mTOR-dependent pathway, Autophagy 7 (7) (2011) 748–759.

[169] D.J. Lager, Q. Qian, R.J. Bengal, M. Ishibashi, V.E. Torres, The pck rat: a new model that resembles human autosomal dominant polycystic kidney and liver disease, Kidney Int. 59 (1) (2001) 126–136.

[170] L.A. Smith, N.O. Bukanov, H. Husson, R.J. Russo, T.C. Barry, A.L. Taylor, D.R. Beier, O. Ibraghimov-Beskrovnaya, Development of polycystic kidney disease in juvenile cystic kidney mice: insights into pathogenesis, ciliary abnormalities, and common features with human disease, J. Am. Soc. Nephrol. 17 (10) (2006) 2821–2831.

[171] M. Moser, A. Pscherer, C. Roth, J. Becker, G. Mucher, K. Zerres, C. Dixkens, J. Weis, L. Guay-Woodford, R. Buettner, et al., Enhanced apoptotic cell death of renal epithelial cells in mice lacking transcription factor AP-2beta, Genes Dev. 11 (15) (1997) 1938–1948.

[172] P.J. Winyard, J. Nauta, D.S. Lirenman, P. Hardman, V.R. Sams, R.A. Risdon, A.S. Woolf, Deregulation of cell survival in cystic and dysplastic renal development, Kidney Int. 49 (1) (1996) 135–146.

[173] B. Goilav, L.M. Satlin, P.D. Wilson, Pathways of apoptosis in human autosomal recessive and autosomal dominant polycystic kidney diseases, Pediatr. Nephrol. 23 (9) (2008) 1473–1482.

[174] H. Li, P. Wang, Q. Sun, W.X. Ding, X.M. Yin, R.W. Sobol, D.B. Stolz, J. Yu, L. Zhang, Following cytochrome c release, autophagy is inhibited during chemotherapy-induced apoptosis by caspase 8-mediated cleavage of Beclin 1, Cancer Res. 71 (10) (2011) 3625–3634.
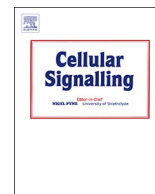
Increased mTOR and suppressed autophagic flux in the heart of a hypomorphic *Pkd1* mouse model of autosomal dominant polycystic kidney disease

Daniel J. Atwood, Deepak Pokhrel, Carolyn N. Brown, Sara J. Holditch, Dheevena M. Bachu, Andrew Thorburn, Katharina Hopp, Charles L. Edelstein*

Division of Renal Diseases and Hypertension, University of Colorado Anschutz Medical Campus, Aurora, Colorado, USA

ABSTRACT

Cardiac hypertrophy is common in autosomal dominant polycystic kidney disease (ADPKD) patients. We found increased heart weight in $Pkd1^{RC/RC}$ and $Pkd2^{WS25/+}$ mouse models of ADPKD. As there is a link between increased heart weight and mammalian target of rapamycin (mTOR), the aim of the study was to determine mTOR complex 1 and 2 signaling proteins in the heart in the $Pkd1^{RC/RC}$ mouse model of PKD. In 70 day old $Pkd1^{RC/RC}$ hearts, on immunoblot analysis, there was a large increase in p-AMPK^{Thr172}, a known autophagy inducer, and an increase in p-Akt^{Ser473} and p-Akt^{Thr308}, but no increase in other mTORC1/2 proteins (p-S6$^{Ser240/244}$, p-mTOR^{Ser2448}). In 150 day old $Pkd1^{RC/RC}$ hearts, there was an increase in mTORC1 (p-S6$^{Ser240/244}$) and mTOR-related proteins (p-Akt^{Thr308}, p-GSK3β^{Ser9}, p-AMPK^{Thr172}). As the mTOR pathway is the master regulator of autophagy, autophagy proteins were measured. There was an increase in p-Beclin-1 (BECN1), an autophagy regulator and activating molecule in Beclin-1-regulated autophagy (AMBRA1), a regulator of Beclin that play a role in autophagosome formation, an early stage of autophagy. There was a defect in the later stage of autophagy, the fusion of the autophagosome with the lysosome, known as autophagic flux, as evidenced by the lack of an increase in LC3-II, a marker of autophagosomes, with the lysosomal inhibitor bafilomycin, in both 70 day old and 150 day old hearts. To determine the role of autophagy in causing increased heart weight, $Pkd1^{RC/RC}$ were treated with 2-deoxyglucose (2-DG) or Tat-Beclin1 peptide, agents known to induce autophagy. 2-DG treatment from 150 to 350 days of age, a time period when increased heart weight developed, did not reduce the increased heart weight. Unexpectedly, Tat-Beclin 1 peptide treatment from 70 to 120 days of age resulted in increased heart weight. In summary, there is suppressed autophagic flux in the heart at an early age in $Pkd1^{RC/RC}$ mice. Increased mTOR signaling in older mice is associated suppressed autophagic flux. There was a large increase in p-AMPK^{Thr172}, a known autophagy inducer, in both young and old mice. 2-DG treatment did not impact increased heart weight and Tat-Beclin1 peptide increased heart weight.

1. Introduction

ADPKD is the most common life threatening genetic condition [1,2]. Most cases of ADPKD are caused by mutations to either the *PKD1* (~80% of cases) or *PKD2* (~12% of cases) genes. The disease is characterized by slowly growing and persistent renal cysts that eventualy cause end-stage renal disease [1]. The growth of cysts in the kidney results in hypertension, chronic kidney disease and end stage kidney disease requiring dialysis and kidney transplantation [1,2]. ADPKD is as common as 1 in 400 persons. Abnormalities of signaling pathways in PKD kidneys include mTORC1, cAMP, AMP-activated protein kinase

(AMPK), signal transducer and activator of transcription (STAT), Wnt, G-protein, proto-oncogene tyrosine-protein kinase Src (c-Src), mitogen-activated protein kinase (MAPK), epidermal growth factor (EGFR), cyclin-dependent kinase (CDK), intracellular calcium, p53, Myc and calcium-sensing receptor signaling pathways [3]. Activation of the calcium-sensing receptor increases intracellular calcium and decreases cAMP and mTOR in *PKD1* deficient proximal tubular epithelial cells [4]. Selective calcium-sensing receptor activation in *PKD1* deficient proximal tubular epithelial cells restores altered mitochondrial function that is thought to play a role in cyst formation [5]. Hyper-proliferation, increased fluid secretion, increased apoptosis and impaired autophagy

---

* Corresponding author at: Division of Renal Diseases and Hypertension, Univ. of Colorado Anschutz Medical Campus, Box C281, 12700 East, 19th Ave, Aurora, CO 80045, USA.
E-mail address: Charles.edelstein@cuanschutz.edu (C.L. Edelstein).

in the cells lining the kidney cysts are all characteristic of ADPKD [6–9].

Cardiac disease is the commonest cause of death in ADPKD patients [10]. ADPKD patients have left ventricular hypertrophy (LVH) out of proportion to the degree of hypertension [11]. As complications of ADPKD like LVH are common, the health care burden of LVH in ADPKD patients is large. Thus, understanding the pathophysiology of cardiac hypertrophy in PKD and testing therapies to reduce cardiac hypertrophy in PKD are very important.

mTOR is a serine/threonine protein kinase that regulates cell growth, cell proliferation, cell survival, protein synthesis, autophagy, and transcription [12]. The mTOR pathway is a central regulator of mammalian metabolism and physiology [13]. mTOR exists in two distinct structural and functional complexes, mTORC1 and mTORC2, that are both known to regulate cardiac structure and function in models of cardiac hypertrophy. Studies show conflicting results on whether activation of mTORC1 and 2 in the heart promotes or improves cardiac hypertrophy [14]. While mTOR activation in the kidney is known to worsen PKD [15], mTOR activation in the heart in PKD has not been detailed. In the present study, we found increased heart weight in 180 day old $Pkd1^{RC/RC}$ and 116 day old $Pkd2^{WS25/-}$ mice with ADPKD and heart weight was decreased by an mTOR antisense oligonucleotide (ASO), that inhibits both mTORC1 and 2, in $Pkd2^{WS25/-}$ mice. We have previously shown the successful impact of treatment with an mTOR ASO on kidney cyst growth in $Pkd2^{WS25/-}$ mice [16]. Thus, we measured heart weight and mTORC1 and 2 proteins in the heart in $Pkd1^{RC/RC}$ mice, a hypomorphic model of ADPKD.

ADPKD is caused by mutations in two genes, *PKD1* or *PKD2*, which encode polycystin-1 (PC-1) and -2 (PC-2), respectively. Both PC-1 and PC-2 are known to modulate the mTOR pathway. PC-1 deficiency causes upregulation of the mTOR pathway via tuberous sclerosis complex 2 (TSC2) [17–20]. PC-2 modulates the mTOR pathway in human embryonic stem cell cardiomyocytes [21]. There is thought to be an emerging link between polycystins and the mTOR/4E-BP1 pathway in PKD [20]. As PC-1 and PC-2 are abnormal in both the kidneys and heart in ADPKD, we hypothesized that there would be mTOR activation in the heart in ADPKD mouse models that have a global gene defect that includes the heart.

In addition to being a master regulator of metabolism, mTORC1 is also a master regulator of autophagy [22] and mTOR activation inhibits autophagy [23]. Thus, we hypothesized that upregulation of mTOR would be associated with suppressed autophagy in the heart. Signaling pathways controlled by AMPK are also central to cellular metabolism [24–26]. AMPK is a universal regulator of autophagy [27]. Activation of AMPK is known to inhibit mTOR via unc-51- like autophagy activating kinase (ULK1) and activate autophagy. Because of the connection between AMPK, mTOR and autophagy, we also measured AMPK in the $Pkd1^{RC/RC}$ hearts during a time course of PKD.

2. Methods

2.1. In vivo model

$Pkd1^{RC/RC}$ mice have a hypomorphic *Pkd1* gene mutation orthologous of PKD patient disease variant, *PKD1* p. R3277C (*Pkd1*) [28]. $Pkd1^{RC/RC}$ mice in the C57BL/6 background have cysts at birth that progressively enlarge from 1 month of age and older [29,30]. At 120 days of age, the two kidney to total body weight ratio, a marker of kidney size, in $Pkd1^{RC/RC}$ mouse kidneys is approximately double that of wild type controls and the percentage of kidney that is cystic is approximately 17% [31]. At 120 days of age, $Pkd1^{RC/RC}$ mice have abnormal kidney function as indicated by increased BUN and serum creatinine compared to wild type controls [31]. There is an increase in markers of mTORC1 (pS6 and p4E-BP1) in non-cystic areas of $Pkd1^{RC/RC}$ kidneys compared to wild type and pS6 and p4E-BP1 staining is present in cells lining kidney cysts [31]. Cyst expansion and size correlates with increased tubular cell proliferation [28] and there is

apoptosis in the cells lining the cysts in $Pkd1^{RC/RC}$ mice [31]. Wild type C57BL/6J mice (#000664) were purchased from Jackson Laboratories (Bar Harbor, ME, USA). All experiments were conducted with adherence to the National Institutes of Health Guide for the Care and Use of Laboratory Animals. The animal protocol was approved by the Animal Care and Use Committee of the University of Colorado at Denver. Mice were maintained on a standard diet with standard pathogen-free housing conditions, and food and water were freely available.

2.2. Cardiac dimensions

Transverse heart sections were stained with hematoxylin-eosin and analyzed using Aperio ImageScope macros. Intra-ventricular septum (IVS) width and left ventricular wall (LVW) width were measured as described previously [32].

2.3. Experimental in vivo protocol

2-Deoxyglucose (2-DG) has been shown to be an autophagy inducer in macrophages [33], cancer cells [34], endothelial cells [35] and hypothalamic cells via activation of AMPK [36]. Additionally, in patients with prostate cancer, administration of 2-DG for 14 days resulted in increased autophagy in peripheral blood mononuclear cells (PBMCs), as measured by decreased P62/SQSTM1 (p62) [37]. 2-DG can stimulate autophagy by ER stress rather than ATP depletion [38]. 2-DG or vehicle (normal saline) was given via I.P. injection at a dose of 600 mg/kg/day on weekdays from ages 70–120 days old or from 150 to 350 days old. 2-DG was purchased from Sigma Aldrich (Cat no. D8375).

Tat-Beclin 1 peptide is a known autophagy inducer when given to mice [39–41]. Mice were treated with Tat-Beclin 1 peptide or vehicle (normal saline) via I.P. injection at a dose of 20 mg/kg/day on weekdays from 70 to 120 days of age. A cell permeable Tat-Beclin 1 peptide was manufactured by the Peptide Core at the Univ. of Colorado Anschutz Medical Campus. The sequence of the Tat-Beclin D11 peptide was RRRQRRKKRGYGGDHWIHFTANWV [40].

$Pkd1^{RC/RC}$ mice were treated with the mTORC1 inhibitor, sirolimus or the mTOR kinase inhibitor, torin2, that inhibits both mTORC1 and 2, as we have previously described [31]. $Pkd2^{WS25/+}$ mice with ADPKD were treated with an mTOR ASO, that inhibits both mTORC1 and 2, as we have previously described [16]. Han: SPRD (Cy/+) rats with ADPKD were treated with the mTOR kinase inhibitor, PP242, that inhibits both mTORC1 and 2, as we have described [42].

2.4. Measurement of autophagic flux

The number of autophagosomes in a cell can increase, either due to increased formation or due to decreased degradation by the lysosome [43]. To investigate whether there is increased autophagosome synthesis or decreased degradation by the lysosome, mice were injected intra peritoneal (I.P.) with the lysosomal proton pump inhibitor, bafilomycin (1.75 mg/kg) or vehicle 2 h before sacrifice. After sacrifice LC3-II, a marker of autophagosomes and p62, a marker of autophagosome degradation was measured with bafilomycin or vehicle.

2.5. Immunoblot analysis

Protein was isolated from cells and tissues using RIPA, cOmplete protease and phoSTOP phosphatase inhibitor cocktails (Sigma). Homogenates were centrifuged and supernatant was taken for protein quantification by Bio-Rad (Hercules, CA, USA) DC Protein Assay as described by manufacturer. Samples were mixed with Laemmli Sample Buffer and boiled for 5 min. Samples were run on 8–15% polyacrylamide gels. Proteins were then transferred to 0.45 μm PVDF membranes, blocked with 2.5% evaporated milk, and probed with antibodies listed in Supplementary Table 1. Blots were developed by chemiluminescence and analyzed for densitometry using ImageJ

(National Institutes of Health).

2.5.1. Antibodies

Supplementary Table 1 lists the antibodies used in this study. The specificity of each of the antibodies used has been validated by the vendor (Cell Signaling Technology, Danvers, MA).

2.6. Statistical analysis

Data sets were analyzed by the non-parametric unpaired Mann Whitney test. Multiple group comparisons are performed using analysis of variance (ANOVA) with post-test according to Newman-Keuls. Single group comparisons were made using students t-test. A *p*-value of < 0.05 was considered statistically significant. Values are expressed as means ± SEM.

3. Results

3.1. Increased heart weight in rodent PKD models

Heart weight was analyzed from various published datasets of our group. Heart weight in $Pkd1^{RC/RC}$ mice was not increased in 70, 90, 120 and 150 day old mice but increased in 180 day old and 270 day old mice compared to strain/age matched wild types. In 120 day old $Pkd1^{RC/RC}$ mice we have demonstrated that the mTORC1 inhibitor, sirolimus and the mTOR kinase inhibitor, torin2, reduce PKD [31]. Heart weights were determined in mice from this published study [31]. In 120 day old $Pkd1^{RC/RC}$ mice treated with sirolimus or the mTOR kinase inhibitor, torin 2, the increase in heart weight did not reach statistical significance (Table 1). In 116 day old $Pkd2^{WS25/-}$ mice we have demonstrated that treatment with an mTOR antisense oligonucleotide (ASO) that inhibits both mTORC1 and 2, resulted in decreased PKD [44]. Heart weights were determined in $Pkd2^{WS25/-}$ mice from this published study [44]. The increase in heart weight in 116 day old $Pkd2^{WS25/-}$ mice was decreased by the mTOR ASO (Table 1). In 116 day old heterozygous $Pkd2^{WS25/+}$ mice that do not have PKD, the heart weight was increased compared to age matched littermate controls (Table 1). We have demonstrated that the mTOR kinase inhibitor, PP242, decreased PKD at 8 weeks of age in the Cy/+ rat model [42].

Table 1
Heart weight in rodent PKD models.

Model	Species	Age (days)	HW/BW (%)	Ref
+/+	Mouse	70	0.50 ± 0.03	
$Pkd1^{RC/RC}$ (B6)	Mouse	70	0.56 ± 0.04	
+/+	Mouse	90	0.64 ± 0.07	
$Pkd1^{RC/RC}$ (B6)	Mouse	90	0.63 ± 0.03	
+/+	Mouse	120	0.54 ± 0.07	
$Pkd1^{RC/RC}$ (B6)	Mouse	120	0.54 ± 0.07	
+/+	Mouse	150	0.49 ± 0.02	
$Pkd1^{RC/RC}$ (B6)	Mouse	150	0.52 ± 0.01	
+/+	Mouse	180	0.57 ± 0.08	
$Pkd1^{RC/RC}$ (B6)	Mouse	180	0.71 ± 0.09**	
+/+	Mouse	270	0.53 ± 0.06	
$Pkd1^{RC/RC}$ (B6)	Mouse	270	0.66 ± 0.07***	
$Pkd1^{RC/RC}$ (B6) + Veh	Mouse	120	0.47 ± 0.04	[34]
$Pkd1^{RC/RC}$ (B6) + Torin2	Mouse	120	0.58 ± 0.05	[34]
$Pkd1^{RC/RC}$ (B6) + Sirolimus	Mouse	120	0.55 ± 0.02	[34]
+/+	Mouse	116	0.52 ± 0.04	[9]
$Pkd2^{WS25/-}$ (B6) + Scr ASO	Mouse	116	0.69 ± 0.07*	[9]
$Pkd2^{WS25/-}$ (B6) + mTOR ASO	Mouse	116	0.55 ± 0.03*	[9]
+/+	Rat	56	0.43 ± 0.02	[35]
Cy/+ plus Veh	Rat	56	0.52 ± 0.02*	[35]
Cy/+ plus PP242	Rat	56	0.44 ± 0.01*	[35]

+/+ = wild type, HW/BW (%) = heart weight to body weight ratio (%), *P < .05, **P < .01, ***P < .001, Cy/+ = Han:SPRD rat, Torin2 and PP242 = mTOR kinase inhibitors, Scr = scrambled, ASO = antisense oligonucleotide, B6 = C57BL/6 background, Veh = vehicle, Ref = reference.
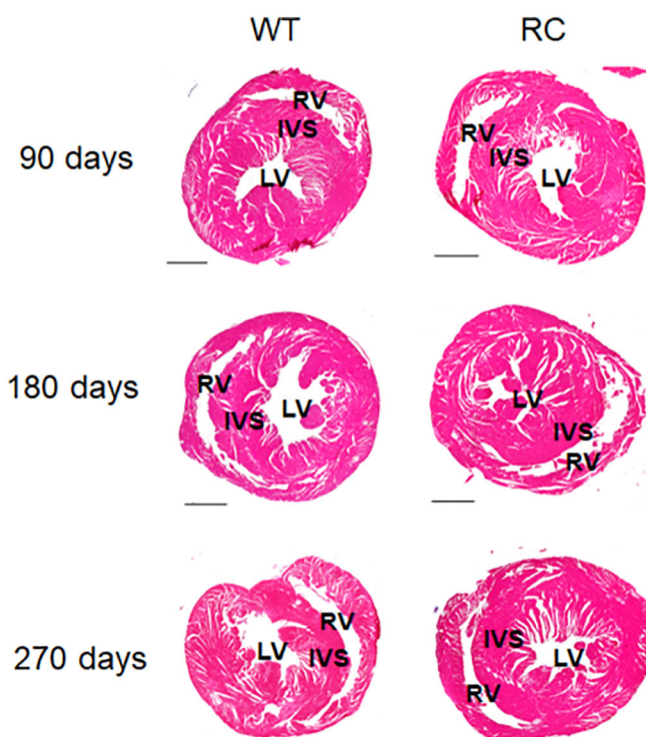
Age (days)	WT	RC	WT	RC
	IVS	IVS	LVW	LVW
90	372 ± 39	482 ± 88	558 ± 114	498 ± 48
180	372 ± 59	601 ± 46 *	438 ± 45	640 ± 24**
270	456 ± 41	817 ± 237*	634 ± 91	883 ± 53*

Fig. 1. Cardiac hypertrophy in 180 and 270 day old $Pkd1^{RC/RC}$ mice. Representative hematoxylin-eosin stained transverse sections of heart at the same magnification are demonstrated. There was no difference in size of intra-ventricular septum (IVS), left ventricular (LV) wall and right ventricle (RV) in 90 day old $Pkd1^{RC/RC}$ (RC) hearts compared to wild type (WT) controls. There was an increase in both intra-ventricular septum (IVS) and LV wall size in 180 and 270 day old RC hearts compared to WT controls. Measurements (μm) of IVS, LVW and RV are shown in the table. n = 4–5 per group. *P < .05, **P < .01. LVW = left ventricle wall. Scale bar = 1000 μm.

Heart weights were determined in Cy/+ rats from this published study [42]. The increase in heart weight in Cy/+ rats was decreased by the mTOR kinase inhibitor, PP242, that inhibits both mTORC1 and 2 (Table 1). Thus, the effect of mTOR inhibition on heart weight is variable depending on the inhibitor used, the model of PKD and the timing of administration of mTOR inhibitors.

3.2. Cardiac hypertrophy in 180 and 270 day old $Pkd1^{RC/RC}$ mice

IVS and LVW were measured in 90, 180 and 270 day old hearts. The increase in IVS in 80 day old mice did not reach statistical significance. The increase in heart weight in 180 and 270 day old $Pkd1^{RC/RC}$ mice (Table 1) was associated with cardiac hypertrophy. There was an increase in both IVS and LVW in 180 and 270 day old $Pkd1^{RC/RC}$ hearts compared to wild type controls (Fig. 1).

3.3. p-Akt^{Thr308}, p-Akt^{Ser473} and p-AMPK^{Thr172}, but not other mTORC1 and 2 proteins, were increased in 70 day old $Pkd1^{RC/RC}$ hearts

p-Akt^{Thr308}, that is directly upstream of mTORC1 and p-Akt^{Ser473}, a marker of mTORC2 activation, were increased in 70 day old $Pkd1^{RC/RC}$ hearts compared to wild type controls (Fig. 2). p-S6$^{Ser240/244}$ and p-
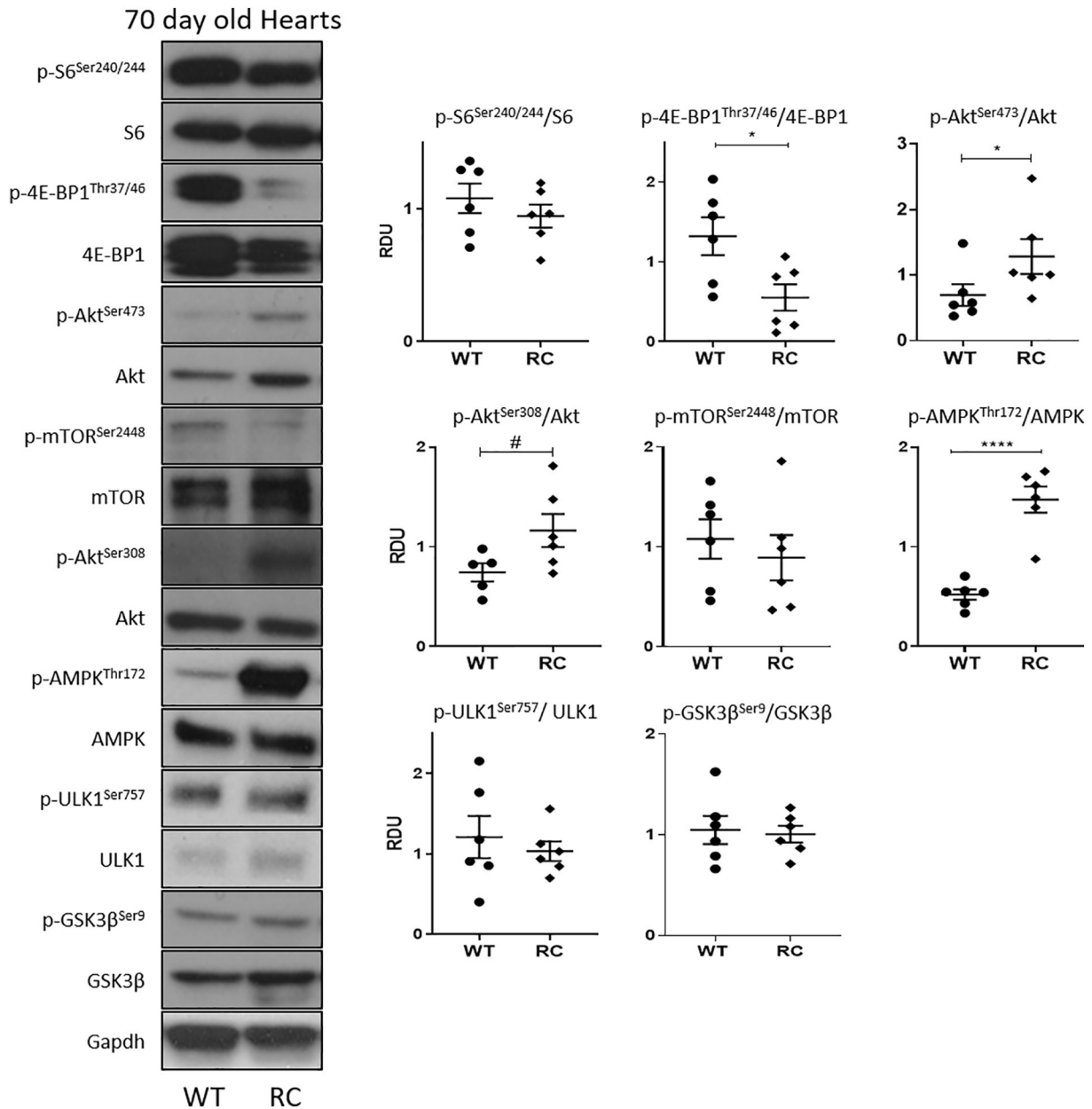
Fig. 2. p-Akt^{Thr308}, p-Akt^{Ser473} and p-AMPK^{Thr172}, but not other mTORC1 and 2 proteins, were increased in 70 day old *Pkd1*$^{RC/RC}$ hearts. Immunoblot analysis was performed for p-S6$^{Ser240/244}$, p-Akt^{Thr308}, p-Akt^{Ser473}, p-4E-BP1$^{Thr37/46}$, p-mTOR^{Ser2448}, p-AMPK^{Thr172}, p-ULK1^{Ser757} and p-GSK3β^{Ser9} in 70 day old *Pkd1*$^{RC/RC}$ (RC) hearts compared to wild type (WT) controls. RDU = relative densitometry units corrected for GAPDH. Data is expressed as a mean $+/-$ SEM, $n = 6$ per treatment group. *$P < .05$, ****$P < .0001$.

mTOR^{Ser2448}, markers of mTORC1 activation were unchanged in 70 day old *Pkd1*$^{RC/RC}$ hearts compared to wild type controls (Fig. 2). p-4E-BP1$^{Thr37/46}$ that is immediately downstream of mTORC1 was decreased in 70 day old *Pkd1*$^{RC/RC}$ hearts compared to wild type controls (Fig. 2). p-AMPK^{Thr172} was more than 3 -fold increased in 70 day old *Pkd1*$^{RC/RC}$ hearts compared to wild type controls (Fig. 2). p-ULK1^{Ser757}, that is phosphorylated by mTOR, and pGSK3β^{Ser9}, that is a target of Akt, were unchanged in 70 day old *Pkd1*$^{RC/RC}$ hearts compared to wild type controls (Fig. 2).

3.4. p-S6$^{Ser240/244}$, p-Akt^{Thr308}, p-AMPK^{Thr172} and p-GSK3β^{Ser9} were increased in 150 day old Pkd1$^{RC/RC}$ hearts

p-S6$^{Ser240/244}$, a marker of mTORC1 activation, and p-Akt^{Thr308}, that is directly upstream of mTORC1 were increased in 150 day old *Pkd1*$^{RC/}$

^{RC} hearts compared to wild type controls (Fig. 3). p-4E-BP1$^{Thr37/46}$ was increased in 150 day old *Pkd1*$^{RC/RC}$ hearts compared to wild type controls, but there was no increase when corrected for total 4E-BP1. p-mTOR^{Ser2448} and p-Akt^{Ser473}, a marker of mTORC2 activation, were unchanged in 150 day old *Pkd1*$^{RC/RC}$ hearts compared to wild type controls (Fig. 3). As seen in 70 day old *Pkd1*$^{RC/RC}$ hearts, p-AMPK^{Thr172} was much increased (more than 2-fold) in 150 day old *Pkd1*$^{RC/RC}$ hearts compared to wild type controls (Fig. 3). p-GSK3β^{Ser9}, that is directly phosphorylated by Akt was increased in 150 day old *Pkd1*$^{RC/RC}$ hearts compared to wild type controls (Fig. 3). When nutrients are sufficient, mTORC1 phosphorylates ULK1 at Ser^{757}. p-ULK1^{Ser757} was unchanged in 150 day old *Pkd1*$^{RC/RC}$ hearts compared to wild type controls (Fig. 3).
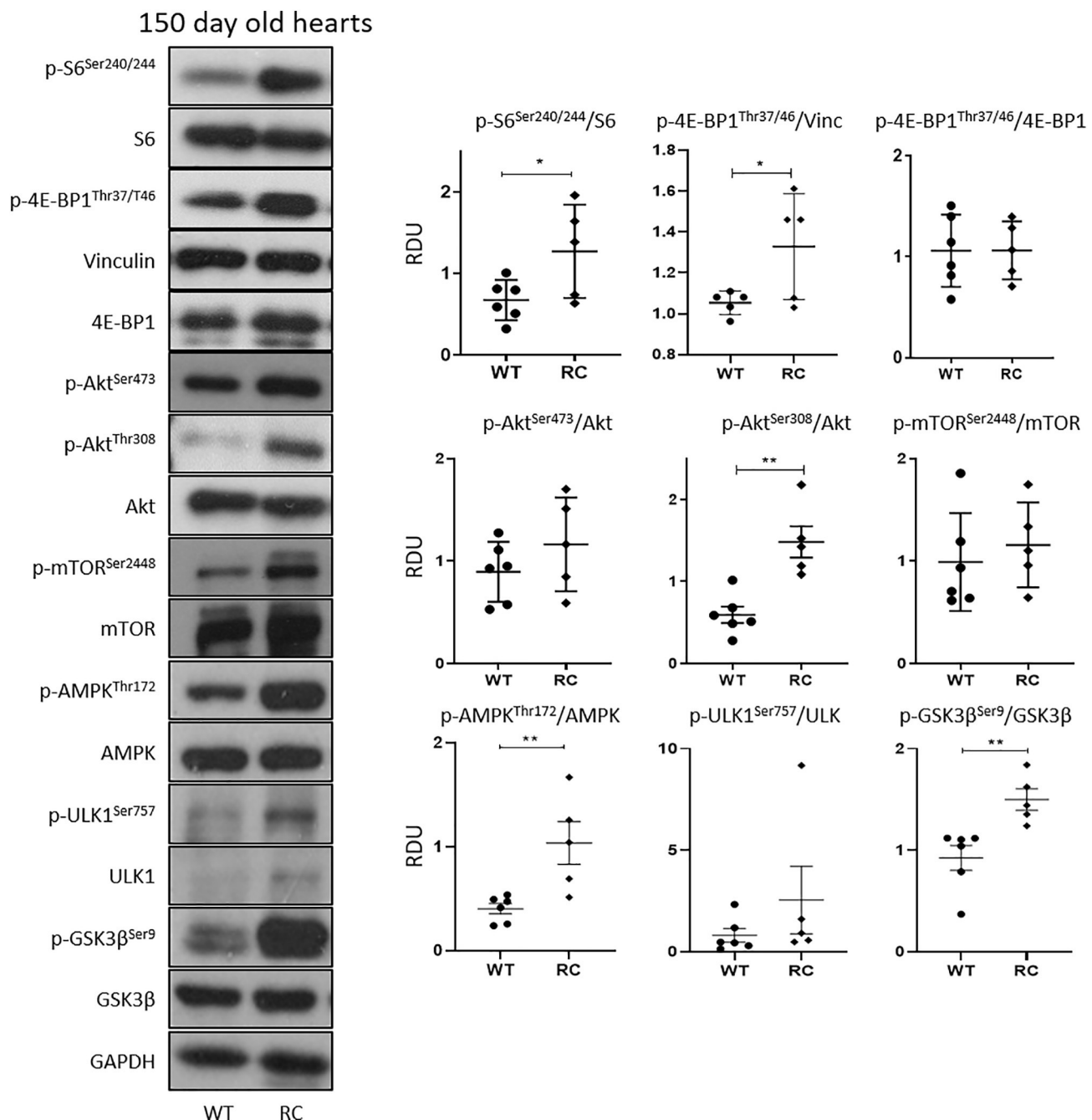
Fig. 3. p-S6$^{Ser240/244}$, p-Akt^{Thr308}, p-AMPK^{Thr172} and p-GSK3β^{Ser9} were increased in 150 day old *Pkd1*$^{RC/RC}$ hearts. Immunoblot analysis was performed for p-S6, p-Akt^{Thr308}, p-4E-BP1$^{Thr37/46}$, p-mTOR^{Ser2448}, p-Akt^{Ser473}, p-AMPK^{Thr172}, p-ULK1^{Ser757} and p-GSK3β^{Ser9} in 150 day old *Pkd1*$^{RC/RC}$ (RC) hearts compared to wild type (WT) controls. Both p-4E-BP1$^{Thr37/46}$ corrected for the loading control vinculin (Vinc) and p-4E-BP1 corrected for total 4E-BP1 are shown. RDU = relative densitometry units corrected for GAPDH. Data is expressed as a mean $+/-$ SEM, $n = 6$ per treatment group. $*P < .05$, $**P < .01$.

3.5. Autophagic flux is suppressed in hearts from both young and older *Pkd1*$^{RC/RC}$ mice

In the present study, autophagic flux was measured by comparing the expression of LC3-II in animals treated with and without a lysosomal inhibitor, bafilomycin. If the expression of LC3-II increases in the presence of bafilomycin, it can be inferred that the animal is continually producing LC3-II. No increase in LC3-II with bafilomycin indicates a defect in autophagic flux, the fusion of autophagosomes with the lysosome. In 70 and 150 day old wild type hearts, there was a significant increase in LC3-II expression after treatment with bafilomycin, indicating autophagic flux (Fig. 4). In 70 day old *Pkd1*$^{RC/RC}$ hearts, there

was a decrease in basal LC3-II compared to wild type (Fig. 4). In 70 and 150 day old *Pkd1*$^{RC/RC}$ hearts, there was no increase in LC3-II with bafilomycin indicating suppressed autophagic flux (Fig. 4). p62, a marker of autophagic cargo, is another method of determining flux as p62 is destroyed by the lysosome much like LC3-II. There was no change in p62 between 70 and 150 day old *Pkd1*$^{RC/RC}$ hearts compared to wild type controls (Fig. 4). However, in 150 day old wild type hearts, bafilomycin treatment caused a larger build up of p62 than in *Pkd1*$^{RC/RC}$ hearts (Fig. 4). As p62 is a marker of autophagosomes, the smaller increase of p62 with bafilomycin in *Pkd1*$^{RC/RC}$ hearts suggests suppressed autophagic flux.
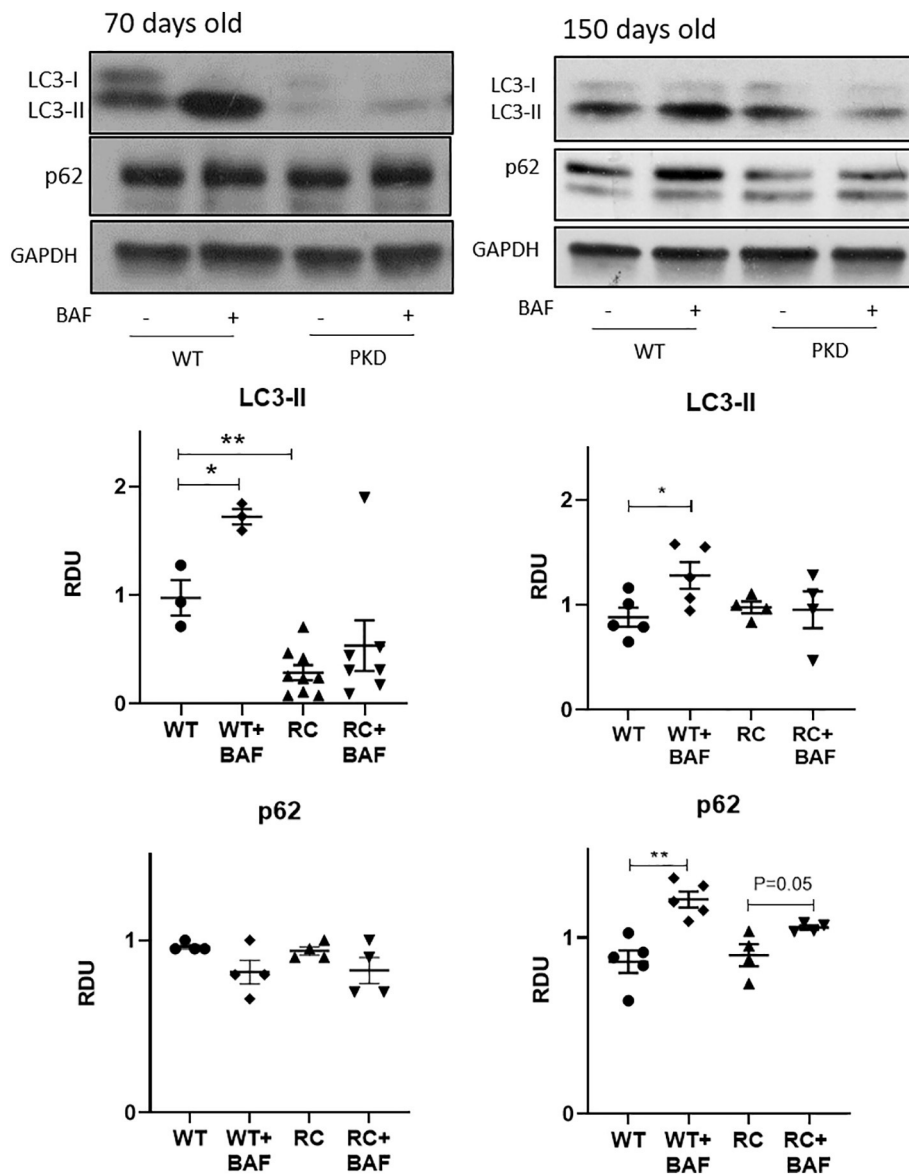
Fig. 4. Autophagic flux is suppressed in hearts from both young and older *Pkd1*[RC/RC] mice. Mice were treated with bafilomycin (Baf) 1.75 mg/kg 2 h before sacrifice. Immunoblot analysis for LC3-II and p62 in the heart was performed in Baf and vehicle treated 70 and 150 day old *Pkd1*[RC/RC] mice (PKD) and age matched wild type (WT) control mice. RDU = relative densitometry units corrected for GAPDH. Data is expressed as a mean $+/-$ SEM, n = 6 per treatment group. *$P < .05$, **$P < .01$.

3.6. Autophagy proteins p-BECN1[Ser15] and AMBRA1 were increased in 150 day old Pkd1[RC/RC] hearts

p-BECN1[Ser15], an important regulator of autophagosome formation [45] and AMBRA1 (activating molecule in Beclin1-regulated autophagy), a positive regulator of the BECN1 [46] were increased in 150 day old *Pkd1*[RC/RC] hearts compared to wild type controls (Fig. 5). Autophagy related proteins Atg3, Atg12-5 complex and Rab9a, a marker of Atg5–independent alternative autophagy pathway was unchanged in 150 day old *Pkd1*[RC/RC] hearts compared to wild type controls (Fig. 5).

3.7. Treatment of mice with 2-DG does not decrease heart weight. Treatment of mice with Tat-Beclin 1 peptide results in increased heart weight

Suppressed autophagic flux was seen in 70 and 120 day old *Pkd1*[RC/RC] hearts. Thus, the effect of autophagy inducers on heart weight was determined, with the idea that autophagy induction may impact heart weight. Mice were treated with 2-DG from 70 to 120 days of age, a time

before increased heart weight and from 150 to 350 days old, a time period when increased heart weight developed. 2-DG treatment from 70 to 120 days did not decrease heart weight (Fig. 6A). 2-DG treatment from 150 to 350 days of age resulted in an increase in heart weight that did not reach statistical significance (Fig. 6A). In support of an increase in heart weight with 2-DG treatment, the increase in heart weight between 150 and 350 days of age was significantly more with 2-DG that with vehicle (Fig. 6B). Mice were treated with the autophagy-inducing Tat-Beclin 1 peptide from 70 to 120 days of age, a time period before there is increased heart weight. Tat-Beclin 1 treatment from 70 to 120 days of age resulted in increased heart weigh (Fig. 6C).

4. Discussion

ADPKD patients, despite therapy with angiotensin converting enzyme (ACE) inhibitors, have higher left ventricular mass index (LVMI) than healthy controls [47]. In the HALT-PKD study, despite standard blood pressure control on an ACE inhibitor or angiotensin receptor
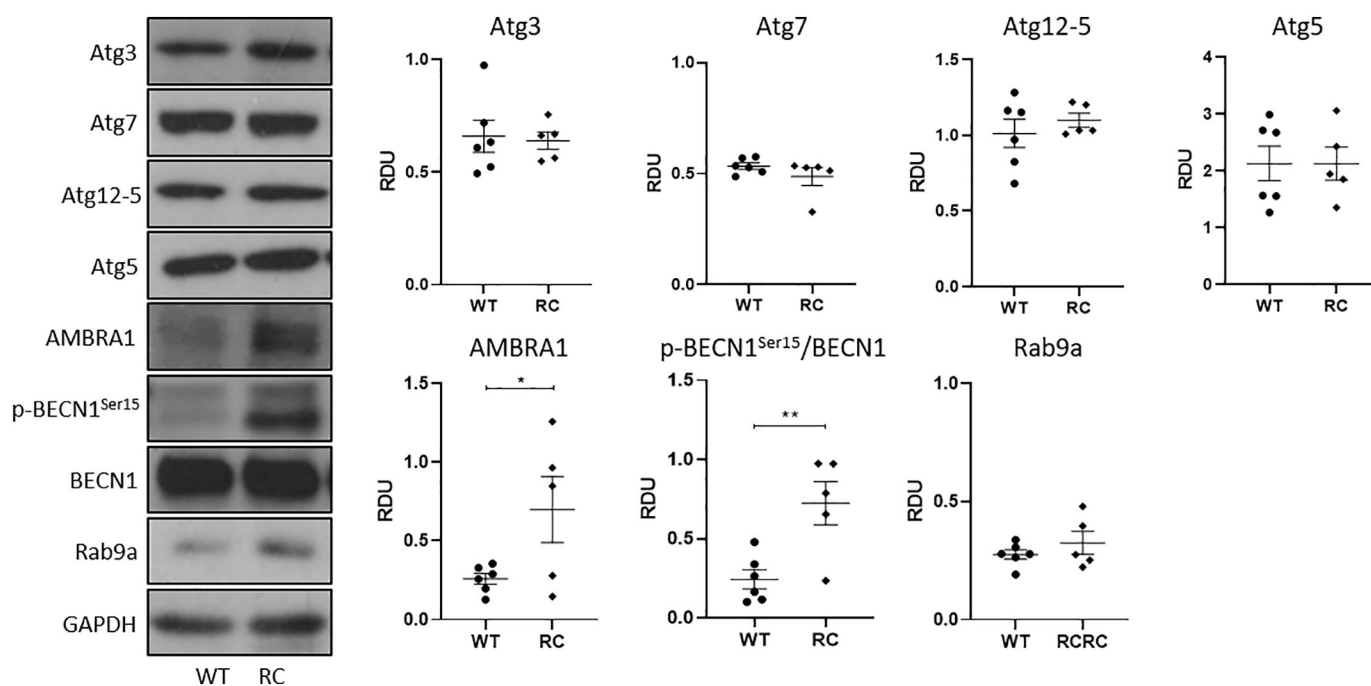
Fig. 5. Autophagy proteins p-BECN1^{Ser15} and AMBRA1 were increased in 150 day old $Pkd1^{RC/RC}$ hearts. Immunoblot analysis was performed for autophagy related proteins Atg3, Atg12-5 complex and Rab9a, BECN1, AMBRA1 in 150 day old $Pkd1^{RC/RC}$ (RC) hearts compared to wild type (WT) controls. RDU = relative densitometry units corrected for GAPDH. Data is expressed as a mean $+/-$ SEM, n = 6 per treatment group. *$P < .05$, **$P < .0001$.

blocker (ARB), few patients had increased LVMI on MRI scan, but many were in the upper range of normal (there was no specific comparison to the general population) [48]. In patients from the ALADIN-trial, left ventricle (LV) function determined by speckle-tracking echocardiography is impaired early and somatostatin-analogue therapy improves LV dysfunction in this population [49]. Thus, there is increased LVMI in ADPKD patients and describing the pattern and understanding the pathophysiology of cardiac disease in ADPKD in rodents is important in providing clues to develop future therapies to treat the cardiac disease in PKD patients.

There are reasons to suspect that mTOR would be activated in the enlarged heart in PKD. Firstly, mTOR is activated in the kidney [15] and liver [50] in ADPKD. Secondly, there is a known connection between abnormalities in PC-1 and PC-2 and mTOR, a known mediator of cardiac hypertrophy [20]. Thirdly, the present study shows that mTORC1/2 inhibition with an ASO that blocks both mTORC1 and 2, resulted in decreased heart weight in $Pkd2 -/-$ mice (Table 1). However, in 120 day old $Pkd1^{RC/RC}$ mice, that do not yet have increased heart weight, sirolimus and the mTOR kinase inhibitor, Torin2, had a tendency to increase heart weight (Table 1). Thus, the effect of mTOR inhibition on the heart may depend on the PKD model and whether the mTOR inhibitor is given before or after the onset of increased heart weight.

Studies show conflicting results on the role of mTORC1 and 2 in non PKD models of cardiac hypertrophy. Sirolimus, an mTORC1 inhibitor that blocks S6K attenuates cardiac hypertrophy [51], but mTORC1 (Raptor) or mTORC2 (Rictor) knockout in the heart worsens cardiac hypertrophy [52,53]. In the present study, we show that p-S6$^{Ser240/244}$, a marker of mTORC1, is activated in the heart at 150 days old, a time point before the onset of measurable increased heart weight at 180 day of age. At 70 days old there was a decrease in p-4E-BP1 in $Pkd1$ RC/RC mouse kidneys. It is known that cardiac-specific 4E-BP1 knockout improves cardiac hypertrophy in a non PKD model [54]. Thus the decrease in p-4E-BP1 in 70 day old mice seen in the present study may be an early compensatory mechanism to try to reduce cardiac hypertrophy. Thus while it is known that there are changes in mTOR proteins in the heart in non PKD models of cardiac hypertrophy, mTOR activation in

the heart in PKD has not previously been described and is the focus of the present study.

Proteins that are known to be both upstream and downstream of mTORC1 were activated in $Pkd1^{RC/RC}$ hearts. In 150 day old hearts there was an increase in p-Akt^{Thr308}, a protein kinase that is activated by insulin and various growth and survival factors and via growth factor-stimulated PI3K activity. Akt is known to directly phosphorylate mTORC1 (17) or phosphorylate and inactivate TSC-2, an inhibitor of mTOR [55,56]. In the present study, there was increased p-Akt^{Thr308} and p-S6$^{Ser240/244}$, a marker of mTORC1, in 150 day old hearts. There was an increase in p-GSK3β^{Ser9} in 150 day old hearts. GSK3 (GSK3α and GSK3β) regulate many cellular processes by directly phosphorylating substrates, that include metabolic enzymes, transcription factors, cell-cycle regulatory proteins, and cytoskeletal proteins [57,58]. GSK3 is a well-characterized Akt target and Akt's phosphorylation of GSK3β is inhibitory [59]. Therefore, in $Pkd1^{RC/RC}$ hearts, Akt's phosphorylation of GSK3β could result in inhibitory effects of GSK on cellular processes decreasing the direct phosphorylation of metabolic enzymes, transcription factors, cell-cycle regulatory proteins, and cytoskeletal proteins. mTOR signaling pathways in $Pkd1^{RC/RC}$ hearts are demonstrated in Fig. 7.

As mTOR activation is known to inhibit autophagy, we measured autophagic flux in the heart during a time-course of the PKD. In 70 and 120 day old $Pkd1^{RC/RC}$ hearts there was suppressed autophagic flux. The suppressed autophagic flux in 70 day old mice occurred before activation of mTORC1 or 2 suggesting that the suppressed autophagy was not related to mTORC1 or 2. We also measured other autophagy related proteins in PKD hearts. Autophagy related 5 (Atg5) is an important protein involved in the extension of the phagosome membrane in autophagic vesicles and is activated by Atg7. In the conventional autophagy pathway, two autophagy related proteins (Atg12 and Atg5) form a complex with other proteins such as LC3-II in order to elongate the phagosome and fully engulf autophagic cargo [60–63]. There is also an Atg5-independent mechanism of autophagy, called alternative autophagy, utilizing Rab9a, a small GTPase, that is recruited to autophagosome-like vacuoles after autophagosomal maturation resulting in autophagosome-like vacuole enlargement and eventual lysosomal
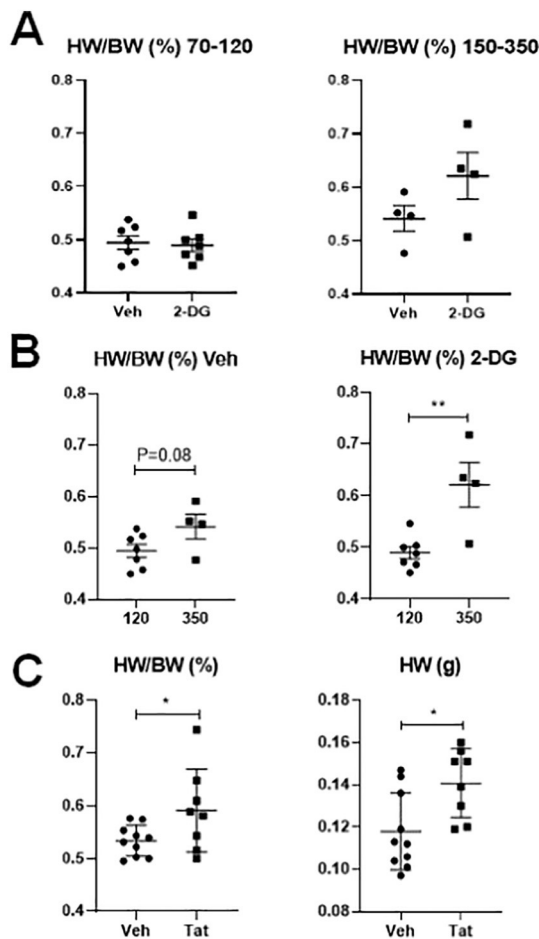
Fig. 6. Treatment of *Pkd1*[RC/RC] with 2-DG does not decrease heart weight. Treatment of *Pkd1*[RC/RC] with Tat-Beclin 1 peptide results in increased heart weight. *Pkd1*[RC/RC] mice were treated with 2-deoxy glucose (2-DG) or vehicle (Veh) from 70 to 120 days of age and from 150 to 350 days of age or TatBeclin1 peptide (Tat) or vehicle (Veh) from 70 to 120 days of age. (A) Heart weight/body weight (HW/BW) (%) in mice treated with Veh or 2-DG from 70 to 120 days of age and 150–350 days of age. (B) HW/BW (%) at 120 days vs. 350 days in mice treated with either Veh or 2-DG. (C) HW/BW (%) in mice treated with Veh or Tat.

Fig. 7. mTOR signaling in *Pkd1*[RC/RC] hearts. The potential connections between the mTOR signaling proteins that were increased in *Pkd1*[RC/RC] hearts is demonstrated. In 70 day old hearts, there was an increase in p-AMPK[Thr172], p-Akt[Ser473] and p-Akt[Thr308]. In 150 day old hearts, there was an increase p-AMPK[Thr172], p-S6[Ser240/244], p-Akt[Thr308] and p-GSK3β[Ser9]. AMPK has been shown to be an upstream kinase necessary for activation of both p-Akt[Ser473] and p-Akt[Thr308] in metabolic stress, tumorigenesis and drug resistance [74]. However, AMPK is also known to inhibit p-Akt[Thr308] [75]. Akt activation can also prevent phosphorylation of AMPK at Thr[172] [75]. While p-GSK3β[Ser9] is usually inhibited by mTOR activation, p-GSK3β[Ser9] can also activate mTORC1 [76]. GSK3 is a well -characterized Akt target and Akt's phosphorylation of GSK3β is inhibitory [59]. p-S6[Ser240/244] is a marker of mTORC1 and is usually inhibited by AMPK via ULK1 [23].

fusion [64]. There was no change in Atg7, Atg12-5 complex, or Rab9a in PKD hearts, but a lack of increase of LC3-II with bafilomycin suggested that the autophagy defect in PKD hearts was related to a lysosomal defect.

Beclin1 (BECN1; coiled-coil, myosin-like BCL2-interacting protein) is an important regulator of early autophagosome formation [45]. BECN1 plays a role in autophagy initiation by regulating the autophagy-promoting activity of the Class III PI 3-kinase, Vps34, and BECN1 and is involved in the formation of autophagosome membranes. AMBRA1 (activating molecule in Beclin1-regulated autophagy) is required for BECN1 activity [46]. AMBRA1 interacts with BECN1 at the initiation of autophagy and promotes the binding between BECN1 and its target kinase, Vps34. In the present study there was an increase in both AMBRA1 and p-BECN1[Ser15] in 150 day old hearts indicating that the proximal stages of autophagy were intact. There was decreased autophagic flux, the fusion of the autophagosome with the lysosome, a distal stage of autophagy. These findings suggest that the defect in autophagy in 150 day old PKD hearts may be due to a more distal lysosomal defect rather than a defect in the more proximal steps involving autophagy related proteins, BECN1 and AMBRA1.

There was a large increase in p-AMPK[Thr172] in both young (70 day old) and older (150 day old) hearts at a time when there was suppressed

autophagic flux but not yet increased heart weight. AMP activated protein kinase (AMPK), is a key energy sensor that regulates cellular metabolism to maintain energy homeostasis. There are a variety of physiological conditions that change the ATP to AMP ratio leading to the activation of AMPK, including mitochondrial inhibition, nutrient starvation and exercise [65]. AMPK is known to inhibit mTORC1 and it has recently been demonstrated that mTORC1 also directly down-regulates AMPK signaling [66]. One of the functions of AMPK is to promote autophagy by regulation of the mammalian autophagy-initiating kinase, ULK1, a homologue of yeast Atg1. In the present study, activation of AMPK was not associated with changes in ULK1 phosphorylation, suggesting that AMPK phosphorylation is not a mediator of autophagy via ULK1. AMPK has other autophagy-related functions in regulating mitochondrial homeostasis: biogenesis, fission and mitophagy. AMPK is activated in response to mitochondrial damage, as well as under other low ATP conditions to ensure that there is generation of new mitochondria [65]. In summary, the increase in AMPK in *Pkd1*[RC/RC] hearts may be an attempt to repair a mitochondrial defect.

To determine the mechanistic effect of suppressed autophagy in causing increased heart weight, mice were treated with known autophagy inducers 2-DG or Tat-Beclin 1 peptide. 2-DG has been shown to induce autophagy and activate AMPK [67]. 2-DG treatment in mice has been shown to reduce cyst growth, but the effect on cardiac hypertrophy was not determined [68]. In the present study, 2-DG treatment, from 150 to 350 days of age, a time period when increased heart weight developed, did not reduce increased heart weight and had a tendency to increase heart weight. Tat-Beclin 1 peptide is a cell-penetrating autophagy-inducing peptide that induces autophagy *in vivo* in mice through interaction with the autophagy suppressor GAPR-1/GLIPR2 that promotes the release of BECN1 from the Golgi, resulting in enhanced early autophagosome formation [39–41]. Tat-Beclin 1 treatment from 70 to 120 days of age resulted in increased heart weight. Suppressed autophagic flux in 70 day old mice occurred before the onset of increased heart weight and the increased heart weight with Tat-Beclin1 treatment at this time suggested that suppressed autophagy may be a mechanism to prevent cardiac hypertrophy in young PKD mice and that inducing autophagy may interfere with this process resulting in increased heart weight. The studies with 2-DG and Tat- Beclin 1 peptide suggest that autophagy induction in the heart does not improve increased heart weight.

There are reasons to suspect that the increased heart weight in mice is due to more than hypertension: The known expression of PC1 and PC2 in cardiac tissue suggests that there are direct effects of PC1 and PC2 on cardiac function [69]. There is evidence that PC-2 modulates intracellular calcium cycling, contributing to the development of heart failure in *Pkd2* mutant zebrafish and in *Pkd2+/−* mice that do not have PKD [70]. The present study confirmed increased heart weight in *Pkd2*^WS25/− mice that do not have PKD. Abnormalities in PC-1 have also been implicated in causing heart disease. In mice with a conditional silencing of PC-1 selectively in cardiomyocytes subjected to mechanical stress there was decreased cardiac function relative to littermate controls [71]. The hypothesis that cardiac hypertrophy in PKD is due to more than just hypertension is supported by human studies in which there is LVH in normotensive patients [72,73].

In summary, there is mTORC1 activation in the heart in older *Pkd1*^RC/RC mice associated with suppressed autophagic flux. In younger mice suppressed autophagic flux in the heart was not associated with mTORC1 activation. There was a defect in autophagic flux, the fusion of phagosomes with the lysosome, rather than the more proximal autophagy steps involving autophagy related proteins. There was a large increase in p-AMPK^Thr172, a known autophagy inducer, in both young and old mice perhaps as a compensatory mechanism to suppressed autophagy. Treatment with the autophagy inducer, 2-DG, did not impact increased heart weight but treatment with Tat Beclin1 peptide increased heart weight.

Acknowledgements

Appendix A. Supplementary data

Supplementary data to this article can be found online at https://doi.org/10.1016/j.cellsig.2020.109730.

References

[1] P.D. Wilson, Polycystic kidney disease, N. Engl. J. Med. 350 (2) (2004) 151–164.
[2] G.M. Fick, P.A. Gabow, Natural history of autosomal dominant polycystic kidney disease, Annu. Rev. Med. 45 (1994) 23–29.
[3] C. Bergmann, et al., Polycystic kidney disease, Nat. Rev. Dis. Primers 4 (1) (2018) 50.
[4] A. Di Mise, et al., Activation of Calcium-Sensing Receptor increases intracellular calcium and decreases cAMP and mTOR in PKD1 deficient cells, Sci. Rep. 8 (1) (2018) 5704.
[5] A. Di Mise, et al., Activation of the calcium-sensing receptor corrects the impaired mitochondrial energy status observed in renal polycystin-1 knockdown cells modeling autosomal dominant polycystic kidney disease, Front. Mol. Biosci. 5 (2018) 77.
[6] K. Ravichandran, C.L. Edelstein, Polycystic kidney disease: a case of suppressed autophagy? Semin. Nephrol. 34 (1) (2014) 27–33.
[7] P. Zhu, et al., Autophagy activators suppress cystogenesis in an autosomal dominant polycystic kidney disease model, Hum. Mol. Genet. 26 (1) (2017) 158–172.
[8] L. Peintner, C. Borner, Role of apoptosis in the development of autosomal dominant polycystic kidney disease (ADPKD), Cell Tissue Res. 369 (1) (2017) 27–39.
[9] K.L. Nowak, C.L. Edelstein, Apoptosis and autophagy in polycystic kidney disease (PKD), Cell. Signal. 68 (2020) 109518.
[10] G.M. Fick, et al., Causes of death in autosomal dominant polycystic kidney disease, J. Am. Soc. Nephrol. 5 (12) (1995) 2048–2056.
[11] A.B. Chapman, et al., Left ventricular hypertrophy in autosomal dominant polycystic kidney disease, J. Am. Soc. Nephrol. 8 (8) (1997) 1292–1297.
[12] M. Laplante, D.M. Sabatini, mTOR signaling in growth control and disease, Cell 149 (2) (2012) 274–293.
[13] R.A. Saxton, D.M. Sabatini, mTOR signaling in growth, metabolism, and disease, Cell 168 (6) (2017) 960–976.
[14] C.G. Proud, Ras, PI3-kinase and mTOR signaling in cardiac hypertrophy, Cardiovasc. Res. 63 (3) (2004) 403–413.
[15] I. Zafar, et al., Sirolimus attenuates disease progression in an orthologous mouse model of human autosomal dominant polycystic kidney disease, Kidney Int. 78 (8) (2010) 754–761.
[16] K. Ravichandran, et al., Antisense-mediated angiotensinogen inhibition slows polycystic kidney disease in mice with a targeted mutation in Pkd2, Am. J. Physiol. Ren. Physiol. 308 (4) (2015) F349–F357.
[17] R. Dere, et al., Carboxy terminal tail of polycystin-1 regulates localization of TSC2 to repress mTOR, PLoS ONE 5 (2) (2010) e9239 (Electronic Resource).
[18] D. Mekahli, et al., Polycystin-1 but not polycystin-2 deficiency causes upregulation of the mTOR pathway and can be synergistically targeted with rapamycin and metformin, Pflugers Arch. 466 (8) (2014) 1591–1604.
[19] J.M. Shillingford, et al., The mTOR pathway is regulated by polycystin-1, and its inhibition reverses renal cystogenesis in polycystic kidney disease, Proc. Natl. Acad. Sci. U. S. A. 103 (14) (2006) 5466–5471.
[20] A. Boletta, Emerging evidence of a link between the polycystins and the mTOR pathways, Pathogenetics 2 (1) (2009) 6.
[21] J. Lu, et al., Polycystin-2 plays an essential role in glucose starvation-induced autophagy in human embryonic stem cell-derived cardiomyocytes, Stem Cells 36 (4) (2018) 501–513.
[22] Y.C. Kim, K.L. Guan, mTOR: a pharmacologic target for autophagy regulation, J. Clin. Invest. 125 (1) (2015) 25–32.
[23] J. Kim, et al., AMPK and mTOR regulate autophagy through direct phosphorylation of Ulk1, Nat. Cell Biol. 13 (2) (2011) 132–141.
[24] A. Gonzalez, et al., AMPK and TOR: the Yin and Yang of cellular nutrient sensing and growth control, Cell Metab. 31 (3) (2020) 472–492.
[25] D.G. Hardie, B.E. Schaffer, A. Brunet, AMPK: an energy-sensing pathway with multiple inputs and outputs, Trends Cell Biol. 26 (3) (2016) 190–201.
[26] D.G. Hardie, S.A. Hawley, J.W. Scott, AMP-activated protein kinase–development of the energy sensor concept, J. Physiol. 574 (Pt 1) (2006) 7–15.
[27] M. Hoyer-Hansen, M. Jaattela, AMP-activated protein kinase: a universal regulator of autophagy? Autophagy. 3 (4) (2007 Aug) 381–383.
[28] K. Hopp, et al., Functional polycystin-1 dosage governs autosomal dominant polycystic kidney disease severity, J. Clin. Invest. 122 (11) (2012) 4257–4273.
[29] K. Hopp, et al., Tolvaptan plus pasireotide shows enhanced efficacy in a PKD1 model, J. Am. Soc. Nephrol. 26 (1) (2015) 39–47.
[30] E.K. Kleczko, et al., CD8(+) T cells modulate autosomal dominant polycystic kidney disease progression, Kidney Int. 94 (6) (2018) 1127–1140.
[31] S.J. Holditch, et al., A study of sirolimus and an mTOR kinase inhibitor (TORKi) in a hypomorphic Pkd1 mouse model of autosomal dominant polycystic kidney disease (ADPKD), Am. J. Physiol. Ren. Physiol. 317 (1) (2019) F187–F196.
[32] P.A. Doevendans, et al., Cardiovascular phenotyping in mice, Cardiovasc. Res. 39 (1) (1998) 34–49.
[33] F. Matsuda, J. Fujii, S. Yoshida, Autophagy induced by 2-deoxy-D-glucose suppresses intracellular multiplication of Legionella pneumophila in A/J mouse macrophages, Autophagy 5 (4) (2009) 484–493.
[34] R.S. DiPaola, et al., Therapeutic starvation and autophagy in prostate cancer: a new paradigm for targeting metabolism in cancer therapy, Prostate 68 (16) (2008) 1743–1752.
[35] Q. Wang, et al., 2-Deoxy-D-glucose treatment of endothelial cells induces autophagy by reactive oxygen species-mediated activation of the AMP-activated protein kinase, PLoS One 6 (2) (2011) e17234.
[36] T.S. Oh, et al., Hypothalamic AMPK-induced autophagy increases food intake by regulating NPY and POMC expression, Autophagy 12 (11) (2016) 2009–2025.
[37] M. Stein, et al., Targeting tumor metabolism with 2-deoxyglucose in patients with castrate-resistant prostate cancer and advanced malignancies, Prostate 70 (13) (2010) 1388–1394.
[38] H. Xi, et al., 2-Deoxy-D-glucose activates autophagy via endoplasmic reticulum stress rather than ATP depletion, Cancer Chemother. Pharmacol. 67 (4) (2011) 899–910.
[39] A. Shirakabe, et al., Drp1-dependent mitochondrial autophagy plays a protective role against pressure overload-induced mitochondrial dysfunction and heart failure, Circulation 133 (13) (2016) 1249–1263.
[40] S. Shoji-Kawata, et al., Identification of a candidate therapeutic autophagy-inducing peptide, Nature 494 (7436) (2013) 201–206.
[41] Y. Sun, et al., Beclin-1-dependent autophagy protects the heart during sepsis, Circulation 138 (20) (2018) 2247–2262.
[42] K. Ravichandran, et al., An mTOR kinase inhibitor slows disease progression in a rat model of polycystic kidney disease (PKD), Nephrol. Dial. Transplant. 30 (1) (2014) 45–53.
[43] D.J. Klionsky, et al., Guidelines for the use and interpretation of assays for monitoring autophagy (3rd edition), Autophagy 12 (1) (2016) 1–222.
[44] K. Ravichandran, et al., An mTOR anti-sense oligonucleotide decreases polycystic kidney disease in mice with a targeted mutation in Pkd2, Hum. Mol. Genet. 23 (18) (2014) 4919–4931.
[45] X.H. Liang, et al., Induction of autophagy and inhibition of tumorigenesis by beclin 1, Nature 402 (6762) (1999) 672–676.
[46] G.M. Fimia, et al., Ambra1 regulates autophagy and development of the nervous system, Nature 447 (7148) (2007) 1121–1125.
[47] M. Pietrzak-Nowacka, et al., Autosomal dominant polycystic kidney disease and hypertension are associated with left ventricular mass in a gender-dependent manner, Kidney Blood Press. Res. 36 (1) (2012) 301–309.
[48] R.D. Perrone, et al., Cardiac magnetic resonance assessment of left ventricular mass in autosomal dominant polycystic kidney disease, Clin. J. Am. Soc. Nephrol. 6 (10) (2011) 2508–2515.
[49] L. Spinelli, et al., Left ventricular dysfunction in ADPKD and effects of octreotide-LAR: a cross-sectional and longitudinal substudy of the ALADIN trial, Int. J. Cardiol. 275 (2019) 145–151.
[50] C. Spirli, et al., Mammalian target of rapamycin regulates vascular endothelial growth factor-dependent liver cyst growth in polycystin-2-defective mice,

Hepatology 51 (5) (2010) 1778–1788.

[51] J.R. McMullen, et al., Inhibition of mTOR signaling with rapamycin regresses established cardiac hypertrophy induced by pressure overload, Circulation 109 (24) (2004) 3050–3055.

[52] P. Shende, et al., Cardiac raptor ablation impairs adaptive hypertrophy, alters metabolic gene expression, and causes heart failure in mice, Circulation 123 (10) (2011) 1073–1082.

[53] P. Shende, et al., Cardiac mTOR complex 2 preserves ventricular function in pressure-overload hypertrophy, Cardiovasc. Res. 109 (1) (2016) 103–114.

[54] D. Zhang, et al., MTORC1 regulates cardiac function and myocyte survival through 4E-BP1 inhibition in mice, J. Clin. Invest. 120 (8) (2010) 2805–2816.

[55] K. Inoki, et al., TSC2 is phosphorylated and inhibited by Akt and suppresses mTOR signalling, Nat. Cell Biol. 4 (9) (2002) 648–657.

[56] B.D. Manning, L.C. Cantley, AKT/PKB signaling: navigating downstream, Cell. 129 (7) (2007) 1261–1274.

[57] M.A. Hermida, J. Dinesh Kumar, N.R. Leslie, GSK3 and its interactions with the PI3K/AKT/mTOR signalling network, Adv. Biol. Regul. 65 (2017) 5–15.

[58] R.S. Jope, G.V. Johnson, The glamour and gloom of glycogen synthase kinase-3, Trends Biochem. Sci. 29 (2) (2004) 95–102.

[59] D.A. Cross, et al., Inhibition of glycogen synthase kinase-3 by insulin mediated by protein kinase B, Nature 378 (6559) (1995) 785–789.

[60] N. Mizushima, Y. Ohsumi, T. Yoshimori, Autophagosome formation in mammalian cells, Cell Struct. Funct. 27 (6) (2002) 421–429.

[61] P. Jiang, N. Mizushima, Autophagy and human diseases, Cell Res. 24 (1) (2014) 69–79.

[62] N. Mizushima, et al., Autophagy fights disease through cellular self-digestion, Nature 451 (7182) (2008) 1069–1075.

[63] N.N. Noda, F. Inagaki, Mechanisms of autophagy, Annu. Rev. Biophys. 44 (1) (2015) 101–122.

[64] Y. Nishida, et al., Discovery of Atg5/Atg7-independent alternative macro-autophagy, Nature 461 (2009) 654.

[65] S. Herzig, R.J. Shaw, AMPK: guardian of metabolism and mitochondrial homeostasis, Nat. Rev. Mol. Cell Biol. 19 (2) (2018) 121–135.

[66] N.X.Y. Ling, et al., mTORC1 directly inhibits AMPK to promote cell proliferation under nutrient stress, Nat. Metab. **2** (1) (2020) 41–49.

[67] D. Zhang, et al., 2-Deoxy-D-glucose targeting of glucose metabolism in cancer cells as a potential therapy, Cancer Lett. 355 (2) (2014) 176–183.

[68] I. Rowe, et al., Defective glucose metabolism in polycystic kidney disease identifies a new therapeutic strategy, Nat. Med. 19 (4) (2013) 488–493.

[69] I.Y. Kuo, A.B. Chapman, Polycystins, ADPKD, and cardiovascular disease, Kidney Int. Rep. 5 (4) (2020) 396–406.

[70] E. Giehl, et al., Polycystin 2-dependent cardio-protective mechanisms revealed by cardiac stress, Pflugers Arch. 469 (11) (2017) 1507–1517.

[71] Z. Pedrozo, et al., Polycystin-1 is a cardiomyocyte mechanosensor that governs L-type Ca2+ channel protein stability, Circulation 131 (24) (2015) 2131–2142.

[72] A. Bardaji, et al., Left ventricular mass and diastolic function in normotensive young adults with autosomal dominant polycystic kidney disease, Am. J. Kidney Dis. 32 (6) (1998) 970–975.

[73] F.A. Valero, et al., Ambulatory blood pressure and left ventricular mass in normotensive patients with autosomal dominant polycystic kidney disease, J. Am. Soc. Nephrol. 10 (5) (1999) 1020–1026.

[74] F. Han, et al., The critical role of AMPK in driving Akt activation under stress, tumorigenesis and drug resistance, Nat. Commun. 9 (1) (2018) 4728.

[75] Y. Zhao, et al., ROS signaling under metabolic stress: cross-talk between AMPK and AKT pathway, Mol. Cancer 16 (1) (2017) 79.

[76] R. Mancinelli, et al., Multifaceted roles of GSK-3 in cancer and autophagy-related diseases, Oxidative Med. Cell. Longev. 2017 (2017) 4629495.

ELSEVIER

Cellular
Signalling
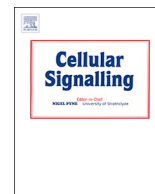
The effect of trehalose on autophagy-related proteins and cyst growth in a hypomorphic Pkd1 mouse model of autosomal dominant polycystic kidney disease

Daniel J. Atwood, Carolyn N. Brown, Sara J. Holditch, Deepak Pokhrel, Andrew Thorburn, Katharina Hopp, Charles L. Edelstein*

Department of Medicine, Division of Renal Diseases and Hypertension, University of Colorado Anschutz Medical Campus, Aurora, CO, USA

ABSTRACT

Autosomal dominant polycystic kidney disease (ADPKD) is a common inherited disorder characterized by kidney cyst growth often resulting in end-stage renal disease. There is growing attention on understanding the role of impaired autophagy in ADPKD. Trehalose (TRE) has been shown to increase both protein stability and aggregate clearance and induce autophagy in neurodegenerative diseases. TRE treatment in wild type mice compared to vehicle resulted in increased expression in the kidney of Atg12–5 complex and increased Rab9a, autophagy-related proteins that play a role in the formation of autophagosomes. Thus, the aim of the study was to determine the effect of TRE on cyst growth and autophagy-related proteins, in the hypomorphic $Pkd1^{RC/RC}$ mouse model of ADPKD. $Pkd1^{RC/RC}$ mice were treated 2% TRE in water from days 50 to 120 of age. TRE did not slow cyst growth or improve kidney function or affect proliferation and apoptosis in $Pkd1^{RC/RC}$ kidneys. In $Pkd1^{RC/RC}$ vs. wild type kidneys, expression of the Atg12–5 complex was inhibited by TRE resulting in increased free Atg12 and TRE was unable to rescue the deficiency of the Atg12–5 complex. Rab9a was decreased in $Pkd1^{RC/RC}$ vs. wild type kidneys and unaffected by TRE. The TRE-induced increase in p62, a marker of autophagic cargo, that was seen in normal kidneys was blocked in $Pkd1^{RC/RC}$ kidneys. In summary, the autophagy phenotype in $Pkd1^{RC/RC}$ kidneys was characterized by decreases in crucial autophagy-related proteins (Atg12–5 complex, Atg5, Atg16L1), decreased Rab9a and increased mTORC1 (pS6$^{S240/244}$, pmTOR^{S2448}) proteins. TRE increased Atg12–5 complex, Rab9a and p62 in normal kidneys, but was unable to rescue the deficiency in autophagy proteins or suppress mTORC1 in $Pkd1^{RC/RC}$ kidneys and did not protect against cyst growth.

1. Introduction

Autosomal Dominant Polycystic Kidney Disease (ADPKD) is one of the most common genetic disorders in the world. The majority of ADPKD cases can be explained by mutations to either *PKD1* (~80% of cases) or *PKD2* (~12% of cases) and the disease is defined by slowly growing and persistent renal cysts that eventualy cause end-stage renal disease [1]. Hyper-proliferation, increased apoptosis and impaired autophagy in the kidney are all characteristic of ADPKD [2–5]. Autophagy is the process in which cellular components, such as damaged organelles and misfolded proteins, are degraded and recycled [6]. In conventional autophagy, two autophagy-related proteins (ATGs), Atg12 and Atg5 form a complex, recruiting other proteins such as microtubule-associated protein 1A/1B light chain 3B (LC3) to the growing autophagosome membrane in order to elongate and fully engulf

autophagic cargo [6–9]. The Atg12–5 complex also binds to Atg16 which is required for the localization of Atg5 and Atg12 to the phagophore assembly site and for the elongation of isolation membranes (also called phagophores) during mammalian autophagy [10]. The association of the Atg12–5 complex with Atg16 unmasks a membrane-binding site in Atg5 and allows Atg5 to bind to phagophore precursors [11]. LC3-I is converted into the phosphatidylethanolamine (PE)-conjugated form, LC3-II, which allows conjugation to the phagosome membrane and LC3-II is the most reliable marker of completed autophagosomes [12]. The amount of LC3-II can increase in cells due to increased production or a block in autophagosome-lysosome fusion or a defect in lysosome function. If the basal increase in LC3-II is due to increased autophagosome production, then it is expected that lysosomal inhibition will further increase LC3-II (i.e. increased autophagic flux) [12]. The amount of sequestome 1/p62 (p62) a marker of autophagic

cargo, is another method of determining autophagic flux as p62 can be destroyed by the lysosome much like LC3. In general, an increase in p62 indicates suppressed autophagic flux [13].

Recent studies have also discovered an Atg5/7-independent mechanism of autophagy, called alternative autophagy, in which autophagosomes are generated in a Ras-related protein Rab9a (Rab9a)-dependent manner by the fusion of isolation membranes with vesicles derived from the trans-Golgi and late endosomes [14,15]. Rab proteins are small GTPases that belong to the Ras-like GTPase superfamily and regulate vesicle trafficking [16]. Rabs are related to autophagy by regulating the transport and fusion of autophagosomes [16,17]. Beclin1 is essential to the initiation of autophagy in both the canonical and alternative autophagy pathways [18]. Beclin1 plays a role in the initial steps in the assembly of autophagosomes from pre-autophagic structures by recruitment and activation of the class III phosphatidylinositol 3-kinase complex.

It has been demonstrated that there is suppressed autophagic flux in Pkd1 −/− cells [3,19] and in mouse PKD kidneys [20]. Stimulating autophagy has been shown to slow the progression of ADPKD in zebrafish [3]. Autophagy inducers like sirolimus, deoxy glucose and metformin are known to slow cyst growth in PKD [19,21,22]. In the present study, in normal kidneys both ex vivo and in vivo, we determined that the non-reducing glucose disaccharide, trehalose (TRE) had the potential to increase autophagy by increased expression of Atg12–5 complex and increased Rab9a. Thus, the aim of the study was to determine the effect of TRE on autophagy-related protein expression, especially Atg12–5 complex, Rab9a, and p62 as well as cyst growth in a *Pkd1*[RC/RC] mice, a hypomorphic *Pkd1* mouse model.

TRE is found in most organisms other than vertebrates and in common food supplements [23–25]. TRE is a natural sugar often used to preserve the flavor, texture, and color of dehydrated and frozen foods by preventing protein degradation [26]. The cryo-protective properties of TRE are linked to its chemical chaperone properties, which influence protein folding through direct protein-TRE interactions resulting in protein stability and reduced accumulation of misfolded proteins [25]. The autophagy inducing effect of TRE in Huntington's disease results in the stabilization of the toxic mutant huntingtin protein, resulting in less aggregation and enhanced clearance of soluble mutant huntingtin [27]. Thus, TRE has dual protective effects as both an inducer of autophagy and a chemical chaperone [27–30]. While TRE has been shown to increase both protein stability and aggregate clearance [27,29,32], it is unknown if this property increases the stability of Atg12–5 or its ability to form a complex. Also, *Pkd1*[RC/RC] mice that were used in the present study, have a missense pkd1 allele, matching a human disease variant, PKD1 p. R3277C (Pkd1[RC]) [33]. The PC1[RC] protein is a temperature-sensitive folding mutant, with a ∼ 65% reduction in PC1[RC] protein levels relative to wild-type PC1 [33]. Given that Pkd1[RC] is thought to be a folding mutant, we were interested to determine whether the PKD caused by Pkd1[RC] could benefit from a chemical chaperone like TRE that increases protein stablity.

2. Methods

2.1. Trehalose assay

Trehalose was measured in serum and kidney per manufacturer's instructions using an enzymatic assay kit from Megazyme, Inc. (Chicago, IL, USA) (Product code K-TREH). The Trehalose test kit is a method for the measurement and analysis of trehalose in foods, beverages and other materials. The principle of the assay is that trehalose is hydrolysed to D-glucose by trehalase and the D-glucose released is phosphorylated by the enzyme hexokinase (HK) and adenosine-5′-triphosphate (ATP) to glucose-6-phosphate (G-6-P) with the simultaneous formation of adenosine-5′-diphosphate (ADP). In the presence of the enzyme glucose-6-phosphate dehydrogenase (G6P-DH), G-6-P is oxidized by nicotinamide-adenine dinucleotide phosphate (NADP +) to

gluconate-6-phosphate with the formation of reduced nicotinamide-adenine dinucleotide phosphate (NADPH). The amount of NADPH formed in this reaction is stoichiometric with the amount of D-glucose and with twice the amount of trehalose. NADPH is measured by the increase in absorbance at 340 nm. D-glucose and trehalose standard solutions were assayed as positive controls. A standard curve was determined for each assay performed.

2.2. In vivo models

Pkd1[RC/RC] mice have a hypomorphic *Pkd1* gene mutation orthologous of PKD patient disease variant, *PKD1* p. R3277C (*Pkd1*) [33]. *Pkd1*[RC/RC] mice in the C57BL/6 background have small cysts as early as postnatal day 12 [34,35]. Cyst expansion and size correlates with increased tubular cell proliferation [33]. Wild type C57BL/6 J mice (#000664) were purchased from Jackson Laboratories (Bar Harbor, ME, USA). All experiments were conducted with adherence to the National Institutes of Health Guide for the Care and Use of Laboratory Animals. The animal protocol was approved by the Institutional Animal Care and Use Committee of the University of Colorado at Denver. Mice were maintained on a standard diet with standard pathogen-free housing conditions, and food and water were freely available.

2.3. Experimental in vivo protocol

Glucose/sucrose, that is sweeter than TRE, in the drinking water has the potential to increase water intake, suppress ADH and slow cyst growth. However, it has been shown that mice fed drinking water supplemented with sucrose have a slightly increased cystic phenotype compared to untreated mice, supporting studies that sugar consumption has the potential to worsen ADPKD [36]. Thus we used tap water rather than glucose or sucrose in the drinking water as the control for TRE. A concentration of 2% TRE (mass/volume) in tap water was chosen for in vivo experiments, based on published studies [27–30,37]. Male C57BL/6 *Pkd1*[RC/RC] mice were treated with 2% TRE in water from days 64 to 70 of age (short-term study) or days 50 to 120 of age (long-term study). TRE was purchased from Sigma-Aldrich (St. Louis, MO, USA).

2.4. Ex vivo assay

Fresh kidney was homogenized on ice with a sonicator for 30 s in lysis buffer containing 10 mM Tris-HCL (pH 7.5), 10 mM NaCl, 0.1% Triton-X100, 10% Glycerol, cOmplete protease and PhosSTOP phosphatase inhibitor cocktails (Sigma), and 1 mM PMSF. The homogenate was then centrifuged at 14,000RPM at 4 °C. Supernatant was then immediately incubated with concentrations of 0, 10, 25, 100, and 250 mM TRE, or 250 mM Glucose or 250 mM sucrose in DMEM + 10% FBS for 30 min in an incubator at 37 °C in 1.7 mL Eppendorf tubes. Protein quantification was then performed by Bio-Rad (Hercules, CA, USA) DC Protein Assay as described by manufacturer and immunoblot analysis was performed as described below.

2.5. Water intake study

58 day old wild type mice were given either water or 2% TRE in water for 5 days. Starting the second to last day, the mice were placed in metabolic chambers for 16 h and fluid intake was measured.

2.6. Measurement of kidney function

Blood urea nitrogen (BUN) was measured with a BioAssay Systems (Hayward, CA, USA) Urea Assay Kit according to manufacturer's instructions (DIUR-100).

2.7. Immunoblot analysis

Protein was isolated from cells and tissues using RIPA, cOmplete protease and phoSTOP phosphatase inhibitor cocktails (Sigma). Homogenates were centrifuged and supernatant was taken for protein quantification by Bio-Rad (Hercules, CA, USA) DC Protein Assay as described by manufacturer. Samples were mixed with Laemmli Sample Buffer and beta-mercaptoethanol and boiled for 5 min. Samples were run on 4–15% polyacrylamide gels. Proteins were then transferred to 0.45 μm PVDF membranes, blocked with 2.5% evaporated milk, and probed with antibodies listed in Supplemental Table 1. Blots were developed by chemiluminescence and analyzed for densitometry using ImageJ.

2.8. Antibodies

Supplemental Table 1 lists the antibodies used in this study. The specificity of each of the antibodies used has been validated by the vendor (Cell Signaling Technology, Danvers, MA).

2.9. Routine histology

Tissues were fixed overnight in 10% formalin at 4 °C. They were transferred to fresh 70% ethanol and left overnight at 4 °C; this process was repeated twice more. Next, the tissues were processed and embedded in paraffin wax using Leica systems. Tissues were sectioned at 4 μm and baked at 60 °C for 2 h. Kidneys were stained with hematoxylin-eosin and cystic index and number was quantified on two sections per mouse (left and right kidney) using a NIS Elements macro as previously published [35]. Cyst index or cyst number were expressed as the percentage of the cross-sectional area or number per cross sectional area, respectively. Areas with tissue tears and bubbles that were identified with higher magnification (40×) were excluded from analysis.

2.10. Immunohistochemistry protocol

Tissue sections were deparaffinized and rehydrated, then antigen unmasking was performed in sodium citrate buffer (pH 6.0) for 25 min at 100 °C. After rinsing sections for 10 min in cold tap water, endogenous peroxidase activity was blocked by immersing the sections in 3% hydrogen peroxide for 10 min, followed by a 5-min rinse in deionized water. Blocking was performed using Vectastain® Elite® ABC Kit blocking serum for 30 min at room temperature. Primary antibodies were diluted in tris-buffered saline with Tween20 (TBST) as indicated in Supplemental Table 1 and incubated overnight at 4 °C in a humidified chamber. Immunoreactions were detected using the Vectastain® standard protocol with 3,3′-diaminobenzidine tetrahydrochloride hydrate (DAB) counterstained with hematoxylin. Slides were subsequently dipped 1–3 times in 0.3% acid alcohol, then dehydrated and mounted. DAB positive staining was analyzed using Aperio ImageScope macros.

2.11. Terminal deoxynucleotidyl transferase dUTP nick end labeling (TUNEL) staining protocol

TUNEL staining was performed on tissue sections using Promega DeadEnd™ Colorimetric Apoptosis Detection System Kit following the manufacturer's instructions.

2.12. Quantitation of immunohistochemical staining

The number of positive staining cells was counted using the Aperio ImageScope, Leica Biosystems, by an observer blinded to the treatment modality. Non-cystic tubules were defined as tubules less than 50 μm in diameter. 15–20 fields of view (40× magnification) devoid of cysts in the cortex per sample were randomly selected for quantitation in non-cystic tubules. To avoid sensitivity and selection artifacts between non-cystic tubules and dilated possibly pre-cystic tubules, as well as potential changes in tubular epithelium lining massive cysts, positive staining was counted in cysts of approximately 75-200 μm diameter. 50–75 cortical cysts per tissue section were randomly selected for histological analysis.

2.13. Immunofluorescence

Fixation of tissue, preparation of slides and immunofluorescence was performed as we have previously described [38]. Slides were imaged using an Olympus FV1000 confocal laser scanning microscope with a 100× oil objective. Images were taken of cortical tubular regions. Co-localization analysis was performed using the Coloc2 plugin in ImageJ (U.S. National Institutes of Health, Bethesda, Maryland, USA).

2.14. Statistical analysis

Data sets were analyzed by the non-parametric unpaired Mann Whitney test. Multiple group comparisons are performed using analysis of variance (ANOVA) with post-test according to Newman-Keuls. Single comparisons were made using students t-test. A p-value of < 0.05 was considered statistically significant. Values are expressed as means ± SEM.

3. Results

3.1. TRE is detected in blood and kidney

TRE can be rapidly degraded into glucose by the brush border saccharidase, trehalase, which is present in the intestinal brush borders of most mammals including mice. Thus it was important to determine that TRE was absorbed into the blood. TRE was detected in serum and kidney in TRE–treated mice (Supplemental Fig. S1).

3.2. TRE supplementation did not increase water intake

In order to ensure that the any observed effects of TRE on cyst growth were not the result of increase water intake, which has been shown to slow cyst growth in rats [39], a preliminary water intake study was performed. Fifty eight day old wild type mice were given either vehicle (tap water) or 2% TRE in tap water for 5 days and then water intake, urinary arginine vasopressin (AVP), and serum copeptin were measured. While there was an upward trend in water intake with TRE treated mice, there were no significant differences in AVP or serum copeptin in vehicle or TRE –treated mice (Fig. 1).

3.3. Short term supplementation with TRE increased markers of autophagy

In order to determine the immediate effects of TRE treatment, wild type and $Pkd1^{RC/RC}$ mice were given either VEH or 2% TRE in tap water for 6 days (64–70 days of age) and then sacrificed. After TRE treatment, Atg12–5 complex levels were significantly increased in wild type mice but remained unchanged with TRE in $Pkd1^{RC/RC}$ mice which had higher baseline levels compared to wild type mice on immunoblot analysis (Fig. 2). However, no significant changes in free Atg12 expression were observed. As Atg12–5 complex formation is linked with autophagy stimulation, additional autophagy associated proteins were measured. In the canonical autophagy pathway, LC3-II and p62, markers of autophagosomes and autophagic cargo respectively, were measured [9]. LC3-II and p62 expression was nearly 2-fold higher in $Pkd1^{RC/RC}$ mice compared to wild type (Fig. 2). Treatment with TRE decreased LC3-II expression in $Pkd1^{RC/RC}$ mice but had no effect on p62, suggesting decreased autophagosome production. Rab9a has been implicated in the formation of autophagosomes in the Atg5/7-independent alternative autophagy pathway [15]. TRE supplementation caused a significant
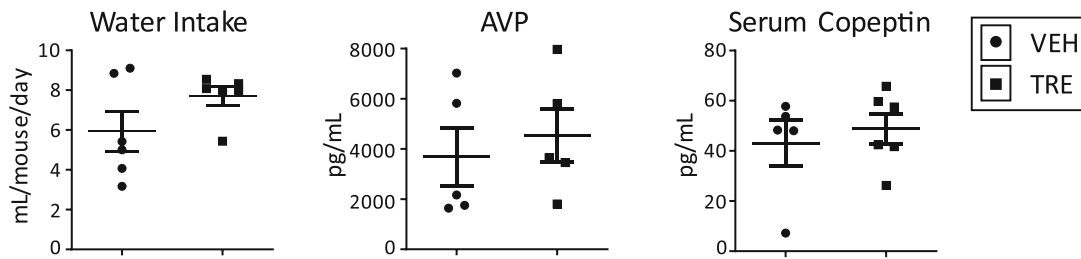
Fig. 1. Trehalose (TRE) does not significantly affect water intake, urinary vasopressin (AVP), or serum copeptin.
Animals were given either tap water (VEH) or 2% TRE in tap water for 5 days from ages 58–63 days old and water intake was recorded. Then urinary vasopressin and serum copeptin were measured. Data is expressed as a mean $+/-$ SEM. $n = 5$–6 per group.

increase in Rab9a in both wild type and *Pkd1*[RC/RC] mice (Fig. 2). Additionally, Beclin1 was examined as it is essential to the initiation of autophagy in both the canonical and alternative autophagy pathways [18]. *Pkd1*[RC/RC] mice had a significant decrease in pBeclin1[S15] compared to wild type mice and TRE supplementation caused non significant increases in pBeclin1[S15] in both wild type and *Pkd1*[RC/RC] mice compared to vehicle (Fig. 2B).

3.4. TRE increased Atg12–5 complex ex vivo

In order to confirm the effect of TRE to increase the Atg12–5 complex in wild type mice, ex vivo experiments on kidney homogenates from wild type mice were performed. Kidney homogenates from wild type mice were incubated with increasing concentrations of TRE in DMEM and with glucose at the highest concentration. Incubation with TRE at 10, 25 and 100 mM concentrations significantly increased the levels of the Atg12–5 complex in homogenized wild type kidneys compared to vehicle and 250 nM TRE (Fig. 3). Additionally, incubation with 250 mM glucose caused a non significant decrease in Atg12–5 complex expression. TRE also significantly increased LC3-II expression,

independent of concentration used, with no increase with glucose supplementation. Only 25 mM TRE increased P62 expression. Neither TRE nor glucose supplementation had an effect on Rab9a protein expression. In order to control that autophagic-stimulation was not a nonspecific osmotic stress response, kidney homogenates were incubated with or without 250 mM sucrose. There was no difference in LC3, p62 or Atg12–5 in kidney homogenates treated with or without sucrose (Supplemental Fig. S2).

3.5. Long term TRE supplementation did not slow cyst growth or improve kidney function

Next, the effect of long-term supplementation with TRE on cyst growth was determined in mice treated from 50 to 120 days of age (70 days of treatment). Water intake in TRE treated animals was significantly higher, approximately 15% more than with vehicle (Fig. 4A). However, previous studies have shown that a close to 7 –fold increase in water intake had no effect on plasma vasopressin levels or cyst burden in *Pkd1*[RC/RC] mice [39] and as such this 15% increase in water intake with TRE was not expected to have any impact on the study. There was
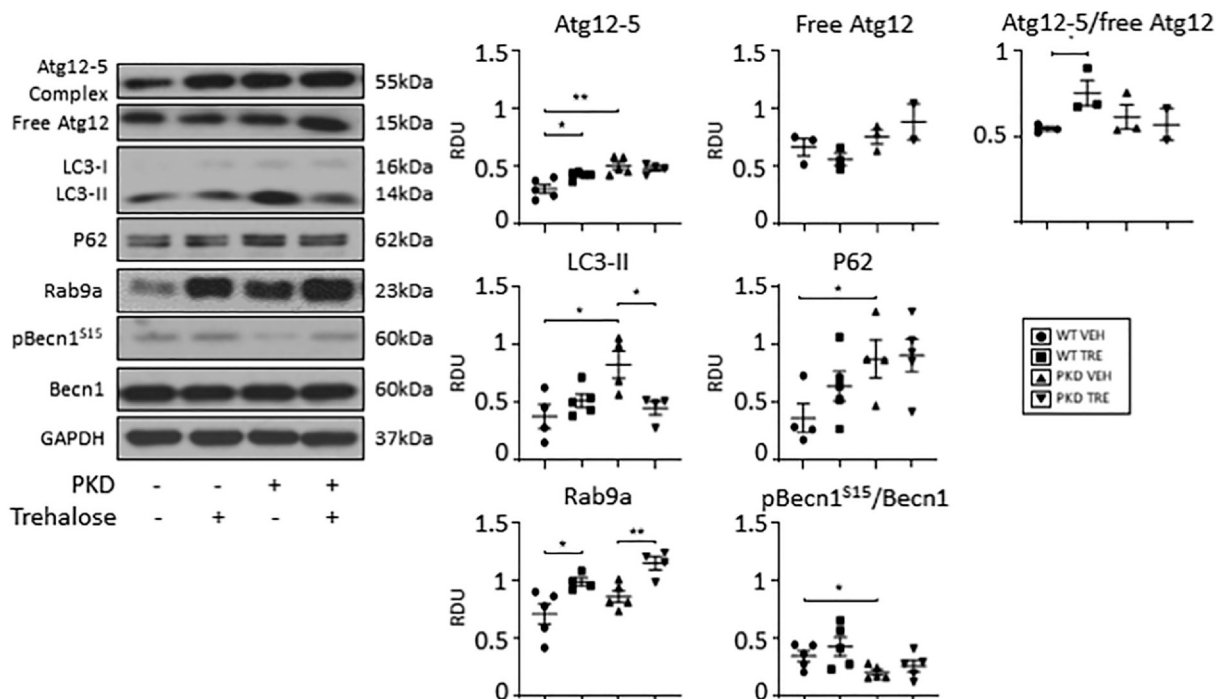

Fig. 2. Atg12–5, LC3-II, p62 were increased and pBeclin1[S15] was decreased in *Pkd1*[RC/RC] (PKD) vs. wild type (WT) kidneys. Short-term trehalose (TRE) supplementation increased Atg12–5 complex in WT but not *PKD* kidneys and increased Rab9a in both WT and PKD kidneys.
Animals were treated for 6 days from 64 to 70 day of age with TRE or vehicle (VEH). Immunoblot analysis was performed for LC3-II, p62, Atg12–5 complex, free Atg12, Rab9a and pBeclin1 (Becn1)[S15]. RDU = relative densitometry units corrected for GAPDH. Data is expressed as a mean $+/-$ SEM, $n = 4$–6 per treatment group. *$P < 0.05$, ** $P < 0.01$.
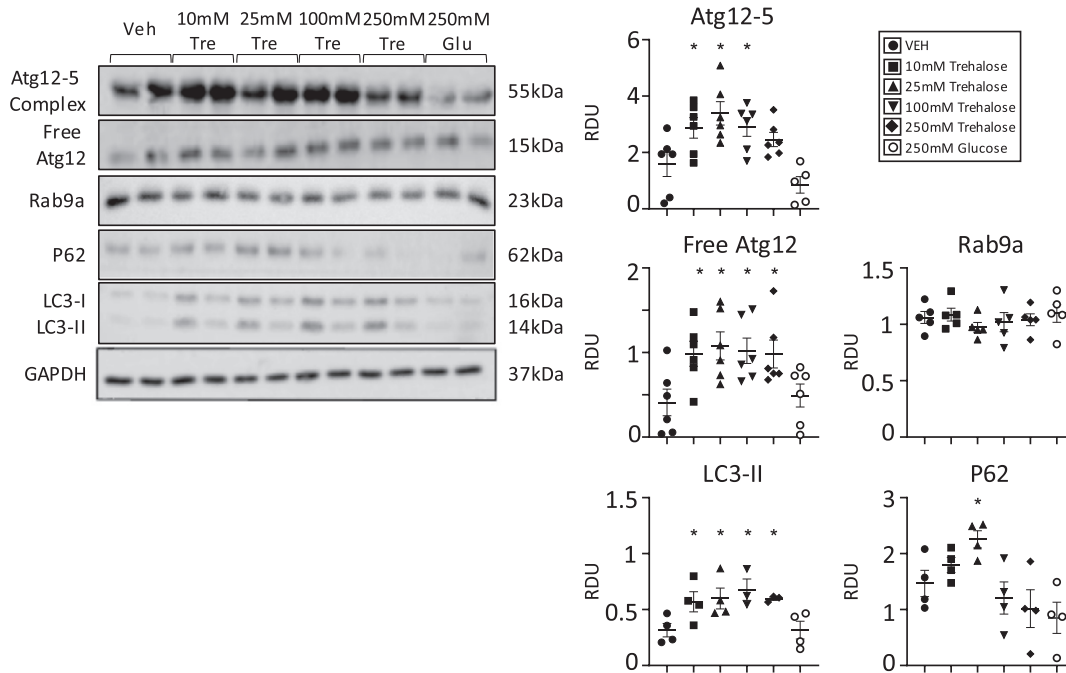
Fig. 3. Trehalose (TRE) increases autophagy proteins Atg12–5, p62, LC3-II ex vivo.
Homogenized wild type mouse kidneys were incubated in a test tube with increasing concentrations of TRE or glucose (GLU) and were then immunoblotted for Atg12–5, p62, LC3-II and Rab9a proteins. RDU = relative densitometry units corrected for GAPDH. Data is expressed as a mean $+/-$ SEM. n = 4–6 per treatment group. P $<$ 0.05 versus vehicle (VEH) and 250 nM TRE.

an increase in 2 K/TBW ratio between 64 day old historical control mice and 120 day old mice treated with vehicle or TRE (Supplemental Fig. S3). Long-term treatment with TRE from 50 to 120 days old had no impact on cyst growth or cyst number as determined by 2KW/TBW ratio, cyst number and cyst index (Fig. 4A). Long term treatment with TRE did not improve kidney function as measured by BUN (Fig. 4A). Representative kidney sections from vehicle and TRE-treated $Pkd1^{RC/RC}$ mice are demonstrated in Fig. 4A. There were no cysts present in wild type mice treated with TRE. Histological analysis of cystic tubules in age matched littermate $Pkd1^{RC/RC}$ mice showed no significant differences in proliferation, as determined by PCNA staining, or apoptosis, as determined by TUNEL staining, in TRE vs. vehicle treated mice (Fig. 4B). Histological analysis of non cystic tubules in vehicle and TRE-treated wild type and age matched littermate Pkd1$^{RC/RC}$ mice showed no significant differences in PCNA TUNEL staining, between groups (Fig. 4B).

3.6. TRE was unable to rescue the deficiency of the Atg12–5 complex or increase Rab9a in Pkd1$^{RC/RC}$ kidneys

Next, the effects of long-term supplementation with TRE on autophagy-related protein expression was determined in mice treated from 50 to 120 days of age (70 days of treatment). Immunoblot analysis revealed that TRE treatment significantly increased Atg12–5 complex expression in wild type kidneys but was unable to rescue the complex in $Pkd1^{RC/RC}$ mice, which was effectively absent (Fig. 5). This was reflected in free Atg12 levels, which were unchanged between treatment groups but were 7-fold higher in $Pkd1^{RC/RC}$ mice compared to wild type (Fig. 5). The increase in Atg12–5 complex in wild type mice treated with TRE was not caused by increased abundance of Atg12 and Atg5 as the levels of free protein was not changed. Additionally, Atg5 levels in $Pkd1^{RC/RC}$ animals were approximately half that of wild type animals. This suggests that there is both decreased Atg5 available for Atg12 to bind to and that their ability to form a complex is also impaired. Without the Atg12–5 complex, canonical autophagy cannot proceed so we examined the alternative autophagy pathway. Levels of the

alternative autophagy pathway marker Rab9a were also significantly decreased in $Pkd1^{RC/RC}$ compared to wild type mice and not changed between treatment groups, which is surprising as one would expect the Atg5-independent alternative autophagy pathway to ramp up activity in the absence of Atg5 as has been previously described [15,40]. The canonical autophagy pathway-associated proteins LC3-II and p62 were both significantly increased with TRE treatment in wild type animals (Fig. 5), indicating a change in the autophagy pathway preventing turnover and degradation of LC3-II and p62 [7,41,42]. To determine whether the increased in LC3-II and p62 in wild type kidneys treated with TRE (Fig. 5) was due to increased autophagic flux or due to inhibition of autophagic degradation, wild type mice were treated with TRE + vehicle vs. TRE+ bafilomycin A1 (a lysosomal inhibitor) 1.75 mg/kg IP at 2 h before sacrifice. If the amount of LC3-II increases further in the presence of lysosomal protease inhibitors like bafilomycinA1, this indicates an increase in autophagic flux [41]. However, if LC3-II does not increase further with lysosomal inhibitors, this indicates that autophagosome accumulation occurred due to inhibition of autophagic degradation, for example, blockage of autophagosome-lysosome fusion [41]. There was no further increase in LC3-II or p62 in kidneys treated with TRE + bafilomycin A1 vs TRE alone suggesting that the increase in LC3-II and p62 was due to inhibition of autophagic degradation (Supplemental Fig. S4). It is not recommended that the conversion of LC3-I to LC3-II be used as a marker of autophagy as LC3-I is technically less sensitive to detection by antibodies that also detect LC3-II [12]. LC3-I is labile and more sensitive to freeze-thawing and degradation in SDS buffer and the amount of LC3-I is cell and stress specific.

pBeclin1^{S15} and the alternative autophagy pathway marker Rab9a were not affected by TRE treatment in wild type mice, suggesting that TRE mainly acts on the canonical autophagy pathway in the long term. pBeclin1^{S15} was upregulated in vehicle treated $Pkd1^{RC/RC}$ mice compared to wild type and was reduced to near wild type levels with TRE treatment.

On immunofluorescence staining for Rab9a and LAMP2 (lysosomal marker), TRE did not affect the co-localization of Rab9a and LAMP2
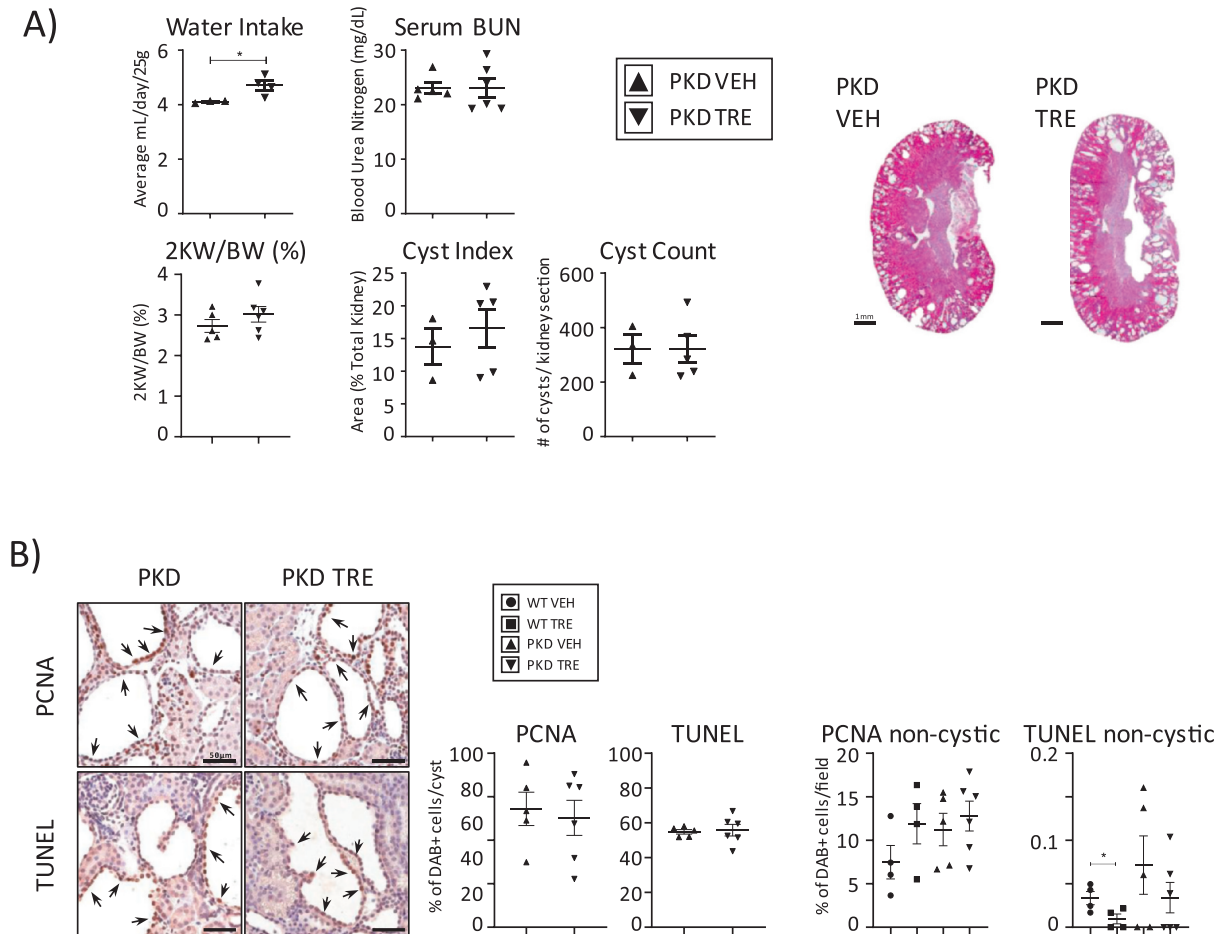
Fig. 4. Long-term trehalose (TRE) supplementation did not improve kidney weight, cyst number, cyst index, BUN, tubular cell proliferation or tubular cell apoptosis. Animals were treated from 50 to 120 days of age with either vehicle (VEH) or TRE. (**A**) In older mice (120 days of age), water intake was slightly increased by TRE compared to no significant increase in water intake in younger mice (63 d old) (Fig. 1). Kidney weight was measured by two kidney weight to body weight ratio (2KW/BW%). Cyst number and cyst index (percentage of the cross-sectional area of the kidney that was cystic) were determined. Renal function was assessed by BUN. Representative kidney cross sections at the same magnification stained with hematoxylin-eosin are shown. Data is expressed as a mean $+/-$ SEM, $n = 3-6$ per treatment group. $*P < 0.05$. (**B**) Immunohistochemistry for markers of proliferation (PCNA) and apoptosis (TUNEL) was performed and quantitated in cyst lining cells and non cystic tubules. Data is expressed as a mean $+/-$ SEM, $n = 4-6$ per treatment group.

suggesting that TRE does not increase the localization of Rab9a in the lysosome (Supplemental Fig. S5).

3.7. TRE increased pAMPK^{T172} and pGSK-3β^{S9} in wild type kidneys. TRE had no effect on mTORC1, mTORC2 and autophagy-related proteins (Atg3 and 7)

The effect of PKD and TRE on mTORC1/2 proteins, autophagy-related proteins, pAkt^{S308}, phospho AMP-activated protein kinase (pAMPK^{T172}) and phospho glycogen synthase kinase-3β (pGSK-3β^{S9}) is demonstrated in Fig. 6. Atg16L1 was decreased in *Pkd1*$^{RC/RC}$ vs. wild type kidneys. Markers of mTORC1 (pmTOR^{S2448} and pS6$^{S240/244}$) were increased in *Pkd1*$^{RC/RC}$ vs. wild type kidneys and unaffected by TRE. pAkt^{S473}, a marker of mTORC2 and pAkt^{S308} that is upstream of mTOR were decreased in *Pkd1*$^{RC/RC}$ kidneys and unaffected by TRE. pAMPK^{T172} expression was increased in *Pkd1*$^{RC/RC}$ vs. wild type kidneys, increased by TRE in wild type kidneys and unaffected by TRE in *Pkd1*$^{RC/RC}$ kidneys. pGSK-3β^{S9} expression was increased by TRE in wild type kidneys. pGSK-3β^{S9} was decreased in *Pkd1*$^{RC/RC}$ kidneys compared to wild type kidneys and unaffected by TRE in *Pkd1*$^{RC/RC}$ kidneys. TRE had no effect on Atg 3 or Atg7.

4. Discussion

Hyper-proliferation, increased apoptosis and impaired autophagy in the kidney are all characteristics of ADPKD [2–5]. Inhibition of proliferation with sirolimus or everolimus has been shown to decrease cyst growth and improve kidney function in mice [21,43]. The mTOR inhibitors, sirolimus and everolimus, are known autophagy inducers [12]. Autophagy is an essential cellular process in which damaged organelles and misfolded proteins are sequestered by the autophagosome and then degraded after fusing with a lysosome [6]. Several studies show that this process is suppressed in ADPKD [2,3,36] and stimulating autophagy has been shown to slow the progression of ADPKD in zebrafish [3]. TRE is a non-reducing glucose disaccharide that is found in most organisms other than vertebrates and in common food supplements [23–25]. TRE is known to increase autophagy in several animal models of neurological disorders [27–29]. It is also known to stabilize proteins and cell membranes in response to freezing and dehydration [23]. Thus agents that induce autophagy, like the food additive TRE, have a potential therapeutic value to stabilize autophagy proteins and the Pkd1^{RC} mutant protein and decrease cyst growth in ADPKD.

In the present study, TRE did not decrease cyst growth. mTOR inhibitors and AMPK activators are known to decrease cyst growth in PKD [21,22]. TRE did not decrease pmTOR activation or further increase pAMPK^{T172} in *Pkd1*$^{RC/RC}$ mice and this could partly explain why TRE
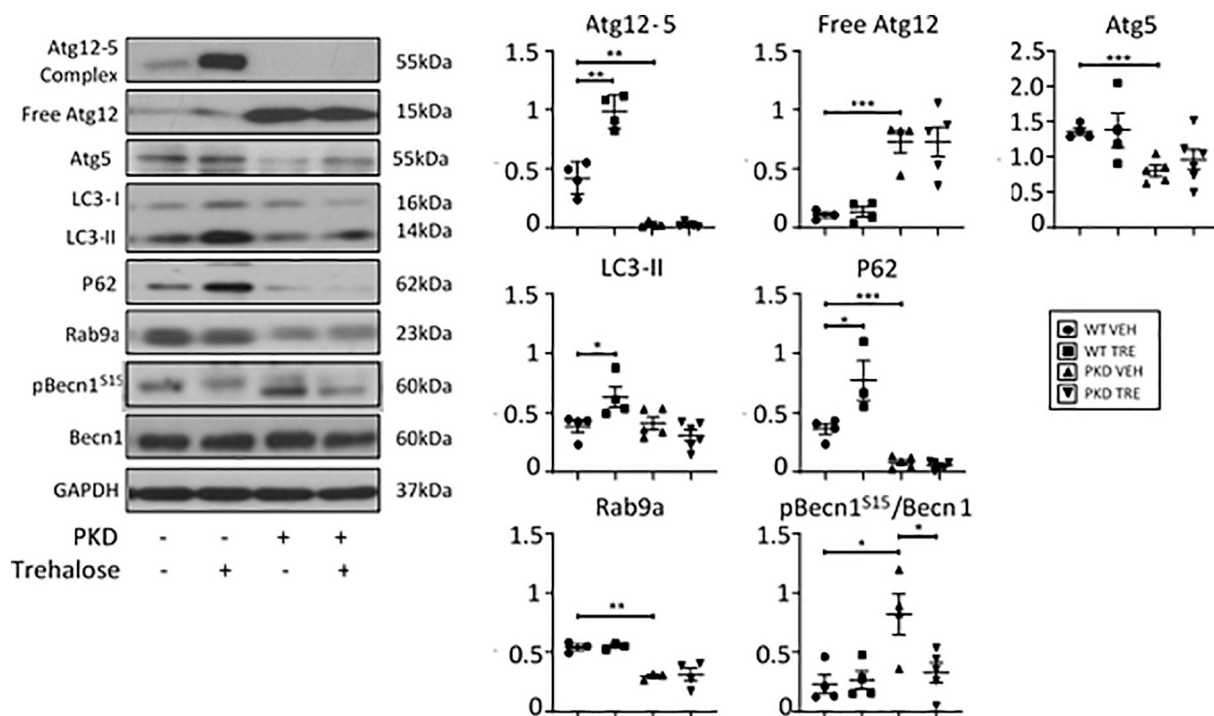
Fig. 5. Long-term trehalose (TRE) supplementation resulted in an increase in Atg12–5, LC3-II, and p62 in wild type (WT) but not *Pkd1*[RC/RC] kidneys. Atg12–5 complex was absent and free Atg12 was increased in *Pkd1*[RC/RC] kidneys.

Animals were treated for 70 days from 50 to 120 days of age with either vehicle (VEH) or TRE. Immunoblot analysis was performed for Atg12–5 complex, free Atg12, free Atg5, LC3-II, p62, Rab9a and pBeclin (Becn1)[S15]. RDU = relative densitometry units corrected for GAPDH. Data is expressed as a mean $+/-$ SEM, n = 4–6 per treatment group. *P $<$ 0.05 ** P $<$ 0.01, ***P $<$ 0.001.
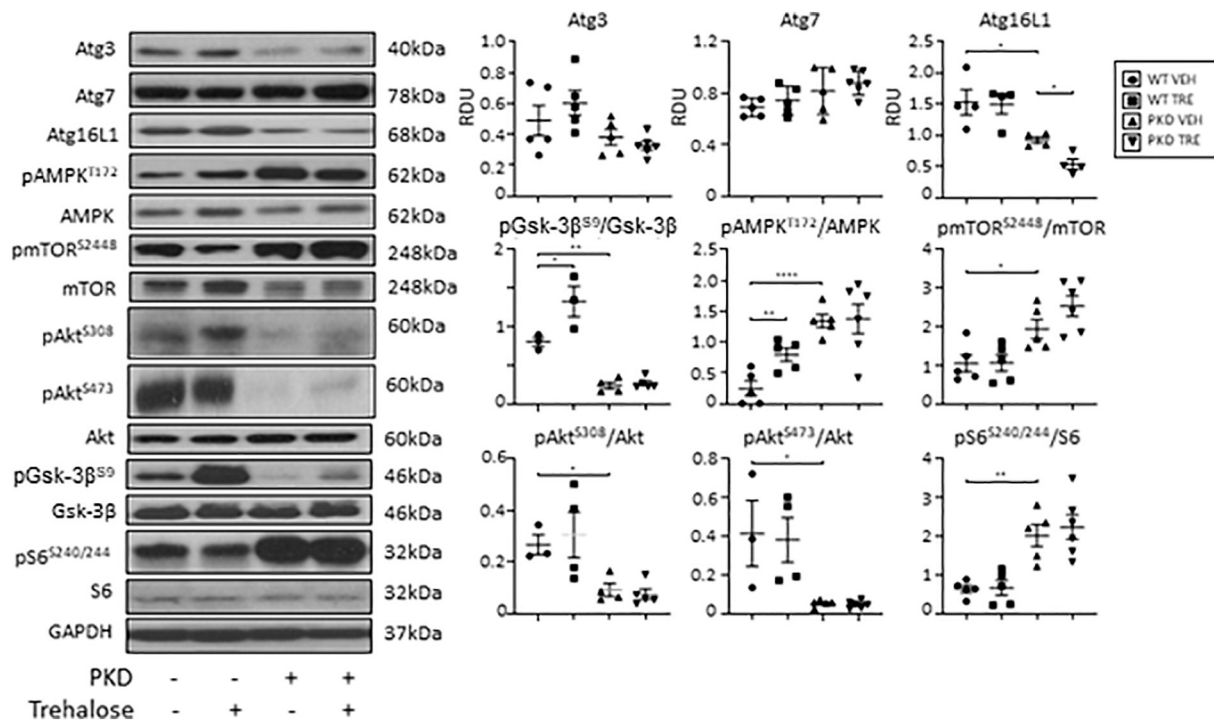
Fig. 6. Autophagy phenotype in *Pkd1*[RC/RC] kidneys: Increase in mTORC1 (pmTOR[S2448], pS6), decrease in mTORC2 (pAkt[S473]), decrease in Atg16L1, pGSK-3β[S9] and pAkt[S308] in *Pkd1*[RC/RC] (PKD) vs. wild type (WT) kidneys that was not affected by trehalose (TRE).

Animals were treated for 70 days from 50 to 120 days of age with either vehicle (VEH) or TRE. The effect of PKD and TRE on mTORC1 (pmTOR[S2448], pS6), mTORC2 (pAkt[S473]), pAkt[S308], pGSK-3β[S9] and autophagy-related proteins Atg3, Atg7 and Atg16L1 in WT and PKD kidneys was determined. RDU = relative densitometry units corrected for GAPDH. Data is expressed as a mean $+/-$ SEM, n = 3–6 per treatment group. *P $<$ 0.05 ** P $<$ 0.01, ***P $<$ 0.001, ****P $<$ 0.0001.

was not protective against cyst growth. In this regard, TRE is known to be an mTOR-independent autophagy inducer by acting as a chemical chaperone [29]. In this study, TRE and mTOR inhibition with sirolimus have an additive effect on the clearance of aggregate-prone proteins because of increased autophagic activity in a model of Huntingtons disease.

In the conventional autophagy pathway, two autophagy-related proteins (Atg12 and Atg5) form a complex with other proteins such as LC3-II in order to elongate the phagosome and fully engulf autophagic cargo [6–9]. Deficiency in the Atg12–5 complex is known to impair autophagy leading to several diseases such as asthma, lupus erythematosus, and Crohn's disease, as well as several types of cancer [44–48]. There is also an Atg5-independent mechanism of autophagy, called alternative autophagy, utilizing Rab9a, a small GTPase, that is recruited to autophagosome-like vacuoles after autophagosomal maturation resulting in autophagosome-like vacuole enlargement and eventual lysosomal fusion [14,15,17]. TRE has been gaining attention recently regarding activating the autophagy pathway. TRE supplementation of the diets of mice with Parkinson's and Huntington's disease reduces disease severity and increases lifespan by increasing aggregate clearance via an mTOR-independent autophagy pathway [27–30]. The effect of TRE on Atg12–5 complex and Rab9a is not known. Thus, the first aim of the study was to determine the effect of TRE on autophagy-related proteins especially Atg12–5 complex, Rab9a and p62. Both in 70 and 120 day old wild type kidneys in vivo and in kidney homogenates from wild type mice ex vivo, TRE resulted in increased expression of the Atg12–5 complex and increased Rab9a. In the ex vivo experiments, the increase in Atg12–5 complex was accompanied by the increase in LC3-II and p62, markers of autophagic vesicles and cargo, respectively [7,42]. These studies demonstrate for the first time that TRE was able to increase Atg12–5 and Rab9a, in wild type kidneys, reinforcing its potential as an autophagy inducer. Thus, we hypothesized that supplementing the diet with TRE would increase expression of the Atg12–5 complex and increase Rab9a in $Pkd1^{RC/RC}$ kidneys.

In both in vivo and ex vivo experiments in wild type kidneys, TRE successfully increased the amount of Atg12–5 complex. This effect was not seen in $Pkd1^{RC/RC}$ mice. 70 day old $Pkd1^{RC/RC}$ kidneys had higher levels of Atg12–5 complex than wild type mice while in older 120 day old mice, Atg12–5 complex was unexpectedly absent. Conversely, the opposite was found of pBeclin1^{S15,} whose levels in 70 day old $Pkd1^{RC/RC}$ mice were slightly more than half the levels of wild type mice. This was reversed in 120 day old mice, with $Pkd1^{RC/RC}$ mice having 3-fold higher levels of pBeclin1^{S15} compared to wild type, but this difference was eliminated with TRE treatment. Thus, while TRE had an effect on Atg12–5 complex and Rab9a in wild type kidneys, it did not affect these autophagy-related proteins in $Pkd1^{RC/RC}$ kidneys.

Lack of an effect of TRE on autophagy-related proteins in $Pkd1^{RC/RC}$ kidneys was associated with the lack of an effect on cyst growth and kidney function. Lack of a protective effect in PKD was associated with the inability of TRE to impact proliferation and apoptosis, processes that are crucial to increase cyst growth. Another study has also showed the lack of a therapeutic effect of TRE on ADPKD [36]. There are important differences between the published study and our study. In the published study, a different ADPKD model, the $Pkd1$ miRNA transgenic mouse, was used. In the published study, TRE exhibited no effects on the mRNA levels of any of the measured autophagy proteins in either wild-type or diseased mice, while our study showed an effect of TRE on protein expression of Atg12–5 complex, Rab9a, p62 and LC3-II, pGSK-3β^{S9} and pAMPK^{T172} in normal kidneys and LC3-II, Rab9a and pBeclin1^{S15} in $Pkd1^{RC/RC}$ kidneys. Tubular apoptosis was not described in the published study whereas we found that TRE had no effect on tubular apoptosis in both cystic and non cystic tubules in $Pkd1^{RC/RC}$ kidneys. Pro-inflammatory or glycolysis related genes were studied in the published study, whereas we focused on the effect of TRE on autophagy-related proteins especially Atg12–5 complex.

A limitation of the current study is that treatment was started at 50 days of age, a time point when there was already a significant cyst burden [33]. In the younger (70 day old) mice, an increase in the alternative autophagy pathway protein, Rab9a, was seen with TRE. This effect was lost with long term treatment in older (120 day old) mice. If treatment was started at a younger age it is possible that the beneficial effect would have been maintained.

Finally, we noted a distinct autophagy-related phenotype in $Pkd1^{RC/RC}$ mouse kidneys compared to wild type kidneys. There was a decrease in Atg12–5 complex, increased free Atg12 and decreased Rab9a in 120 day old $Pkd1^{RC/RC}$ kidneys that was not present in 70-day old kidneys. There was an increase in LC3-II and p62 in 70-day old $Pkd1^{RC/RC}$ kidneys that was not present in 120-day old kidneys. TRE increased Rab9a in 70-day old but not in 120-day old kidneys. The difference in autophagy proteins between 70 and 120-day old kidneys suggest that older age, worse polycystic kidney disease and worse kidney function in 120-day old mice vs. 70-day old mice [43] affects autophagy and the response to TRE. In this regard, aging is known to have significant effects on autophagy [50]. Atg3 and Atg16L1 are E2 enzymes essential for the LC3 lipidation process of autophagosomes. A large protein complex consisting of Atg5, Atg12 and Atg16L1 has recently been shown to be essential for the elongation of isolation membranes (also called phagophores) during mammalian autophagy [10]. Atg5 and Atg7 are key proteins involved in the extension/development of the autophagosomal membrane [12]. Atg16L1 and Atg5 were decreased in $Pkd1^{RC/RC}$ vs. wild type kidneys confirming defects in autophagosome development and the autophagic process in PKD. mTORC1 is a known inhibitor of autophagy [12]. Markers of mTORC1 (pmTOR^{S2448} and pS6) were increased in $Pkd1^{RC/RC}$ kidneys. TRE had no effect on these mTORC1 markers confirming its known mTOR-independent actions [29]. In contrast to mTORC1, mTORC2 is a known inducer of autophagy and knockout of mTORC2 results in suppressed autophagy [29]. pAkt^{S473}, a marker of mTORC2 was decreased in $Pkd1^{RC/RC}$ kidneys consistent with suppressed autophagy. Akt is a serine/threonine-specific protein kinase activated by PI-3 kinase (PI3K) that is part of the PI3K/Akt/mTORC1 pathway [51]. Pharmacological inhibition of Akt promotes nuclear translocation of TFEB, lysosomal biogenesis and autophagy [52]. pAkt^{S308}, was decreased in $Pkd1^{RC/RC}$ kidneys and unaffected by TRE. Phosphorylation of AMP-activated protein kinase (AMPK) that plays a role in cellular energy homeostasis and autophagy induction was increased in $Pkd1^{RC/RC}$ kidneys, increased by TRE in wild type kidneys and unaffected by TRE in $Pkd1^{RC/RC}$ kidneys. In this regard, the AMPK activator metformin is known to protect against PKD in mice [22]. The serine/threonine kinase glycogen synthase kinase-3β (GSK-3β) that functions in a wide range of cellular processes and is known to induce apoptosis and proliferation in cancer [53] was decreased in $Pkd1^{RC/RC}$ kidneys and unaffected by TRE. In summary, the autophagy phenotype in $Pkd1^{RC/RC}$ kidneys was characterized by decreases in crucial autophagy-related proteins (Atg12–5 complex, Atg5, Atg16L1), decreased Rab9a, increased mTORC1 (inhibitor of autophagy) and decreased mTORC2 (inducer of autophagy).

In conclusion, the present study shows a newly described effect of TRE to increase expression of Atg12–5 complex and increase Rab9a expression in normal kidneys. However, the effect of long term TRE treatment on Atg12–5, Rab9a and other autophagy proteins was not seen in $Pkd1^{RC/RC}$ kidneys associated with a lack of protection against cyst growth.

Declaration of Competing Interest

Acknowledgements

Appendix A. Supplementary data

Supplementary data to this article can be found online at https://doi.org/10.1016/j.cellsig.2020.109760.

References

[1] P.D. Wilson, Polycystic kidney disease, N. Engl. J. Med. 350 (2) (2004) 151–164.
[2] K. Ravichandran, C.L. Edelstein, Polycystic kidney disease: a case of suppressed autophagy? Semin. Nephrol. 34 (1) (2014) 27–33.
[3] P. Zhu, et al., Autophagy activators suppress cystogenesis in an autosomal dominant polycystic kidney disease model, Hum. Mol. Genet. 26 (1) (2017) 158–172.
[4] L. Peintner, C. Borner, Role of apoptosis in the development of autosomal dominant polycystic kidney disease (ADPKD), Cell Tissue Res. 369 (1) (2017) 27–39.
[5] K.L. Nowak, C.L. Edelstein, Apoptosis and autophagy in polycystic kidney disease (PKD), Cell. Signal. 68 (2020) 109518.
[6] N. Mizushima, et al., Autophagy fights disease through cellular self-digestion, Nature 451 (7182) (2008) 1069–1075.
[7] N. Mizushima, Y. Ohsumi, T. Yoshimori, Autophagosome formation in mammalian cells, Cell Struct. Funct. 27 (6) (2002) 421–429.
[8] P. Jiang, N. Mizushima, Autophagy and human diseases, Cell Res. 24 (1) (2014) 69–79.
[9] N.N. Noda, F. Inagaki, Mechanisms of autophagy, Annu. Rev. Biophys. 44 (1) (2015) 101–122.
[10] K. Ishibashi, et al., Atg16L2, a novel isoform of mammalian Atg16L that is not essential for canonical autophagy despite forming an Atg12-5-16L2 complex, Autophagy 7 (12) (2011) 1500–1513.
[11] M. Walczak, S. Martens, Dissecting the role of the Atg12-Atg5-Atg16 complex during autophagosome formation, Autophagy 9 (3) (2013) 424–425.
[12] D.J. Klionsky, et al., Guidelines for the use and interpretation of assays for monitoring autophagy (3rd edition), Autophagy 12 (1) (2016) 1–222.
[13] T.E. Rusten, H. Stenmark, p62, an autophagy hero or culprit? Nat. Cell Biol. 12 (3) (2010) 207–209.
[14] T. Saito, et al., An alternative mitophagy pathway mediated by Rab9 protects the heart against ischemia, J. Clin. Invest. 129 (2) (2019) 802–819.
[15] Y. Nishida, et al., Discovery of Atg5/Atg7-independent alternative macroautophagy, Nature 461 (2009) 654.
[16] C. Amaya, C.M. Fader, M.I. Colombo, Autophagy and proteins involved in vesicular trafficking, FEBS Lett. 589 (22) (2015) 3343–3353.
[17] T. Nozawa, et al., The small GTPases Rab9A and Rab23 function at distinct steps in autophagy during group a Streptococcus infection, Cell. Microbiol. 14 (8) (2012) 1149–1165.
[18] E. Itakura, et al., Beclin 1 forms two distinct phosphatidylinositol 3-kinase complexes with mammalian Atg14 and UVRAG, Mol. Biol. Cell 19 (12) (2008) 5360–5372.
[19] I. Rowe, et al., Defective glucose metabolism in polycystic kidney disease identifies a new therapeutic strategy, Nat. Med. 19 (4) (2013) 488–493.
[20] F. Belibi, et al., Hypoxia-inducible factor-1alpha (HIF-1alpha) and autophagy in polycystic kidney disease (PKD), Am. J. Physiol. Ren. Physiol. 300 (5) (2011) F1235–F1243.
[21] I. Zafar, et al., Sirolimus attenuates disease progression in an orthologous mouse model of human autosomal dominant polycystic kidney disease, Kidney Int. 78 (8) (2010) 754–761.
[22] V. Takiar, et al., Activating AMP-activated protein kinase (AMPK) slows renal cystogenesis, Proc. Natl. Acad. Sci. U. S. A. 108 (6) (2011) 2462–2467.
[23] C. Olsson, H. Jansson, J. Swenson, The role of Trehalose for the stabilization of proteins, J. Phys. Chem. B 120 (20) (2016) 4723–4731.
[24] J.-C. Argüelles, Why Can't vertebrates synthesize Trehalose? J. Mol. Evol. 79 (3) (2014) 111–116.
[25] K. Hosseinpour-Moghaddam, M. Caraglia, A. Sahebkar, Autophagy induction by trehalose: molecular mechanisms and therapeutic impacts, J. Cell. Physiol. 233 (9) (2018) 6524–6543.
[26] J.N. BeMiller, 3 - Oligosaccharides, in: J.N. BeMiller (Ed.), Carbohydrate Chemistry for Food Scientists, Third edition, AACC International Press, 2019, pp. 49–74.
[27] M. Tanaka, et al., Trehalose alleviates polyglutamine-mediated pathology in a mouse model of Huntington disease, Nat. Med. 10 (2004) 148.
[28] M. Khalifeh, G.E. Barreto, A. Sahebkar, Trehalose as a promising therapeutic candidate for the treatment of parkinson's disease, Br. J. Pharmacol. 176 (9) (2019) 1173–1189, https://doi.org/10.1111/bph.14623.
[29] S. Sarkar, et al., Trehalose, a novel mTOR-independent autophagy enhancer, accelerates the clearance of mutant huntingtin and alpha-synuclein, J. Biol. Chem. 282 (8) (2007) 5641–5652.
[30] Q. He, et al., Treatment with Trehalose prevents behavioral and neurochemical deficits produced in an AAV α-Synuclein rat model of Parkinson's disease, Mol. Neurobiol. 53 (4) (2016) 2258–2268.
[32] P.-F. Wei, et al., Accelerating the clearance of mutant huntingtin protein aggregates through autophagy induction by europium hydroxide nanorods, Biomaterials 35 (3) (2014) 899–907.
[33] K. Hopp, et al., Functional polycystin-1 dosage governs autosomal dominant polycystic kidney disease severity, J. Clin. Invest. 122 (11) (2012) 4257–4273.
[34] K. Hopp, et al., Tolvaptan plus pasireotide shows enhanced efficacy in a PKD1 model, J. Am. Soc. Nephrol. 26 (1) (2015) 39–47.
[35] E.K. Kleczko, et al., CD8(+) T cells modulate autosomal dominant polycystic kidney disease progression, Kidney Int. 94 (6) (2018) 1127–1140.
[36] L.F. Chou, et al., Effect of trehalose supplementation on autophagy and cystogenesis in a mouse model of polycystic kidney disease, Nutrients 11 (1) (2018).
[37] S. Sarkar, et al., Neuroprotective effect of the chemical chaperone, trehalose in a chronic MPTP-induced Parkinson's disease mouse model, NeuroToxicology 44 (2014) 250–262.
[38] A. Akcay, et al., IL-33 exacerbates acute kidney injury, J. Am. Soc. Nephrol. 22 (11) (2011) 2057–2067.
[39] K. Hopp, et al., Effects of hydration in rats and mice with polycystic kidney disease, Am. J. Physiol. Ren. Physiol. 308 (3) (2015) F261–F266.
[40] X. Ao, L. Zou, Y. Wu, Regulation of autophagy by the Rab GTPase network, Cell Death Differ. 21 (3) (2014) 348–358.
[41] N. Mizushima, T. Yoshimori, How to interpret LC3 immunoblotting, Autophagy 3 (6) (2007) 542–545.
[42] T. Lamark, S. Svenning, T. Johansen, Regulation of selective autophagy: the p62/SQSTM1 paradigm, Essays Biochem. 61 (6) (2017) 609.
[43] S.J. Holditch, et al., A study of sirolimus and an mTOR kinase inhibitor (TORKi) in a hypomorphic Pkd1 mouse model of autosomal dominant polycystic kidney disease (ADPKD), Am. J. Physiol. Ren. Physiol. 317 (1) (2019) F187–F196, https://doi.org/10.1152/ajprenal.00051.2019.
[44] A. Poon, et al., ATG5, autophagy and lung function in asthma, Autophagy 8 (4) (2012) 694–695.
[45] J. Hampe, et al., A genome-wide association scan of nonsynonymous SNPs identifies a susceptibility variant for Crohn disease in ATG16L1, Nat. Genet. 39 (2006) 207.
[46] X.H. Liang, et al., Induction of autophagy and inhibition of tumorigenesis by beclin 1, Nature 402 (6762) (1999) 672–676.
[47] M.I. Koukourakis, et al., Beclin 1 over- and underexpression in colorectal cancer: distinct patterns relate to prognosis and tumour hypoxia, Br. J. Cancer 103 (8) (2010) 1209–1214.
[48] X.-J. Zhou, et al., Genetic association of PRDM1-ATG5 intergenic region and autophagy with systemic lupus erythematosus in a Chinese population, Ann. Rheum. Dis. 70 (7) (2011) 1330.
[50] D.C. Rubinsztein, G. Marino, G. Kroemer, Autophagy and aging, Cell 146 (5) (2011) 682–695.
[51] J.K. Chen, et al., Phosphatidylinositol 3-kinase signaling determines kidney size, J. Clin. Invest. 125 (6) (2015) 2429–2444.
[52] M. Palmieri, et al., mTORC1-independent TFEB activation via Akt inhibition promotes cellular clearance in neurodegenerative storage diseases, Nat. Commun. 8 (2017) 14338.
[53] J.A. McCubrey, et al., GSK-3 as potential target for therapeutic intervention in cancer, Oncotarget 5 (10) (2014) 2881–2911.

ARTICLE

Surgical procedures suppress autophagic flux in the kidney

Carolyn N. Brown[1], Daniel Atwood[1], Deepak Pokhrel[1], Sara J. Holditch[1], Christopher Altmann[1], Nataliya I. Skrypnyk[1], Jennifer Bourne[2], Jelena Klawitter[1,3], Judith Blaine[1], Sarah Faubel[1], Andrew Thorburn[4] and Charles L. Edelstein[1]

Abstract

Many surgical models are used to study kidney and other diseases in mice, yet the effects of the surgical procedure itself on the kidney and other tissues have not been elucidated. In the present study, we found that both sham surgery and unilateral nephrectomy (UNX), which is used as a model of renal compensatory hypertrophy, in mice resulted in increased mammalian target of rapamycin complex 1/2 (mTORC1/2) in the remaining kidney. mTORC1 is known to regulate lysosomal biogenesis and autophagy. Genes associated with lysosomal biogenesis and function were decreased in sham surgery and UNX kidneys. In both sham surgery and UNX, there was suppressed autophagic flux in the kidney as indicated by the lack of an increase in LC3-II or autophagosomes seen on immunoblot, IF and EM after bafilomycin A1 administration and a concomitant increase in p62, a marker of autophagic cargo. There was a massive increase in pro-inflammatory cytokines, which are known to activate ERK1/2, in the serum after sham surgery and UNX. There was a large increase in ERK1/2 in sham surgery and UNX kidneys, which was blocked by the MEK1/2 inhibitor, trametinib. Trametinib also resulted in a significant decrease in p62. In summary, there was an intense systemic inflammatory response, an ERK-mediated increase in p62 and suppressed autophagic flux in the kidney after sham surgery and UNX. It is important that researchers are aware that changes in systemic pro-inflammatory cytokines, ERK1/2 and autophagy can be caused by sham surgery as well as the kidney injury/disease itself.

Introduction

Compensatory renal hypertrophy is an important consequence in both glomeruli and tubules following partial or complete UNX performed for renal cancer or for living kidney donors. Excessive compensatory renal hypertrophy can be a maladaptive response that leads to further nephron damage, tubular atrophy, interstitial fibrosis, loss of kidney function and chronic kidney disease[1]. It is well known that pS6, a marker of mTORC1, increases as early as 30 min after UNX and that mTORC1 inhibition with rapamycin can blunt UNX-induced renal hypertrophy[2]. mTOR-mediated phosphorylation of the transcription factor EB (TFEB), a master regulator of lysosomal biogenesis[3], occurs at the lysosomal surface and controls the subcellular localization and activity of TFEB. Thus, the effect of UNX on lysosomal biogenesis and function, which are tightly tied to mTOR function, was determined.

As mTOR and lysosomal function are crucial to autophagy, autophagic flux was determined in vivo in the kidney. LC3-II, a marker of autophagosomes, was measured with and without the lysosomal inhibitor bafilomycin A1 (BafA1). According to the 2016 guidelines for the use and interpretation of assays for monitoring autophagy, if the basal increase in LC3-II is due to increased autophagosome production, then it is expected that lysosomal inhibition will further increase LC3-II (i.e., increased autophagic flux)[4]. Alternatively, if the increase in LC3-II is due to a block in autophagosome-lysosome fusion or a defect in autophagosome degradation by the lysosome, then lysosomal inhibition would not affect LC3-II expression. We measured the increase in LC3-II after lysosomal inhibition and used it to determine the effect of

Correspondence: Charles L. Edelstein (Charles.edelstein@cuanschutz.edu)
[1]Division of Renal Diseases and Hypertension, University of Colorado at Denver, Aurora, CO, USA
[2]Electron Microscopy Center, University of Colorado at Denver, Aurora, CO, USA
Full list of author information is available at the end of the article
Edited by G.M. Fimia

UNX on autophagic flux. The amount of p62/SQSTM1, a marker of autophagic cargo, is another method of determining autophagic flux as p62 can be destroyed by the lysosome much like LC3. In general, an increase in p62 indicates suppressed autophagic flux. p62 was measured in the kidney as an additional marker of autophagic flux[5]. Here, we demonstrated that there was suppressed flux which was associated with lysosomal abnormalities following both sham surgery and unilateral nephrectomy.

Results

Unilateral nephrectomy and sham surgery-dependent mTOR activation are attenuated by rapamycin

The ratio of pS6$^{Ser240/244}$ to total abundance of S6 protein was significantly increased in the kidney after UNX vs. normal and sham surgery (Fig. 1a), consistent with published studies[6,7]. pAkt^{Ser473}, a marker of mTORC2, was significantly increased after both sham surgery and UNX (Fig. 1a). These data indicated that there was increased mTORC2 activation following both sham surgery and UNX, but increased mTORC1 only after UNX.

Rapamycin resulted in a significant decrease in pS6$^{Ser240/244}$ in the kidney after sham surgery and UNX and blunted the increase in pAkt^{Ser473} (Fig. 1b). While rapamycin is known to be an indirect mTORC1 inhibitor, our results confirm previous studies that rapamycin can also inhibit mTORC2[8].

Increased mTOR after sham surgery and unilateral nephrectomy is associated with a lysosomal defect

mTOR is known to regulate TFEB, a master regulator of lysosomal biogenesis[3,9] Quantitative polymerase chain reaction (qPCR) analysis for *Tfeb* and known TFEB-downstream genes *Atp6v0d2*, a vATPase subunit localized to the lysosomal membrane involved in lysosomal acidification[10] and *Lamp2*[11], a lysosomal-associated membrane protein, was performed. There were decreased *Tfeb*, *Atp6v0d2*, and *Lamp2* transcripts in sham surgery and UNX vs. normal kidneys (Fig. 2a). On immunofluorescence of tubular cells in the kidney cortex, there was less nuclear localization of TFEB after sham surgery and UNX vs. normal kidneys (Fig. 2b). Transcription of *Tfeb*-downstream genes and TFEB nuclear localization were not rescued by rapamycin (Fig. 2a, b), indicating that
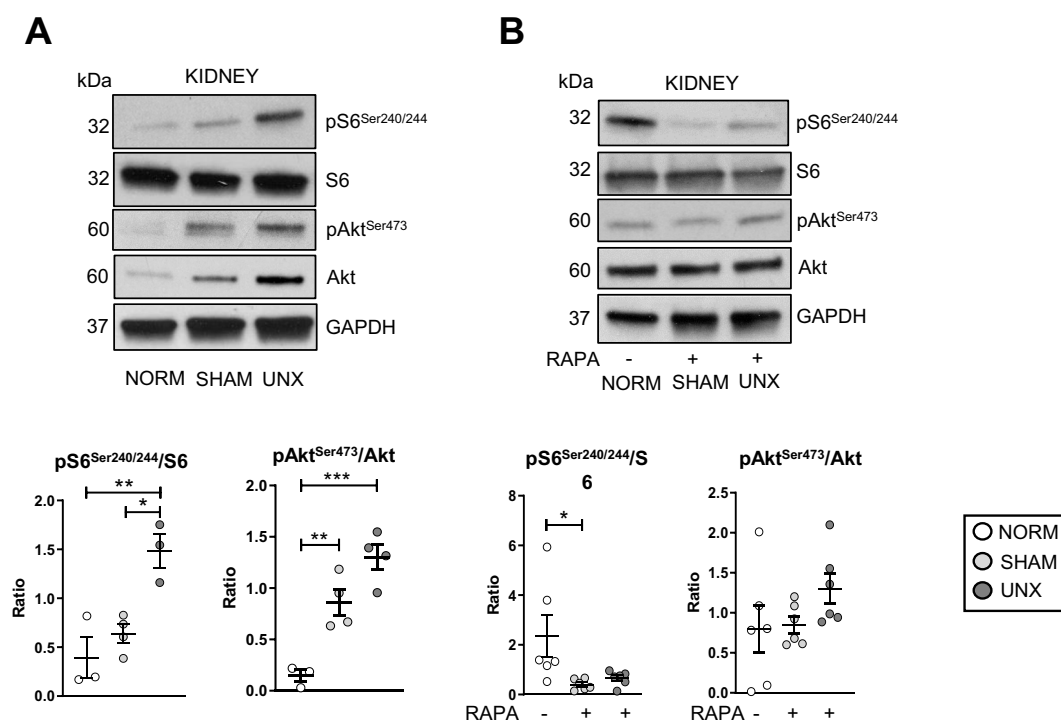

Fig. 1 Increased mTORC1 (pS6Ser240/244) after UNX and mTORC2 (pAktSer473) after sham surgery and UNX in the kidney is attenuated by rapamycin. Mice underwent either no surgical manipulations (NORM), sham surgery (SHAM), or unilateral nephrectomy (UNX) and after 2 h the contralateral kidney was harvested. **A** Representative immunoblots and relative densitometry is shown for mTORC1 (pS6$^{Ser240/244}$) and mTORC2 (pAkt^{Ser473}) substrates in the kidney. *$P < 0.05$, **$P < 0.01$, ***$P < 0.001$. RDU = relative densitometry units corrected for GAPDH. **B** Representative immunoblots and relative densitometry is shown for mTORC1 (pS6) and mTORC2 (pAkt^{Ser473}) substrates in the kidney after treatment of mice with rapamycin (RAPA). *$P < 0.05$, **$P < 0.01$. RDU = relative densitometry units.
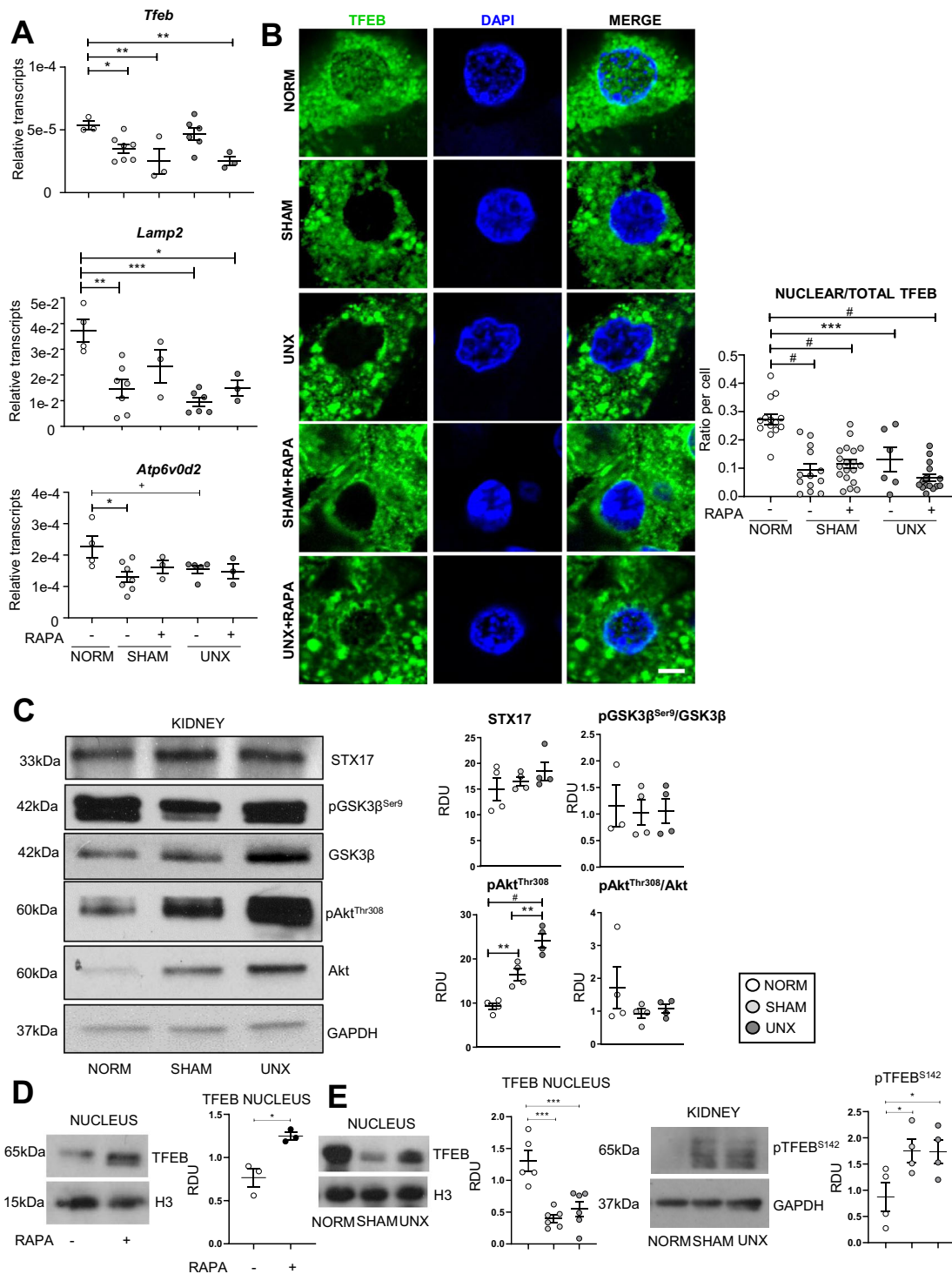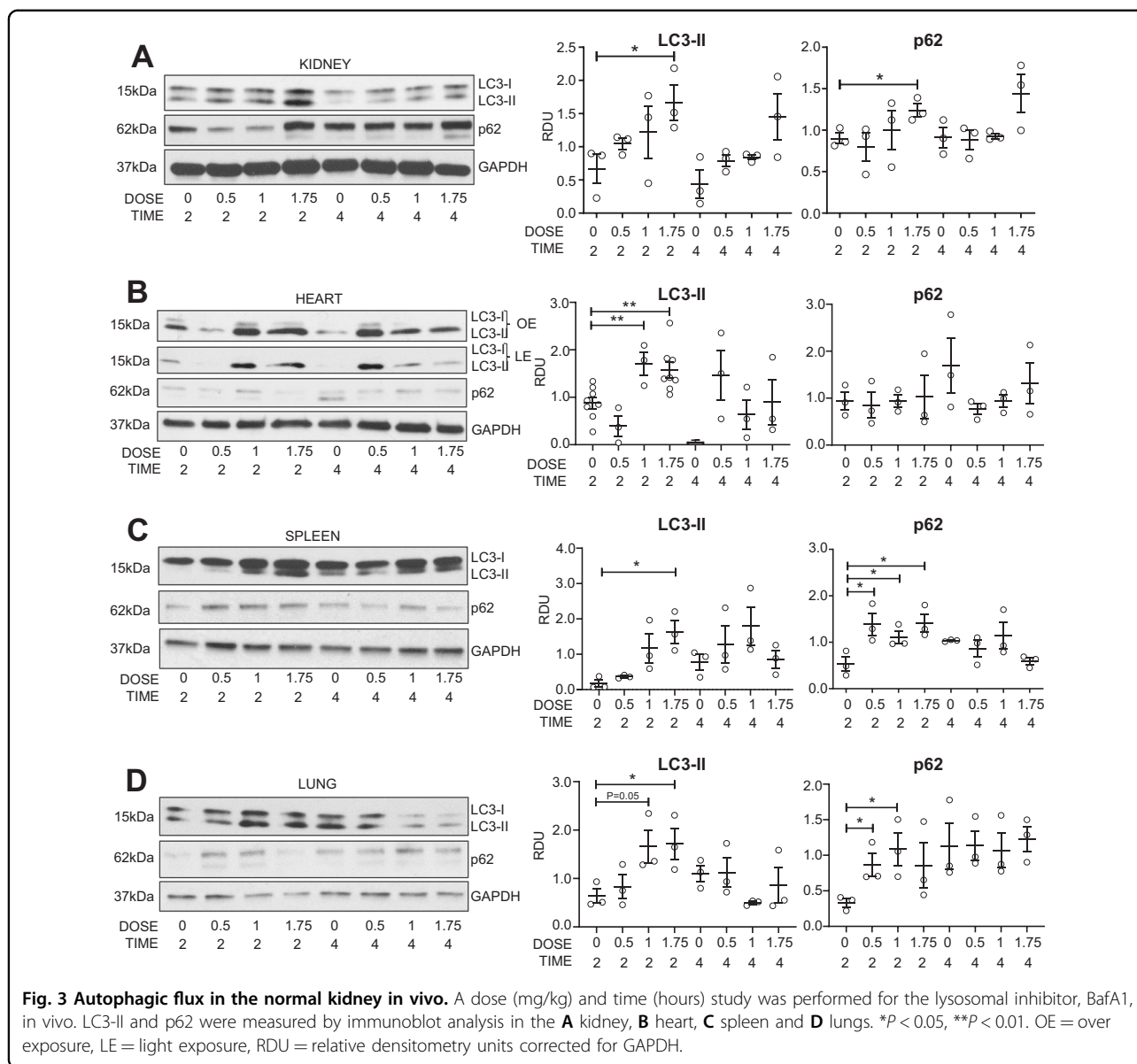
Fig. 2 Sham surgery and unilateral nephrectomy are associated with a lysosomal defect. Mice underwent either no surgical manipulations (NORM), sham surgery (SHAM), or unilateral nephrectomy (UNX) and after 2 h the contralateral kidney was harvested. **A** qPCR analysis of TFEB-downstream genes *Tfeb*, *Atp6v0d2*, and *Lamp2*. **B** Representative proximal tubular cell images of TFEB nuclear versus cytoplasmic localization with quantification showing readings in duplicate for each mouse (Scale bar = 5 μm). **C** Immunoblot analysis for STX17, pGSK3β[Ser9], GSK3β, pAkt[Ser308] and Akt. **D** Immunoblot analysis for TFEB in nuclear extracts from rapamycin -treated (RAPA) mice. **E** Immunoblot analysis for TFEB in nuclear extracts from NORM, SHAM and UNX mice. **F** Immunoblot analysis for pTFEB[S142] in whole kidney extracts from NORM, SHAM and UNX mice. Quantification is corrected for GAPDH unless otherwise indicated. [+]$P = 0.07$, *$P < 0.05$, **$P < 0.01$, ***$P < 0.001$, [#]$P < 0.0001$. RDU = relative densitometry units corrected for GAPDH. H3 = Histone H3.

Fig. 3 Autophagic flux in the normal kidney in vivo. A dose (mg/kg) and time (hours) study was performed for the lysosomal inhibitor, BafA1, in vivo. LC3-II and p62 were measured by immunoblot analysis in the **A** kidney, **B** heart, **C** spleen and **D** lungs. *$P < 0.05$, **$P < 0.01$. OE = over exposure, LE = light exposure, RDU = relative densitometry units corrected for GAPDH.

there may be additional mTOR-independent regulation of TFEB. p-Akt[Thr308], that represses TFEB nuclear translocation independently of mTOR[12], was increased in sham surgery and UNX (Fig. 2c). However, total Akt was also increased and when p-Akt[Thr308] was corrected for total Akt, the increase was not significant (Fig. 2c). Syntaxin 17 (STX17), a vesicle docking protein essential for complete autophagosome-lysosome fusion[13], and phosphorylated glycogen synthase kinase 3 beta (p-GSK3β), that activates a nuclear export signal for TFEB[14], were not different between groups (Fig. 2c). TFEB regulates the expression of genes that encode autophagy-related proteins (Atg)[4]. The autophagy-related proteins, Atg3 and Atg7 play an important role in the LC3 lipidation process that is essential for autophagosome formation[4] Atg3 was

increased in sham surgery and UNX and Atg7 did not change in sham surgery and UNX (Supplementary Fig. S1) suggesting that the decrease in TFEB in the nucleus in sham surgery and UNX did not decrease the expression of Atg7 and 3.

TFEB was measured by immunoblot analysis in nuclear and cytoplasmic fractions of whole kidney from vehicle and rapamycin-treated mice and normal, sham surgery and UNX mice. mTOR inhibition is known to result in a translocation of TFEB to the nucleus[15]. As a positive control, we determined that there was an increase in TFEB in the nucleus in mice treated with rapamycin 10 mg/kg/day via I.P. injection for five days compared to vehicle (Fig. 2d). In agreement with the IF data, there was a decrease in TFEB in the nuclear fraction in sham

surgery and UNX compared to normal (Fig. 2e). On immunoblot analysis, there was no difference in TFEB in the cytoplasmic fractions between the normal, sham and UNX groups (data not shown). TFEB is phosphorylated by mTOR on S142 and S211 serine residues, which play a crucial role in determining TFEB subcellular localization[16]. When these serines are phosphorylated, TFEB is mainly cytosolic and inactive[16]. In whole kidney extracts, there was an increase in pTFEB[S142] in sham surgery and UNX compared to normal controls (Fig. 2f) which is compatible with the cytosolic localization of TFEB with sham surgery and UNX.

Autophagic flux in the normal kidney in vivo

mTOR and lysosomal function that are crucial to autophagy, were affected by sham surgery and UNX. Thus, we hypothesized that sham surgery and UNX would suppress autophagic flux. To determine the optimal BafA1 dose and timing to use in vivo, mice were injected with increasing doses of BafA1. There was a significant increase in LC3-II and increase in p62 in the normal kidney after 2 h of treatment with 1.75 mg/kg BafA1 (Fig. 3a). Administration of 1.75mg/kg BafA1 also resulted in significantly increased LC3-II in the heart, spleen and lung (Fig. 3b–d). LC3-II was corrected for GAPDH. It has been recommended that the amount of LC3-II be compared to actin or GAPDH and not to LC3-I and that conclusions about autophagosome maturation not be made by comparing the amount of LC3-II to LC3-I[4]. The reason is that LC3-I is technically less sensitive to detection by antibodies that also detect LC3-II, LC3-I is labile and more sensitive to freeze-thawing and degradation in SDS buffer and the amount of LC3-I is cell and stress specific. Next, autophagic flux was measured in the kidney and heart after sham surgery and UNX.

Autophagic flux is suppressed in the kidney after sham surgery and UNX

Autophagic flux was measured in the kidney using the method described above (2 h of treatment with 1.75 mg/kg BafA1). Mice underwent either no surgery, sham surgery, or UNX, received either BafA1 or vehicle, and were sacrificed after 2 h (Fig. 4a). LC3-II did not increase with BafA1 after either sham surgery or UNX and p62 was increased in the kidney after sham surgery and UNX vs. normal mice (Fig. 4b). To test if sham surgery affects autophagic flux using independent methods and to determine the localization of autophagooosomes in the kidney, IF and EM analysis for autophagosomes were performed and indicated changes in renal tubules. p62 was significantly increased after both sham surgery and UNX vs. normals on IF analysis (Fig. 4c). As the addition of phosphatidylethanolamine to LC3-I (i.e., LC3-II) cannot be differentiated by molecular weight on IF analysis,

punctate LC3B was used as a measure of autophagosomes. LC3B puncta increased after BafA1 in normal kidneys (Fig. 4c). Significantly increased basal LC3B puncta were detected in both sham surgery and UNX vs. normal and were not further increased by BafA1 on IF analysis (Fig. 4c). There was a significant decrease in LAMP2 after both sham surgery and UNX (Fig. 4c). On EM analysis there was a decrease in the number of lysosomes after both sham surgery and UNX (Supplementary Fig. S2). Co-localization of LAMP2 and LC3B was increased after sham surgery and further increased after UNX similar to what was observed after BafA1 administration (Fig. 4c). These data indicate an increased number of autolysosomes that were unable to break down the autophagosomal cargo and membrane (i.e., LC3-II and p62) suggesting that autophagosome formation was not compromised and that surgery blocks autophagy by causing a defect in the later stages of autophagy[17,18]. EM analysis revealed significantly increased autophagosomes after BafA1 in normal mice (Fig. 4d). There was an increase in basal autophagosomes in both sham surgery and UNX compared to normal, but BafA1 did not induce further increase autophagosomes. These results, which were obtained from 3 independent techniques, indicate that autophagy in renal tubules was suppressed after sham surgery and UNX in the kidney. Further, rapamycin, which did not rescue lysosomal defects (Fig. 2), did not restore autophagic flux in the kidney after sham surgery or UNX (Supplementary Fig. S3).

Metabolomics analysis

Lysosomal defects are known to have effects on availability of amino acids and other metabolites[19]. Thus, metabolomics analysis was performed to determine whether the lysosomal defect and suppressed flux were associated with an altered renal metabolome. Metabolomics analysis was performed on the kidney taken 2 h after sham surgery or UNX (Supplementary Fig. S4A–C). Interestingly, although lysosomal deficiency was similar in both sham surgery and UNX, only fructose phosphate, glycine, and folate (Supplementary Fig. S5A) were affected similarly after sham surgery and UNX. There is little known about the effects of fructose phosphate, glycine, and folate on autophagy[20–22] Most of the metabolites measured were differentially effected by either sham surgery or UNX (Supplementary Fig. S5B–F) or were unchanged by sham surgery or UNX (Supplementary Fig. S6).

Autophagic flux is suppressed in the heart after UNX

The surgical procedure has been shown to affect monocyte subset kinetics in a murine model of myocardial infarction[23] Thus, we determined whether the effects seen following sham surgery and UNX were unique to the kidney or involved the heart as well. BafA1
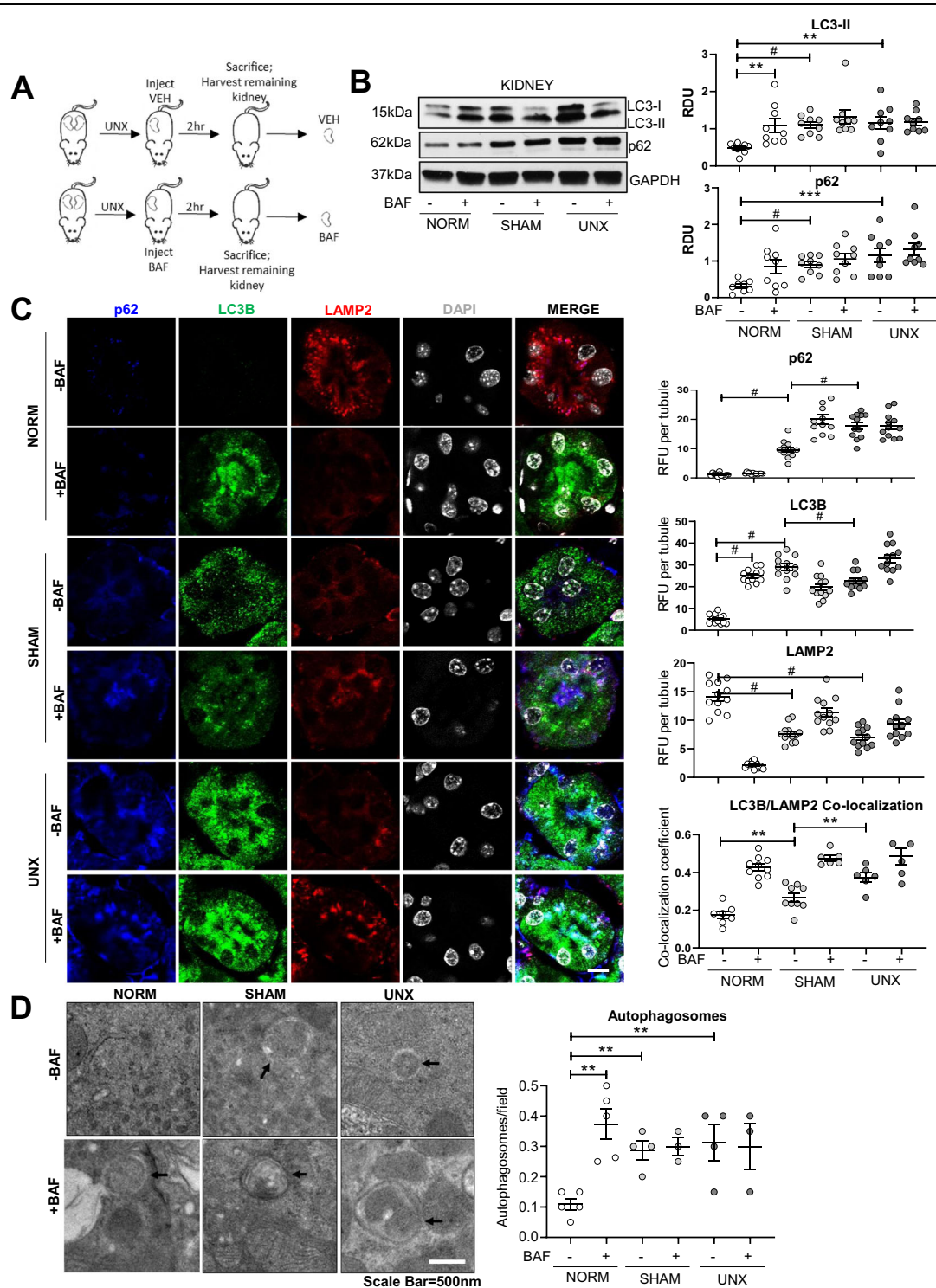
Fig. 4 Suppressed autophagic flux after sham surgery and UNX in the kidney. A Mice underwent either no surgical manipulations (NORM), sham surgery (SHAM), or unilateral nephrectomy (UNX). Each mouse was treated with either vehicle (VEH) or BafA1 (BAF) and after 2 h the contralateral kidney was harvested. **B** Immunoblot analysis of LC3-II and p62 in the kidney with representative densitometry is demonstrated ($n = 9$ per group). Immunoblots were corrected for the endogenous control, GAPDH. RDU = relative densitometry units corrected for GAPDH. **C** Immunofluorescence analysis of punctate LC3B, LAMP2, and p62 per tubule in the kidney with quantification showing readings in duplicate for each mouse. RFU = relative fluorescence units. **D** Transmission electron microscopy for autophagosomes with quantification is demonstrated (arrows=autophagosome). Autophagosomes are quantified per 10 μm^2 field. Scale Bar = 500 nm. **$P < 0.01$, ***$P < 0.001$, #$P < 0.0001$.

resulted in a significant increase in LC3-II in normal hearts (Fig. 3b). There were no significant changes in activation of mTORC1 (pS6 Ser240/244) or mTORC2 activation (pAktSer473) in the heart after sham surgery or UNX (Supplementary Fig. S7A). Unexpectedly, flux (the increase in LC3-II with BafA1) in heart was completely suppressed after UNX, but not sham surgery (Supplementary Fig. S7C). Although rapamycin inhibited mTORC1/2 in the heart (Supplementary Fig. S7B), it did not rescue autophagic flux after UNX (Supplementary Fig. S7D).

Both the sham surgery and bilateral renal ischemia/reperfusion suppressed autophagic flux in the heart

To determine whether other surgical procedures affect autophagic flux, a bilateral renal ischemia/reperfusion (I/R) model of AKI was performed. Mice underwent either no surgery, sham surgery, or I/R for 24 or 72 h. At 24 h after I/R there was a lack of increase in LC3-II with BafA1 suggestive of decreased autophagic flux (Fig. 5a). However, sham I/R surgery in the kidney resulted in an increase in LC3-II with bafilomycin and a decrease in p62 at 24 h suggesting that sham I/R surgery does not suppress autophagic flux (Fig. 5a). Interestingly, in the heart, both sham I/R surgery and I/R at 24 h resulted in suppressed autophagic flux as evidenced by the lack of increase in LC3-II with bafilomycin and an increase in p62 (Fig. 5b). At 72 h after both sham surgery and I/R, autophagic flux normalized in kidney and heart (Fig. 5a, b). These data suggest that sham surgery for renal I/R had different effects on autophagic flux in kidney compared to heart and consistently normalized by 72 h after the procedure.

Pro-inflammatory cytokine "storm" in the serum after sham surgery and UNX

As sham surgery and UNX resulted in changes in autophagy in the kidney and heart, we reasoned that a factor in the serum might be causing these effects. Sham surgical procedures have been shown to cause an inflammatory response[24,23] and production/release of pro-inflammatory cytokines, which are known to affect autophagy[25]. Thus, a panel of pro-inflammatory cytokines was measured in the serum. Mice underwent either no surgery, sham surgery, or UNX and were sacrificed after 2 h. There were massive increases in the serum in IL-1β (up to 50-fold), IL-2, IL-4, IL-6 (up to 100-fold), CXCL1 (also known as IL-8 in humans and KC in mice), IL-12, GM-CSF, IFN-γ in sham surgery and UNX compared to no surgery (Fig. 6a).

To determine whether the pro-inflammatory cytokine "storm" measured in the serum in sham surgery and UNX had an effect on autophagic flux, renal cortical tubular epithelium (RCTE) cells were treated with normal medium or medium containing 10% serum from normal mice, sham surgery or UNX mice. RCTE cells treated with normal medium had a large increase in LC3-II with chloroquine indicating autophagic flux (Fig. 6b). RCTE cells treated with medium containing 10% serum from normal, sham surgery or UNX mice also had a large increase in LC3-II with chloroquin (Fig. 6c). RCTE cells treated with medium containing 10% serum from normal, sham surgery or UNX mice had no change in p62 (Fig. 6c). These data indicate that pro-inflammatory cytokine-rich serum from mice that had sham surgery or UNX did not suppress autophagic flux in RCTE cells.

ERK1/2 inhibition attenuated the increase in p62 seen after sham surgery and unilateral nephrectomy

Pro-inflammatory cytokines have been shown to upregulate pERK1/2[26,27] which can in turn regulate the nuclear localization and activity of TFEB[9] and autophagy[28]. pERK1/2 was significantly increased in sham surgery and UNX vs. normal kidneys (Fig. 7a). Mice were treated with the MEK1/2 inhibitor, Trametinib (1 mg/kg/d IP) that is also a potent ERK1/2 inhibitor, for 3 days and then sham surgery or UNX was performed. Trametinib resulted in a near disappearance of pERK1/2 in sham surgery and UNX kidneys (Fig. 7b). Trametinib resulted in a significant decrease in p62 in sham surgery and UNX kidneys compared to normal kidneys, but did not change the suppressed autophagic flux that was seen in sham surgery and UNX kidneys (Fig. 7c).

Discussion

The major findings of this study are: (1) Increased mTORC1/2 signaling associated with TFEB and lysosomal abnormalities and suppressed autophagic flux in the kidney after both sham surgery and UNX, (2) Large increases in pro-inflammatory cytokines in the serum, and pERK1/2 and p62 in the kidney after sham surgery and UNX. The MEK1/2 inhibitor, trametinib, that also potently inhibits ERK, resulted in decreased p62 in the kidney after sham surgery and UNX. (3) Both sham surgery and renal I/R suppressed autophagic flux in the kidney and heart.

Based on the known role of mTORC1 in compensatory renal hypertrophy[2,7] our data showing increased mTORC1/2 after sham surgery and UNX, and the known role of mTOR in lysosomal biogenesis[3], the effect of UNX on TFEB and lysosomal function was determined. In general, lysosomal defects are characterized by decreased lysosomal biogenesis or impaired lysosomal function (i.e., pH, activity of lysosomal enzymes). LAMP2, a marker of lysosomes, was decreased in both sham surgery and UNX, suggesting decreased lysosomal biogenesis. On qPCR analysis *Lamp2* mRNA was also found to be decreased, suggesting regulation at the
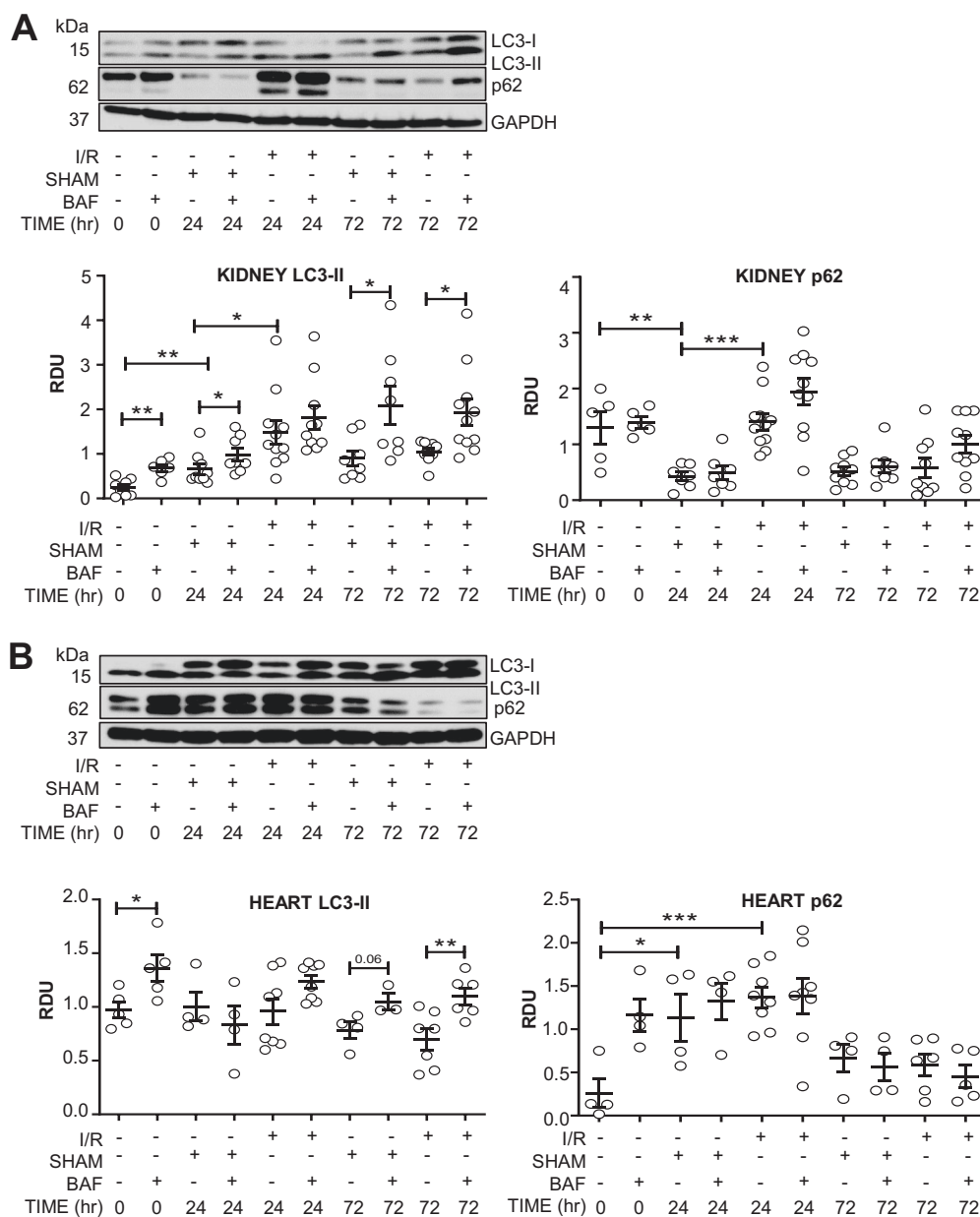
Fig. 5 Both sham surgery and bilateral renal ischemia/reperfusion (24 h) suppressed autophagic flux in the kidney and heart. Autophagic flux normalizes at 72 h. Mice underwent either no surgical manipulations, sham surgery (SHAM), or bilateral renal ischemia/reperfusion (I/R). After 24 h or 72 h, each mouse was treated with either vehicle or BafA1 (BAF) and after 26 h or 74 h of reperfusion, the contralateral kidneys and heart were harvested. Immunoblot analysis of LC3-II and p62 in the kidney (**A**) and the heart (**B**) with representative densitometry is demonstrated. RDU = relative densitometry units corrected for GAPDH. *$P < 0.05$, **$P < 0.01$, ***$P < 0.001$.

transcriptional level. As TFEB is a master regulator of lysosomal biogenesis[9], changes in TFEB were studied. *Tfeb* mRNA in the kidney was decreased after sham and UNX. There was less nuclear localization of TFEB protein, where it induces transcription of target genes, in the kidney after sham surgery and UNX. On nutrient depletion and under abnormal lysosomal storage

conditions TFEB is known to translocate to the nucleus, resulting in the transcription of its target genes such as vesicular ATPases (vATPases) that contribute to lysosomal acidification and function[9]. In this regard, we found mRNA expression of *Atp6v0d2*, a vATPase subunit, to be decreased after sham surgery and UNX. These data suggest that there is a lysosomal defect
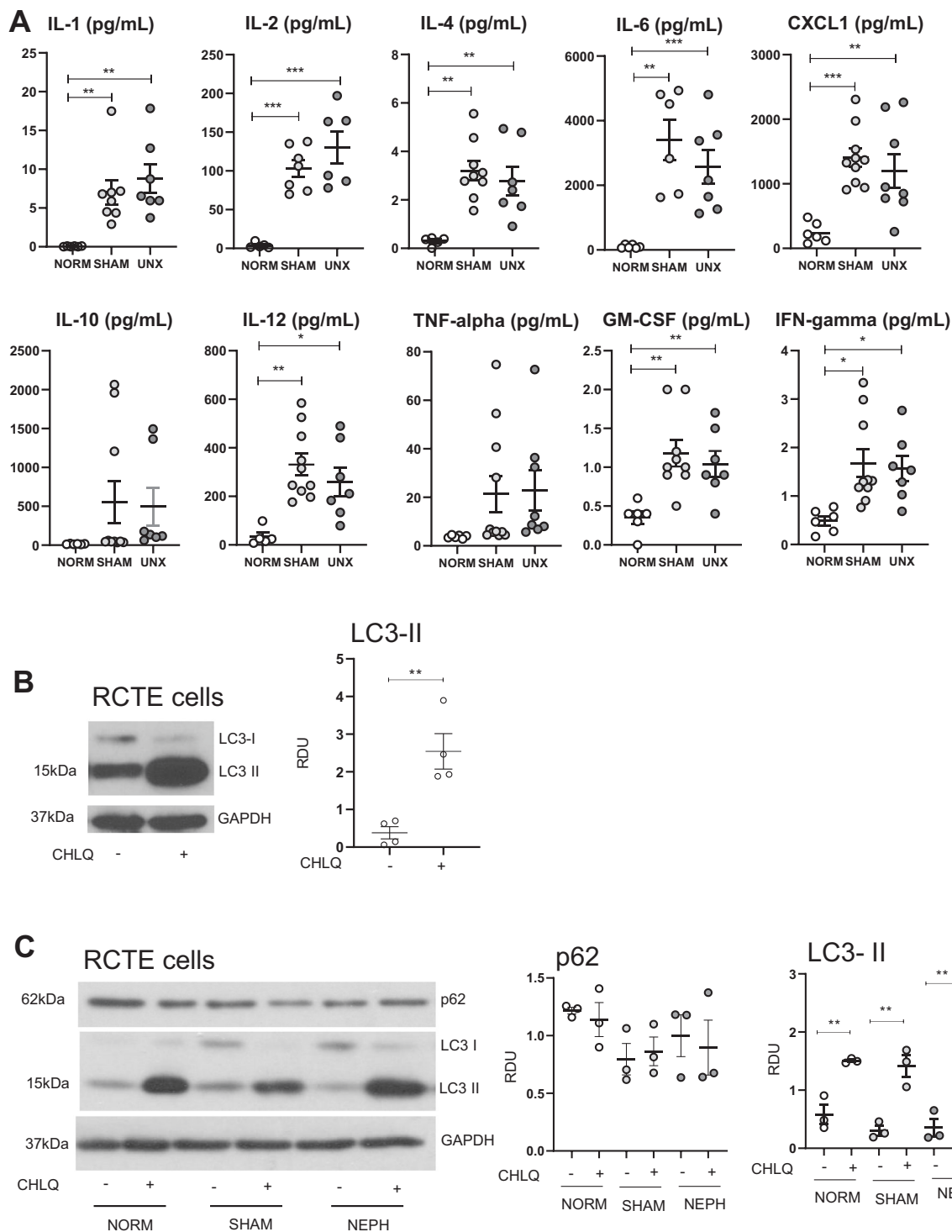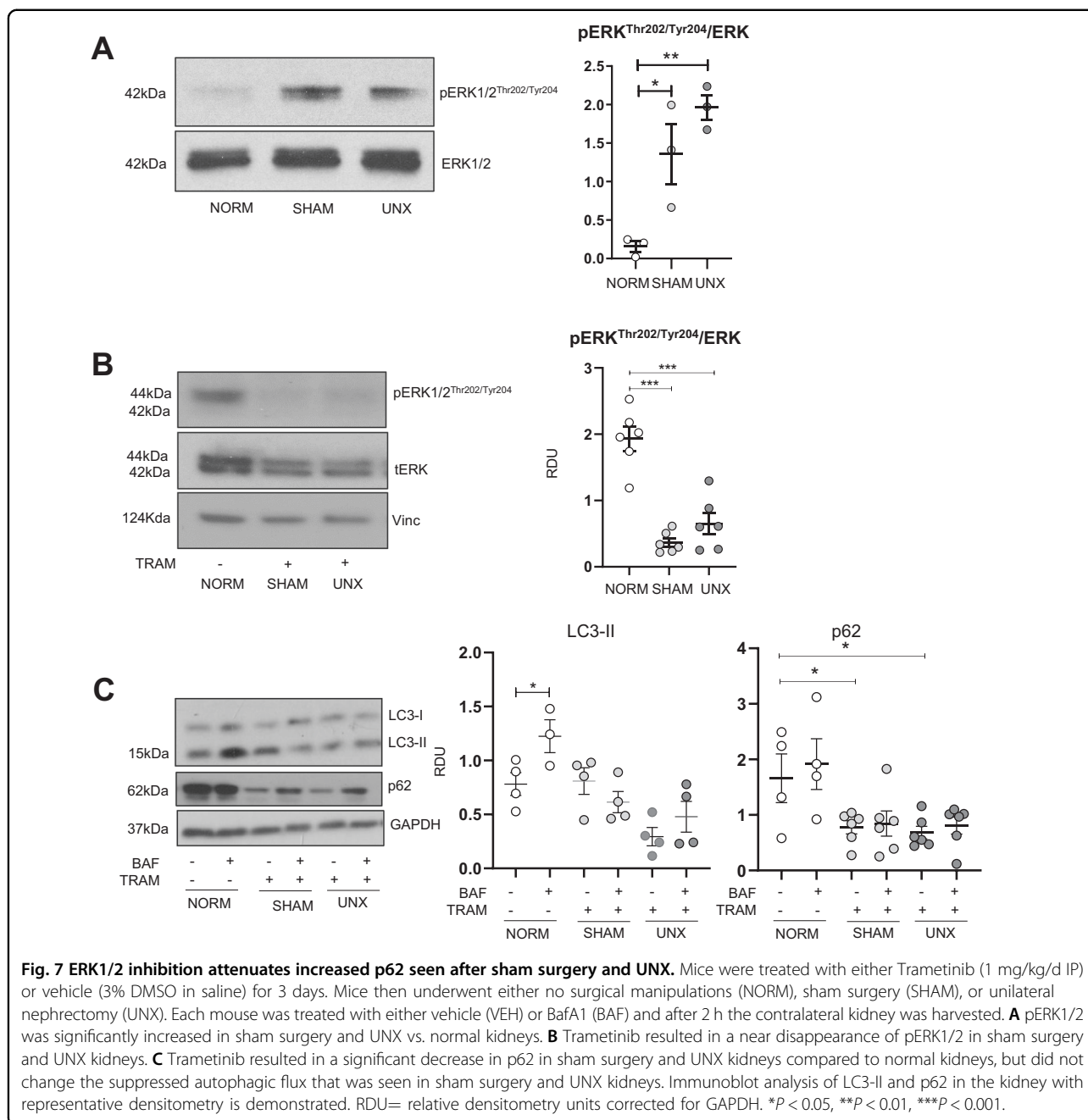
Fig. 6 Pro-inflammatory cytokine "storm" in the serum after sham surgery and UNX. Serum from normal, sham surgery or UNX mice did not suppress autophagic flux in RCTE cells. Mice underwent either no surgery, sham surgery, or UNX and were sacrificed after 2 h. **A** A panel of pro-inflammatory cytokines was measured in the serum: IL-1β, IL-2, IL-4, IL-6, CXCL1 (also known as IL-8 in humans and KC in mice), IL-10, IL-12, GM-CSF, IFN-γ, TNF-α. RCTE cells were treated with **B** normal medium or **C** medium containing 10% serum from normal mice, sham surgery or UNX mice. Immunoblot analysis of LC3-II and p62 in RCTE cells with or without chloroquine (CHLQ) with representative densitometry is demonstrated. Immunoblots were corrected for the endogenous control, GAPDH. *$P < 0.05$, **$P < 0.01$, ***$P < 0.001$.

Fig. 7 ERK1/2 inhibition attenuates increased p62 seen after sham surgery and UNX. Mice were treated with either Trametinib (1 mg/kg/d IP) or vehicle (3% DMSO in saline) for 3 days. Mice then underwent either no surgical manipulations (NORM), sham surgery (SHAM), or unilateral nephrectomy (UNX). Each mouse was treated with either vehicle (VEH) or BafA1 (BAF) and after 2 h the contralateral kidney was harvested. **A** pERK1/2 was significantly increased in sham surgery and UNX vs. normal kidneys. **B** Trametinib resulted in a near disappearance of pERK1/2 in sham surgery and UNX kidneys. **C** Trametinib resulted in a significant decrease in p62 in sham surgery and UNX kidneys compared to normal kidneys, but did not change the suppressed autophagic flux that was seen in sham surgery and UNX kidneys. Immunoblot analysis of LC3-II and p62 in the kidney with representative densitometry is demonstrated. RDU= relative densitometry units corrected for GAPDH. *$P < 0.05$, **$P < 0.01$, ***$P < 0.001$.

(decreased lysosomal biogenesis, decreased lysosomal ATPase) in sham surgery and UNX.

An increase in LC3B/LAMP2 co-localization often indicates an activated autophagy-lysosome pathway. Co-localization of LC3B and LAMP2 was increased after sham surgery and UNX, indicating that there was likely no defect in trafficking. In the context of autophagy, defects in lysosome-autophagosome trafficking and fusion can interfere with autophagic flux. Expression of STX17, which is involved in autophagosome-lysosome fusion, was unchanged, indicating that there was likely no defect in

fusion[13]. These data indicate an increased number of autolysosomes that were unable to break down the autophagosomal cargo and membrane (i.e., LC3-II and p62) suggesting that autophagosome formation or autophagosome-lysosome fusion was not compromised and that surgery blocks autophagy by causing a defect in the later stages of autophagy[17,18].

Next, upstream mechanisms of the lysosomal defect seen after sham surgery and UNX were studied. Transcription of TFEB-downstream genes and TFEB nuclear localization were not rescued by rapamycin, suggesting an

mTORC1/2-independent pathway. pERK1/2, that is known to decrease nuclear localization of TFEB and activity of TFEB[9], was increased in sham surgery and UNX. Akt, has been shown to affect lysosomal biogenesis and function through inhibitory phosphorylation of $TFEB^{Ser466}$[29]. In this regard, there was a large increase in $pAkt^{Ser473}$ (mTORC2-dependent) but not $pAkt^{Thr308}$/ total Akt (mTORC2-independent) after sham surgery and UNX. However, rapamycin that inhibited the increase in mTORC1 ($pS6^{Ser240/244}$) and mTORC2 ($pAkt^{Ser473}$), did not correct the lysosomal abnormalities. GSK3β, that activates a nuclear export signal for TFEB[14], was not significantly affected by sham surgery or UNX. These data indicate that the suppressed flux seen after UNX may be due to mTORC1/2-independent lysosomal dysfunction associated with a large increase in pERK1/2. The idea that signaling in sham surgery and UNX affect TFEB function and induce lysosomal defects led us to determine the effect of sham surgery and UNX on autophagic flux in vivo.

Bafilomycin can initiate autophagosome formation via inhibition of mTORC1 by the Rag signaling molecule[30]. However, in sham surgery mTORC1 (as determined by pS6 immunoblot analysis) was not decreased and in UNX mTORC1 was increased. Excessive exposure time (more than 4 h) of BafA1 can also lead to non-specific effects[4] such as proteasome inhibition[31]. Thus we used BafA1 (1.75 mg/kg) for 2 h that resulted in a significant, consistent, and reproducible increase in LC3-II in kidneys, heart, spleen, and lungs in BafA1-treated mice compared to vehicle-treated mice.
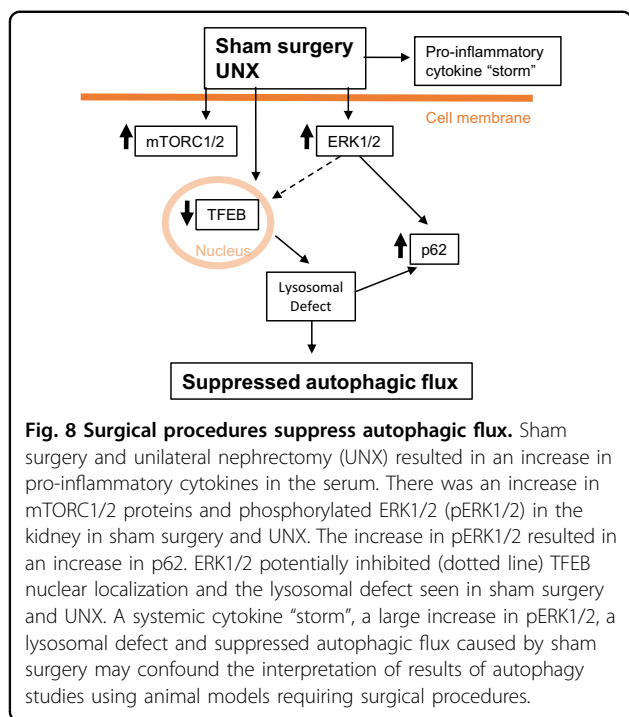
It is known that patients with AKI and patients undergoing surgical procedures especially abdominal surgery have large increases in serum cytokines and that this inflammatory response is associated with liver, lung and heart injury[32,33]. Mouse studies have been performed to better understand how surgical procedures cause a systemic inflammatory response and organ injury. There is a large increase in systemic pro-inflammatory cytokines in a mouse model of ischemic AKI that is associated with histological injury in the lung[24,34] liver[35] and heart[36]. However, the effect of sham surgery on systemic inflammation is less well known. The sham surgical procedure in a mouse model of myocardial infarction can cause a systemic monocyte-induced inflammatory response[23,37] Another study also shows a systemic cytokine response by the surgical procedure to induce mouse myocardial infarction[38]. Our previous study in the same ischemic AKI model used in the present study, demonstrated that 9 cytokines increased as early as 2 h after sham operation compared to baseline[24]. IL-6, but not TNF-α, was increased by sham biliary obstruction surgery or sham partial hepatectomy surgery in mice[39,40] In the present study, we show for the first time that there was a massive increase in pro-inflammatory cytokines in the serum in sham surgery and UNX. It is interesting to speculate whether the inflammatory response caused by sham surgery can cause distant organ injury. In a mouse ischemic AKI model, although there was a systemic inflammatory response caused by sham surgery, the sham surgery did not cause histological lung injury[24]. However, sham surgery for myocardial infarction resulted in a significant change in monocyte subset kinetics in the heart[23]. In future studies, it will be interesting to determine whether sham surgery alone can cause local and distant organ injury.

Pro-inflammatory cytokines have been shown to upregulate pERK1/2[26,27,27] and ERK1/2 can result in an increase in p62[41]. There was a significant increase in p62 in sham surgery and UNX kidneys. p62 functions in both as an autophagy receptor and as a signaling molecule. p62 links cargo proteins with the autophagosome membrane and an increase in p62 is generally indicative of suppressed autophagic flux[35]. The increase in p62 was ERK1/2-dependent as trametinib inhibition of the large increase in pERK1/2 seen in sham surgery and UNX kidneys resulted in a decrease in p62.

There is increased ERK1/2 activation in surgery-induced AKI and inhibition of ERK results in protection against ischemic AKI[42,43] Also in UNX, there is increased ERK1/2 in the remaining kidney[44]. The ERK1/2 pathway is known to regulate autophagy and the effect of ERK1/2 on autophagy is model and stimulus specific[45]. However, the effect of the ERK pathway on autophagy in the context of kidney injury or UNX is not well known. Compatible with our results that increased ERK1/2 in sham surgery and UNX is associated with decreased autophagic flux, it has been shown that increased ERK signaling decreases autophagic flux in pancreatic cancer cells[46]. Also, in ischemic AKI, melatonin resulted in decreased ERK1/2, increased autophagy and functional protection against AKI[47].

The effect of sham surgery and UNX to suppress autophagic flux has not previously been described. This finding is important for researchers performing mouse studies for the following reasons: 1) Suppressed autophagy may account for mouse mortality that is often not reported, 2) Our results exposed a previously under-appreciated impact of sham surgical procedures on lysosomal function, systemic cytokines, pERK1/2, p62 and autophagy. Of importance is that the increase in pro-inflammatory cytokines, pERK1/2 and suppressed autophagic flux caused by sham surgery may have implications for interpreting results of autophagy studies using animal models requiring sham surgery. Thus, caution should be taken with many animal studies where investigators are trying to study effects on autophagy on organ systems, even when the appropriate sham controls are included.

Fig. 8 Surgical procedures suppress autophagic flux. Sham surgery and unilateral nephrectomy (UNX) resulted in an increase in pro-inflammatory cytokines in the serum. There was an increase in mTORC1/2 proteins and phosphorylated ERK1/2 (pERK1/2) in the kidney in sham surgery and UNX. The increase in pERK1/2 resulted in an increase in p62. ERK1/2 potentially inhibited (dotted line) TFEB nuclear localization and the lysosomal defect seen in sham surgery and UNX. A systemic cytokine "storm", a large increase in pERK1/2, a lysosomal defect and suppressed autophagic flux caused by sham surgery may confound the interpretation of results of autophagy studies using animal models requiring surgical procedures.

Suppressed autophagy in the kidney and heart may also explain some of the morbidity seen in patients associated with surgery.

In summary, a method to determine autophagic flux in vivo was developed and demonstrated that surgical procedures suppressed autophagic flux in kidney and heart. There was an increase in serum pro-inflammatory cytokines, and kidney pERK1/2 and p62 after sham surgery and UNX (Fig. 8). Trametinib, a MEK1/2 inhibitor that is also a potent inhibitor of ERK1/2, resulted in a decrease of p62 in sham surgery and UNX kidneys. Description of the effect of sham surgery to suppress autophagy in the kidney and heart is novel. A large increase in pERK1/2, a systemic cytokine "storm and suppressed autophagic flux caused by sham surgery may confound the interpretation of results of autophagy studies using animal models requiring surgical procedures (Fig. 8).

Methods
Drug dosing
5 mg of BafA1 (Cayman Chemical #11038) was dissolved in 1 mL DMSO and diluted to 1 mg/mL in PEG300. Rapamycin was prepared in 28% DMSO in PEG300 and injected IP at 0.5 mg/kg immediately before surgery.

Animals
Wild type male C57BL/6J mice (#000664) at 10 weeks of age were purchased from Jackson Laboratories (Bar Harbor, ME, USA). Mice were randomized to receive either BafA1 or vehicle.

UNX and sham surgery
A laparotomy was performed under isoflurane anesthesia. A silk suture was tied around renal artery/vein and ureter and the kidney was removed, followed by suturing of the muscle and skin. For sham surgery, the same procedure and anesthesia was used in a separate mouse; after maneuvering the kidney out of the body, the kidney was gently caressed with two cotton swabs for 2 min and returned to peritoneum. Normal control animals that did not have any surgical procedure received the same method of sacrifice as the UNX and sham surgery animals: isoflurane overdose followed by cervical dislocation. It was determined that 13 min of 1 liter per minute (LPM) oxygen and 2 LPM isoflurane anesthesia, which were used in the UNX and sham surgery animals, had no effect on autophagic flux (Supplementary Fig. S8A).

Isolation of nuclear and cytosolic fractions
Nuclear and cytoplasmic fractions of whole kidney from vehicle and rapamycin-treated mice and normal, sham surgery and UNX mice were obtained using the NE-PER™ nuclear and cytoplasmic extraction kit (78833) by Thermo-Fisher (Waltham, MA, USA) following manufacturer's instructions.

Bilateral renal ischemia/reperfusion (I/R) surgery
Bilateral renal pedicle clamping for 29 min was performed as previously described[48]. Sham surgery consisted of the same procedure except that clamps were not applied. Normal control animals that did not receive any surgical procedure received the same method of sacrifice as the I/R and sham surgery animals: isoflurane overdose followed by cervical dislocation. It was determined that ketamine/xylazine, which was used in the bilateral ischemia reperfusion and sham surgery animals, had no effect on autophagic flux (Supplementary Fig. S8B).

Immunoblot analysis
Immunoblots were performed as previously described[49]. Briefly, one piece of tissue was immersed in 750 µl tissue lysis buffer (1× RIPA, 1× protease inhibitor, 1× PMSF) and homogenized. Homogenate was centrifuged at 4 °C for 25 min at 15,000 r.p.m. and supernatant was taken for protein quantification by BioRad DC Protein Assay (Hercules, CA, USA). Samples were mixed with Laemmli Sample Buffer and boiled for 5 min. Samples were run on 4–15% gradient precast polyacrylamide gels. Proteins were then transferred to 0.45µm PVDF membranes, blocked with 2.5% evaporated milk, and probed with antibodies listed in Supplementary Table 1. Blots were developed by chemiluminescence and analyzed for

densitometry using ImageJ. 20 μg of protein was loaded in each lane. Serial dilutions of the proteins were loaded to verify that 20 μg was in the linear range for quantitative Western blot detection.

Immunofluorescence

Fixation of tissue, preparation of slides and immuno-fluorescence was performed as we have previously described[50]. Negative controls (secondary antibody only) were tested for each fluorophore used. Slides were imaged using an Olympus FV1000 confocal laser scanning microscope with a 100× oil objective. Images were taken of cortical tubular regions. Co-localization analysis was performed using Olympus FluoView software. Ratio of nuclear-localized protein was calculated by dividing the nuclear fluorescence intensity by the total fluorescence intensity of the same cell.

qPCR analysis

RNA was isolated from kidney tissue using the Qiagen RNeasy kit as described by the manufacturer. cDNA was synthesized using Takara Bio RNA to cDNA kit as described by the manufacturer. 100ng of cDNA was used per reaction with BioRad SYBR green mix and primers as listed in Supplementary Table S2. Ultrapure DNase-/RNase-free water was used as a no template control (NTC). Expression of each gene was corrected for expression of β-actin.

Transmission electron microscopy

Fixation of tissue, processing and sectioning and analysis was performed as described[51]. Sections were imaged on a FEI Tecnai G2 transmission electron microscope (Hillsboro, OR) with an AMT digital camera (Woburn, MA). At least 20 images of proximal renal tubules, where a brush border was clearly seen, were taken per sample. Images were quantified by multiple, independent, blinded observers. Exclusion/inclusion criteria for autophago-somes have been adapted from several sources and are described in Supplementary Table S3.

Metabolomics

Kidney tissue samples were extracted according to a protocol by Yuan et al[52] and analyzed using high-performance liquid chromatography-mass spectrometry (HPLC-MS). After homogenization in 80% methanol solution (volume/volume), samples were incubated for 6–8 h at −80 °C to allow for protein precipitation. Following repeated extraction, samples were centrifuged again and dried in a SpeedVac concentrator (Savant, ThermoFisher, Waltham, MA). Samples were recon-stituted with 20 μl of water/methanol (80:20, volume/volume) and were analyzed using high-performance liquid chromatography-mass spectrometry (HPLC-MS). Sample analysis was performed using an Agilent 1200 series

HPLC system (Agilent Technologies, Palo Alto, CA) interfaced with an ABSciex 5500 hybrid triple quadru-pole/linear ion trap mass spectrometer (Concord, ON, Canada) equipped with an electrospray ionization source operating in the positive/ negative switch mode. Once the data were acquired, MultiQuant (v2.1.1., ABSciex) soft-ware was used for data analysis of 216 unique metabolites. Metabolite peaks were normalized by tissue weight and total area integral of each sample prior to performance of statistical analyses. Analysis of metabolomics data was performed using MetaboAnalyst (metaboanalyst.ca). The Q1 (precursor ion) and Q3 (fragment ion) transitions, the metabolite names, dwell times and the appropriate colli-sion energies for both positive and negative ion modes were adapted from Yuan et al. with several metabolite transitions added by our group. Q1 and Q3 transitions were set to unit resolution for optimal metabolite ion isolation and selectivity. In addition, the polarity switching (settling) time was set to 50 ms. In 1.42 s using a 3-ms dwell time, we were able to obtain 6–14 scans per metabolite peak. Eight μL of sample was injected onto an Amide XBridge HPLC column (3.5 μm; 4.6 mm inner diameter [i.d.] × 100 mm length) (Waters, Milford, MA). The mobile phases consisted of HPLC buffer A (pH = 9.0: 95% (vol/vol) water, 5% (vol/vol) acetonitrile, 20 mM ammonium hydroxide, 20 mM ammonium acetate) and HPLC buffer B: 100% acetonitrile. The HPLC settings were as follows: from 0 to 3 min, the mobile phase was kept at 85% B; from 3 to 22 min, the percentage of solvent B was decreased from 85% to 2% and was kept at 2% for additional 3 min. At minute 26, solvent B was increased again back to 85% and the column flushed for additional 7 min at 85% solvent B.

Measurement of cytokines

A multiplex sandwich immunoassay was used to measure ten inflammatory cytokines (Meso Scale Discovery, MULTI-SPOT Assay System, V-plex Proinflammatory Panel-1 for mice, Catalog no: K15048D-1, Rockville, MD, USA).

In vitro cell experiments

Human primary cells from the normal renal cortical tubular epithelium (RCTE), immortalized with ori-adeno-simian virus 40, were used, as previously described[53]. Briefly, cells were plated 18 h in advance. Once plates had reached 80% confluence, the medium was changed to one of the following: (1) normal medium, (2) medium con-taining 10% serum from normal mice, (3) medium con-taining 10% serum from sham surgery mice, (4) medium containing serum from UNX mice. Cells were then exposed to chloroquine 100 nm or vehicle for measure-ment of autophagic flux as described[54]. After 2 h, protein was isolated from cell lysates and immunoblotted for LC3-II and p62.

Statistical analysis

The sample size was chosen based on our previous experience with similar mouse models and experimental design. All graphs and statistical analyses were managed using GraphPad Prism Software. The Students *t*-test was used to achieve statistical significance between two groups. Multiple group comparisons were performed using one-sided analysis of variance (ANOVA) with posttest according to Tukey. A *P* value of <0.05 was considered statistically significant. Values were expressed as scatter dot plots with each dot representing a separate animal with lines at means and SEM. In all analyses, SEMs were not significantly different between groups. The investigator was blinded to the group allocation when assessing the outcome.

Author details
¹Division of Renal Diseases and Hypertension, University of Colorado at Denver, Aurora, CO, USA. ²Electron Microscopy Center, University of Colorado at Denver, Aurora, CO, USA. ³Department of Anesthesiology, University of Colorado at Denver, Aurora, CO, USA. ⁴Department of Pharmacology, University of Colorado at Denver, Aurora, CO, USA

Author contributions
C.B., D.A., D.P., S.H., A.T., and C.E. performed study concept and design; C.B, D.A., D.P., S.F., A.T., C.E., performed development of methodology and writing, review and revision of the paper; C.B, D.A., D.P., S.H., C.A., N.S., J.B., J.K., J.B., S.F., A.T., and C.E., provided acquisition, analysis and interpretation of data, and statistical analysis; All authors read and approved the final paper.

Ethics approval
No human tissues or samples were used. All experiments were conducted with adherence to the National Institutes of Health Guide for the Care and Use of Laboratory Animals. The animal protocol was approved by the Animal Care and Use Committee of the University of Colorado at Denver.

Conflict of interest
The authors declare no competing interests.

References
1. Fong, D., Denton, K. M., Moritz, K. M., Evans, R. & Singh, R. R. Compensatory responses to nephron deficiency: adaptive or maladaptive? *Nephrology* **19**, 119–128 (2014).
2. Chen, J. K., Chen, J., Neilson, E. G. & Harris, R. C. Role of mammalian target of rapamycin signaling in compensatory renal hypertrophy. *J. Am. Soc. Nephrol.* **16**, 1384–1391 (2005).
3. Napolitano, G. & Ballabio, A. TFEB at a glance. *J. Cell Sci.* **129**, 2475–2481 (2016).
4. Klionsky, D. J. et al. Guidelines for the use and interpretation of assays for monitoring autophagy (3rd edition). *Autophagy* **12**, 1–222 (2016).
5. Rusten, T. E. & Stenmark, H. p62, an autophagy hero or culprit? *Nat. Cell Biol.* **12**, 207–209 (2010).
6. Chen, J. K., Chen, J., Thomas, G., Kozma, S. C. & Harris, R. C. S6 kinase 1 knockout inhibits uninephrectomy- or diabetes-induced renal hypertrophy. *Am. J. Physiol. Ren. Physiol.* **297**, F585–F593 (2009).
7. Chen, J. K. et al. Phosphatidylinositol 3-kinase signaling determines kidney size. *J. Clin. Invest.* **125**, 2429–2444 (2015).
8. Sarbassov, D. D. et al. Prolonged rapamycin treatment inhibits mTORC2 assembly and Akt/PKB. *Mol. Cell* **22**, 159–168 (2006).
9. Settembre, C. et al. TFEB links autophagy to lysosomal biogenesis. *Science* **332**, 1429–1433 (2011).
10. Palmieri, M. et al. Characterization of the CLEAR network reveals an integrated control of cellular clearance pathways. *Hum. Mol. Genet.* **20**, 3852–3866 (2011).
11. Settembre, C. et al. A lysosome-to-nucleus signalling mechanism senses and regulates the lysosome via mTOR and TFEB. *EMBO J.* **31**, 1095–1108 (2012).
12. Palmieri, M. et al. mTORC1-independent TFEB activation via Akt inhibition promotes cellular clearance in neurodegenerative storage diseases. *Nat. Commun.* **8**, 14338 (2017).
13. Yoshii, S. R. & Mizushima, N. Monitoring and measuring autophagy. *Int J. Mol. Sci.* **18**, 9 (2017).
14. Li, L. et al. A TFEB nuclear export signal integrates amino acid supply and glucose availability. *Nat. Commun.* **9**, 2685 (2018).
15. Martina, J. A., Chen, Y., Gucek, M. & Puertollano, R. MTORC1 functions as a transcriptional regulator of autophagy by preventing nuclear transport of TFEB. *Autophagy* **8**, 903–914 (2012).
16. Napolitano, G. et al. mTOR-dependent phosphorylation controls TFEB nuclear export. *Nat. Commun.* **9**, 3312 (2018).
17. Rajan, R. et al. Quantifying autophagosomes and autolysosomes in cells using imaging flow cytometry. *Cytom. A.* **87**, 451–458 (2015).
18. Pugsley H. R. Assessing autophagic flux by measuring LC3, p62, and LAMP1 co-localization using multispectral imaging flow cytometry. *J. Vis. Exp.* 55637 (2017).
19. Lawrence, R. E. & Zoncu, R. The lysosome as a cellular centre for signalling, metabolism and quality control. *Nat. Cell Biol.* **21**, 133–142 (2019).
20. Cai, C. C. et al. Glycine protects against hypoxic-ischemic brain injury by regulating mitochondria-mediated autophagy via the AMPK pathway. *Oxid. Med Cell Longev.* **2019**, 4248529 (2019).
21. Yin, X. et al. Autophagy regulates abnormal placentation induced by folate deficiency in mice. *Mol. Hum. Reprod.* **25**, 305–319 (2019).
22. Zhao, Y. et al. Folic acid deficiency increases brain cell injury via autophagy enhancement after focal cerebral ischemia. *J. Nutr. Biochem.* **38**, 41–49 (2016).
23. Hoffmann, J. et al. Sham surgery and inter-individual heterogeneity are major determinants of monocyte subset kinetics in a mouse model of myocardial infarction. *PLoS ONE* **9**, e98456 (2014).
24. Hoke, T. S. et al. Acute renal failure following bilateral nephrectomy is associated with cytokine-mediated pulmonary injury. *J. Am. Soc. Nephrol.* **18**, 155–164 (2006).
25. Ge, Y., Huang, M. & Yao, Y. M. Autophagy and proinflammatory cytokines: interactions and clinical implications. *Cytokine Growth Factor Rev.* **43**, 38–46 (2018).
26. Gao, B., Calhoun, K. & Fang, D. The proinflammatory cytokines IL-1beta and TNF-alpha induce the expression of Synoviolin, an E3 ubiquitin ligase, in mouse synovial fibroblasts via the Erk1/2-ETS1 pathway. *Arthritis Res. Ther.* **8**, R172 (2006).
27. Sheng, W. et al. Pro-inflammatory cytokines and lipopolysaccharide induce changes in cell morphology, and upregulation of ERK1/2, iNOS and sPLA(2)-IIA expression in astrocytes and microglia. *J. Neuroinflammation.* **8**, 121 (2011).
28. Bryant, K. L. et al. Combination of ERK and autophagy inhibition as a treatment approach for pancreatic cancer. *Nat. Med.* **25**, 628–640 (2019).
29. Palmieri, M., Pal, R. & Sardiello, M. AKT modulates the autophagy-lysosome pathway via TFEB. *Cell Cycle* **16**, 1237–1238 (2017).
30. Li, M. et al. Suppression of lysosome function induces autophagy via a feedback down-regulation of MTOR complex 1 (MTORC1) activity. *J. Biol. Chem.* **288**, 35769–35780 (2013).
31. Barth, S., Glick, D. & Macleod, K. F. Autophagy: assays and artifacts. *J. Pathol.* **221**, 117–124 (2010).
32. Simmons, E. M. et al. Plasma cytokine levels predict mortality in patients with acute renal failure. *Kidney Int.* **65**, 1357–1365 (2004).

33. Kato, M. et al. Elevated plasma levels of interleukin-6, interleukin-8, and granulocyte colony-stimulating factor during and after major abdominal surgery.[see comment]. *J. Clin. Anesthesia.* **9**, 293–298 (1997).

34. Andres-Hernando, A. et al. Splenectomy exacerbates lung injury after ischemic acute kidney injury in mice. *Am. J. Physiol. Ren. Physiol.* **301**, F907–F916 (2011).

35. Golab, F. et al. Ischemic and non-ischemic acute kidney injury cause hepatic damage. *Kidney Int.* **75**, 783–792 (2009).

36. Prud'homme, M. et al. Acute kidney injury induces remote cardiac damage and dysfunction through the galectin-3 pathway. *JACC Basic Transl. Sci.* **4**, 717–732 (2019).

37. Gao, E. et al. A novel and efficient model of coronary artery ligation and myocardial infarction in the mouse. *Circ. Res.* **107**, 1445–1453 (2010).

38. Nossuli, T. O. et al. A chronic mouse model of myocardial ischemia-reperfusion: essential in cytokine studies. *Am. J. Physiol. Heart Circ. Physiol.* **278**, H1049–H1055 (2000).

39. Bemelmans, M. H., Gouma, D. J., Greve, J. W. & Buurman, W. A. Cytokines tumor necrosis factor and interleukin-6 in experimental biliary obstruction in mice. *Hepatology* **15**, 1132–1136 (1992).

40. Wang, H. et al. Interplay of hepatic and myeloid signal transducer and activator of transcription 3 in facilitating liver regeneration via tempering innate immunity. *Hepatology* **51**, 1354–1362 (2010).

41. Kim, J. H. et al. Raf/MEK/ERK can regulate cellular levels of LC3B and SQSTM1/p62 at expression levels. *Exp. Cell Res.* **327**, 340–352 (2014).

42. Alderliesten, M. et al. Extracellular signal-regulated kinase activation during renal ischemia/reperfusion mediates focal adhesion dissolution and renal injury. *Am. J. Pathol.* **171**, 452–462 (2007).

43. Collier, J. B., Whitaker, R. M., Eblen, S. T. & Schnellmann, R. G. Rapid renal regulation of peroxisome proliferator-activated receptor gamma coactivator-1alpha by extracellular signal-regulated Kinase 1/2 in physiological and pathological conditions. *J. Biol. Chem.* **291**, 26850–26859 (2016).

44. Han, S. J., Jang, H. S., Kim, J. I., Lipschutz, J. H. & Park, K. M. Unilateral nephrectomy elongates primary cilia in the remaining kidney via reactive oxygen species. *Sci. Rep.* **6**, 22281 (2016).

45. Cagnol, S. & Chambard, J. C. ERK and cell death: mechanisms of ERK-induced cell death-apoptosis, autophagy and senescence. *FEBS J.* **277**, 2–21 (2010).

46. Kinsey, C. G. et al. Protective autophagy elicited by RAF->MEK->ERK inhibition suggests a treatment strategy for RAS-driven cancers. *Nat. Med.* **25**, 620–627 (2019).

47. Yang, J. et al. Melatonin pretreatment alleviates renal ischemia-reperfusion injury by promoting autophagic flux via TLR4/MyD88/MEK/ERK/mTORC1 signaling. *FASEB J.* **34**, 12324–12337 (2020).

48. Fox, B. M. et al. Metabolomics assessment reveals oxidative stress and altered energy production in the heart after ischemic acute kidney injury in mice. *Kidney Int.* **95**, 590–610 (2019).

49. Holditch, S. J. et al. A study of sirolimus and an mTOR kinase inhibitor (TORKi) in a hypomorphic Pkd1 mouse model of autosomal dominant polycystic kidney disease (ADPKD). *Am. J. Physiol. Renal Physiol.* **317**, F187–F196 (2019).

50. Akcay, A. et al. IL-33 exacerbates acute kidney injury. *J. Am. Soc. Nephrol.* **22**, 2057–2067 (2011).

51. Bourne, J. N. Analyzing synaptic ultrastructure with serial electron microscopy. In: *Neuromethods: Transmission Electron Microscopy Methods for Understanding the Brain* (2016).

52. Yuan, M., Breitkopf, S. B., Yang, X. & Asara, J. M. A positive/negative ion-switching, targeted mass spectrometry-based metabolomics platform for bodily fluids, cells, and fresh and fixed tissue. *Nat. Protoc.* **7**, 872–881 (2012).

53. Loghman-Adham, M., Nauli, S. M., Soto, C. E., Kariuki, B. & Zhou, J. Immortalized epithelial cells from human autosomal dominant polycystic kidney cysts. *Am. J. Physiol. Ren. Physiol.* **285**, F397–F412 (2003).

54. Mauthe, M. et al. Chloroquine inhibits autophagic flux by decreasing autophagosome-lysosome fusion. *Autophagy* **14**, 1435–1455 (2018).
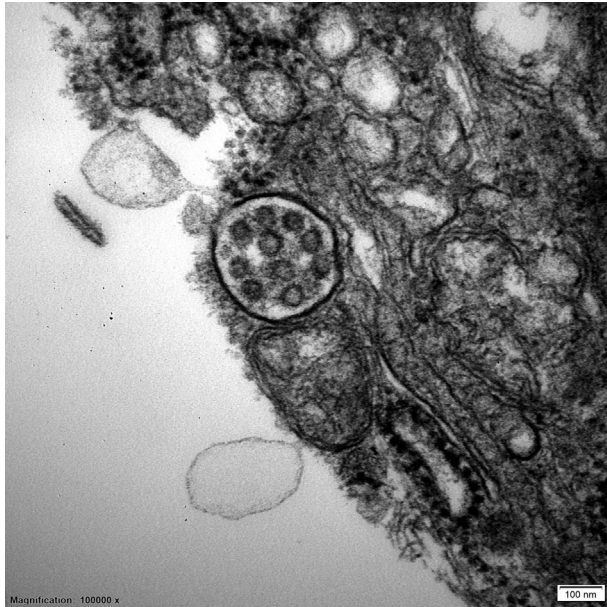
Figure 1 | Multivesicular body in a podocyte of a patient with lupus nephritis who tested negative for coronavirus disease 2019. Uranyl acetate-lead citrate, original magnification ×10,000. To optimize viewing of this image, please see the online version of this article at www.kidney-international.org.

nonspecific. Endocytic vesicles may be coated by proteins, such as clathrin. The presence of coating proteins may cause an electron-dense area around these vesicles giving the appearance of a viral "corona."[4] Su *et al.*[1] found SARS-CoV nucleoprotein in renal tubules by immunohistochemistry, but the presence of a viral protein does not necessarily mean the presence of complete viral particles. Why MVBs occur so commonly in podocytes and uncommonly in tubular epithelial cells is unclear.

Transmission EM of tissue sections is not a specific or sensitive method for the detection of viral particles; there are numerous structures found by EM that resemble viruses (so-called viral-like particles), such as the well-known endothelial tubuloreticular inclusions (also called myxovirus-like particles). Therefore, caution is suggested when identifying a virus by EM in tissue sections. Immunohistochemistry may also result in nonspecific staining, particularly in renal tubules. Two recent case reports of collapsing glomerulopathy in COVID-19–positive patients failed to identify the virus in the kidney biopsy by *in situ* RNA analysis.[5,6] Another case report describing a patient with collapsing glomerulopathy also failed to find viral RNA in tissue extracted from the biopsy but demonstrated "viral particles" (with the appearance of MVBs) in podocytes.[2] Further molecular studies for the presence of the viral genome in renal parenchymal cells would be important in deciding whether SARS-CoV-2 truly infects the kidney.

1. Su H, Yang M, Wan C, et al. Renal histopathological analysis of 26 postmortem findings of patients with COVID-19 in China. *Kidney Int.* 2020;98:219–227.
2. Kissling S, Rotman S, Gerber C, et al. Collapsing glomerulopathy in a COVID-19 patient. *Kidney Int.* 2020;98:228–231.
3. Ghadially FN. Multivesicular bodies and R-bodies. In: Ghadially FN, ed. *Ultrastructural Pathology of the Cell and Matrix.* 4th ed. Vol. 2. Boston, MA: Butterworth-Heinemann; 1997:632–639.
4. Marsh M, McMahon HT. The structural era of endocytosis. *Science.* 1999;285:215–220.
5. Larsen CP, Bourne TD, Wilson JD, et al. Collapsing glomerulopathy in a patient with COVID-19. *Kidney Int Rep.* 2020;5:935–939.
6. Peleg Y, Kudose S, D'Agati V, et al. Acute kidney injury due to collapsing glomerulopathy following COVID-19 infection. *Kidney Int Rep.* 2020;5:940–945.

Edward Calomeni[1], Anjali Satoskar[1], Isabelle Ayoub[2], Sergey Brodsky[1], Brad H. Rovin[2] and Tibor Nadasdy[1]

[1]*Department of Pathology, The Ohio State University, Columbus, Ohio, USA; and* [2]*Department of Medicine, The Ohio State University, Columbus Ohio, USA*

Correspondence: *Tibor Nadasdy, The Ohio State University, 320 W. 10th Avenue, M018 Starling Loving Hall, Columbus, Ohio 43210, USA. E-mail:* tibor.nadasdy@osumc.edu

Autophagy inhibition by chloroquine and hydroxychloroquine could adversely affect acute kidney injury and other organ injury in critically ill patients with COVID-19

To the editor: We read the letter by Izzedine *et al.*[1] with great interest, especially the discussion of renal adverse effects of drug treatment options for coronavirus disease 2019 (COVID-19). We would like to draw particular attention to the potential adverse effect of chloroquine and hydroxychloroquine, the lysosomotropic antimalarial drugs that may inhibit the infection of severe acute respiratory syndrome coronavirus 2 by reducing the entry and replication of the virus. Severe acute respiratory syndrome coronavirus 2 enters cells via endocytosis by binding of its trimeric spike protein to cell surface receptors including angiotensin-converting enzyme 2. Expression of angiotensin-converting enzyme 2 is high in proximal tubular cells in the human kidney (see Supplementary Figure S1 and Supplementary References). Based on the *in vitro* observation of inhibitory effects of chloroquine and hydroxychloroquine, clinical studies of their treatment in COVID-19 patients are under way. However, we believe that these lysosomotropic agents have the potential to make acute kidney injury (AKI) and other organ failures worse due to their known effect to increase lysosomal pH and inhibit autophagy,[2] a fundamental mechanism for the survival of injured cells. Chloroquine mainly inhibits autophagy by
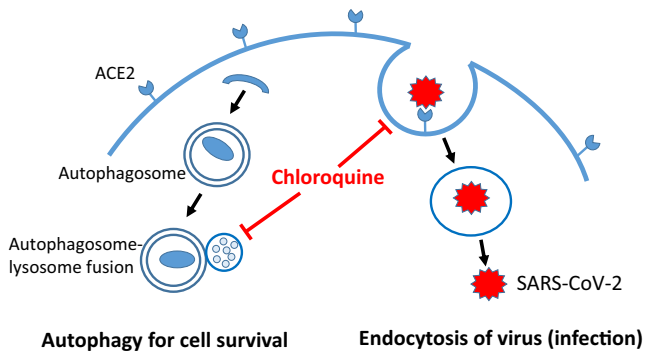
Figure 1 | Chloroquine could be a double-edged sword. Chloroquine may slow virus infection and replication early but may later potentiate tissue damage and worsen acute organ injury by inhibiting autophagy. ACE2, angiotensin-converting enzyme 2; SARS-CoV-2, severe acute respiratory syndrome coronavirus 2.

impairing autophagosome-lysosome fusion and the degradative activity of the lysosome.[2] Also, chloroquine can induce an autophagy-independent severe disorganization of the Golgi and endosomal-lysosomal systems that may contribute to its effect on autophagosome-lysosome fusion.[2] Inhibition of autophagy by chloroquine results in the accumulation of damaged mitochondria due to the lack of clearance via mitophagy, which, together with attendant oxidative stress, leads to renal tubular dysfunction.[3] In patients, chloroquine increases cancer cell killing by inhibiting autophagy, an idea being tested in clinical trials.[4] In mouse models of septic AKI, autophagy protects against renal tubule injury and pharmacological inhibition of autophagy with chloroquine worsens kidney damage.[5] Chloroquine also blocks autophagic flux and worsens both ischemic and cisplatin-induced nephrotoxic AKI in mice.[6] Chloroquine has also been shown to be nephrotoxic by autophagy-dependent as well as autophagy-independent pathways, including interference with the cyclic adenosine monophosphate production and signaling in distal tubular cells.[7] In other preclinical studies, chloroquine inhibits autophagy and worsens ischemic cardiac injury[8] and sepsis-induced liver or lung injury.[9,10] Thus, chloroquine could be a double-edged sword: it may slow virus infection and replication early, but may later potentiate tissue damage and worsen acute organ injury by inhibiting autophagy (Figure 1). We write to strike a cautionary note on using chloroquine or hydroxychloroquine in COVID-19 patients with acute organ injury including AKI.

SUPPLEMENTARY MATERIAL
Supplementary File (PDF)
Figure S1. Angiotensin-converting enzyme 2 (ACE2) is the functional cellular receptor for SARS-CoV-2.
Supplementary References.

1. Izzedene H, Jhaveri KD, Perazella MA. COVID-19 therapeutic options for patients with kidney disease. *Kidney Int*. 2020;97:1297–1298.
2. Mauthe M, Orhon I, Rocchi C, et al. Chloroquine inhibits autophagic flux by decreasing autophagosome-lysosome fusion. *Autophagy*. 2018;14:1435–1455.
3. Festa BP, Chen Z, Berquez M, et al. Impaired autophagy bridges lysosomal storage disease and epithelial dysfunction in the kidney. *Nat Commun*. 2018;9:161.
4. Levy JMM, Towers CG, Thorburn A, et al. Targeting autophagy in cancer. *Nat Rev Cancer*. 2017;17:528–542.
5. Mei S, Livingston M, Hao J, et al. Autophagy is activated to protect against endotoxic acute kidney injury. *Sci Rep*. 2016;6:22171.
6. Jiang M, Wei Q, Dong G, et al. Autophagy in proximal tubules protects against acute kidney injury. *Kidney Int*. 2012;82:1271–1283.
7. Wang B, Guo H, Ling L, et al. The chronic adverse effect of chloroquine on kidney in rats through an autophagy dependent and independent pathways. *Nephron*. 2020;144:96–108.
8. Ma X, Liu H, Foyil SR, et al. Impaired autophagosome clearance contributes to cardiomyocyte death in ischemia/reperfusion injury. *Circulation*. 2012;125:3170–3181.
9. Lin CW, Lo S, Perng DS, et al. Complete activation of the autophagic process attenuates liver injury and improves survival in septic mice. *Shock*. 2014;41:241–249.
10. Zhao H, Chen H, Xiaoyin M, et al. Autophagy activation improves lung injury and inflammation. *Inflammation*. 2019;42:426–439.

Charles L. Edelstein[1,2], Manjeri A. Venkatachalam[3] and Zheng Dong[4,5]

[1]Division of Renal Diseases and Hypertension, University of Colorado Anschutz Medical Campus, Aurora, Colorado, USA; [2]Department of Medicine, Rocky Mountain Regional Veterans Affairs Medical Center, Aurora, Colorado, USA; [3]Department of Pathology, University of Texas Health Science Center at San Antonio, San Antonio, Texas, USA; [4]Department of Cellular Biology and Anatomy, Medical College of Georgia at Augusta University, Augusta, Georgia, USA; and [5]Department of Medical Research, Charlie Norwood Veterans Affairs Center, Augusta, Georgia, USA

Correspondence: *Charles L. Edelstein, Division of Renal Diseases and Hypertension, University of Colorado Anschutz Medical Campus, Box C281, 12700 East 19th Avenue, Aurora, CO 80045, USA. E-mail: Charles.edelstein@cuanschutz.edu*

Could ferritin help the screening for COVID-19 in hemodialysis patients?

To the editor: The screening for coronavirus disease 2019 (COVID-19) is challenging: many patients are asymptomatic, viral RNA detection in a nasopharyngeal swab is falsely negative in 30%, and a pulmonary computed tomography scan is useless in patients with no pulmonary involvement.[1,2]

In our hemodialysis center, following the Kidney Disease Improving Global Outcomes recommendations, ferritin levels are measured each month to detect iron deficiency.[3] In April 2020, there were 22 COVID-19 cases that had occurred within the 270 patients undergoing hemodialysis at our hemodialysis center. We noticed that ferritin levels were very high in these patients (Figure 1). When monthly ferritin levels were measured in April, 1 of our female patients had an unusually high ferritin level of 3806 ng/ml compared with 531 ng/ml previously. A clinical examination showed no clinical symptoms of COVID-19, but she was tested by nasopharyngeal swab and was shown to be positive.

We compared ferritin levels in patients undergoing hemodialysis who tested positive and negative for COVID-19 at our